AWARD NUMBER: W81XWH-20-1-0682

TITLE: A Novel Approach Combining Oncolytic Virotherapy and Dual Immune Checkpoint Blockade for Metastatic Osteosarcoma

PRINCIPAL INVESTIGATOR: Jaime F. Modiano, VMD, PhD

CONTRACTING ORGANIZATION: University of Minnesota, Minneapolis, MN

REPORT DATE: October 2023

TYPE OF REPORT: Annual

PREPARED FOR: U.S. Army Medical Research and Development Command
Fort Detrick, Maryland 21702-5012

REPORT DOCUMENTATION PAGE

Form Approved
OMB No. 0704-0188

1. REPORT DATE	2. REPORT TYPE	3. DATES COVERED
October 2023	Annual	01Sep2022-31Aug2023

4. Title and subtitle

A Novel Approach Combining Oncolytic Virotherapy and Dual Immune Checkpoint Blockade for Metastatic Osteosarcoma

5a. CONTRACT NUMBER
W81XWH-20-1-0682

5b. GRANT NUMBER
CA190276

5c. PROGRAM ELEMENT NUMBER

6. AUTHOR(S)
Jaime F. Modiano, VMD, PhD
Shruthi Naik, PhD

E-Mail: modiano@umn.edu

5d. PROJECT NUMBER
00081767

5e. TASK NUMBER

5f. WORK UNIT NUMBER

7. PERFORMING ORGANIZATION NAME(S) AND ADDRESS(ES)

University of Minnesota
Veterinary Clinical Sciences and Masonic Cancer Center 420 Delaware St. SE
Minneapolis, MN 55455

Mayo Clinic College of Medicine
Department of Molecular Medicine
200 First Street, NW
Rochester, MN 55905

8. PERFORMING ORGANIZATION REPORT NUMBER

9. SPONSORING / MONITORING AGENCY NAME(S) AND ADDRESS(ES)

U.S. Army Medical Research and Development Command
Fort Detrick, Maryland 21702-5012

10. SPONSOR/MONITOR'S ACRONYM(S)

11. SPONSOR/MONITOR'S REPORT NUMBER(S)

12. DISTRIBUTION / AVAILABILITY STATEMENT
Approved for Public Release; Distribution Unlimited

13. SUPPLEMENTARY NOTES

14. ABSTRACT

Osteosarcoma is one of the most common cancers of children and adolescents and young adults (AYAs). The outcomes for with metastatic osteosarcoma are especially dismal because there are no effective options to treat this condition. Our objectives are to tilt the immune landscape of metastatic osteosarcoma from immunosuppression to immunoreactivity, and to generate pre-clinical support to translate this innovative immunotherapy for the treatment of children and AYAs with metastatic bone cancer. To achieve this, we propose to combine an oncolytic virus, which will kill tumor cells and activate the immune system in the tumor environment, with a drug that blocks the myeloid checkpoint to enhance phagocytosis and antigen presentation as well as the immune exhaustion checkpoint to enhance tumor killing by T cells and NK cells. We will define optimal combinations in lab animal models and subsequently use these data to translate the approach into a therapy for dogs with naturally occurring metastatic osteosarcoma, which will serve as a clinically realistic model in the pathway towards applying this therapy to treat children and AYAs with metastatic osteosarcoma.

15. SUBJECT TERMS

Osteosarcoma, metastasis, tumor immunity, oncolytic virotherapy, vesicular stomatitis virus, immune checkpoints, CD47, PD-1, PD-L1, drug development, animal models.

16. SECURITY CLASSIFICATION OF:			17. LIMITATION OF ABSTRACT	18. NUMBER OF PAGES	19a. NAME OF RESPONSIBLE PERSON
					USAMRDC
a. REPORT	b. ABSTRACT	c. THIS PAGE	Unclassified	221	19b. TELEPHONE NUMBER *(include area code)*
Unclassified	Unclassified	Unclassified			

Standard Form 298 (Rev. 8-98)
Prescribed by ANSI Std. Z39.18

TABLE OF CONTENTS

1. Introduction

Osteosarcoma is one of the most common cancers of children and adolescents and young adults (AYAs). In particular, the outcomes for patients with metastatic disease are dismal because there are no effective options for this condition. We have recognized that the mutational profiles in osteosarcoma create fertile environments for immunotherapy, and that the immune response is an important determinant of disease progression. These discoveries are foundational components of this project. In particular, immunotherapy is an appealing modality to treat metastatic cancer not only because tumors that are resistant to conventional treatment, such as radiation and chemotherapy, can be attacked with immunologic approaches, but also because this modality can reach tumors that are inaccessible for conventional treatments. For osteosarcoma, the inaccessibility of metastasis is a major factor that influences prognosis. Our recent work shows that osteosarcomas segregate into distinct groups with "immunologically silent" and "immunologically aware" tumors[1]. Patients with immunologically aware tumors have significantly better outcomes than patients with immunologically silent tumors. However, rationally designed immunotherapies have yet to be tested in the setting of metastatic osteosarcoma.

Immunotherapies, particularly checkpoint inhibitors (CPIs), designed to reactivate suppressed immune cells against tumors has revolutionized the management of patients with advanced melanoma and lung cancer, and they represent promising treatment approaches for many other cancers. But despite the success in these areas, many cancers are unresponsive to immune checkpoint blockade. Even among patients with cancers that are approved indications for immune checkpoint blockade, many patients are unresponsive to - or relapse after treatment. Immunotherapy resistance has been attributed to an exclusion or dearth of immune cells in the tumor microenvironment (TME). Oncolytic viruses are an emerging form of immunotherapy designed to selectively kill tumor cells and induce an inflammatory immune response in tumors. Preclinical studies using the oncolytic Vesicular stomatitis virus (VSV) that we are employing in this project can be administered systemically to reach and selectively replicate in tumor tissues leading to their destruction and consequent recruitment and activation of immune cells to the TME[2,3]. We hypothesize that combining systemic VSV therapy with CPI therapy can induce a potent and durable antitumor immune response that delivers clinical benefit in the treatment of metastatic osteosarcoma.

There are many challenges associated with the investigation of novel immunotherapies, and particularly combinatorial approaches. These difficulties are compounded in childhood cancers, and in particular in osteosarcoma which is a very rare tumor. We have thus learned about pathogenesis of this disease using conventional laboratory animal models (mice), but these models have limitations for therapy development. Studying spontaneous dog cancers as models to develop new therapies has gained favor due to the similarities in incidence and natural history of these diseases. Dogs are treated with similar protocols and dosing schedules as humans, providing a clinically realistic setting for drug development in a compressed timeline. Furthermore, canine clinical trials will almost always include animals of both sexes, allowing sex to be considered among the important biological variables. Biological samples to monitor safety, clinical toxicities, and local and systemic immune responses can be obtained from veterinary patients, so in addition to potential improvements in treatment modalities and dose schedules, veterinary trials also create opportunities to identify companion biomarkers to predict patient responses[4].

This project is designed to begin to address the potential to reach and manage metastatic osteosarcoma lesions by combining oncolytic VSV with ONIx, a novel CPI dually targeted to activate the CD47:SIRPα and PD-1:PD-L1 pathways. Therapies that block the interaction of CD47 and SIRPα stimulate tumor cell phagocytosis, while inhibitors of the PD-1:PD-L1 pathway stimulate T-cell activation that work in concert to induce anti-tumor immune responses[5]. This combination therapy is being studied in dogs with metastatic osteosarcoma with correlative studies to identify and investigator biomarkers of response.

2. Keywords

Osteosarcoma, metastasis, tumor immunity, oncolytic virotherapy, vesicular stomatitis virus, immune checkpoints, CD47, PD-1, PD-L1, drug development, animal models.

3. Accomplishments

NOTES REGARDING NO COST-EXTENSIONS: ON 4/February/2021, the PIs received an email notice from DOD describing the concern shared by CDMRP about the impacts of COVID-19 on Service Members and the public, and specifically on the challenges it posed to ongoing research. In that email, we were asked to disclose significant COVID-19-related developments that would impact performance of this project.

On 25/May/2021, Dr. Modiano (contact PI) notified Dr. Senkevitch (Program Officer) that our laboratories had been operating at less than full capacity due to the COVID-19 responses adopted by our institutions, which were magnified by supply chain disruptions, which continue to this day, and by personnel departures.

On 7/March/2022, Dr. Modiano confirmed in emails to Dr. Senkevitch and to Jodi Cardoza (Grants Specialist) that a no-cost extension would be needed to complete the objectives of the project. Both responded with assurance that a no-cost extension would likely be awarded. On 23/June, Dr. Senkevitch notified the PI that a Year 2 Annual Report was due 9/30/22. At this time a DD882 would not be needed.

On 8/August/2022, the University of Minnesota Sponsored Programs Administration Officer (Brett Carlson) submitted a formal request on the PI's behalf to request a 1-year no-cost extension. The request was acknowledged by Ms. Cardoza, and the no-cost extension was subsequently approved.

On 13/May/2023, Dr. Modiano requested a final 1-year no-cost extension to fulfill the aims of the project, which was granted.

This Technical Report is submitted to document progress from the inception of the progress through the end of the 3rd year, following the milestones in the approved SOW.

- **What are the major goals of the project?**

The project has three specific aims:

Specific Aim 1: Optimize dose and schedule for combination VSV-IFNβ-NIS and P-DIC (now called Onco-Immune Accelerator or ONIx) in mouse models of metastatic osteosarcoma.

Milestone: Project Specific Approvals by Local IACUC and IBC. Completed.
Note: A 3-year renewal of the IACUC protocol was approved during year-3, with appropriate modifications accounting for alternative strategies implemented to achieve the project goals.

Milestone: Project Specific Approvals by ACURO. Completed.
Note: The updated (new) IACUC protocol was approved by ACURO in August of 2023.

Milestone: Production of VSV-IFNβ- NIS for mouse studies. Completed.

Milestone: Production of P-DIC (ONIx). Completed.

Milestone: Cell authentication. Ongoing throughout the project.

Milestone: Define toxicity of combination VSV-IFNβ-NIS and P-DIC (ONIx). Ongoing.

Milestone: Define optimal dose for combination VSV-IFNβ-NIS and P-DIC (ONIx). Ongoing.

Milestone: Complete necropsies. Ongoing.

Milestone: Data analysis; organization and conclusions. Ongoing.

Milestone: Quality control and quality assurance for data – manuscript preparation and submission. Ongoing.

Specific Aim 2: Define immunological effects and mechanism of action for combination VSV IFNβ-NIS and P-DIC

Milestone: Assessment of immune response induced by VSV-IFNβ-NIS and P-DIC (ONIx) in mice with metastatic osteosarcoma. Ongoing.

Note: We modified the objectives to use alternative models of sarcoma to account for weaknesses of the K7M2 model. The MC17 syngeneic murine sarcoma model was successfully established for preclinical evaluation of oncolytic VSV combination immunotherapy approaches. Preliminary data indicate that single dose systemic therapy with oncolytic VSV-IFNβ-NIS significantly delays tumor growth in mice with subcutaneous murine sarcoma tumors. An orthotopic intratibial model is also being established to assess impact of combination immunotherapy on metastatic disease progression.

Milestone: Data analysis; organization and conclusions. Ongoing.

Milestone: Quality control and quality assurance for data – manuscript preparation and submission. Ongoing.

Specific Aim 3: Characterize safety, efficacy, and immunomodulatory effects of VSV-IFNβ- NIS and P-DIC (ONIx) in dogs with naturally occurring metastatic osteosarcoma

Milestone: Production of in vivo grade VSV-IFNβ-NIS for use in canine studies. Completed.

- Note, a new clinical-grade batch of VSV-IFNβ-NIS was produced, and QC testing was completed in 2022 to ensure the test article being used in these studies was active.

Milestone: Production of in vivo grade P-DIC (ONIx). Completed.

Note: Production of a new batch of ONIx is in progress.

Milestone: Identify safe dose to guide clinical development. We have demonstrated that systemic VSV-IFNβ-NIS therapy, administered as two consecutive doses of $3x10^9$ TCID50/kg, in combination with 2mg/kg ONIx administered twice weekly for 2 weeks was well tolerated in one dog with metastatic osteosarcoma. Ongoing.

Milestone: Assessment of immune response induced by VSV-IFNβ-NIS and P-DIC (ONIx) in dogs with metastatic osteosarcoma. Ongoing .

Note: we have expanded eligibility to dogs with inoperable or metastatic sarcomas and have designed alternative approaches to characterize the synergy of VSV and ONIx in vitro using resources from a completed canine clinical study.

Milestone: Data analysis; organization and conclusions. Ongoing.

Milestone: Quality control and quality assurance for data – manuscript preparation and submission. Ongoing.

Milestone: Planning for pediatric clinical trial planning (translation to humans). A clinical trial synopsis to evaluate neoadjuvant systemic VSV therapy in patients with sarcoma undergoing metastatectomy has been developed. A retrospective study to evaluate historic outcomes from patients undergoing metastatectomy of sarcoma pulmonary metastases is currently being completed. Ongoing.

- **What was accomplished under these goals?**

FORMATTING NOTE: The figures that illustrate the data referenced in the text have been moved to the end of the document to simplify formatting and to ensure that the document remains readable across platforms (Macintosh/Windows).

Milestone: Project Specific Approvals by Local IACUC and IBC. Completed.
University of Minnesota IACUC protocol 2004-38033A was approved on July 20, 2020. The three-year renewal for University of Minnesota IBC protocol (new number assigned, 2106-39146H) was approved on October 22, 2021 (previous IBC approval date 1805-35967H). The 3-year renewal for the IACUC protocol, with the new ID 2304-40976A, was approved on July 10, 2023. The University of Minnesota IBC protocol 2106-39146H remains in effect until October 21, 2024.

Mayo Clinic IACUC protocol A00005309-20 was approved on September 30, 2020. The 3-year renewal for this protocol, with the new ID A00005309-20-R23, was approved on September 27, 2023, and has been submitted to ACURO for review and approval.

Milestone: Project Specific Approvals by ACURO. Completed.
ACURO approval for Proposal Number CA190276, Award Number W81XWH-20-1-0682 was obtained on November 20, 2020. ACURO approval for the updated University of Minnesota IACUC protocol was obtained on August 8, 2023, with a minor modification to allow dogs as small as 7.5 kg approved on September 13, 2023.

Protocols have been renewed and updated to remain in compliance with animal welfare and proposed protocol modifications.

Milestone: Production of VSV-IFNβ- NIS. Completed.

Production of a new batch of recombinant VSV-cIFNβ-NIS for veterinary studies was completed in March 2022 using processes similar to those defined for GMP production of clinical grade VSV. Briefly, recombinant VSV-cIFNβ-NIS was produced in a human suspension cell line and purified by tangential flow filtration. Following production, the new virus batch was subject to quality control (QC) testing including assays to confirm potency, purity, sterility, functional activity, and sequence identity. This new

virus preparation is being used canine studies. The virus batch undergoes routine quality control testing to ensure that it remains uncontaminated and that it potency and infectivity are stable.

Table 1. Testing and validation of VSV-cIFNβ-NIS batch 2022-01

Date of production	03/25/2022
Titer	$4.8x10^{10}$ $TCID_{50}$ units/ml
Total protein concentration	6115 ug/ml
Total DNA concentration	8035 ng/ml
Benzonase concentration	<0.4ng/ml
Endotoxin level	2.6 EU/ml
Sequence analysis	completed
VSV N gene	$4.23x10^{11}$ copies/ml
Sterility testing	No growth after 14 days

Milestone: Production of P-DIC (ONIx). Completed.
We had a pre-existing batch of P-DIC (now called Oncoimmunology accelerator, or ONIx) that was sufficient for pilot studies (see below for experimental data using ONIx in pilot mouse studies). This product had been previously tested for sterility and potency, and the data were provided in the original grant application.

Production of ONIx for this project was delayed because of the response to the COVID-19 pandemic. The University of Minnesota maintained minimal operations from March 2020 until approx. May of 2021, primarily focused on development of COVID-19 tests, ventilators, and other procedures that aided the national response to this public health crisis. Laboratories and facilities, including the Molecular Cell Therapy Center, where drug production for ONIx was to take place, were closed as part of the need to avoid having people in close contact, as well as to divert all physical resources (pipettes, glassware, etc.) to COVID-related research, development, diagnosis, treatment, and response operations.

In May of 2021, PIs at the University of Minnesota were directed to submit individual plans to resume work under the umbrella of a University Health Sciences-wide “Sunrise Plan.” With few exceptions, the individual plans required staff to work in staggered shifts with a maximum occupancy in labs of 50%. As part of the implementation of that plan, Dr. Vallera was able to resume synthesis of ONIx and complete the batch for pre-clinical work (in mice and dogs). The production run was completed on May 27, 2021, and vialed for use in 3-mL vials at a concentration of 9 mg/mL (total yield = 3.1g). Purity of the product was confirmed by SDS-PAGE **(Figure 1).**

Sterility testing for ONIx was completed through IDEXX laboratories (**See report as an appendix**). Potency testing (measured as displacement of anti-CD47 and anti-PD-L1 antibodies from human A549 and canine CLBL-1 cells was completed. We confirmed that ONIx binds canine CLBL-1 cells with comparable affinity to human A549 cells **(Figure 2).**

Whereas there are robust methods to measure the pharmacokinetics (PK) and pharmacodynamics (PD) of VSV[6], we had been using CD47-driven phagocytosis assays with mouse J774 cells as effectors and Raji lymphoma cells as targets to investigate ONIx PK and PD by evaluating CD47 blockade[7,8]. However, these assays are extremely laborious and, in our hands, poorly reproducible among different operators. It takes considerable effort to master the methodology.

Antibody displacement (**Figure 3**) is a reasonable method to evaluate the presence of ONIx, but it does not provide a definitive measure of biological activity. Thus, as part of our efforts to improve quantification, we requested a cell line from Dr. Lin at AstraZeneca that would allow us to measure the effect of ONIx to inhibit PD-1 signaling in a Jurkat indicator cell line *in vitro*[9]. After extensive negotiations, AstraZeneca did not agree to provide the materials requested. However, over the past 15 months or so, several companies, including Promega and Eurofins Discovery have developed bioassays to measure the activity of biological products, including those intended for immune checkpoint blockade.

We obtained a sample kit from Promega to evaluate its utility to quantify blockade of the immune exhaustion checkpoint by ONIx. The principle of the assay is shown in **Figure 4A**. Briefly, the assay consists of incubating an artificial antigen-presenting cell (APC) line engineered to express a molecule that activates the T-cell receptor of human Jurkat T-cells, with a Jurkat cell line that has been modified to express PD-1. Jurkat cells were originally derived from a human T-cell leukemia, so they are immortalized. But they have been an exceptional tool for immunologists for decades because the physiology of the biochemical pathways stemming from the T-cell receptor that control interleukin (IL)-2 production and IL-2 receptor expression remain intact[10]. Therefore, these cells meet essential criteria to understand basic mechanisms of T-cell activation. Because they have been extensively studied and characterized, the cells also have provided tools for development of clinical laboratory assays such as the ones described here.

Antigen receptor-mediated or biochemical activation of the Jurkat cells is determined based on the activity of a reporter gene. The Jurkat cells for the assay have been further modified to include a firefly luciferase (fLuc) gene controlled by the nuclear factor of activated T-cells (NFAT)-dependent promoter. Upon T-cell (or Jurkat cell) activation, a biochemical cascade of events leads to translocation of NFAT transcription factors from the cytoplasm to the nucleus, with consequent transcription of NFAT-regulated genes (including IL-2). Because the fLuc gene in Jurkat cells is controlled exclusively by NFAT, the fLuc reporter is silent in unstimulated cells, but it produces protein in activated cells. The protein can then be measured by adding substrate (luciferin) and measuring light emission in a standard luminometer. In the absence of PD-1 ligation, the cells should produce high levels of fLuc (light emission) upon activation. However, in the modified, PD-1-expressing Jurkat cells, ligation of PD-1 by PD-L1 (expressed by the artificial APC), will attenuate fLuc expression and the light signal.

Figure 4B shows the positive control data from our experiment. We did not receive APCs without PD-L1 as part of the sample kit, so as a positive control, we stimulated the Jurkat cells using a combination of phorbol myristate acetate (PMA) and ionomycin (P/I). This combination, which activates protein kinase C (PKC) and increases the concentration of cytosolic ionized calcium, bypasses antigen receptor signals and leads to synchronous activation of 80-100% of the cells[11]. The data show that unstimulated Jurkat cells produced small levels of light that were detectable above background in the assay, and stimulation with P/I increased light emission by more than 100-times. As predicted by the assay design, the addition of artificial APCs expressing PD-L1 attenuated the light signal by more than one order of magnitude, providing confirmation of the principle on which the assay is based: ligation of PD-1 (expressed by the Jurkat cells) by PD-L1 (expressed by the artificial APCs) significantly interrupts T-cell signaling and activation, even when that activation uses pharmacological agents that bypass the antigen receptor.

With the confirmation of the positive control, we could use the assay to evaluate ONIx activity. **Figure 4C** shows a dose response relationship where Jurkat cells incubated with artificial APCs were treated with decreasing concentrations of ONIx. The Y axis in the figure is truncated to show the dose response relationship, as it would be masked by the inclusion of the full dynamic range of activation using P/I. This is expected: pharmacological activation of T cells using P/I produces greater than 5 to 10-fold higher levels of measurable signal than physiologic (or semi-physiologic) activation through the antigen

receptor. The data indicate that the addition of ONIx reversed the inhibition seen by engagement of PD-L1 and suggest that levels as low as 5 µg/ml could be reliably detected in samples using this assay.

Finally, we evaluated the potential for using this assay to establish measures of PK and PD in the canine METEOR trial (more details about the trial are described below). We investigated the possible interference of canine serum (the biological sample format) in the assay. **Figure 4D** shows that, unexpectedly, normal canine serum (added to 10% of the assay by volume) inhibited the activation of Jurkat cells in the assay, and the addition of PD-L1-expressing artificial APCs had no further effect. Previous work has shown that canine serum can contain xenoantibodies that promote complement-dependent killing of human cells[12], but there was no complement added to the cultures. We have considered the possibility that there is enough complement present in the canine serum to mediate this effect, which could be inactivated by heating the serum at 56°C for 15-60 minutes. However, that could also inactivate other critical components we want to measure in the assay, including ONIx. At the present time, we are investigating the mechanisms through which canine serum might cause inhibition of the assay signal and ways to overcome that working in collaboration with Promega. Promega has also agreed to provide a comparable bioassay to measure CD47 blockade, which could be used in combination with or instead of the PD-1 blockade assay.

As noted above, Eurofins Discovery has also developed similar assays, also based on the use of genetically modified Jurkat cells, a different set of reporters (evaluating receptor assembly instead of transcriptional activity), and artificial APCs. We have obtained a sample kit to evaluate the Eurofins PD-1 blockade bioassay in our system, and the initial experiments to test the kit are scheduled for October 19 and 20, 2023. Depending on the results (dynamic range, confirmation of ONIx activity, inhibition by canine serum or lack thereof), we also plan to test the Eurofins CD47 blockade bioassay kit and decide which of these various kits, if any, will be the best suited to establish ONIx PK and PD in vivo. If we determine that none of the kits is suitable, for example, due to cell death induced by canine serum, we will use the antibody displacement assays (**Figure 3**) to establish the presence of ONIx and reconsider use of the phagocytosis assay described above as a measure of activity.

Milestone: Cell authentication. Ongoing.
The PI labs follow rigorous SOPs for cell authentication. Authentication of cell lines, including newly obtained K7M2, F420, and F331 cell lines, has proceeded according to SOPs since lab work resumed for this project.

Milestone: Define toxicity of combination VSV-IFNβ-NIS and P-DIC (ONIx). Ongoing.
To confirm the safety of VSV and ONIx combination therapy, a pilot study was carried out in the well-established A20 (Balb/c) murine lymphoma model. Mice with established A20 tumors were treated with either PBS, VSV ($1x10^8$ $TCID_{50}$/mouse), ONIx (5mg/kg for 6 doses), or combination of VSV and ONIx. Mice were monitored for adverse events, including weight loss. The results show that all treatments, including combination therapy were well tolerated, with minimal transient weight loss and resumption of weight gain in mice at approximately the same rate as the controls (**Figure 5**).

Milestone: Define optimal dose for combination VSV-IFNβ-NIS and P-DIC (ONIx). Ongoing.
Continuing our efforts to investigate the combination therapy in the most commonly used pre-clinical model of osteosarcoma, we obtained K12 and K7M2 cells from the National Cancer Institute (NCI) for use in this project under a multi-institutional Materials Transfer Agreement. Neither cell line was modified with reporters for *in vivo* imaging or with a known antigen for immunological studies. Thus, our first step was to genetically edit the cells to express luciferase for *in vivo* tracking and ovalbumin to test antigen-specific immune responses. We generated a genetically edited K12 cell line incorporating chicken ovalbumin (OVA), as a target antigen for immune cells and Gaussia luciferase (Gluc) as a reporter for *in vivo* imaging using CRISPR-Cas9. Integration of the Gluc-OVA cassette in frame into the *Rosa26* locus was confirmed by sequencing, however, unlike MC17 cells which we previously modified

using the same methodology[13], the cells did not show significant Gluc activity *in vitro*, and certainly not enough for *in vivo* experiments (**Figure 6**).

The K12-17 cells also failed to form subcutaneous (sq) tumors in syngeneic Balb/c recipient mice when injected at $2x10^6$ cells per mouse. Our attempts to introduce exogenous genes into K7M2 cells failed repeatedly. Thus, we obtained a K7M2 cell line that is stably transfected with fLuc (K7M2-fLuc) from Dr. Brock Lindsey at West Virginia University[14]. It took several months to obtain these cells due to the challenges associated with the COVID-19 pandemic, as Dr. Lindsey's lab had to wait until they could return to the laboratory in-person to expand cells and ship them. We received K7M2 cells on February 10, 2021, expanded them, and submitted them for authentication and *Mycoplasma* testing to IDEXX BioResearch. The cells passed QC (authenticated as K7M2, were negative for all *Mycoplasma sp*.). They also expanded *in vitro* with an estimated doubling time of 22-24 hours and had robust fLuc activity (**Figure 7**).

We had to wait several months to start the *in vivo* experiments , as the animal facilities at the University of Minnesota were also experiencing a severe shortage of caretaker staff during the COVID pandemic and PIs were asked to reduce the number and frequency of animal experiments, or not to start any new ones until further notice when staffing could be restored.

We finally were able to initiate up a titration experiment on May 10, 2022. Groups of three female Balb/c mice received $2.5x10^5$, $5x10^5$, or $1x10^6$ K7M2-fLuc cells by tail vein injection. One group of three Balb/c mice received $2x10^6$ K7M2-fLuc cells as a sq injection.

Viable cells were identified using *in vivo* imaging 24 hours after the injection (**Figure 8**). However, most of the activity in the mice receiving tail vein injections was seen in the spleen, with no luciferin conversion above background noted in the lung fields for any mouse. Viable cells were seen at the site of tumor implantation in all of the mice that received sq injections. Unlike what has been previously reported (see for example, reference[15]), we did not see any significant tracking of tumor cells to the lungs based on imaging over a 12-week experimental period. Rather, the luciferin-converting activity remained in the abdomen (anatomically, in the area where the spleen is located), showing peak activity at 24 hours, then waning progressively over the next eight weeks, and increasing again slightly in some mice between weeks 8-12 (**Figures 8 and 9**).

Two mice that received K7M2 cells in the tail vein (one at the $1x10^6$ cells dose and one at the $5x10^5$ cells dose) developed tumors at the injection site, which were grossly evident approximately 11 weeks after inoculation. These tumors, which probably arose from cells that extravasated at the time of injection, grew slowly, did not impair the quality of life of the mice, and were readily apparent in the *in vivo* imaging studies. The potential extravasation did not impede systemic distribution of the cells through the vascular system, as there were no obvious differences in the whole body imaging for these mice compared to the other two mice in each of their groups. We terminated the experiment for futility after 12 weeks. At the end of the experiment, the mice were humanely sacrificed, and a complete necropsy was performed on each mouse. Necropsies were done systematically, starting with a complete examination of the abdomen for evidence of metastasis and collection of the spleen with gross examination for evidence of tumor growth. No other abdominal organs were collected, as there was no evidence of gross metastasis or tumor growth (luciferin conversion *in vivo*) in the abdomen outside of the spleen for any animal. The chest cavity was then carefully opened without perforating the diaphragm by removing the skin and carefully transecting the ribs at the left costochondral junctions. The lungs were allowed to deflate to examine the chest cavity for gross metastasis (none was noted). The trachea was transected above the mediastinal entry, and the lungs were gently inflated *in situ* by infusing 10% neutral buffered formalin through the tracheal transection. The inflated lungs were then removed from the chest cavity and examined for evidence of gross metastasis. **Figure 10** shows a mass measuring approximately 3 mm in diameter seen in the single mouse that received $5x10^5$ cells

and developed a tumor in the tail (**Figures 8 and 9**). The tail tumors were collected from both mice in which they were grossly apparent.

No gross tumors were seen in any of the mice that received sq K7M2-fLuc cells, consistent with the observation that the fLuc activity in those mice had waned. A prominent sq fat pad was collected from one mouse to assess if there was evidence of a tumor remnant. The tissue collected consisted of skin, subcutis, multiple small quiescent mammary, glands and ducts, abundant adipose tissue and a lymph node. There were no significant abnormalities detected.

Histopathologic examination of the lungs, spleens, and tails showed that three mice (one in the group receiving $1x10^6$ cells and two in the group receiving $5x10^5$ cells) had microscopic evidence of tumors in the lungs (**Figure 11**). The tumors were similar in all cases (in the lungs, and in the two mice that had tumors in the tail), consisting of unencapsulated, moderately well-demarcated, densely cellular masses that were consistent with a diagnosis of sarcoma. The neoplastic cells were arranged into ill-defined broad sheets to poorly formed bundles and streams, and they were supported by a fine fibrovascular stroma. Rarely, between neoplastic cells, there were scant amounts of wispy, fibrillary, eosinophilic material (possible osteoid). The neoplastic cells were plump, spindle shaped, with indistinct cell borders, and they had large amounts of eosinophilic to amphophilic cytoplasm. The nuclei were round to oval with vesicular chromatin, and they had up to three prominent, magenta nucleoli. There was marked anisocytosis and anisokaryosis throughout the tumors.

The lungs of every mouse in the experiment also showed evidence of inflammation: there was diffuse, mild, alveolar vascular congestion, and mild increased cellularity of the alveolar septa, owing to increased large round mononuclear cells (macrophages) and small lymphocytes. Particularly at the edge of the sections, there were foci of atelectasis. The spleens showed diffuse, moderate congestion and extramedullary hematopoiesis, although a component of inflammation could not be excluded. The lung pathology was atypical and suggestive of an inflammatory or immune response which possibly eliminated the tumor cells or rejected an incipient tumor. The spleen pathology could be within the confines of what is normally observed for this strain of mouse (Balb/c), but it also could reflect inflammation or immune stimulation in response to the tumor cells that were retained in the spleen (presumably within the reticuloendothelial system). In particular, the fact that cells tracked to the spleen first could be the cause of why a strong anti-tumor immune response might have been generated, as the spleen in a major immune organ in mice. It is interesting that two of the three mice that developed lung metastasis had tumors in the tail, as these tumors might have provided a source of metastatic cells (outside of the spleen). This would be consistent with the observed metastasis of K7M2 cells injected intratibially[14-16]. **A copy of the full pathology report is included as an appendix**.

Nonetheless, it was clear from these experiments that the tail vein model of K7M2-fLuc cells (at least using the cells from West Virginia University) will not be useful for our experiments. We thus obtained K7M2-fLuc cells from a different source (Dr. Steve Dow, Colorado State University). We received these cells in August of 2022, but the viability was poor, and we have had limited success expanding them.

We attempted one more experiment with unmodified (no fLuc transgene) K7M2 cells from NCI that grew exceptionally well in culture. Groups of 4 Balb/c mice were inoculated with $5x10^5$ K7M2 cells iv to assess the effect of ONIx vs. placebo. Two mice were inoculated with K7M2 cells at the same concentration and sacrificed at Day-5 to assess for the presence of microscopic lung tumors. Mice received 5 mg/kg ONIx (or PBS for the placebo control) on days 12, 14, 19, and 21. Mice were humanely euthanized on Day 28 of the experiment. The presence of tumors in the lungs and other organs was evaluated grossly at necropsy, and microscopically (in the lungs) for all of the mice. As per the experiments described above, none of the mice developed detectable tumors within the 28-day experimental period. However, we were able to document that ONIx was safe based on the absence

of adverse events on weight gain (**Figure 12**) or other physical and qualitative metrics (no changes in the texture or appearance of hair coat, no changes in activity or behavior, etc.).

Upon our consultation with other osteosarcoma experts who have used the K7M2 model, we learned that it is not unusual for K7M2 cells to track to the spleen. But under conditions when the experiment works as intended, the cells will then appear in the lungs (either cells trapped in the lungs will grow out or cells growing in the spleen will migrate to the lungs). As noted above, published data state that when the experiment is successful, this should happen within about 2 weeks after a $1x10^6$ cell injection into the tail vein, and within about 3 weeks after a $5x10^5$ cell injection into the tail vein[15,16]. The possible reasons for the unexpected results in this experiment, and observations to support or refute them, include:

1. *Poor cell viability*: this is unlikely. The cells were >99% viable when they were prepared for injection (based on trypan blue exclusion) and viable cells were detectable in the mice for several weeks based on fLuc expression (luciferin conversion).

2. *Aged or senescent cells*: Previous work indicates cells were used for *in vivo* experiments between passages 1 and 10[15,16]. The cells we obtained from NCI, West Virginia University, and Colorado State University did not have information about passage number, so it is impossible for us to know the length of time cells were cultured before we received them. In our hands, cells were only passaged three to five times after thawing before mouse injections.

3. *Poor injection technique with cells exiting the vasculature*: This is possible, albeit unlikely. Two mice did show local growth of tumor cells at the injection site, suggesting at least some cells might have been deposited outside the vein. However, all the mice showed evidence of cells tracking to the spleen (**Figures 8 and 9**), and the fLuc activity was consistent for every mouse in each group with a predictable dose response (**Figure 9**), suggesting that all of the mice received approximately the intended dose of cells into the vasculature.

4. *The cells were rejected by the mouse hosts*: we believe this is the most likely possibility. As described in the results of the microscopic pathology examination above, there was evidence of inflammation in the lungs of the mice, also showing a dose response, and the spleens showed evidence of extramedullary hematopoiesis, or possibly inflammation. In addition, three mice had evidence of micrometastasis, indicating that the cells did have the potential to colonize the lungs. They just did not do so with the expected efficiency or frequency.

While we cannot be certain about the reason why the K7M2 cells might have failed to establish tumors or been rejected by most of the mice in this experiment (both those receiving tail vein injections and those receiving sq injections), there are at least three possible explanations. One explanation is that there are subtle differences in Balb/c mice from different vendors. The tumor microbiome of mice purchased from different vendors has been shown to have important differences that mediate the baseline of inflammation and impact systemic immune responses[17,18]. There are also subtle differences in genetic drift among colonies maintained at different locations and under different husbandry conditions, which, for example, significantly impact susceptibility to conditions such as epilepsy[19]. We obtained our mice from Jackson Labs. Other investigators report obtaining mice from Envigo or from the NCI. Another explanation is that the fLuc transgene can act as a neoantigen in immunocompetent animals, enhancing the likelihood of immune rejection[20,21]. Although this is not a universal phenomenon[22], it seems to be an area of increasing concern among investigators using syngeneic, transplantable cancer models, to the extent that groups have developed mice that are tolerant to the immunodominant epitopes of common reporters such as green fluorescent protein (GFP) and fLuc[23]. Finally, the K7M2 model also has been shown to express high levels of endogenous retrovirus sequences, such as gp70, which may initiate or enhance anti-tumor responses in this model[24].

Based on our experience so far, we have concluded that despite published data, the K7M2 model (and its non-metastatic counterpart, K12) are challenging to work with. Although previous reports describe the models as reliable transplantable tumors in the orthotopic and experimental metastasis (intravenous, or iv) settings[14-16,25], we have had limited success to reproducibly establish these models of tumor growth and metastasis in both of our labs, even as we have tested K12 and K7M2 cells from various different sources. Data regarding the success (or failure) rate for tumor take of these cells are largely unpublished, but other investigators have relayed to us (confidentially) that failure to form tumors is not a rare event in this model. Given the inconsistent performance of the K12 andK7M2 models, we have started working on alternative models to address this milestone.

As noted above, the K12 and K7M2 tumors are syngeneic with Balb/c mice. In addition to their inconsistent growth *in vivo*, immunological reagents for Balb/c mice are more limited than those for other strains, such as C57B/6 (B6), creating yet another obstacle for use of these models. With this in mind, we obtained the F420 and the F331 murine osteosarcoma cell lines from Dr. Jason Yustein (Baylor University; now at Emory University). These cells were derived from tumors isolated from genetically engineered B6 mice, and they grow in syngeneic B6 hosts as local sq tumors as well as in the lungs after intraosseous or iv injection[26]. These tumor models appear to have the advantage of being amenable to genetic modification, while retaining their tumor-forming capacity.

We received cells on February 1, 2022, and so far, we have focused on growing the F420 model. A microsatellite profile (single tandem repeats) was generated for the cells at IDEXX BioResearch, and the cells were shown to be negative for *Mycoplasma sp.* The cells grow reliably *in vitro*, and we have shown that they can be modified to express GFP and fLuc transgenes via lentivirus transduction (approximately 5% efficiency in our initial experiments). We obtained high-titer lentivirus encoding GFP-fLuc to optimize the transduction conditions and sort for GFP-positive cells for *in vivo* inoculation into immunocompetent B6 hosts, but these experiments failed to generate stable transfectants. The F420 model will remain a focus of our experiments to define the effects and optimal combinations of VSV-IFNβ-NIS and ONIx in the mice. Experiments to verify the capability of F420, F331, and MC17 cells to colonize the lungs after intravenous injection are scheduled to begin on October 10, 2023 (date mice are scheduled for delivery), with the actual injections scheduled to be done on October 19, 2023, and the endpoint set 30 days later or earlier, if the mice show clinical signs of disease progression.

Another approach we have taken is to develop the methylcholanthrene-17 (MC17) murine sarcoma model as an alternative to intravenous or sq osteosarcoma models. Our experience with MC17 at the University of Minnesota is described in greater detail below, and we have also now established the MC17 model has now at the Mayo Clinic. Briefly, MC17 tumor cells ($3x10^5$ cells in 100 µl) were implanted subcutaneously in syngeneic C57Bl/6 mice. Tumors formation was efficient and consistent with tumor uptake in ~90% of mice undergoing implantation. Ten days following tumor implantation (tumor volume range ~50-100 mm^3), mice were treated with a single IV dose of 100ul PBS or $5x10^8$ $TCID_{50}$ (~$2x10^{10}$ $TCID_{50}$/kg) VSV-IFNβ-NIS. Mice were closely monitored for acute adverse events including weight loss and deterioration of body condition. Our early results show that systemic VSV therapy was well tolerated with no significant weight loss observed in mice (**Figure 13A**) and resulted in delayed tumor growth (**Figure 13B**). Comparison of tumor burden at 7 days post treatment showed significant inhibition of tumor growth at 7 days post treatment (**Figure 13C**). We have now established the MC17 syngeneic murine sarcoma model in the Naik lab.

MC17 represents a fibrosarcoma, but it provides a reliable model for drug development. Importantly, it is especially recalcitrant to conventional immunotherapy (MC17 is a prototypical “cold tumor”). Yet, MC17 can respond to unconventional immunotherapies. For example, we have developed a molecule called epidermal growth factor (EGF) bispecific angiotoxin (eBAT), which is a polypeptide ligand targeted toxin (LTT) that consists of full-length human epidermal growth factor (EGF) linked to the amino

terminal fragment (ATF) of human urokinase plasminogen-type activator (uPA) and to a *Pseudomonas* exotoxin (PE) that has been genetically modified to enhance its cytotoxicity and reduce its immunogenicity.

As part of our experiments to develop this model, we have shown that the drug, eBAT, has activity against a wide variety of sarcomas, effectively targeting sarcoma stem cells[27-29]. eBAT also kills activated endothelial cells, potentially depleting or normalizing tumor vasculature[30]. But most importantly for this discussion, eBAT remodels the immune and inflammatory TME by targeting uPA receptor (uPAR)-expressing, immunosuppressive myeloid cells, potentially enhancing the immune response against tumors. We tested this premise using MC17 and a uPAR-knockout (KO) derivative of MC17 called D10, and a mouse-specific version of the drug eBAT, called meBAT that incorporates mouse uPA[13]. Anti-mouse uPAR antibodies do not bind to D10 cells, indicating that the CRISPR KO created the desired phenotype. The biding affinity of meBAT to wild type (WT) MC17 cells, as determined by fluorescence intensity and the proportion of bound cells, was higher than that of eBAT, and binding of both eBAT and meBAT was reduced, although not fully abrogated in D10 cells (**Figure 14**). This suggests that eBAT and meBAT can likely bind cells by interacting with either or both uPAR and EGF receptors (EGFR).

Both WT MC17 cells and D10 cells were resistant to eBAT cytotoxicity *in vitro* (**Figure 15**). Both toxins were capable of killing mouse sarcoma cells, as shown by the dose dependent elimination of K7M2 cells. Resistance to bacterial toxins that target protein synthesis has been attributed to loss of the pro-apoptotic BH3-only protein, Bim[31]. But for our purpose, the MC17/D10 model has been exceptionally useful because the resistance to meBAT and eBAT has allowed us to *focus our attention on the impact of these drugs on remodeling the TME* (comparable to our plan with VSV and ONIx). Our data show that uPAR expression is not necessary for tumor formation, as both MC17 and D10 achieved log-growth and generated tumors that reached endpoint (maximum diameter of 1.5 cm or any ill health effects on the mouse host). But uPAR deficiency in the tumor cells retarded their growth *in vivo*: the median time to endpoint was 24 days for MC17 cells and 47 days for D10 cells (**Figure 16** inset). On the other hand, systemic uPAR deficiency in the TME (*i.e.*, germ line uPAR KO hosts) did not impair tumor growth (**Figure 16**).

As is common for sarcomas[32], MC17 tumors attracted large numbers of TAMs into the TME. In this case, we documented infiltration of the tumor by TAMs by immunostaining with the mouse macrophage specific antibody, F4/80 and examined whether eBAT could deplete TAMs by targeting uPARs, which they express in abundance. WT MC17 tumors from WT B6 mice and uPAR-deficient (D10) tumors from uPAR-KO mice were immunostained with the F4/80 antibody. The data indicate that eBAT or meBAT treatment had no effect on TAMs from D10 (uPAR-KO) tumors growing in uPAR-KO mice, whereas they were almost completely ablated in WT MC17 tumors grown in WT B6 mice (**Figure 17**). This shows that macrophage depletion by eBAT was dependent on the expression of uPAR in the tumor and/or in the TME.

To further define the impact of remodeling the MC17 immune landscape, we created uPAR-WT and uPAR-KO bone marrow chimeras (see **Figure 18** for an illustration of the experiment). Engraftment efficiency was approx. 75-85% for both groups, providing WT controls and mice with only hematopoietic (+/- vascular) cells lacking uPARs. Mice were injected with mCherry-labeled MC17 cells and treated with eBAT or meBAT for two consecutive Mon-Wed-Fri cycles. **Figure 19** shows that, despite the fact that MC17 cells are resistant to eBAT and meBAT, both drugs reduced the tumor burden in mice whose hematopoietic cells expressed WT uPAR. The therapeutic benefit was completely ablated in mice whose hematopoietic cells had uPAR knocked out.

Consistent with what we observed in the WT and germline uPAR KO mice, eBAT and meBAT remodeled the myeloid landscape of the MC17 sarcomas. The total numbers of $CD11b^+$ myeloid cells were similar in the WT and uPAR-KO bone marrow recipients. However, TAMs were significantly reduced in mice treated with meBAT (**Figure 20 and Table 2**) and a significant number of $CD11b^+$ cells in the WT bone marrow recipients were also positive for mCherry (**Figure 21**), suggesting these myeloid cells had been reprogrammed from an immunosuppressive phenotype to a pro-immune phenotype and had almost certainly engulfed $mCherry^+$ MC17 tumor cells (doublet conjugate cells would have been excluded by the staining protocol). The increased myeloid cell phagocytosis was not seen in the uPAR-KO bone marrow recipients. This pro-immune myeloid remodeling appeared to be functionally significant: we observed a reproducible increase of $CD3^+$ T cells infiltrating the TME in the WT bone marrow recipients (**Figures 22 and 23**), whereas virtually no T cells were present in the TME of the uPAR-KO bone marrow recipients, and the overall survival time (based on time to a tumor endpoint) was also improved in in the WT bone marrow recipients (**Figure 24**) as compared with the uPAR-KO bone marrow recipients.

Table 2. meBAT Ablates F480+ TAMs.

Group/Treatment	% TAMs in TME (range across all of the tumor)
WT BM/PBS	21.8 (17.7 - 27.7)
WT BM/meBAT	5.1* (1.4 - 19.6)
uPAR-KO BM/PBS	11.4 (7.4 - 21.0)
uPAR-KO BM/meBAT	17.8 (1.6 - 34.1)

WT = wild type; BM = bone marrow; PBS = phosphate buffered saline; KO = knockout. uPAR-KO BM are the chimeric mice with targeted uPAR deficiency in bone marrow cells; *=statistically different from other conditions, with a p value <0.05.

The alterations in myeloid populations induced by eBAT and meBAT were specific to the tumor environment, as *neither depletion nor alterations in phenotypes were observed in peripheral blood from the same mice*. Our preliminary assessments indicate that there were no differences in the number of microvessels (based on CD31 immunostaining in the tumor; **Figure 25 and Table 3**), although we cannot exclude the possibility that eBAT or meBAT influence the distribution of vessels, potentially leading to vascular normalization. Here, we will extend these observations to examine whether eBAT and meBAT normalize tumor vasculature and alter the immune landscape in the TME, and whether these effects enhance infiltration and activity of cytotoxic T cells and NK cells.

Table 3. Microvessel density (%$CD31^+$ cells) in MC17 tumors treated with vehicle or meBAT.

uPAR BM	WT		KO	
Treatment	**PBS**	**meBAT**	**PBS**	**meBAT**
Average percentage of $CD31^+$ cells (SD)	0.940 (0.51)	1.313 (0.20)	1.423 (1.58)	3.864 (0.36)
Range of CD31+ cells across the tumor (%)	0.220-2.75	0.487-3.01	0.078-3.52	1.89-6.51

uPAR-BM refers to the source of bone marrow cells: WT = wild type; KO = uPAR knockout.

Treatment: PBS = phosphate buffered saline; meBAT (2 cycles of 50 µg/kg).

In the interim, while the MC17 model was being developed to Mayo Clinic, Dr. Naik carried out a pilot study in the well-established A20 murine lymphoma model to confirm the safety of combination VSV and P-DIC combination therapy. This was done concurrently with the tolerability experiment described in **Figure 5**. The results show that mice that received both VSV and combination therapy had transient tumor remissions (including formation of scabs on the tumor site), with a significant survival benefit compared to PBS treatment (**Figure 26**). These data support further analysis of this combination therapy in relevant murine sarcoma models.

Milestone: Complete necropsies. Ongoing.
Dr. Modiano, Ms. Schulte, and Dr. Kim performed necropsies for the experiments using MC17 at the University of Minnesota. As described above, Dr. Modiano and the lab staff completed necropsies on the mice inoculated with K7M2-fLuc cells and with K12 cells. Necropsies will continue to be performed for all experimental animals.

Dr. Naik is developing this aspect of the project as described above and in the Milestones for Aim 2.

Milestone: Data analysis; organization and conclusions. Ongoing.
The project investigators have been holding regular meetings to update the status of the project.

Milestone: Quality control and quality assurance for data – manuscript preparation and submission. Ongoing.
QC and QA for data are performed on a continuous basis. We have presented the MC17 data at national and international meetings. A draft manuscript describing the eBAT mechanisms of action data described in this report is under review by the coauthors and is planned for submission before the end of 2023, as is a manuscript describing the toxicology of eBAT. We will continue to accrue data for the osteosarcoma experiments and consider publication of a manuscript if we can form a consensus around publication of negative data from the K12/K7M2 model.

Specific Aim 2: Define immunological effects and mechanism of action for combination VSV IFNβ-NIS and P-DIC (ONIx)

Milestone: Assessment of immune response induced by VSV-IFNβ-NIS and P-DIC in mice with metastatic osteosarcoma. Ongoing.

Milestone: Assessment of immune response induced by VSV-IFNβ-NIS and P-DIC in mice with metastatic osteosarcoma. Ongoing.

Pilot data were generated for this milestone, which were highly informative. The effect of VSV and ONIx combination therapy in murine tumors especially on the immune landscape has not been previously established.

To fill this gap in knowledge, Dr. Naik's group initially conducted two pilot studies: the first to establish murine sarcoma models in the lab and the second to perform a detailed immune assessment of VSV and ONIx combination therapy in the well-established A20 murine lymphoma model.

To establish sarcoma models in the lab, we initially did a pilot study by implanting $5x10^6$ K7M2 osteosarcoma cells (from NCI) sq in syngeneic Balb/c mice. Tumor growth was quite slow in this model with only 50% of mice developing tumors (N=4). Tumor bearing mice were treated with PBS or $1x10^8$ $TCID_{50}$ VSV (per mouse) given intravenously. Mice were sacrificed on study day 4 to optimize methods to measure intra-tumoral immune infiltration and antitumor immunity.

Preliminary assessment of CD8 T-cells and macrophages in peripheral blood mononuclear cells (PBMCs), spleen and tumor (**Figure 27**) show *(a)* a notable increase of CD8 T-cells in PBMCs but not in tumor and spleen; and *(b)* an increase in macrophages in PBMCs, spleen, and tumor. Additional and larger experiments will be needed to confirm these findings. Addition of checkpoint inhibition dually targeted to macrophages (CD47) and T-cells (PD-1), *i.e.*, ONIx, may potently activate antitumor responses mediated by these immune cell populations. PD-1 expression was increased on CD4 and CD8 T-cells in the blood and spleen (**Figure 28**) suggesting addition of a PD-1 inhibitor, *i.e.*, ONIx, would be a potent activator of antitumor immune responses. We have also established the MC17 murine sarcoma model in Dr. Naik's lab and have conducted a pilot study demonstrating that single dose systemic VSV therapy was safe and delayed tumor growth in this model (**Figure 13**).

A detailed assessment of the efficacy of combination therapy with VSV and either ONIx or PD-1 inhibitor in the A20 tumor model was carried out: A20 tumor bearing mice were treated with PBS, VSV, or combination therapy VSV + ONIx or VSV + αPD-1. In this study, a higher dose of VSV was utilized and toxicity was observed following systemic VSV administration. Most of the mice that received systemic VSV monotherapy were euthanized due to excessive weight loss. Interestingly combining systemic VSV therapy with either ONIx or an αPD-1 antibody had reduced toxicity and most mice recovered following transient weight loss. These data suggest that addition of CPI can mitigate potential toxicity of oncolytic virotherapy, and they show that combination therapy with both VSV + ONIx and VSV + αPD-1 induce durable tumor remission in a subset of tumor bearing mice (**Figure 29**) compared to rapidly growing tumors in the majority of PBS treated mice (though there was spontaneous tumor remission observed in some PBS treated mice). Near the end of the study, mice were euthanized and splenocytes were analyzed by ELISPOT assay to detect immune responses against PHA (positive control), VSV antigen, and MHC-I specific tumor associated AH1 antigen[33]. These data indicate show that VSV treatment increases overall activated T-cell responses, VSV specific T-cell responses, and detectable responses against the AH1 tumor associated antigen (**Figure 29**). VSV and tumor specific T-cell responses were generally higher in mice that had complete response to combination therapy compared to mice that did not respond, suggesting that development of virus and tumor specific T-cell responses may correlate with therapeutic response.

Milestone: Data analysis; organization and conclusions. Ongoing.
Emerging data support the hypothesis of synergy between VSV-IFNβ-NIS and ONIx. Data analysis is ongoing in real time and the investigators meet regularly to discuss data, reach consensus for the conclusions, and decide on next steps for experiments and reporting.

Milestone: Quality control and quality assurance for data – manuscript preparation and submission. Ongoing.
QC and QA for data are performed on a continuous basis in real time.

Specific Aim 3: Characterize safety, efficacy, and immunomodulatory effects of VSV-IFNβ- NIS and P-DIC (ONIx) in dogs with naturally occurring metastatic osteosarcoma

Milestone: Production of in vivo grade VSV-IFNβ-NIS. Completed.
Please see milestones for specific aim 1. A new batch of *in vivo* grade VSV-IFNβ-NIS for the canine clinical trial was produced by the Mayo Clinic investigators.

Milestone: Production of *in vivo* grade P-DIC (ONIx). Completed.
Please see milestones for specific aim 1. Release assays for sterility and potency have been completed and assays for stability are scheduled semiannually throughout the project period. This milestone was accelerated and ONIx was produced in a single batch, which should be sufficient to assess if there is

a biological effect at 2 mg/kg dose after VSV administration. Our second batch of ONIx, however, will provide sufficient drug for dose escalation if enough dogs are enrolled and if escalation is warranted.

Milestone: Identify safe dose to guide clinical development. Ongoing.
The mouse experiments shown as part of Aims 1 and 2 show that ONIx at a dose of 5 mg/kg is safe in mice. This dose equivalent might be higher than the maximal dose we will be able to administer to dogs, as the dose required to achieve a therapeutic effect might be no higher than 1-2 mg/kg (1/6 of the effective mouse dose).

Milestone: Assessment of immune response induced by VSV-IFNβ-NIS and P-DIC (ONIx) in dogs with metastatic osteosarcoma.

The study parameters were extensively reviewed, and the METEOR (metastatic experimental osteosarcoma research) study opened in August of 2022. A Data Safety Monitoring Board comprised by Dr. Antonella Borgatti (board certified veterinary oncologist and Director of the Clinical Investigation Center of the University of Minnesota College of Veterinary Medicine), Dr. Michael Conzemius (board certified veterinary surgeon and former Director of the Clinical Investigation Center of the University of Minnesota College of Veterinary Medicine), and Dr. Aaron Rendahl (biostatistician) has been assembled to oversee the canine clinical study and ensure safety criteria are rigorously followed.

The enrollment web page and study details are available at z.umn.edu/meteor. The first eligible dog whose owners applied for the study was screened on the week of September 5, 2022. The dog was a 1.75 years-old spayed female spaniel that was diagnosed with a primary osteosarcoma of the left distal femur on May 3, 2022 (**Figure 30**). The family decided to pursue standard of care (amputation followed by adjuvant chemotherapy). The dog's affected limb was amputated on May 12, 2022, and adjuvant chemotherapy was started with carboplatin (300mg/m^2) three weeks later on June 2, 2022, with the intent to administer between four and six cycles once every three weeks. On the same date when the initial chemotherapy was administered, two pulmonary nodules were visible radiographically, although they did not meet the complete criteria for definitive diagnosis of metastatic disease. A second dose of carboplatin was administered on June 23, 2022. Mild lymphocytosis and eosinophilia were the only abnormalities noted in the laboratory testing done on that date. On July 14, 2022, the dog had neutropenia, so chemotherapy was delayed. Imaging showed evidence of progressive disease (increased size of the pulmonary nodules), so the chemotherapy protocol was switched to doxorubicin (30 mg/m^2), with the intent to administer between four and six cycles once every three weeks. The neutropenia had resolved by July 21, 2022, which allowed for the first dose of doxorubicin to be administered. A second dose was given on August 4, 2022, but by August 18, 2022, there was evidence of further disease progression (**Figure 30**) and chemotherapy was discontinued. The family was given options to discontinue treatment and switch to palliative care, begin an experimental rescue protocol using Losartan and toceranib (+/- propranolol), or screen for eligibility for the METEOR study. They elected the latter.

The dog completed screening for METEOR on September 6, 2022, and was deemed to be eligible to enroll. The dog was hospitalized on July 12 and released from the hospital and back to the family on September 16, 2022. Two consecutive doses of VSV-cIFNβ-NIS ($5x10^9$ $TCID_{50}$/kg) were administered on September 12 and 13, 2022. A mild (not clinically significant) decrease in platelet count and a mild (not clinically significant) increase in circulating levels of fibrinogen were noted on September 14, 2022, about 24 hours after the second dose of VSV-cIFNβ-NIS. Given that these laboratory changes were deemed to be non-clinically significant, the first dose of ONIx (2 mg/kg) was administered on September 14, 2022, as per the protocol. On September 15, 2022, the dog showed grade-1, gastrointestinal adverse events (inappetence and vomiting). The signs were managed medically and a second dose of ONIx was given on September 16, 2022. Laboratory testing revealed recovery of platelets and fibrinogen back to baseline levels and a slight decrease in red cell mass, probably attributable to the

blood obtained for laboratory sampling over the experimental treatment period. It should be noted that the dog was not anemic. The dog was discharged on September 16, 2022, and returned on September 19, 2022, to receive a third dose of ONIx in the outpatient setting. Laboratory testing showed that all hematology and serum biochemistry values were within the specified reference ranges for the clinical laboratory, with resolution of all prior mild abnormalities. The family reported that the dog had persistent inappetence and nausea (determined to remain as a grade-1 adverse event), although without vomiting. These gastrointestinal signs continued to be managed medically and the dog improved and resumed eating. The dog showed signs of disease progression and was humanely euthanized on day 47 after initiating therapy. A five-week survival time is comparable to the expected survival time for dogs with metastatic osteosarcoma that receive rescue therapies. More dogs will need to be treated to determine efficacy; however, the side effects were much milder than what would be expected with treatment using cytotoxic chemotherapy. Therefore, even if this provided equivalent efficacy, it might still provide an alternative to manage patients with advanced disease.

Blood, serum, urine, and feces obtained prior to and during the 24 hours after VSV administration were banked for viral shedding and VSV pharmacokinetic studies. Serum samples obtained prior to any treatment, after VSV, and for the first hour after ONIx were also banked for ONIx pharmacokinetic studies. PBMCs for immunological analysis were collected at time points before treatment and after the administration of the test articles. This will be repeated for all enrolled dogs. If three dogs complete the study without severe adverse events attributable to ONIx, we will consider a dose escalation.

In humans receiving PD-1/PD-L1 immune checkpoint inhibition therapy, the gastrointestinal system is one of the most commonly affected organ systems and is responsible for the most frequent emergency visits resulting from immune-related adverse events[34], so the observed adverse gastrointestinal events in this dog were not unexpected. Mild (grade-1 and grade-2) gastrointestinal adverse events, including diarrhea, nausea, vomiting, constipation, and dyspepsia were also observed in clinical trials of CD47 blockade[35], so the signs in this first dog treated by ONIx could be due to either the effects of PD-1 blockade, CD47 blockade, or both. Optimistically, the observed, mild gastrointestinal toxicity suggests that ONIx is indeed biologically active at the dose given.

Since the METEOR study opened and started enrolling dog patients, we followed 29 dogs with osteosarcoma treated at the University of Minnesota that would qualify based on the diagnosis and treatment to offer entry into the study. Many of these dogs have remained in remission (so they are not eligible), and others either succumbed to their disease before they could enroll in the study, or the owners declined participation.

We also had approximately 14 inquiries regarding dogs treated elsewhere (not at the University of Minnesota). Two dogs were eligible and were screened. One was enrolled and completed participation (described above). The other dog showed progression and was humanely euthanized before it could receive treatment. The remaining dogs were not eligible to enroll (outside the weight limit, had not developed metastatic disease, etc.) We had a new external inquiry this week and the dog meets the criteria, so we plan on screening. The enrollment for the study lagged behind our expectations (we normally expect approximately 20-25% enrollment, whereas here we had 1 of 40, or 2.5%). So, to accelerate enrollment we expanded the eligibility to allow inoperable/metastatic sarcomas, otherwise using the same criteria as before.

As of the date of this report, we have had a total of 61 contacts from owners that had interest in the study. Most of the new contacts have been from owners of dogs with other metastatic sarcomas (chondrosarcoma, fibrosarcoma, hemangiosarcoma). None of the dogs have enrolled, for some of the same reasons stated above, and also because owners have been reluctant to hospitalize their dog for 4 days. The hospitalization requirement is due to an abundance of caution from the Minnesota State Veterinarian, making sure that the potential for any shed VSV to infect a susceptible farm animal (horse,

cow, pig, goat, sheep) is minimized. We agree this is reasonable and will continue to work within these parameters to identify eligible dogs. In terms of its potential translation to humans, VSV is currently administered in the outpatient setting (in clinical trials), and we don't anticipate hospitalization would be a barrier.

Nevertheless, we have devised an alternative to understand how VSV and ONIx might synergize to activate the immune system to fight tumors. We have taken advantage of our previous VIGOR study, where 22 dogs with primary osteosarcoma received VSV in the neoadjuvant setting, and for which we have stored cell lines and PBMCs collected prior to and after VSV treatment. We are using those samples to understand if and how VSV might prime tumor and immune cells to alter their biological behavior through *in vitro* assays.

The plan is to perform assays for transposase-accessible chromatin using sequencing (ATAC-seq) to evaluate regions of accessible (open) and inaccessible (closed) chromatin and RNA sequencing (RNAseq) to evaluate the relationship of chromatin states to the transcriptome in osteosarcoma cell lines cultured in conventional 2-dimensional plastic dishes and in 3-dimensional matrix, which might simulate the conditions in the actual tumor. We will perform the same assays in PBMCs from the same dogs that were used to derive the cell lines, both in PBMCs collected from prior to VSV treatment and 7 days after VSV treatment. The PBMCs will undergo stimulation *in vitro* using P/I (for maximal stimulation as a positive control), ONIx, and P/I + ONIx. **Figure 31** shows a schematic description of these experiments. We are providing data for the initial pilot experiments done in five well-characterized osteosarcoma cell lines and in three samples of PBMCs obtained from normal, healthy dogs to develop the methodology.

Osteosarcoma cell lines OSCA-8, OSCA-32, OSCA-40, OSCA-71, and OSCA-78 were cultured as described above; cells were collected after three days in culture and dry pellets were stored at -20°C for DNA extraction as recommended by the protocols from the supplier. PBMCs were cultured in suspension media without further stimulation or stimulated using P/I. At the end of a 3-day culture period, cells were sorted into unstimulated, naïve ($CD44^{dim}/CD62L^{bright}$) CD4 and CD8 cells and activated ($CD44^{bright}/CD62L^{dim}$) CD4 and CD8 cells using antibody labeling and a flow activated cell sorter (**Figure 32**). Dry pellets from the sorted cells were similarly stored at -20°C for DNA extraction as recommended by the protocols from the supplier. One of the PBMC samples only yielded enough stimulated CD8 cells to include in the downstream procedures and analyses.

DNA extraction and ATAC-seq proceeded according to the supplier's protocols through the University of Minnesota Genomics Center (UMGC). The ATAC-seq data passed all the QC metrics for release. Sequences were mapped to CanFam6.0 (Ensembl), with alignment, per sample peak calling, QC, and group level consensus peaks called using the PEPATAC pipeline. For consensus peak generation, the pipeline performs the following steps: 1. Overlapping peaks are identified among all the project samples. 2. For each set of overlapping peaks, the consensus peak's coordinates are defined as the coordinates of the peak with the maximum score among the set of overlapping peaks. 3. Any peaks that extend beyond chromosomes are trimmed. 4. Peaks present in ≥ 2 samples, with scores ≥1, are retained. Consensus peaks were called using all CD4 and CD8 T-cell samples as a group and all osteosarcoma samples as a group. The individual peak sets were used for differential accessibility (DA) analysis. The Csaw pipeline was used to generate counts for each peak region for each sample and the DESeq pipeline was used for count normalization and DA analysis.

Figure 33 shows principal component analysis (PCA) for CD4 (n=4) and CD8 (n=5) sorted T-cell samples. The samples are labeled as unstimulated ($CD44^{dim}/CD62L^{bright}$) CD4 and CD8 cells and as stimulated ($CD44^{bright}/CD62L^{dim}$) CD4 and CD8 cells. The strongest difference between samples was whether or not they were stimulated (PC1 accounting for approx. 76% of the variance). **Figure 33** also shows PCA analysis for 5 osteosarcoma cells lines. Four of the cell lines generated data from paired

(2-dimensional and 3-dimensional) cultures. The OSCA-32 cell line did not grow in 3-dimensional cultures and only data from the 2-dimensional cultures is shown. For these cells, the strongest difference was the culture condition, although the impact was much smaller than what was observed by T-cell stimulation (PC1 accounting for approx. 58% of the variance).

Figure 34 shows volcano plots to identify differentially expressed genes in the T-cell sample groups. DA regions were identified from the T- cell consensus peaks and showed significant differences between unstimulated CD4 (open chromatin regions de-enriched, or to the negative $\log_2$ scale in the X-axis of the figure) and CD8 T-cells (open chromatin regions enriched, or to the positive $\log_2$ scale in the X-axis of the figure). The data provide additional confidence in the quality, as the open chromatin regions in CD4 and CD8 cells are consistent include genes that would be expected to be differentially expressed in these cell types. The peaks were mapped based on the closest protein coding gene to assign gene name labels. Any region where the closest genes were predicted transcripts (vs. known protein-coding genes), *i.e.*, identified as ENSCAFXXXX, were excluded from the labels. The red and green colors represent variance in the $\log_2$ expression levels along a scale of ± 3 (X-axis). The red and blue colors represent a false discovery rate (FDR) <0.05 as a cutoff for significance (Y-axis).

Somewhat surprisingly, ATAC-seq showed virtually no differential enrichment of open chromatin states between stimulated CD4 and CD8 cells (**Figure 34**). This does not mean there are no differences. It simply means that the differences are overwhelmed by the similarity of enriched open chromatin regions near genes that control proliferation, differentiation (to effector and memory cells), and survival. This can be readily appreciated in the bottom two panels of **Figure 34**, which show volcano plots for unstimulated vs. stimulated CD4 and CD8 cells. While there are some minor differences, it is readily apparent that most of the enriched and de-enriched open chromatin regions are conserved between both cell types. This suggests that, at least at this level of resolution, we might be able to infer the presence of unstimulated or resting CD4 cells and CD8 cells in bulk ATAC-seq analysis of osteosarcomas, but we would need deeper sequencing in order to be able to confidently infer the presence of activated CD4 cells vs. activated CD8 cells in the same samples.

We applied the same methods to analyze DA chromatin regions for the osteosarcoma cells. As was seen in the PCA analysis above, **Figure 35** shows that the magnitude of difference between the osteosarcoma cells cultured under different conditions was smaller than what we observed in unstimulated vs. stimulated T-cells. In this case, we relaxed the stringency to identify significant peaks, so the red and green colors represent variance in the $\log_2$ expression levels along a scale of ± 2 (X-axis), while the red and blue colors still represent a false discovery rate (FDR) <0.05 as a cutoff for significance (Y-axis). Results of gene set enrichment analysis (GSEA) for the osteosarcoma cells cultured under different conditions showed that transcriptional programs that regulate metastasis, “cancer”, cell cycle, and resistance to chemotherapy were among those that were enriched in the hydrogel cultures. This suggests that ATAC-seq is sufficiently sensitive to segregate among different cancer cell behaviors, and we should be able to establish if and how VSV might have impacted the tumors using bulk sequence analyses. The experiments using the VIGOR trial samples are in progress and we expect data will be available before the end of this final no-cost extension period.

Additional experiments that were supported by this project, which are related to our overall objectives, although not explicitly stated in the specific aims, are described in detail below under the heading, “Other Related Work”.

Milestone: Data analysis; organization and conclusions. This is ongoing, as described above.

Milestone: Quality control and quality assurance for data – manuscript preparation and submission. This is ongoing, as described above. The manuscript for the VIGOR clinical trial is now accepted for publication in the journal *Molecular Therapy – Oncolytics*. The data shown below regarding repression

of PTEN in canine and human osteosarcoma are published in the journal *Cancer Genetics*. The data describing the eBAT mechanisms of action in sarcomas and the safety profile of the drug in pre-clinical settings are in the last stages of author review for submission.

Milestone: Planning for pediatric clinical trial planning (translation to humans). Ongoing.

At Mayo Clinic, Dr. Naik and Dr. Steven Robinson, a medical oncologist with a focus on sarcoma treatment have worked together to develop a clinical trial outline to evaluate systemic oncolytic VSV therapy in combination with checkpoint blockade to be given in the neoadjuvant setting in sarcoma patients scheduled to undergo metastatectomy. Drs. Robinson and Naik have recruited a team including surgery fellow, Dr. Jack Sample, and undergraduate research fellow, Coryn Ferguson, to collate data from patients with sarcoma undergoing pulmonary metastatectomy at Mayo Clinic between 2008-2018. This analysis will yield information on this patient population receiving treatment at Mayo including number of patients, subsequent treatments, and clinical outcomes.

At the University of Minnesota, Dr. Modiano has initiated discussions with Drs. Brenda Weigel, Emily Greengard, and Andrea Espejo-Freire to develop plans for translating this therapy into adult patients as well as children and AYAs with osteosarcoma and/or other sarcomas. The sarcoma teams from Mayo Clinic and the University of Minnesota are developing plans to introduce trials using combinations of oncolytic virotherapy and immune checkpoint blockade to patients.

- **Other related work**

In addition to the work described here, the COVID-19-related laboratory closures gave us the opportunity to make progress on various other related fronts that are highly pertinent to this project.

First, being confined to working from home provided an opportunity to refine our understanding of how spontaneous canine cancers should be used in the context of "models" for human disease. In particular, we know that there are important similarities in the biology and natural history of osteosarcoma in humans and dogs[36], but we wished to address the persistent questions regarding the major difference in age of susceptibility for osteosarcoma in humans, where the age distribution is bimodal with the major peak in adolescence, and in dogs, where the age distribution is also bimodal but has its major peak in older adults.

These efforts culminated in a peer reviewed publication (perspective) in the journal *Aging and Cancer*[37], where we propose that the excess cancer risk seen in humans and in domestic dogs is driven in large part by the technological gains that have extended lifespans beyond the evolutionarily adapted limits for both species. Notably, this has only happened in humans and in dogs (to a lesser extent, perhaps, in domestic cats and in pet/laboratory mice bred and kept in captivity), and suggests that, even as the relative frequency of tumor types diagnosed in humans and dogs is different, the overall lifetime risk of cancer is comparable because both species exceed their evolutionarily adapted cancer protective mechanisms. **A copy of the manuscript is included as an appendix**.

It follows from this perspective that causality of osteosarcoma might be different for pediatric human cases where the major influence seems to come from genetic predisposition (*i.e.*, syndromic) or from a confluence of rare, random events leading to malignancy[38] and for older canine cases where the major influence is from risk associated with aging. As such, human pediatric osteosarcoma and canine osteosarcoma could be considered convergent (rather than homologous) diseases with potentially different causation but comparable tissue organization. We have followed this line of investigation with additional experiments using whole exome sequencing analysis, whole transcriptome sequencing analysis, and methylome analysis. Some of these experiments were supported <u>in part</u> by DOD grant CA170218 (*i.e.*, methylome sequencing), and by DOD grant CA190276, which is the subject of this

report (*i.e.*, whole transcriptome sequencing for one of the canine osteosarcoma cohorts used as a comparison in the *Molecular Therapy* manuscript). In addition to our previously published work in this field[1,39,40], we are preparing additional manuscripts from these data, which will be forwarded to our program officers once they are published in the peer reviewed literature and/or deposited in pre-print servers. One such manuscript shows results from our parallel analysis of the mutational landscapes of canine and human osteosarcoma. The data indicate that there are some conserved events in both species, but these are immersed among many critical differences of the genes that undergo recurrent mutation, copy number gains, and copy number losses. One of the most significant differences was the distribution of COSMIC signature imprints, suggesting that distinct mechanisms are responsible for creating the mutational landscape and the genomic chaos in osteosarcoma from both species (**Figure 36**).

Another manuscript describing different mechanisms through which the *PTEN* gene is inactivated in canine and human osteosarcoma is published and the data described herein can be found in the original manuscript, **included as an appendix to this report**)[41]. The data show that in dogs, the genomic localization of the *PTEN* gene near the distal terminus of the q arm of canine chromosome 26 (CFA26) appears to create a unique vulnerability under conditions of genomic instability. So, in canine osteosarcoma, which is characterized by loss of function of *TP53* and genomic chaos, *PTEN* seems to be recurrently deleted, and the transcript levels (and hence, presumably, the functional protein) are directly related to the *PTEN* copy number in the tumors. In humans, however, the *PTEN* locus is located near the middle of chromosome 10. This region seems to be less susceptible to deletion; and yet, *PTEN* transcripts in human osteosarcomas seem to be universally silenced, independent of their stable copy number status. We found that a portion of the *PTEN* promoter that seems to be required for inducible expression of the gene is heavily methylated in virtually all of the human osteosarcomas analyzed, leading to silencing and loss of inducibility. Thus, *PTEN* loss seems to favor development of aggressive osteosarcomas in dogs, whereas *PTEN* silencing by methylation seems to be almost a requisite event for the development or progression of osteosarcomas in humans. We conclude from these data that *PTEN* inactivation is achieved as a terminal event in both canine and human osteosarcomas. But this occurs via independent mechanisms, and it is not shared by all of the tumors. That is, more than half of canine osteosarcomas retain one, and more often two copies of the *PTEN* gene, and the gene is expressed robustly in those tumors.

Knowing this, we would argue that canine osteosarcoma is not a good model, for example, to test strategies that reverse *PTEN* methylation, and more generally to study risk, susceptibility, or causation of human osteosarcoma, or even to test therapies targeted at certain mutations or genome abnormalities that might be present in one species, but not the other. On the other hand, the observation that transcriptional programs, global patterns of methylation, and inferred cellular distribution are conserved across species[1,39] suggests that canine osteosarcoma may be a very suitable “model” to study how disrupting the organization of the tumor tissue by attacking the tumor microenvironment could improve outcomes. This is especially relevant to this project.

One intriguing finding in this study was that the gene encoding the Fas death receptor (*FAS* or CD95) is closely linked to *PTEN* in both species. We previously showed that neoadjuvant therapy using a non-replicating adenovirus encoding Fas ligand stimulated antitumor immunity in dogs, but only when the malignant tumor cells themselves did not express Fas (*i.e.* when Fas expression was confined to cells in the tumor microenvironment)[4]. Like *PTEN*, copy number loss of *FAS* in dogs was associated with decreased expression in the tumors, making this therapy appropriate for only a subset of the dogs. In humans, *FAS* seems to be silenced by methylation, so the adenovirus-Fas ligand therapy would have had much greater potential benefit.

We are complementing these experiments using single cell sequencing and spatial genomics of canine and human osteosarcomas, which will further refine our understanding of the tumor microenvironment and highlight opportunities to address this disease using immunomodulation.

We have also continued to analyze data from our previously completed VSV clinical trial in dogs with naïve osteosarcoma (the VIGOR study; **a copy of the accepted manuscript is attached as an appendix to this report**). The data described herein can be found in the original included manuscript[6]. The summary that follows includes the most recent work, which was done in part during the COVID shutdown while the PI and staff salaries were supported in part by this grant, and which is especially pertinent to this project.

We evaluated event free survival (EFS) and overall survival from dogs in the VIGOR study and compared them to two contemporary cohorts of dogs with appendicular osteosarcoma with no evidence of metastasis. The first cohort (n = 57) included dogs seen at the U of M Veterinary Medical Center (VMC) between July 2011 and July 2018, where there was intent to treat with standard-of-care surgery and adjuvant carboplatin chemotherapy, and that had a successful limb amputation and completed at least one cycle of adjuvant chemotherapy. The second control cohort was from a study recently published by the National Cancer Institute's Comparative Oncology Trials Consortium (COTC). This cohort included 157 dogs with primary appendicular, non-metastatic osteosarcoma enrolled between November 2015 and February 2018 that were treated with standard-of-care surgery and adjuvant carboplatin chemotherapy[42]. The COTC cohort was made available as a control dataset for evaluation of novel neoadjuvant or adjuvant treatments for osteosarcoma.

Overall survival for dogs showed a "tail" of long-term survivors, including 4 dogs that were still alive at the time of this report. Three dogs were excluded from survival analysis: two dogs that were eventually diagnosed with an indication other than osteosarcoma (one rhabdomyosarcoma of bone and one hemangiosarcoma of bone) and one dog that died immediately after surgery due to hypovolemic shock, yielding a cohort of 20 evaluable VSV-cIFNβ-NIS treated dogs. When compared to the control cohorts, neoadjuvant VSV-cIFNβ-NIS therapy did not significantly improve EFS or overall survival, but importantly it did not worsen survival outcomes. We analyzed long-term survivorship of evaluable VSV-cIFNβ-NIS treated dogs by tabulating the proportion of dogs with survival that exceeded the 75th percentile value of the COTC cohorts (479 days). In this analysis, the VMC cohort showed that 26% of dogs exceeded the overall survival benchmark of 479 days, virtually identical to the proportion of dogs in the COTC cohort. In contrast, the VIGOR study cohort had a higher-than-expected proportion of long-term survivors, with 35% of dogs exceeding the benchmark of 479 days). This potential efficacy signal was intriguing and noteworthy, although the sample size was insufficient to predict with high certainty whether this finding will be reproducible in a larger sample set.

To begin to establish a mechanism for this response, we completed next generation RNA sequencing for tumor samples from dogs in the VIGOR study. Tumor biopsies were obtained from dogs prior to treatment and 10 days after administration of neoadjuvant VSV (at the time of amputation and prior to chemotherapy. mRNA was extracted from the biopsies and subjected to next-generation RNA sequencing. Tumor samples for sequencing were not available for dogs in either of the clinical control cohorts, but they were available for a fourth independent cohort of dogs, obtained from the Canine Comparative Oncology and Genomics Consortium, Inc. (CCOGC). Dogs from the CCOGC cohort were selected based on having received standard of care therapy (amputation plus adjuvant chemotherapy) with relevant survival metadata. The overall survival for dogs in this group was comparable to that of the two control cohorts (VMC and COTC). Sample processing and next-generation RNA sequencing for this group were supported, in part, with funds from this project.

We looked for evidence of an immune component in the tumor response using the gene cluster expression summary score (GCESS) method to summarize co-regulated gene clusters in tumor

samples and their association with outcome[1]. Pre- and post-treatment samples from primary osteosarcoma and metastatic osteosarcoma tumors segregated together, separate from both the cell lines derived from the pre-treatment tumors as well as from normal skin biopsy samples obtained from the same dogs at the time of amputation. This suggested that the composition of the microenvironment was a stronger driver of clustering than any traits associated with malignant transformation. Fourteen gene clusters were identified and were apparent in unsupervised hierarchical clustering heatmaps, including the immune and cell cycle gene clusters previously identified in canine and human osteosarcoma[1]. The distribution of cell cycle and immune GCESS across tumor samples, cell lines, and skin biopsy samples was predictable, with no immune transcripts identified in the osteosarcoma cell lines. VSV treatment did not significantly impact the GCESS score of pre- versus post-treatment tumor specimens.

When we analyzed the association between GCESS and survival, we observed that the dogs with the highest CD8-related immune GCESS had longer survival times. This relationship was not observed for the CD37-positive monocyte-related GCESS, and somewhat surprisingly, it was also not evident for the cell cycle GCESS. To assess whether neoadjuvant VSV was associated with the improved survival of dogs with higher CD-8 positive GCESS scores, we examined the relationship between GCESS and survival in the 23 dogs from the CCOGC cohort. When comparing the VIGOR study dogs and the CCOGC cohorts, we noted that a higher immune GCESS was associated with a longer survival in both groups, but the effect was larger in the VSV-treated group. Specifically, all the dogs with longer survival had higher CD8 GCESS, but not all the dogs with higher CD8 GCESS had longer survival in the CCOGC group, whereas in the VIGOR group, all of the dogs with higher CD8 GCESS had longer survival.

Our efforts in single cell sequencing and spatial genomics experiments have yielded data that will allow us to create single cell atlases for circulating canine leukocytes, for canine tumor cell diversity, and for infiltrating immune cells in tumors, as well as information to integrate these data into the correct spatial localization of tumors which will improve our immunotherapy applications.

We collected samples from six dogs with primary osteosarcoma, henceforth referred to as OS tissues and three samples from short term cultures of osteosarcoma cells, henceforth referred to as OS cells, to understand the heterogeneity of tumor cells depleted of stroma. We have also collected three samples of canine peripheral blood leukocytes, henceforth referred to as WBCs, and aggregated data from three additional samples originating from canine spleens: one hemangiosarcoma, one histiocytic sarcoma, and one sample of reactive canine spleen adjacent to a region of complex nodular hyperplasia/stromal sarcoma. All have been processed for single cell RNA sequencing on the 10X Genomics Chromium platform. Sequencing data are pending for the three most recent osteosarcoma samples from disaggregated fresh tumors, which are undergoing quality control metrics or are in the sequencing queue. Gene expression data have been remapped to CanFam6 (Tasha-Boxer), which is the latest canine genome assembly available in Ensembl. The results are consistent with data mapped to all other available canine genome builds, except CanFam6 is more extensively annotated. The samples included in the analyses for this report are listed in **Table 4** below.

The analyses shown below are preliminary interpretations from the extensive datasets we have gathered. We have followed standard methods and also developed new methods to filter low quality data from the single cell sequencing samples, including steps for removing data from dead or dying cells and from events capturing two (or more) cells in a single drop. Eliminating duplicates is especially critical to develop a robust atlas of expression that includes specific transcripts associated with individual cells with the least amount of noise in the data. For example, this would avoid assigning transcripts of a capture that included a CD8 T-cell and a neutrophil in the analysis, as this would create ambiguity in the assignment of genes expressed to both lineages.

Table 4. Samples Included in the Analysis

Sample Source	ID
OS Tissue*	DOS-2101 DOS-2301 DOS-2302
OS Cells	DOS-075 DOS-110 DOS-0952
WBCs	WBC-1 (Dog_1_YP) WBC-2 (141517) WBC-3 (1832517)
Spleen Tissues Splenic hemangiosarcoma Splenic histiocytic sarcoma Normal spleen adjacent to splenic stromal sarcoma	 DHSA-2101 DHSA-2102 DHSA-2104
*Data from OS tissue sample DOS-2304 are available and undergoing QC; cells from OS tissue samples DOS-2305 and DOS-2308 have been processed and are in the sequencing queue.	

Dead and dying cells accounted for a very small proportion of the populations in the white blood cell samples, as these were processed immediately and with minimal manipulations (RBC lysis). Dead and dying cells accounted for greater proportion of cells in the cryopreserved tumor samples and the freshly processed tumor samples, as these required extensive manipulation (recovery of the surgical sample, processing in the pathology laboratory, storage at 4°C, and finally, enzymatic digestion and mechanical disruption to recover cells from the tissue stroma). Duplicate cell captures were consistent with the predictions from 10X Genomics, and they were proportional to the total number of events captured. An example of the data from the three canine leukocyte samples using these quality control metrics is shown in **Figure 37**.

Figure 38 illustrates a newly developed method to exclude dead and dying cells. The distribution of transcript abundance and gene abundance in live cells from WBC (n=3), OS cells (n=3), OS tissues (n=3), and splenic samples (n=3) are included to show that the distributions follow predictable patterns after cells where low numbers of expressed genes (approx. <200) are excluded.

We aggregated the data from the samples shown in **Figure 38** and visualized them using K-means clustering (n=20) on a UMAP plot (**Figure 39)**. The number of clusters for this analysis was determined somewhat arbitrarily to provide a reasonable depth of resolution of unique cell types, and it appears to provide a reasonable starting point as shown in the additional figures below.

We next examined the composition of individual groups of samples that comprised the aggregate UMAP plot. **Figure 40A** represents the three WBC samples. As we would have predicted, and as could be inferred from the data shown in **Figure 37**, the composition of the three WBC samples was remarkably similar, showing several consistent clusters located along the right side of the UMAP plot (*i.e.*, separated along the most distinct component of the data). Based on the gene complement expressed by the cells in each cluster, we could infer they represent defined populations of white blood cells, including neutrophils, two populations of myeloid cells, one or perhaps two closely related populations of monocytes, at least three populations of T-cells, including regulatory T-cells, and one or perhaps two closely related populations of B-cells. **Figure 40B** represents the three OS cells samples. Note that the locations of the clusters from these samples are all on the left side of the UMAP plots and do not overlap at all with the locations of the clusters from the WBC samples. This is not surprising, as the OS cells were depleted of inflammatory cells by selection through short term culture. What is most interesting, however, is the separation of each individual sample into multiple clusters of cells (each of which would be predicted to have distinct, active transcriptional programs) and the lack of any relationship among the clusters from the three samples, indicating that there is extensive intratumor heterogeneity and little, if any similarity to the patterns of the transcriptomes among the three samples. In essence, while we can identify genes that are expressed by all the tumor cells (for example, collagen 2A and osteonectin), the overall programs that drive behavior of these cells are individually unique.

Figure 41 represents the three OS tissue samples. In these samples, clusters of cells are present in both the left and right sides of the UMAP plot. It is apparent that each sample includes unique clusters (not seen in any of the other sample), as well as events (cells) located in clusters that are also found in the WBC samples. This is consistent with our predictions, as it indicates that the OS tissue samples included both tumor cells as well as leukocytes, which were either passengers (found within the tumor vessels), residents (macrophages), or infiltrating inflammatory cells. As we expected, similar results were seen in the splenic samples, where there was an even greater preponderance of clusters that aligned with the WBC, consistent with their tissue of origin (not shown).

The observation that there were T-cells and myeloid cells present in the tumors whose transcriptional programs were completely distinct from those in the blood was among the most interesting findings from the data, although this observation was not totally unexpected. The developmental and differentiation programs of T-cells and myeloid cells are highly plastic, and these cells have evolved to adapt to a variety of environments. Work is ongoing to define whether these tumor-associated leukocyte transcriptional programs are associated with specific subsets or populations of T-cells and/or myeloid cells, and/or with migration, differentiation, immunosuppression, activation and/or exhaustion, anergy, memory, or other specific cell states.

It is also worth noting that we have imported publicly available data for human osteosarcomas (tissues), and we observe similar patterns as we see in the canine samples, suggesting the intra-tumor and inter-tumor heterogeneity are similar in canine and human osteosarcoma, even if the driver genes are not. This supports potential applications for comparative assessment of the composition and function of the conserved stromal and immune microenvironments in canine and human osteosarcoma.

Extensive work has been done to develop an atlas of single-cell gene expression for canine leukocytes. We used available reference files for human cells available through the human Database for Immune Cell Expression Data, the Blueprint Encode Data, and the Human Primary Cell Atlas. Generally, this approach showed consistent mapping of cell types from our single cell data across the three human reference datasets (**Figure 42**). However, we recognize that this is imperfect because cell type labels from the human reference datasets are forced onto all of the canine cells. And if a cell type of interest is not in the human reference data set, the best match assigned could be inaccurate. To account for this, we harmonized our data with those of Ammons et al[43] and transferred labels from Ammons's dataset onto ours (**Figure 43**).

There seems to be excellent agreement between the data from Ammons and our data, however, specific assignment for certain individual cells might still be erroneous, as Ammons et al also mapped their data to human reference sources and showed that the prediction scores, at least for neutrophils, CD8 cells, and NK cells, were quite low. In hindsight, these results are also not surprising. NK cells, in particular, show significant differences in phenotype and function among other well characterized species (human, mouse, rat, etc.), as do neutrophils. At first glance, the potential differences in phenotype and function among CD8 cells in different species are perhaps more surprising. But the data remind us that humans and dogs are separated by more than 50 million years of evolution, so it should not be so surprising that canine and human immune cells have acquired divergent functions as part of their adaptation to environment, lifespan, diet, etc. Given this divergence, the fact that we can still observe comparable features in the tumor microenvironments (even if less so in the tumor cells themselves), as described above, is remarkable.

We have recently reached an agreement with scientists at 10X Genomics to create a canine-specific probe set for spatial analysis of formalin-fixed and paraffin embedded (FFPE) samples (the FFPE spatial genomics platforms are highly species-specific). The need for FFPE is because, generally, osteosarcoma samples need to be decalcified to obtain suitable sections for analysis. The hard matrix

in which bone is embedded tends to damage instrumentation and shatter the samples during processing if the calcium apatite is not dissolved. However, Dr. Murugan believes we might be able to process “soft” sections where tumor is enriched from fresh frozen samples, so we are working to acquire those samples to include in our analyses as well.

The development of the canine probe set for FFPE samples will be done as part of a collaboration with the NCI PRECINCT canine immunotherapy consortium and will be made available to the research community. We are delighted to disclose that this effort has been funded as part of a supplement to U01 consortium grants awarded by the NIH/NCI to the two co-investigators at the Mayo Clinic (Dr. Naik) and the University of Minnesota (Dr. Modiano) and to Tufts University. 10X Genomics is also contributing expertise and resources to the effort.

So far, we have processed several canine osteosarcoma samples for FFPE spatial genomics, and we will continue to prioritize these samples as appropriate once the probe sets are finalized and test slides are available.

We have completed a Visium FFPE experiment in a human ovarian cell carcinoma and a human osteosarcoma sample to master the protocols. Based on the successful processing of this sample, we are working to obtain additional human osteosarcoma samples that meet quality control criteria for spatial analysis. These samples will provide a basis of comparison for the spatial organization of human and canine osteosarcomas, which will help guide rational applications for immunotherapy development in canine models. **Figure 44** shows expression data from the human osteosarcoma sample, illustrating the expected low frequency of infiltrating T-cells the compartmentalization of tumor cells, and the diffuse infiltration of macrophages into the tumor.

Final updates on all of the work that has been directly or peripherally supported by this award will be detailed in the 2024 report.

- **What opportunities for training and professional development has the project provided?**

In Dr. Modiano’s lab, one of the technicians involved in the project (Ms. Taylor DePauw) was accepted into graduate school starting in the Fall of 2021. This is a great achievement for a young person who wishes to eventually contribute to the research enterprise as a principal investigator.

Dr. Makielski continues her progression towards independence, having successfully competed for an open position as an Assistant Professor in the Department of Veterinary Clinical Sciences and the University of Minnesota (January 2023). Dr. Makielski is committed to developing an independent research program focused on developing more refined and accurate diagnostic methods and more effective and safer immunological therapies for osteosarcoma. Dr. Makielski also was successful in obtaining funding through a Special Emphasis Research Career Award (SERCA, K01) in Pathology and Comparative Medicine that will support her work in osteosarcoma for the next 5 years.

Ms. Sonam Varnasi (Sonam) completed her Master’s degree in Stem Cell Biology at the University of Minnesota, developing the mouse osteosarcoma models and the phagocytosis assays to quantify ONIx potency. She is currently working as a visiting scientist in the Modiano lab and aims to secure a job working as a scientist in industry.

Ms. Lauren Kreager joined Dr. Modiano’s laboratory as a Researcher-2 (technician) after 3 years working in the lab as an undergraduate student. Her exceptional work, including the pre-clinical (mouse) experiments and the ATAC-seq data presented in this report supported a promotion to Researcher-3 in 2023.

Dr. Julia Medland, who at the start of this project was a veterinary oncology resident at the University of Minnesota, has been working on the single cell sequencing and spatial genomics aspects of the project to characterize the complete diversity of the genomic landscape of osteosarcoma viewed not as a collection of malignant cells, but as a complex, albeit highly organized tissue. She was awarded the VCS-Dr. Gordon Theilen Resident Research Grant from the Veterinary Cancer Society to support her effort on this project. As part of her mentored transition to independence, Dr. Medland co-mentored Ms. Caitlyn Callaghan, who is entering her third year of veterinary school at the University of Minnesota. Dr. Medland has secured a faculty position as Assistant Professor of Oncology at the University of Minnesota (August 2023), where she continues her work as a clinician scientist with an emphasis on translating basic science into new, safe and effective therapies for cancer.

As mentioned above, Ms. Caitlyn Callaghan's is a 3rd-year veterinary student working on the single cell sequencing and spatial genomics aspects of this project. Ms. Callaghan intends to pursue post-graduate training in oncology, retaining a focus on programs that emphasize comparative oncology with aims to improve both human and animal health.

Dr. Aishwarya Sathyanarayan was involved in execution in the preliminary pilot studies in the K7M2, MC17, and A20 mouse models. During COVID-19 she became involved in the institutional response to the pandemic and shifted roles to gain training in viral vector production. She leveraged these skills and decided to take a new position in industry working in a GMP viral vector production role in November 2020. Recruitment to replace Dr. Sathyanarayan' s role was challenging during the pandemic.

Dr. Naik hired Caitlin Preusser as a research technologist following completion of her Bachelor of Science from St. Mary's University, Minnesota. She was recruited into Dr. Naik's lab and has received extensive training in methods in virology, molecular biology, immunology, and executing preclinical in vivo studies in mice. She is now conducting studies independently and is planning to apply to graduate program in biomedical research in Fall of 2024.

Dr. Naik has also recruited a post-doctoral fellow Velia Penza. Dr. Penza completed her PhD in December 2022 and began her post-doctoral fellowship in Dr. Naik's lab in March 2023. She has extensive experience engineering oncolytic virus therapies and is seeking to advance her training in a translational environment.

Finally, Dr. Naik, the Co-PI for this award was promoted to an Associate Consultant and attained her Assistant Professor academic rank at the Department of Molecular Medicine at the Mayo Clinic. She was also the recipient of a U01 award (September 2022) to investigate the immunomodulatory effects of novel oncolytic and immunotherapy combinations in relapsed or refractory lymphoma. Based on her success growing her independent research program, she is currently seeking a faculty position.

- **How were the results disseminated to communities of interest?**

Emerging data from this project have been disseminated through publication of peer reviewed manuscripts and abstracts/posters at scientific meetings (listed below).

- **What do you plan to do during the next reporting period (no-cost extension period) to accomplish the goals?**

We plan to continue pre-clinical development, studies to characterize the mechanisms of action of VSV and ONIx, alone and in combination, and to expand the enrollment of the canine clinical trial.

4. Impact

- **What was the impact on the development of the principal discipline(s) of the project?**

We published a thought-provoking perspective challenging current notions of cancer risk and highlighting novel advantages, as well as limitations of how companion dogs can inform cancer risk in humans.

1. Sarver AL, Makielski KM, DePauw TA, Schulte AJ, Modiano JF. (2022). Increased risk of cancer in dogs and humans: a consequence of recent extension of lifespan beyond evolutionarily determined limitations? (Perspective). Aging and Cancer, 3(1), 3-19. PMID: 35993010. PMCID: PMC9387675.

We documented that canine and human osteosarcoma represent convergent diseases, requiring a deliberate and cautious approach to advancing and/or using canine osteosarcoma as a model for human osteosarcoma.

1. Sarver AL, Mills LJ, Makielski MK, Temiz NA, Wang J, Spector L, Subramanian S, Modiano JF. (2023). Distinct mechanisms of PTEN inactivation in dogs and humans highlight convergent molecular events that drive cell division in the pathogenesis of osteosarcoma. Cancer Genet, 2023 May 20;276-277:1-11. doi: 10.1016/j.cancergen.2023.05.001. Online ahead of print. PMID: 37267683.

Our manuscript describing the safety and immunomodulatory activity of systemic VSV therapy administered in the neoadjuvant setting in dogs undergoing standard of care amputation and chemotherapy following diagnosis of osteosarcoma has been accepted in the journal *Molecular Therapy, Oncolytics*.

1. Makielski KM, Sarver AL, Henson MS, Stuebner KM, Borgatti A, Suksanpaisan L, Preusser C, Tabaran AF, Cornax I, O'Sullivan MG, Chehadeh A, Groschen D, Bergsrud K, Pracht S, Winter AL, Mills LJ, Schwabenlander MD, Wolfe M, Farrar MA, Cutter GR, Koopmeiners JS, Russell SJ, Modiano JF, Naik S. (2023). Oncolytic vesicular stomatitis virus is safe and provides a survival benefit for dogs with naturally occurring osteosarcoma. Mol Ther Oncolytics, accepted for publication. (This manuscript is also available as a bioRxiv preprint at doi: https://doi.org/10.1101/2023.04.16.533664).

We also published a review of more than 20 years of work to refine our understanding of canine osteosarcoma as a pre-clinical model for human osteosarcoma.

1. Sarver AL, Makielski MK, **Modiano JF**. (2022). A contemporary assessment of osteosarcoma: Lessons from a comparative approach. ***Med Res Arch, Med Res Arch,*** 10 (11), 1-21 (online), https://doi.org/10.18103/mra.v10i11.3339

Drs. Naik and Robinson prepared a review of oncolytic virus therapies and platforms that have been evaluated clinically for sarcoma treatment, gaining a perspective on the challenges and medical needs in sarcoma therapy and how OV therapy may be utilized to address them. This manuscript titled "Translation of Oncolytic viruses in Sarcoma" was submitted for review.

The following manuscripts in preparation are expected to be submitted before the end of 2023:

1. Ashley J. Schulte AJ, Lewellen M, Durose W, Nolan E, Taghizadeh L, Todhunter D, Lang HP, Bush C, Brown M, Seelig DM, Schappa JT, O'Sullivan MG, Weigel BJ, Murugan P, Cutter GR, Lund TC, Vallera DA, Modiano JF. Targeting Cells Expressing Urokinase Type Plasminogen

Activator Receptors and Epidermal Growth Factor Receptors in the Sarcoma Environment Enhances Anti-Tumor Activity. (The title might be slightly modified in the final version).

2. Dicovitsky RH, Schappa JT, Schulte AJ, Lang HP, DePauw TA, Lewellen M, Winter AL, Stuebner K, Buettner M, Reid K, Bergsrud K, Pracht S, Chehadeh A, Feiock C, Taras E, Todhunter D, O'Sullivan MG, Carlson T, Meritet D, Henson MS, Weigel BJ, Modiano JF, Borgatti A, Vallera DA. Toxicity profile of eBAT, a bispecific ligand targeted toxin directed to EGFR and uPAR, in the investigational preclinical setting. (The title might be slightly modified in the final version).

We disseminated our findings through abstract and poster presentations at national and international meetings.

1. Schulte AJ, Durose W, Nolan E, Taghizadeh L, Todhunter D, O'Sullivan MG, Seelig D, Vallera DA, Lund TC, Modiano JF. (2022). Therapeutic effect of eBAT is mediated by modulating the tumor microenvironment. Proceedings of the Mid-Year Meeting of the Veterinary Cancer Society
2. Callaghan CM, Sarver AL, Kim JH, Makielski KM, Modiano JF, and Medland JE. (2022). The Immune and Molecular Landscape of Canine Osteosarcoma. Proceedings of the National Veterinary Scholars Symposium, St Paul, MN, August 5, 2022
3. Modiano JF, Schulte AJ, DePauw TA, Khammanivong A, Kim JH, Sarver AL, Cutter GR, Lindquist E, Makielski KM. (2022). Identification and characterization of the cancer permissive environment in companion dogs (Invited oral platform presentation). Proceedings of the Inaugural AACR Cancer and Aging Meeting
4. Kuzmik A*, Medland J*, Makielski K, Chehadeh A, Stuebner K, DePauw T, Kreager L, Callaghan C, Schulte A, Preusser C, Srivastava S, Luethcke R, Dicovitsky R, Lilly R, Parks M, Winter A, Bergsrud K, Feiock C, Greengard E, Weigel B, Largaespada D, Cheng E, Murugan P, Vallera D, Borgatti A, Cutter G, Sarver A, Henson M, Ring A, Naik S, Modiano J. (2023). Development of a novel peptide that simultaneously inhibits the myeloid and immune exhaustion checkpoints as immunotherapy for osteosarcoma (invited oral presentation, J Medland). MIB Agents Osteosarcoma Alliance Factor Osteosarcoma Conference (June 22-24, 2023)
5. Modiano J, Naik S, Ring A. Modulating the Tumor Immune Microenvironment with ONIx, a Peptide for Dual Immune Checkpoint Blockade (Invited oral platform presentation). PEGS Boston Meeting, Boston, MA, May 15-18, 2023

- **What was the impact on other disciplines?**

We have raised awareness and attention of how dogs and humans share a recent history of breaking through their evolutionarily adapted lifespan barriers through technological achievements. Dr. Modiano presented our research, "Identification and Characterization of the Cancer Permissive Environment in Companion Dogs," as oral platform talks at the AACR Aging and Cancer Meeting in San Diego in November of 2022 and at the Protein Engineering and Genomics Symposium (PEGS) Boston Meeting in May of 2023. Dr. Medland presented data on our clinical translation efforts at the FACTOR 2023 osteosarcoma meeting in June of 2023, and she will present data on our work to define the genomic landscape of osteosarcoma at the single cell levels at the annual meeting of the Veterinary Cancer Society in October of 2023

- **What was the impact on technology transfer?**

Nothing to Report

- **What was the impact on society beyond science and technology?**

Our work is highlighting a new opportunity to expand the role of dogs in society, not only as companions and service animals, but as research subjects that can inform methods and strategies to treat, manage, and prevent cancer and to generally help us understand how we can maintain our health through graceful aging. This is especially relevant to military personnel after they leave active service.

5. Changes/Problems

- **Changes in approach and reasons for change**

As described in the Accomplishments section, the K12 and K7M2 mouse osteosarcoma models have not proved to be as reliable as we expected, and so we are developing alternative models to investigate our hypotheses and address the goals of this project, including new cell lines in the C57Bl/6 background and the MC17 sarcoma model.

Recruitment into the canine clinical study has been challenging. We have expanded the eligibility of the trial to include dogs with relapsed or inoperable sarcomas. However, to ensure we can generate data on the synergy of VSV and ONIx, we also have developed an *in vitro* approach to address the hypothesis by utilizing resources of our previous VSV trial (VIGOR) and cutting edge genomic methods (ATAC-seq and RNAseq).

- **Actual or anticipated problems or delays and actions or plans to resolve them**

As we described above, the COVID-19 pandemic and the responses to the pandemic caused significant disruptions to the project. From the departure of a key person (postdoc) at the Mayo site to lab closures that lasted more than a year, to persistent problems sourcing reagents and materials and a very strong and direct request from the U of M administration to consider reducing animal activities due to staffing problems.

Fortunately, as the severity of the pandemic has abated, we have been able to resume work and make progress. We are grateful that the program officers and the agency approved no-cost extensions that will allow us to complete the proposed experiments to achieve our aims.

- **Changes that had a significant impact on expenditures**

The COVID-19 pandemic and the resultant requirement for remote work meant that personnel effort (salary) had to be dedicated to “soft” tasks, including data analysis (see for example the data presented in Figures 3, 4, and 8 of this report), and instead of “hard” tasks (experiments in the lab).

- **Significant changes in use or care of human subjects, vertebrate animals, biohazards, and/or select agents**

We modified the eligibility criteria for dogs to enroll in the clinical study. The changes were approved by the University of Minnesota IACUC and by ACURO

- **Significant changes in use or care of human subjects**

None

- **Significant changes in use or care of vertebrate animals.**

See above.

- **Significant changes in use of biohazards and/or select agents**

None

6. Products

Nothing to Report

7. Participants & Other Collaborating Organizations

What individuals have worked on the project?

Name:	*Jaime Modiano*
Project Role:	*PI*
Researcher Identifier (e.g. ORCID ID):	0000-0001-6398-7648
Nearest person month worked:	2
Contribution to Project:	*Dr. Modiano is the contact PI. He has overseen the work and contributed to the experiments conducted at the University of Minnesota, as well as to the analysis of all project data.*
Funding Support:	*Institutional funds (endowed Chair)*

Name:	*Shruthi Naik*
Project Role:	*Co-PI*
Researcher Identifier (e.g. ORCID ID):	
Nearest person month worked:	4
Contribution to Project:	*Dr. Naik is the Mayo site PI. She has contributed to all the experiments performed at the Mayo Clinic, including supervision of personnel (post-doc) and data analysis.*
Funding Support:	

Name:	*Michael Henson*

Project Role:	*Co-I*
Researcher Identifier (e.g. ORCID ID):	
Nearest person month worked:	1
Contribution to Project:	*Dr. Henson is the clinical lead for the canine clinical study (METEOR). He was involved in study design, organization, and was the attending clinician for the case enrolled in the study.*
Funding Support:	

Name:	*Kelly Makieslki*
Project Role:	*Postdoctoral research associate/Assistant Professor*
Researcher Identifier (e.g. ORCID ID):	
Nearest person month worked:	6
Contribution to Project:	*Dr. Makielski contributed to the experiments performed at the University of Minnesota (in vitro validation of ONIx, MC17 model experiments, and analysis of the VIGOR trial).*
Funding Support:	K01 OD031810

Name:	*Lauren Mills*
Project Role:	*Research Associate*
Researcher Identifier (e.g. ORCID ID):	
Nearest person month worked:	2
Contribution to Project:	*Dr. Mills has been involved in data storage and data management, especially for sequencing data, and she performed the ATAC-seq analysis.*
Funding Support:	

Name:	*Andy Sicheneder*
Project Role:	*Technician*

Researcher Identifier (e.g. ORCID ID):	
Nearest person month worked:	1
Contribution to Project:	*Mr. Sicheneder was responsible for production of ONIx.*
Funding Support:	

Name:	*Mitzi Lewellen*
Project Role:	*Technician*
Researcher Identifier (e.g. ORCID ID):	
Nearest person month worked:	1
Contribution to Project:	*Ms. Lewellen is involved with managing inventories and the animal colonies in the Modiano lab. For this project, she has kept experimental inventories and managed the mouse colonies for the K7M2 and MC17 experiments.*
Funding Support:	

Name:	*Ashley Schulte*
Project Role:	*Technician*
Researcher Identifier (e.g. ORCID ID):	
Nearest person month worked:	3
Contribution to Project:	*Ms. Schulte was the lead scientist in the development of the MC17 model. She also generated the genome-edited mouse osteosarcoma cell lines with assistance from the GESR at the University of Minnesota. She has contributed to QC testing and potency assays for ONIx and has been the lab manager and safety officer for the Modiano lab throughout the project.*
Funding Support:	*Karen Wyckoff Rein in Sarcoma Foundation; Morris Animal Foundation*

Name:	*Taylor DePauw*

Project Role:	*Technician*
Researcher Identifier (e.g. ORCID ID):	
Nearest person month worked:	2
Contribution to Project:	*Ms. DePauw was responsible for leading the ONIx validation studies (in vitro) during year 1. She also was responsible for all purchasing activity and equipment maintenance in the Modiano lab during year 1. Ms. DePauw left the lab to start graduate school at the end of year 1.*
Funding Support:	

Name:	*Lauren Burt (nee, Kreager)*
Project Role:	*Technician*
Researcher Identifier (e.g. ORCID ID):	
Nearest person month worked:	2
Contribution to Project:	*Ms. Kreager joined the lab during year-2 of this project. She assisted with the experiments to develop the mouse models of osteosarcoma and with the experiments for single cell sequencing. She was the lead scientist in the experiments to assess the chromatin landscape in lymphocytes.*
Funding Support:	*Institutional Funds*

Name:	*Julia Medland*
Project Role:	*Resident in Veterinary Oncology/Assistant Professor*
Researcher Identifier (e.g. ORCID ID):	
Nearest person month worked:	1
Contribution to Project:	*Dr. Medland has led the studies to define the genomic landscape of osteosarcoma at the single cell level.*
Funding Support:	*Veterinary Cancer Society/Dr. Gordon Theilen Resident Research Award*

Name:	*Caitlyn Callaghan*
Project Role:	*Veterinary Student*
Researcher Identifier (e.g. ORCID ID):	
Nearest person month worked:	3
Contribution to Project:	*Ms. Callaghan has assisted Dr. Medland in the studies to define the genomic landscape of osteosarcoma at the single cell level.*
Funding Support:	T35 OD011118, “Veterinary Summer Scholars in Comparative Medicine”

Name:	*Caitlin Feiock*
Project Role:	*Assistant Professor*
Researcher Identifier (e.g. ORCID ID):	
Nearest person month worked:	1
Contribution to Project:	*Dr. Feiock is the Research Manager for the University of Minnesota College of Veterinary Medicine Clinical Investigation Center and is coordinating implementation and recruitment for the METEOR Study.*
Funding Support:	Institutional funds

Name:	*Caitlin Preusser*
Project Role:	*Research technologist*
Researcher Identifier (e.g. ORCID ID):	
Nearest person month worked:	6
Contribution to Project:	*Ms. Preusser joined the lab during year-2 of this project. She assisted with the experiments to evaluate the impact of VSV and ONIx in the mouse models and the correlative experiments. Ms. Preusser is the lab manager and safety officer for the Naik lab, where she is also responsible for purchasing activity and equipment maintenance.*

Funding Support:	

Name:	*Velia Penza*
Project Role:	*Post-doctoral fellow*
Researcher Identifier (e.g. ORCID ID):	
Nearest person month worked:	3
Contribution to Project:	*Dr. Penza joined the lab in March 2023. She has bought her experience in conducting preclinical studies in mouse models and tumor immune analysis to help establish the MC17 tumor model and optimize assays to assess tumor immune analysis.*
Funding Support:	

Name:	*Kathy Stuebner*
Project Role:	*Certified Veterinary Technician/Temp-Causal Appointment*
Researcher Identifier (e.g. ORCID ID):	
Nearest person month worked:	1
Contribution to Project:	*Ms. Stuebner was the coordinator for the Clinical Investigation Center of the University of Minnesota College of Veterinary Medicine. She assisted with completion of all the documentation needed to file IACUC and IBC approvals as well as ACURO approvals, as well as with amendments. She prepared the enrollment site for the canine clinical study and was responsible for coordinating release assays for ONIx. She remains involved in our projects and led the completion of ACURO submission for the 3-year renewals*
Funding Support:	

Name:	*Amber Winter*
Project Role:	*Certified Veterinary Technician*
Researcher Identifier (e.g. ORCID ID):	
Nearest person month worked:	1

Contribution to Project:	*Ms. Winter worked with Dr. Modiano and Ms. Stuebner to complete the documentation for IACUC and ACURO approval during year 1.*
Funding Support:	

Name:	*Andrea Chehadeh*
Project Role:	*Certified Veterinary Technician*
Researcher Identifier (e.g. ORCID ID):	
Nearest person month worked:	2
Contribution to Project:	*Ms. Chehade worked with Drs. Modiano and Henson and with Ms. Stuebner to complete preparations for the canine clinical study (METEOR) and is the lead nurse for the study.*
Funding Support:	

Name:	*Aishwariya Sathyanarayan*
Project Role:	*Postdoctoral research associate*
Researcher Identifier (e.g. ORCID ID):	
Nearest person month worked:	2
Contribution to Project:	*Dr. Aishwariya initiated the mouse experiments at Mayo Clinic before COVID-related events forced her relocation from Dr. Naik's lab.*
Funding Support:	

Name:	*Aaron Sarver*
Project Role:	*Assistant Professor*
Researcher Identifier (e.g. ORCID ID):	
Nearest person month worked:	1
Contribution to Project:	*Dr. Sarver was responsible for analysis of the RNAseq data shown in Figure 8.*

Funding Support:	*NIH grant R50 CA211249 (year-1) and Masonic Cancer Center – Cancer Center Core Support Grant P30 CA077598*

Name:	*Davis Seelig*
Project Role:	*Associate Professor*
Researcher Identifier (e.g. ORCID ID):	
Nearest person month worked:	1
Contribution to Project:	*Dr. Seelig was responsible for histopathological analysis of mouse necropsy tissues from the K7M2 study. Dr. Seelig took over as retired as Director of the Masonic Cancer Center Comparative Pathology Shared Resource Core at the beginning of year 2 of this project.*
Funding Support:	*Masonic Cancer Center – Cancer Center Core Support Grant P30 CA077598*

Name:	*Jong Hyuk Kim*
Project Role:	*Assistant Professor*
Researcher Identifier (e.g. ORCID ID):	
Nearest person month worked:	1
Contribution to Project:	*Dr. Kim assisted with the animal experiments and histopathological analysis of mouse necropsy tissues for the MC17 experiments.*
Funding Support:	

Name:	*M. Gerard O'Sullivan*
Project Role:	*Professor*
Researcher Identifier (e.g. ORCID ID):	
Nearest person month worked:	1

Contribution to Project:	*Dr. O'Sullivan was responsible for histopathological analysis of mouse necropsy tissues from the MC17 experiments. Dr. O'Sullivan retired as Director of the Masonic Cancer Center Comparative Pathology Shared Resource Core at the end of year 1 of this project.*
Funding Support:	*Masonic Cancer Center – Cancer Center Core Support Grant P30 CA077598*

Name:	*Sonam Varnasi*
Project Role:	*Master's in Science graduate student*
Researcher Identifier (e.g. ORCID ID):	
Nearest person month worked:	6
Contribution to Project:	*In vivo model development; ONIx/eBAT validation studies.*
Funding Support:	*Institutional funds*

- **Has there been a change in the active other support of the PD/PI(s) or senior/key personnel since the last reporting period?**

Several grants held by the PI at the start of this project have ended (DOD IDEA Award, K01 mentored transition to independence award where the PI was a mentor, T32 support for a postdoc, two fixed cost contracts from Boston Scientific, a contract from Vyriad, and grants from the AKC Canine Health Foundation and Morris Animal Foundation).

New grants awarded to the PI since the start of this project include a grant from Venn Foundation intended to pursue commercialization of inventions in the PI's lab, a competitive renewal from the AKC Canine Health Foundation, two new grants from the AKC Canine Health Foundation, a U01 contract from the NCI, and a K01 mentored transition to independence award from the NIH Office of the Director where the PI is a mentor.

The PI's effort on this grant has not changed.

- **What other organizations were involved as partners?**

The only two organizations involved, University of Minnesota and Mayo Clinic, were listed in the original application.

8. Special Reporting Requirements

None

9. Figures 1-44
(Starting on Next page)

Figure 1

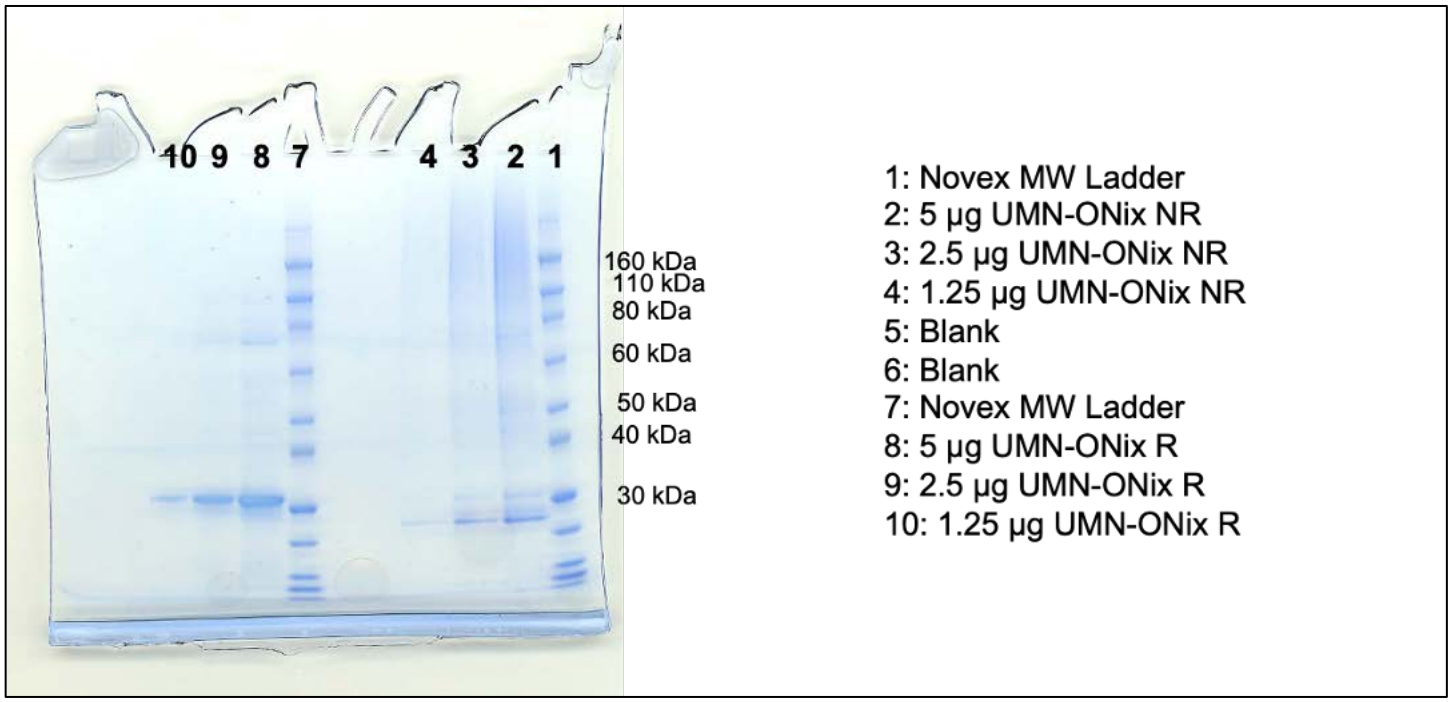

Figure 1. Purity of ONIx determined by gel electrophoresis. Coomassie blue-stained gel showing a titration of the final ONIx peptide under non-reducing conditions (lanes 2-4) and under reducing conditions (lanes 8-10).

Figure 2

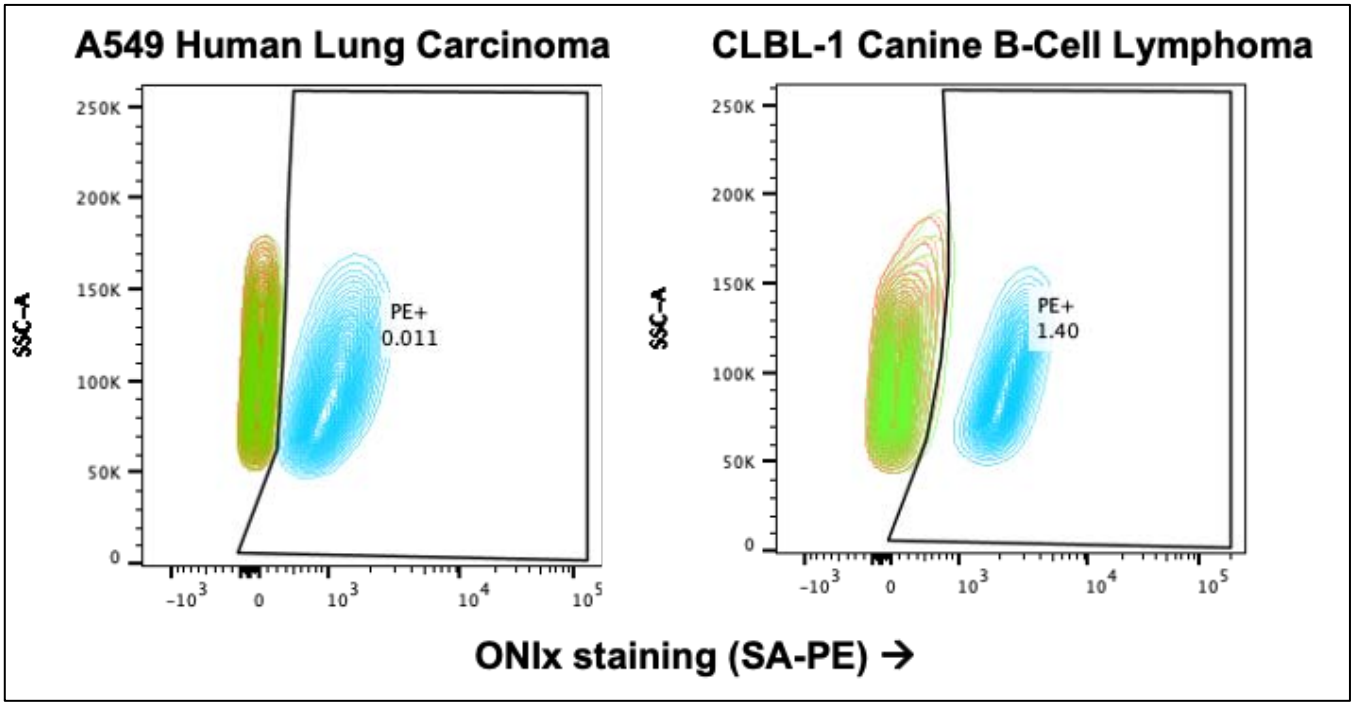

Figure 2. ONIx binds canine cells with approximately equal affinity as human cells. A549 human lung carcinoma cells and canine CLBL-2 B-cell lymphoma cells were stained with biotinylated ONIx alone (brown), streptavidin (SA) conjugated to phycoerythrin (PE) alone (green), or a combination of biotinylated ONIx and SA-PE (blue) and analyzed by flow cytometry. Two-dimensional contour plots show that ONIx staining is similar for both cell lines.

Figure 3

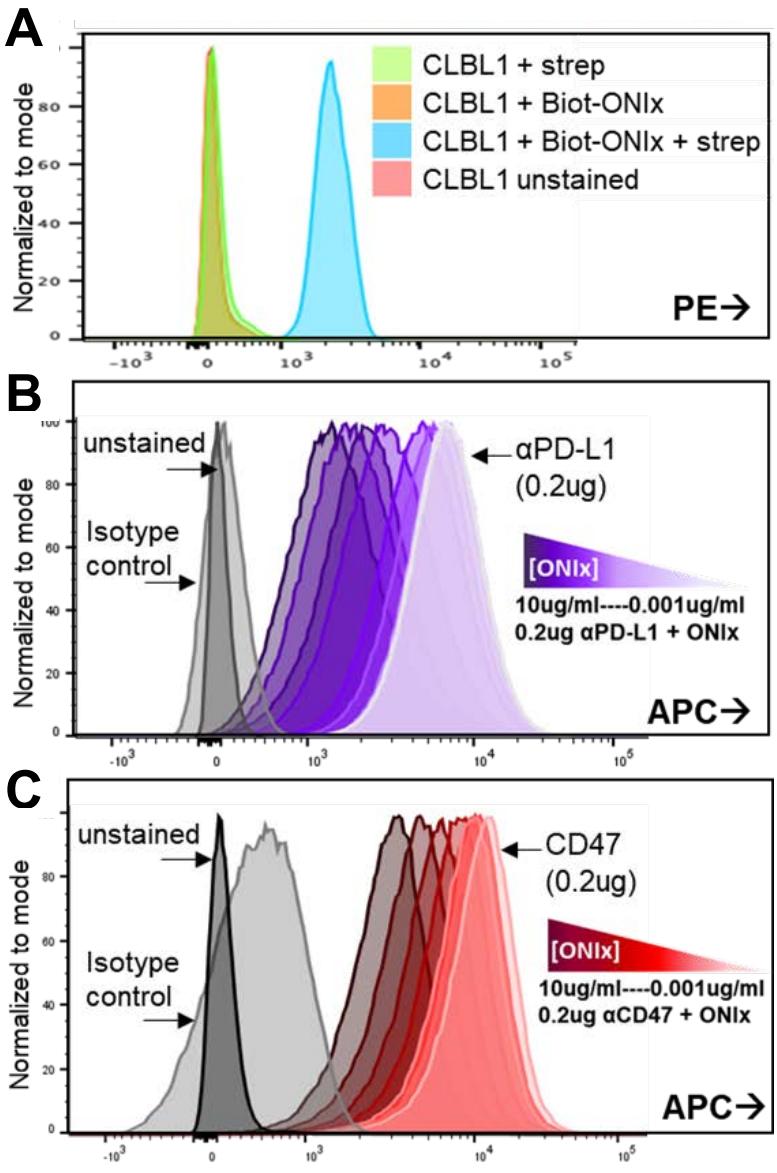

Figure 3. Displacement of anti-PD-L1 and anti-CD47 antibodies by ONIx. A Binding of biotinylated ONIx to CLBL1 cells. B Dose-dependent displacement of anti-PD-L1 antibody (0.2µg/ml) from PD-L1+ mouse 5TGM1 cells by increasing concentrations of ONIx (0.001-10µg/ml). C Displacement of anti-CD47 antibody (0.2µg/ml) from CD47+ mouse 5TGM1 cells by increasing concentrations of ONIx (0.001-10µg/ml).

Figure 4

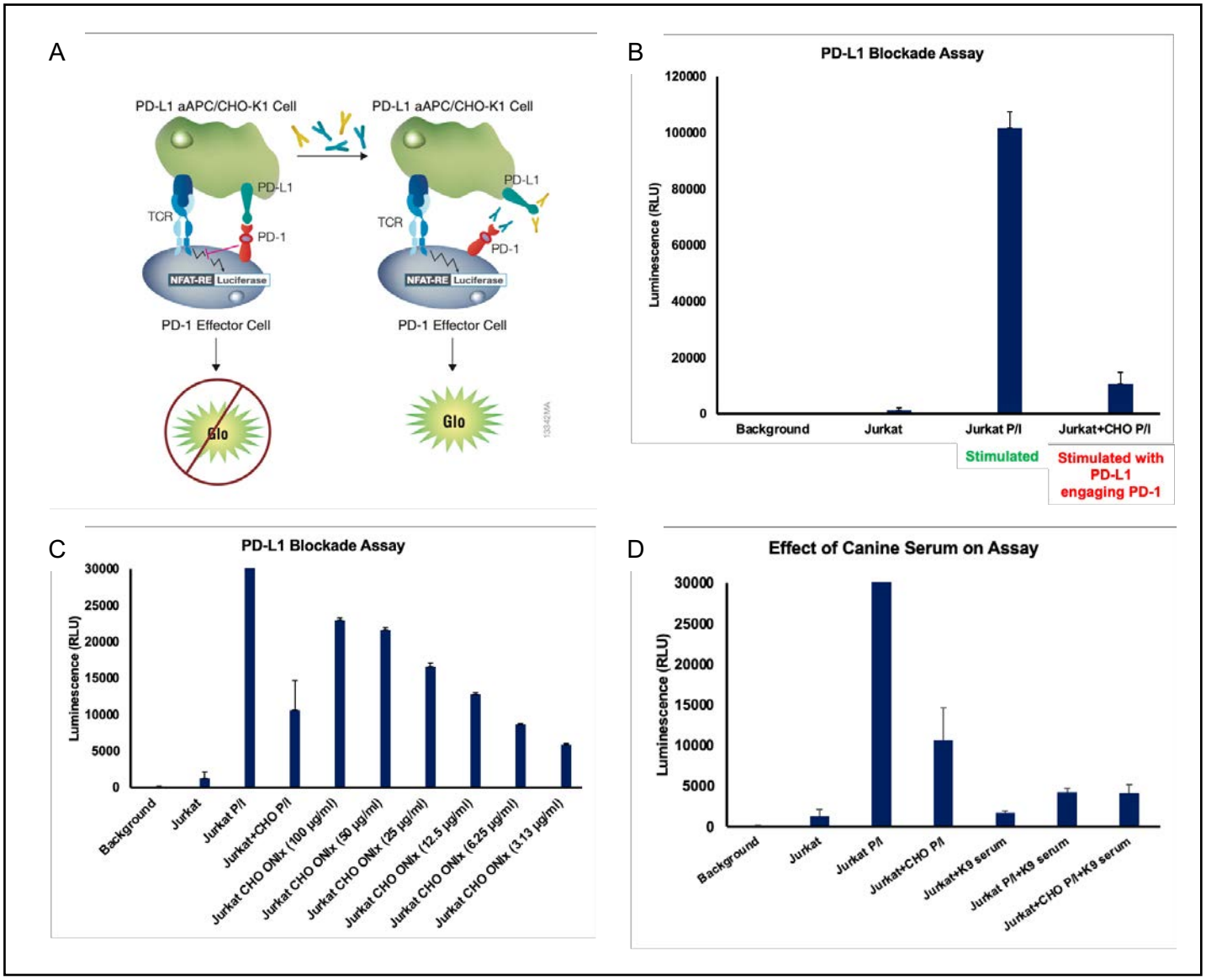

Figure 4. Potential PK/PD bioassay to measure PD-1/PD-L1 checkpoint blockade by ONIx. The Promega PD-1 blockade assay was used to assess the capability of ONIx to block the interactions between PD-1 and PD-L1, allowing for reinvigoration of T cells, as well as its suitability to establish ONIx PK and PD in the VSV + ONIx canine METEOR trial participants. Panel **A** shows the principle of the assay (Promega©). Panel **B** shows the absence of signal when Jurkat cells were excluded from the assay (background), negligible signal when cells were incubated without stimulation (Jurkat), increased signal using the positive control (P/I), and inhibition of the signal by the addition of PD-L1-expressing artificial APCs. Panel **C** shows dose-dependent restoration of Jurkat cell activation when ONIx was added to the assay in the presence of PD-L1-expressing artificial APCs. Panel **D** shows the unexpected inhibition of the assay by canine serum. The mechanisms for this inhibition and ways to overcome it are being investigated in collaboration with Promega.

Figure 5

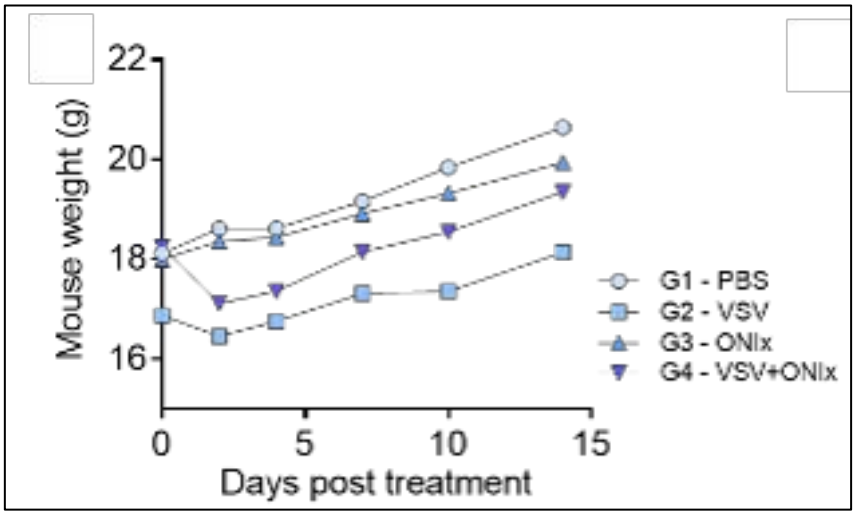

Figure 5. VSV and ONIx combination therapy is well tolerated in tumor bearing mice. Mice were treated as described in the text. ONIx treatment alone did not alter the course of weight gain in the mice. The VSV treatment group included smaller mice (see weight at Day 0) and the trend for weight gain was comparable to the controls. Mice treated with the combination showed transient weight loss, but then resumed weight gain at the same rate as the controls, despite continued treatment with ONIx.

Figure 6

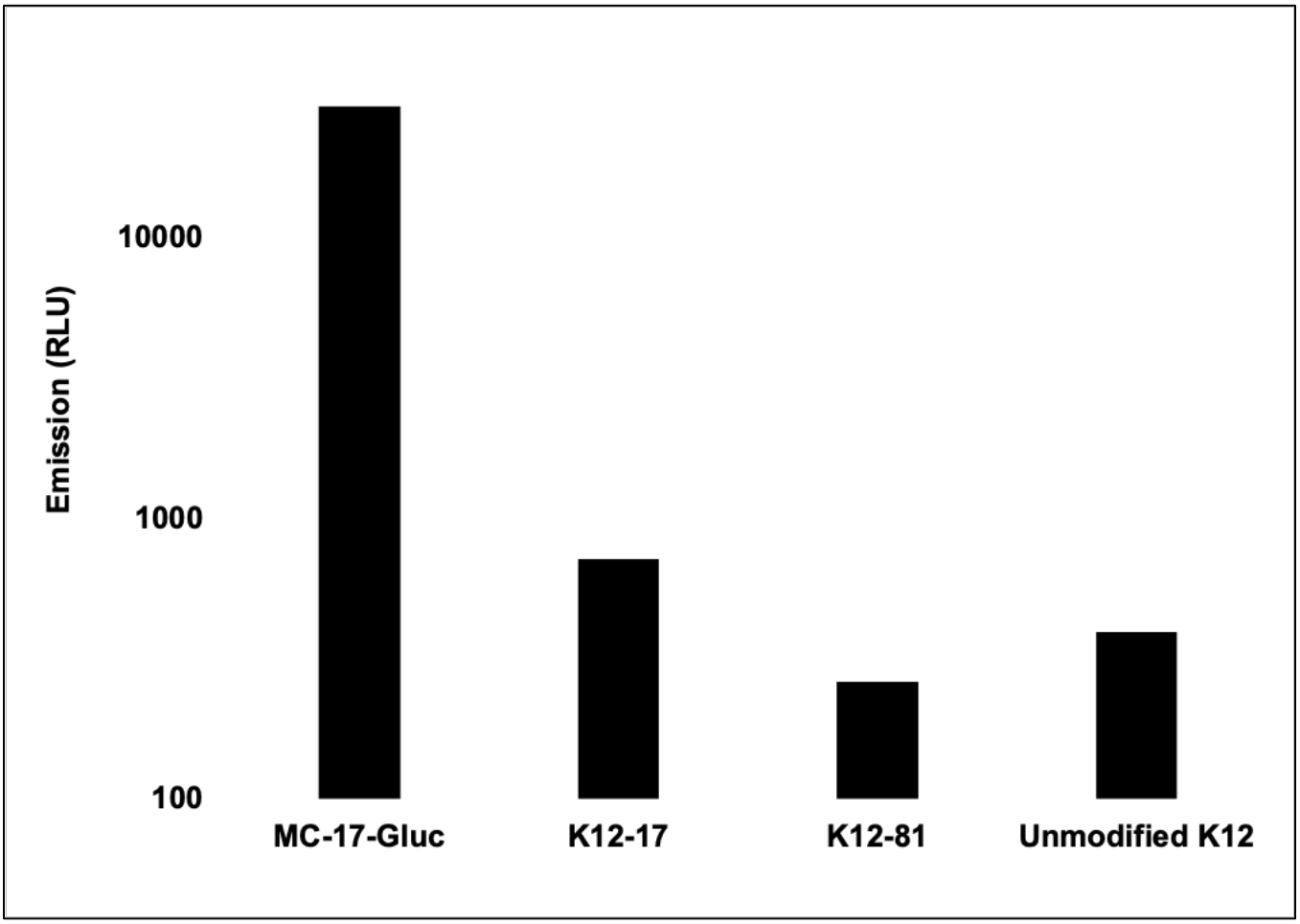

Figure 6. Gaussia Luciferase Activity in MC17 fibrosarcoma and K12 mouse osteosarcoma cells genetically edited to express the *Gluc* gene in the *Rosa 26* locus using CRISPR-Cas9. Culture supernatants were harvested to analyze light emission upon the addition of coelentrazine substrate (Gluc is secreted). Similar results were obtained from cell lysates, to ensure that lack of detectable activity in K12-Gluc clones 17 and 81 was not due to failure of secretion, as well as in live cultured cells imaged on an IVIS spectrum instrument. RLU = relative light units.

Figure 7

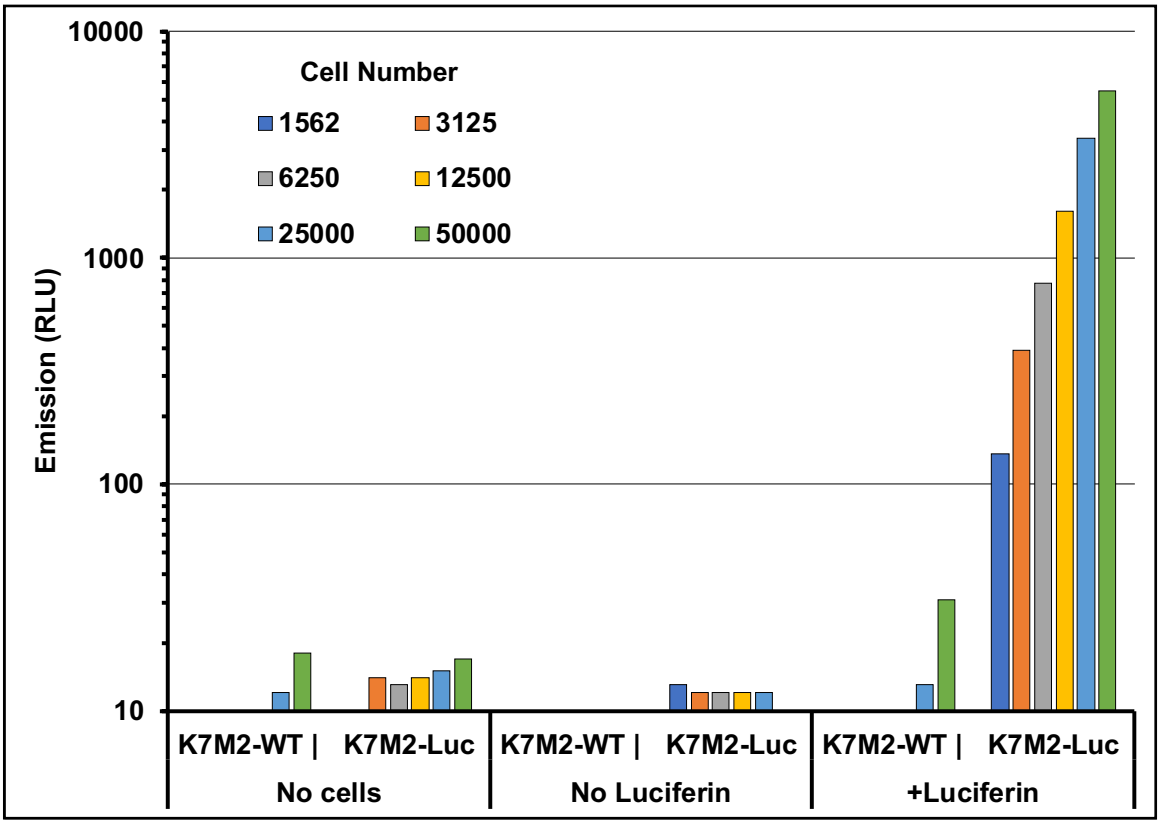

Figure 7. Firefly Luciferase Activity in K7M2-fLuc cells transected with the *Fluc* gene. Wild type K7M2 cells (obtained from the NCI) and K7M2 cells transfected to express firefly luciferase (*Fluc*) were grown in culture and cell-associated luciferase expression was measured in lysates from 2-fold serial dilutions of 50,000 to 1,562 cells. Only the two highest concentrations were used for wild type cells. Controls included omitting cells (media + luciferin substrate) and omitting substrate (media + cell lysate, no luciferin). RLU = relative light units.

Figure 8

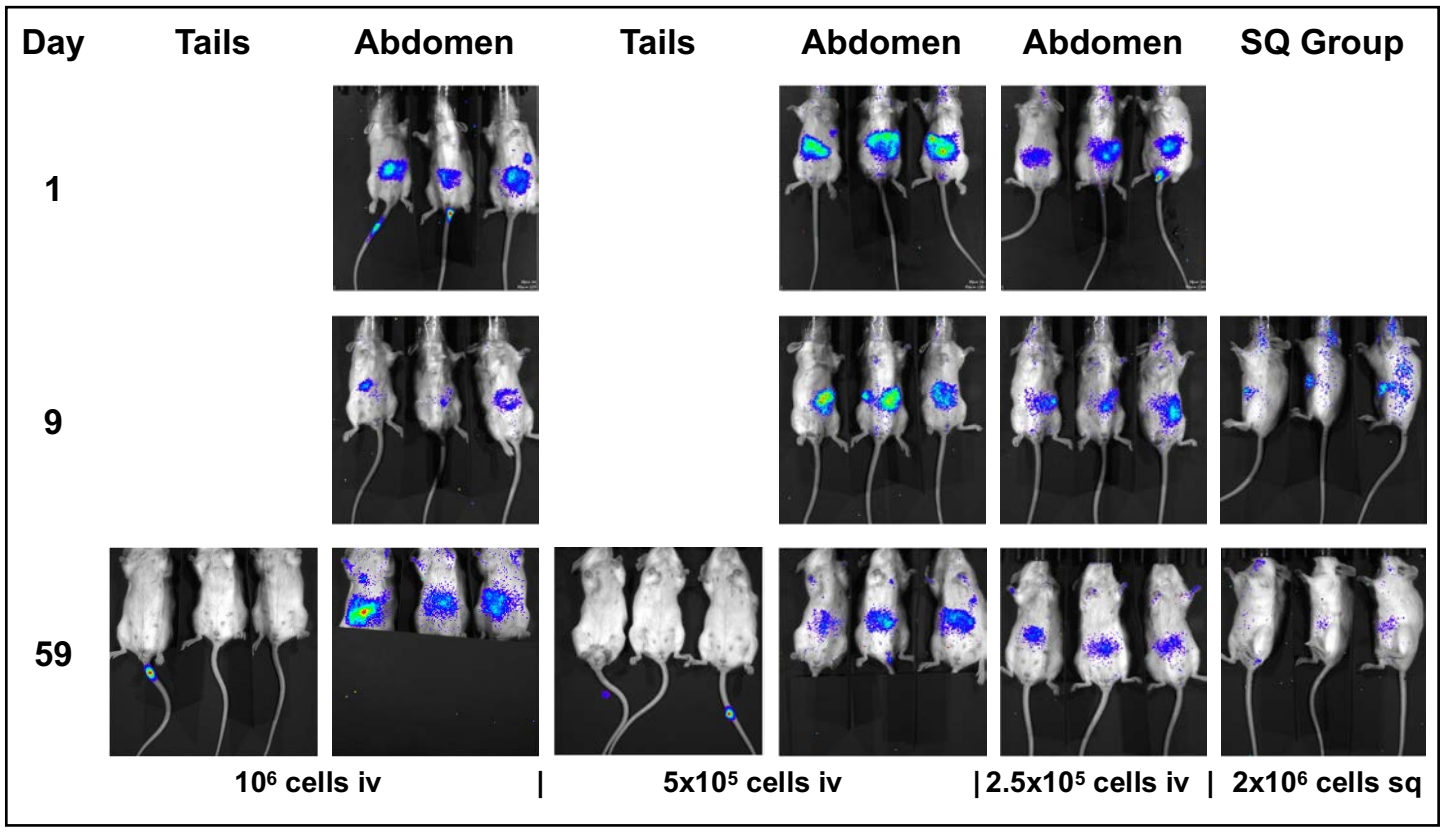

Figure 8. *In vivo* imaging by light emission in mice receiving tail vein or subcutaneous injections of K7M2-fLuc cells. Groups of three mice were injected with K7M2-fLuc cells in the tail vein in 2-fold decrements ($1x10^6$ cells, $5x10^5$ cells, and $2.5x10^5$ cells). In this model, it is reported that iv injection of $1x10^6$ cells results in 100% lung colonization and death (reaching endpoint) of the mice by approximately 2-3 weeks and $5x10^5$ cells results in 100% lung colonization and death by approximately 3-4 weeks. Here, the data indicate that after iv injection, the cells distributed to the abdomen (almost certainly the spleen, based on the anatomical location of the luminescent signal) regardless of cell dose, and they remained in the spleen, where the signal eroded over the course of two months. Two mice (one each in the groups that received $1x10^6$ and $5x10^5$ cells) developed tumors in the tail vertebra near the site of injection, so imaging of the abdomen was also done masking the tail signal to appreciate the presence of cells in the spleen. The abdomens were similarly masked to image the lung fields (images not shown), but signals above background were not apparent without sensitive quantification using the instrument detector (see Figure 9). One group of three mice received $2x10^6$ K7M2 cells subcutaneously (sq). A signal was detectable at the site of injection for approximately one week, but the signal eventually dissipated and returned to baseline.

Figure 9

Figure 9. Quantitative light emission signals from mice injected with K7M2-fLuc cells. Signal quantification was determined using the *Living Image* software (Perkin Elmer). Graphs show luminescence data as counts per second over time for individual mice in the group receiving $1x10^6$ cells iv. Note the relative scale of signals in the single mouse that developed a tail tumor (top), as compared to the signals in the abdomen (spleens), which mostly eroded over time, and the signals in the lung, which increased slightly over background after week 8, but were still about two to three times lower than the signals in the abdomen. The data for mice receiving fewer cells showed similar patterns, with lower (although not proportionate) light emission values.

Figure 10

Figure 10. Image of mass in the lungs from mouse #4. The approx. 3 mm mass is highlighted by the blue oval in the image.

Figure 11

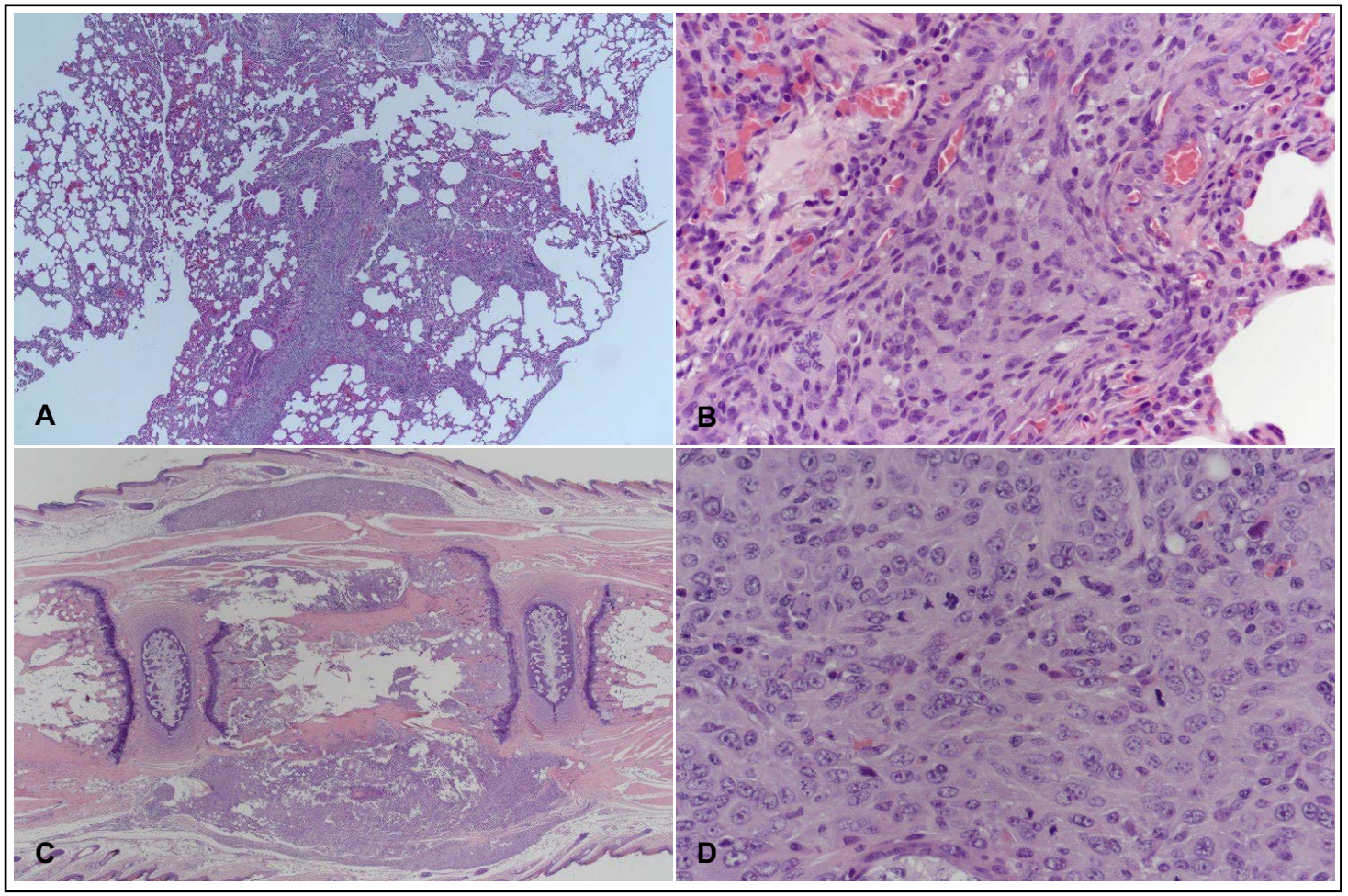

Figure 11. Photomicrographs showing histopathology of tumors in representative sections of the lungs and tail from mouse 3 (injected with $1x10^6$ K7M2 cells iv). A. Lungs, 40x (H&E). Multiple cross sections of vessels have tumor emboli. B. Lungs, 400x (H&E). Higher magnification of tumor emboli. Note multiple mitotic figures, some of which are bizarre. C. Tail, 20x (H&E). Surrounding and infiltrating a vertebra is a sarcoma. D. Tail, 400x (H&E). Higher magnification of the sarcoma. There are numerous mitotic figures, many of which are atypical.

Figure 12

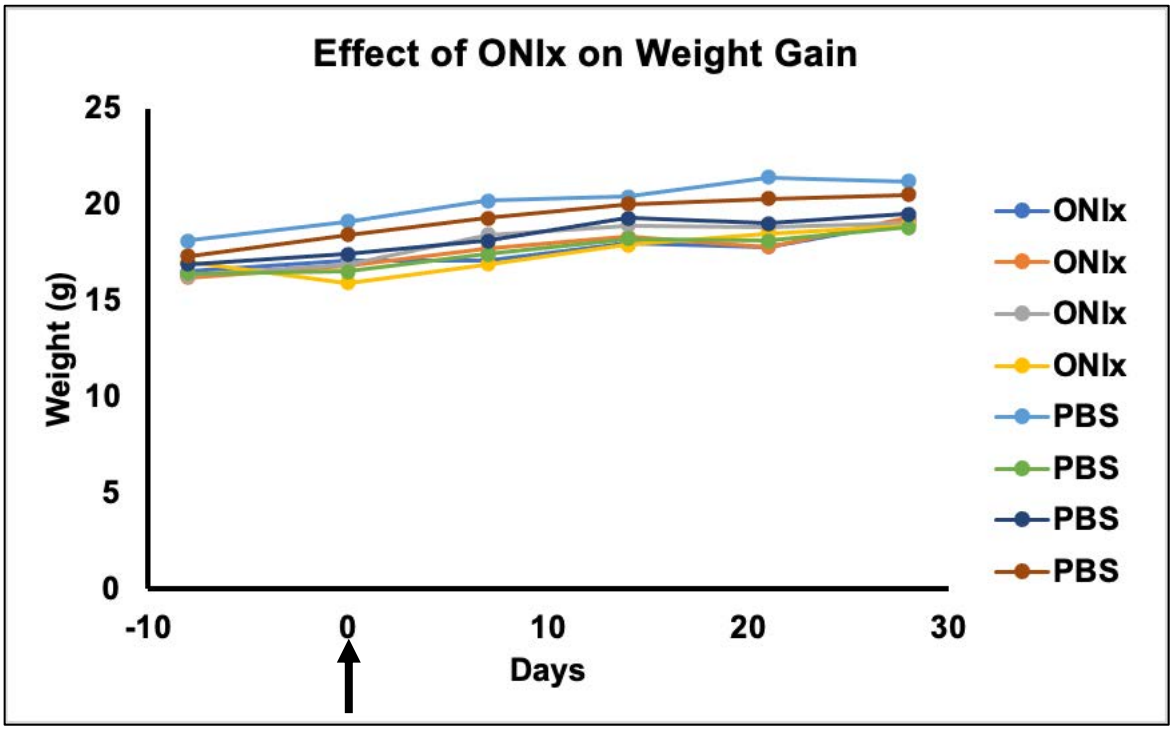

Figure 12. ONIx does not impact weight gain of mice. Mice were inoculated with $5x10^5$ K7M2 cells given iv on day 0 (red arrow) and treated with 2 cycles of ONIx, each 2 days apart (days 12 and 14; days 19 and 21) given sq at 5 mg/kg. The weight of the mice was tracked weekly until the experimental endpoint on day 28. There was no difference in the rate of weight gain in mice that received ONIx as compared to those that received placebo (PBS).

Figure 13

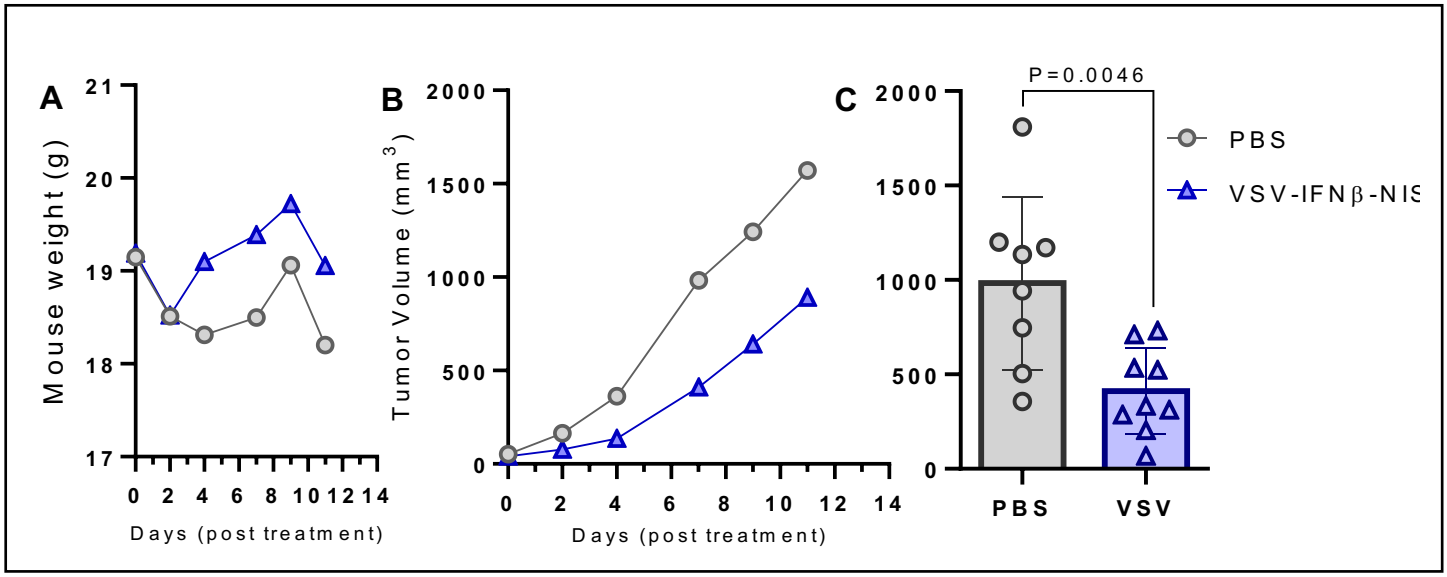

Figure 13. Systemic VSV therapy safe and delays tumor remission of murine sarcoma tumors. C57Bl/6 mice were implanted with MC17 tumor cells subcutaneously in the right flank. Tumor volume was tabulated from serial caliper measurements of tumor diameter. 10 days post tumor implantation, mice were treated with single dose of PBS (100 µl) or $5x10^8$ $TCID_{50}$ VSV-IFNβ-NIS (in 100 µl PBS). Mice were closely monitored for acute adverse events, weight loss, and tumor burden with results showing systemic VSV therapy (A) was well tolerated and did not induce acute toxicities resulting in weight loss, (B) delayed tumor progression, and (C) resulted in significant inhibition of tumor growth based on tumor volume vs. PBS treated mice on day 7 post treatment.

Figure 14

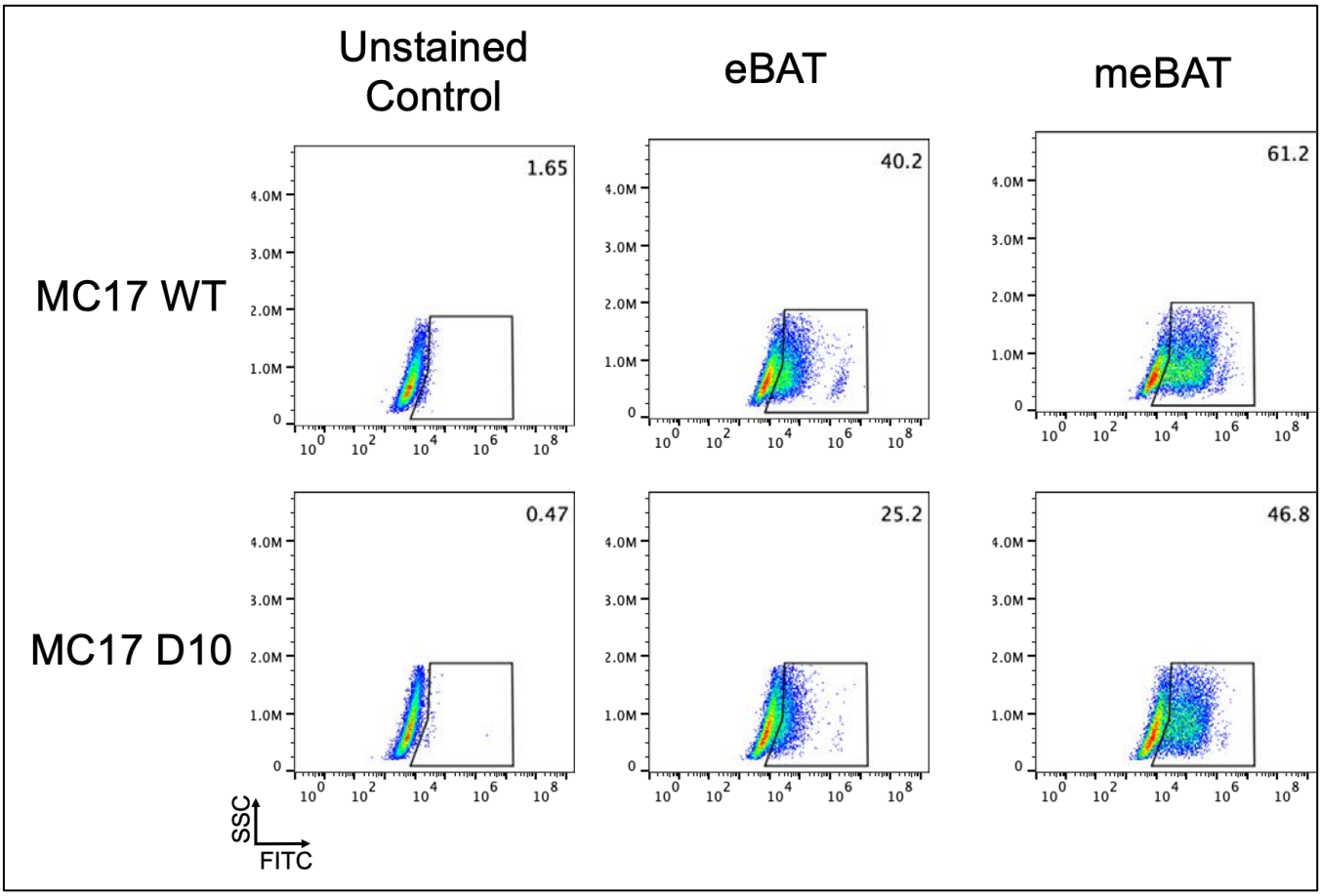

Figure 14. Binding of eBAT and meBAT to MC17 mouse fibrosarcoma cells and to D10 uPAR-KO mouse fibrosarcoma cells. D10 cells were derived from MC17 by CRISPR-Cas9-mediated knockout of uPAR (introduction of a missense mutation in exon 2). The two-dimensional flow cytometry contour plots show fluorescence (x-axis) as a function of cellular complexity (90° light side scatter, y-axis). The top panels represent WT MC17 cells, and the bottom panels represent D10 (uPAR-KO) cells. The panels in the first column from the left are unstained controls. The panels in the second show staining with eBAT-FITC. The panels in the third column show staining with meBAT-FITC. The reduced binding of eBAT and meBAT to D10 cells is attributable to lack of uPAR.

Figure 15

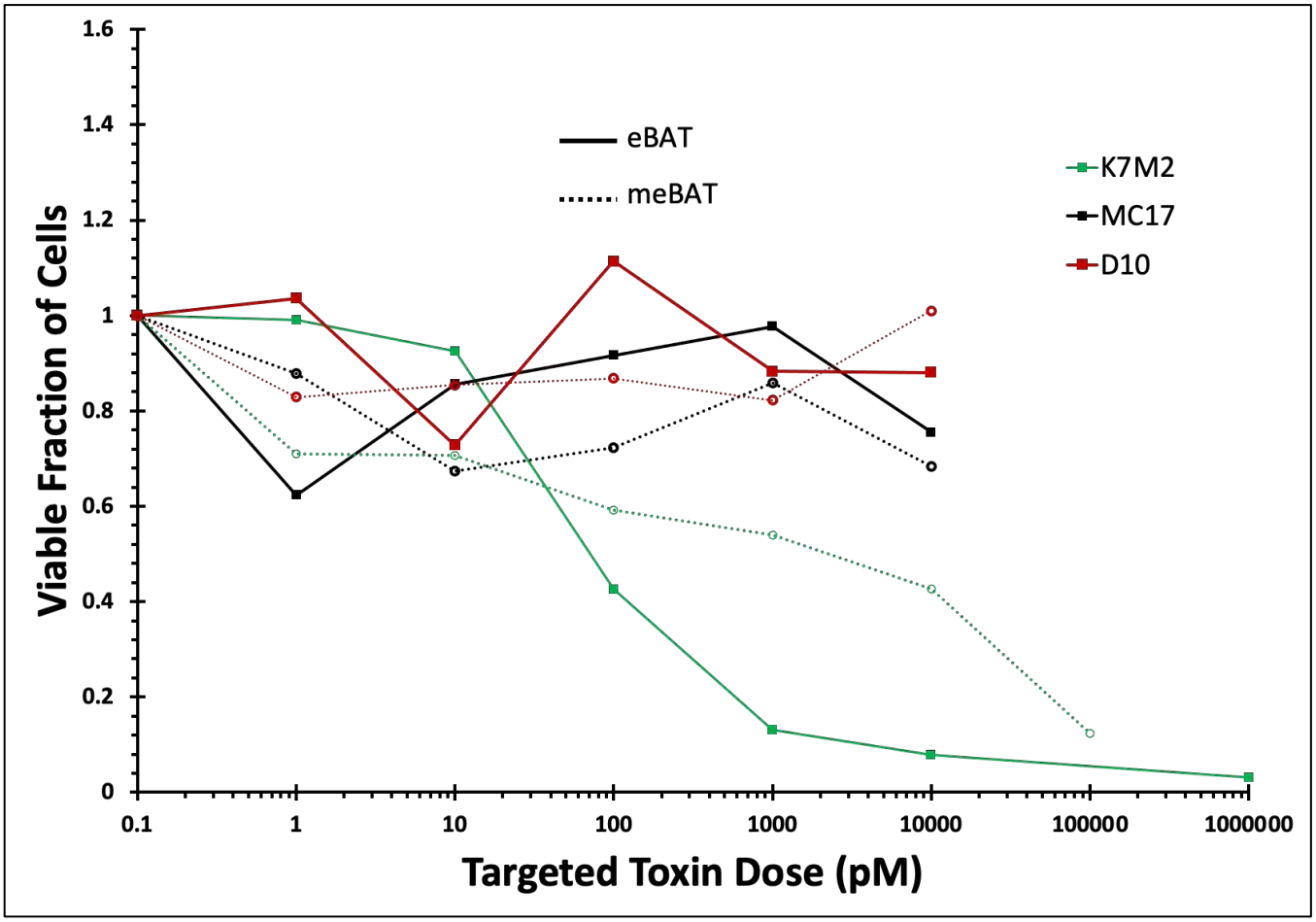

Figure 15. In vitro cytotoxicity of eBAT and meBAT against mouse cells. Graph representing viability from MTS assays as a function of drug dose for mouse K7M2 osteosarcoma cells (green lines), mouse MC17 fibrosarcoma cells (black lines), and mouse D10 uPAR-KO fibrosarcoma cells (red lines) to illustrate the cytotoxic capacity of eBAT (solid lines) and meBAT (dashed lines). Note the remarkable resistance of MC17 and D10 cells to both eBAT and meBAT.

Figure 16

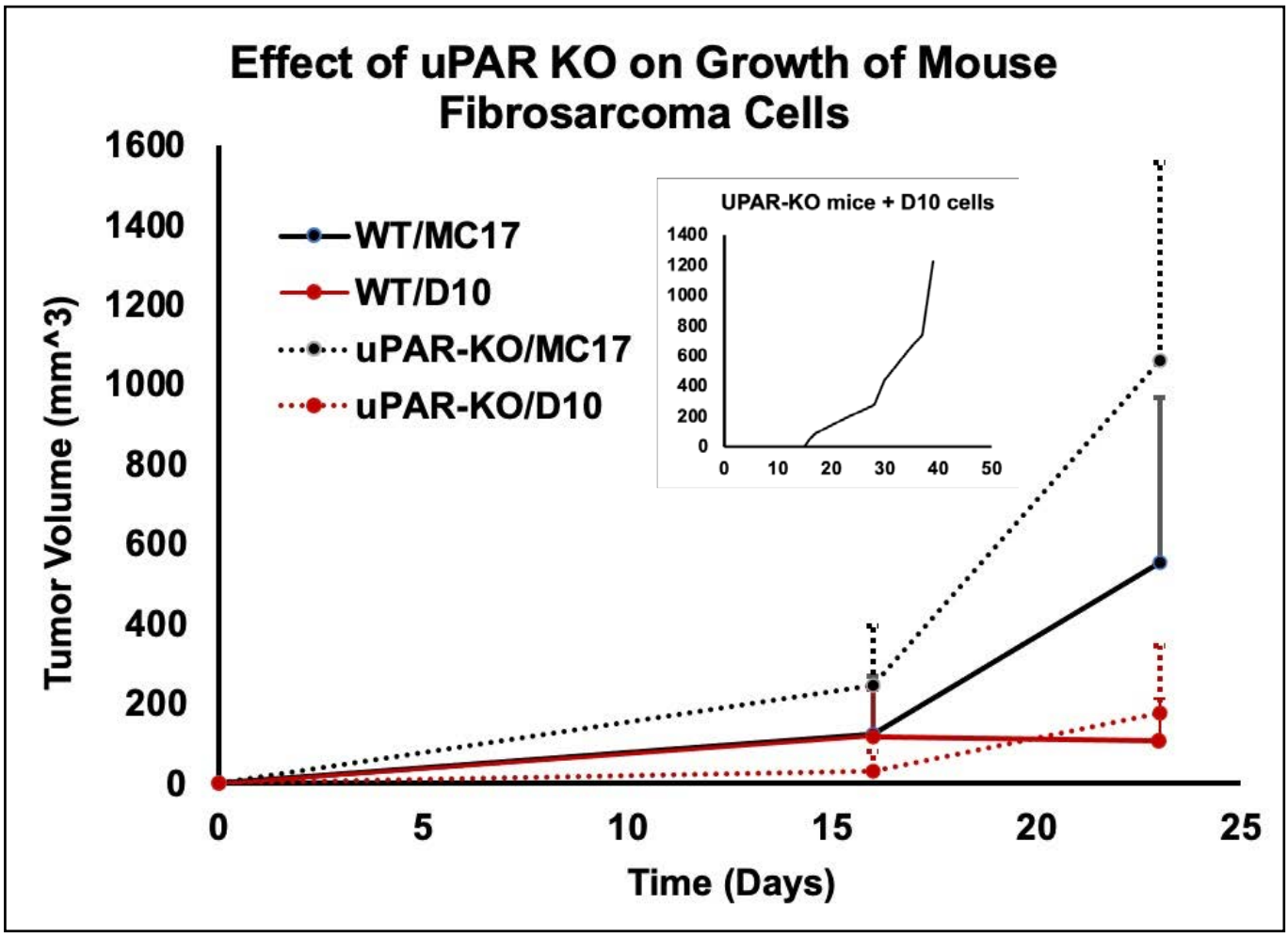

Figure 16. uPAR-KO in tumor cells delays progression but does not abrogate fibrosarcoma formation in WT or uPAR-KO mice. WT MC17 or uPAR-KO D10 cells ($3x10^5$ per mouse) were injected subcutaneously into WT B6 hosts or germ line uPAR-KO B6 hosts. Tumor growth was followed over time. Log growth of the D10 cells was noted starting at Day-28, with tumors, on average, achieving volume of approx. 700-1,200 mm^3 by day 40-47 as shown for uPAR-KO mice (inset).

Figure 17

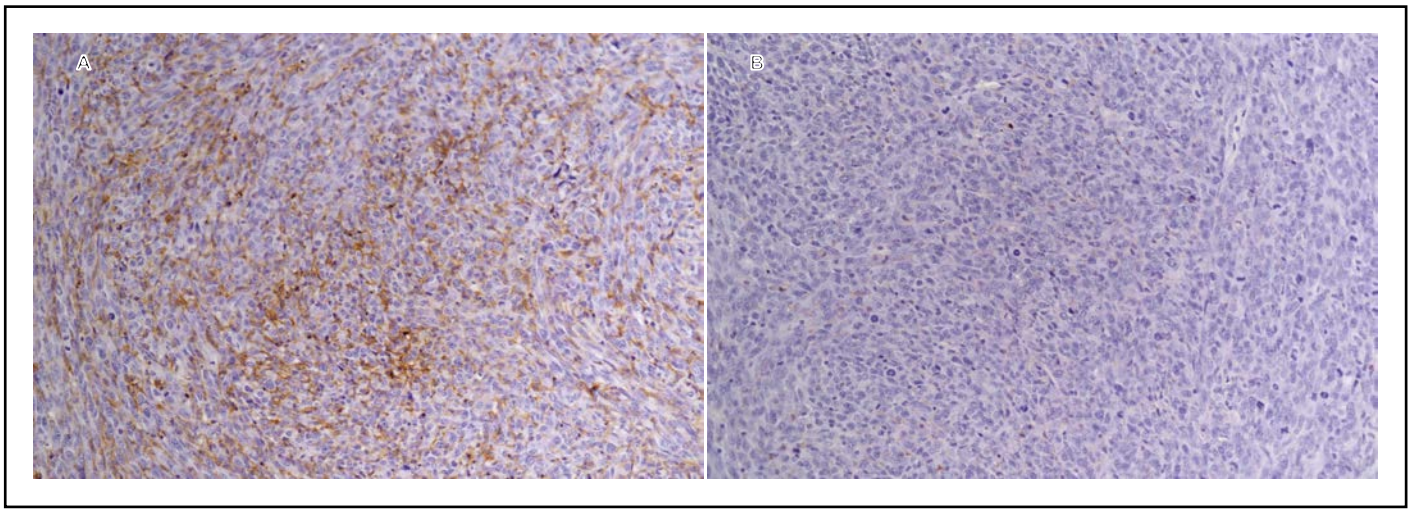

Figure 17. Depletion of F4/80^{+} Immunosuppressive TAMs in mouse sarcoma treated with meBAT. Representative images of sq tumors in B6 recipient mice stained by IHC with antibody F4/80 to document the presence of TAMs (brown staining). Panel **A**: uPAR KO mouse inoculated with $3x10^5$ D10 (uPAR KO) cells and treated with two cycles of meBAT starting on day-16. Panel **B**: WT mouse inoculated with $3x10^5$ WT MC17 cells and treated with two cycles of meBAT starting on day-16. Tumors were harvested at day-28 and day-30, respectively. Note the depletion of TAMs in panel (B) as compared to panel (A). Even though staining in the tumors was variable, decreased F4/80^{+} TAM density was reproducibly observed only in WT mice harboring WT tumors treated with meBAT or eBAT. (Magnification 200x).

Figure 18

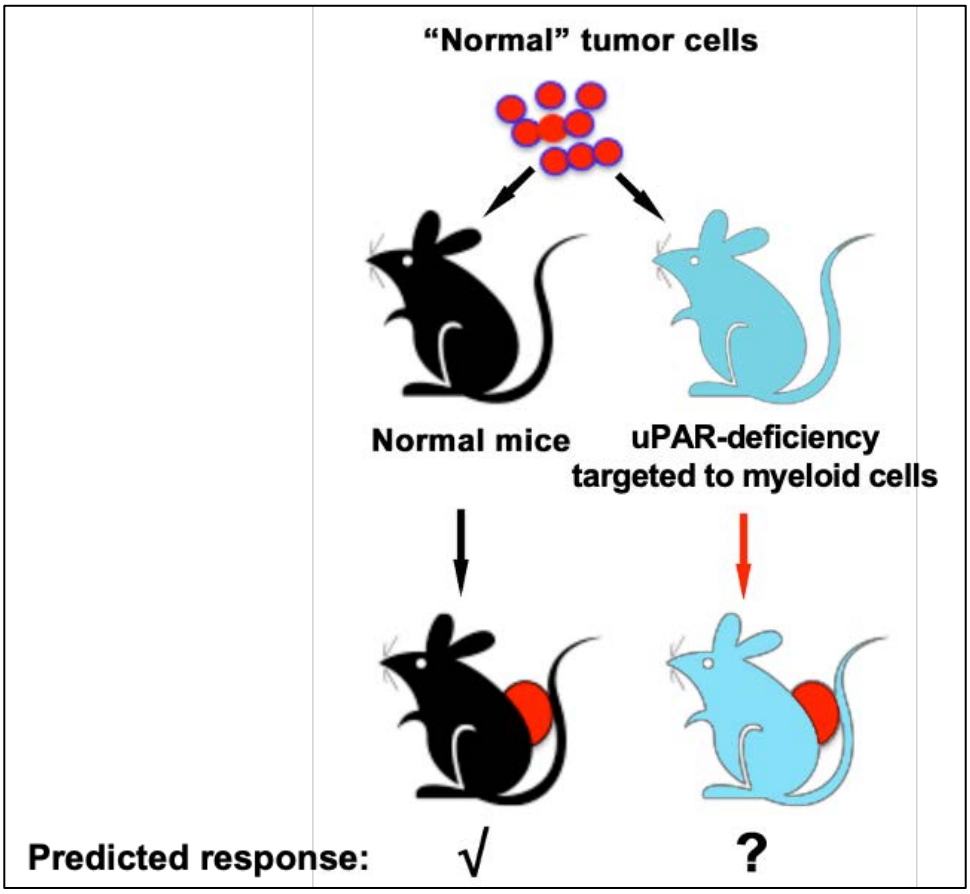

Figure 18. Bone marrow chimeras to test the impact of reshaping the TME. B6 mice that were lethally irradiated and rescued by bone marrow transplantation from WT B6 mice (black) or from B6 uPAR-KO donors (blue) received subcutaneous MC17 implants. Five days after implantation, mice were treated with eBAT, meBAT, or PBS. Tumors (when present) were collected from animals at the endpoint and divided in half for (a) routine pathology and immunohistochemistry, and (b) flow cytometry analysis after disaggregation into single cell suspensions.

Figure 19

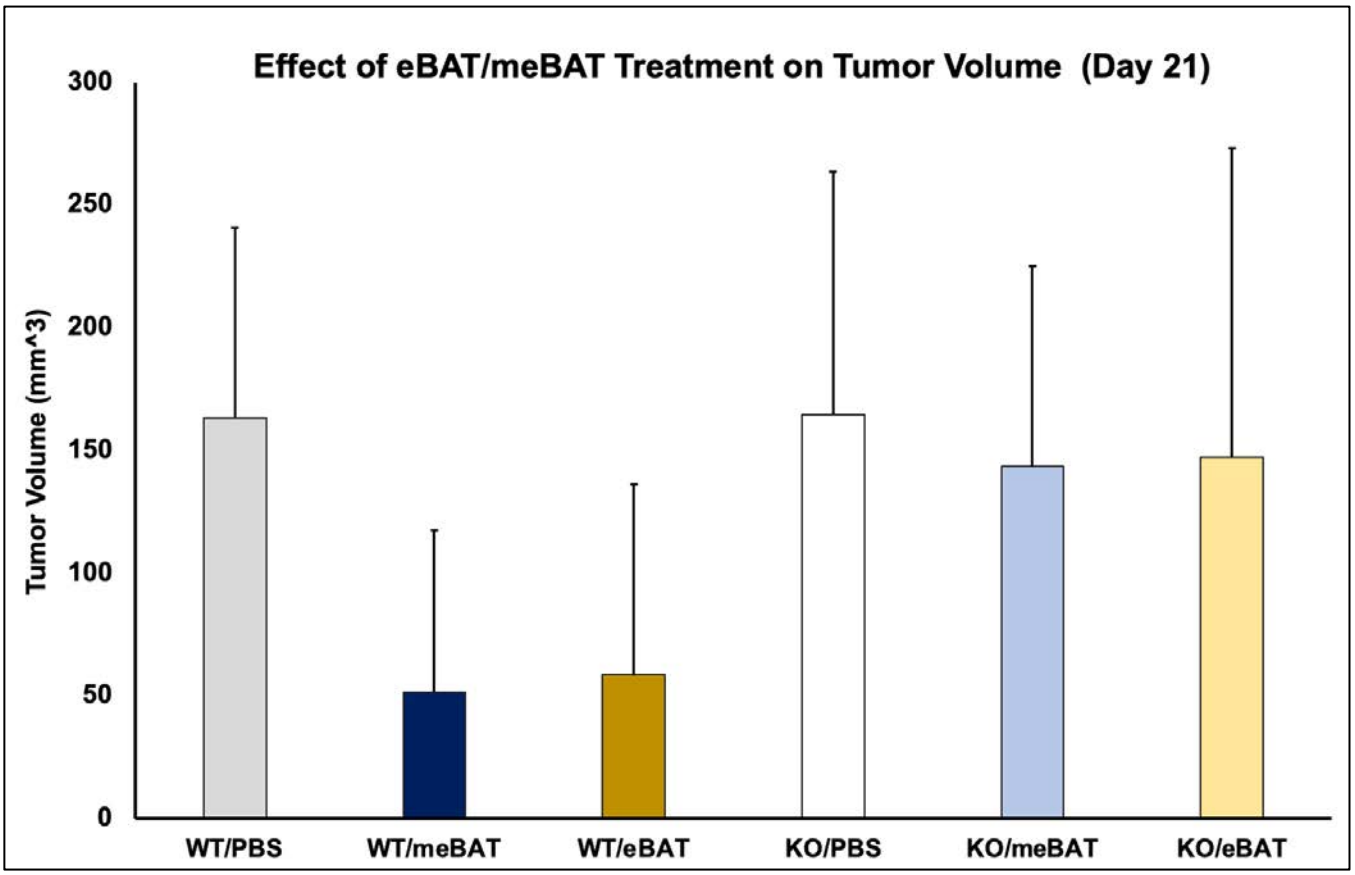

Figure 19. eBAT and meBAT delay growth of MC17 fibrosarcoma in syngeneic mice. Five-week old, WT B6 (CD45.1) mice were lethally irradiated and rescued from death by bone marrow reconstitution using WT (WT) or germline uPAR-KO (KO) B6 (CD45.2) donors. The proportion of CD45.2+ cells in the reconstituted mice was, on average, approx. 75-80%. Three weeks after bone marrow reconstitution, mice were injected subcutaneously with mCherry-labeled MC17 cells, and five days later the mice were treated with phosphate buffered saline (PBS), or with two cycles of meBAT or eBAT. Tumor cells did not engraft in one mouse of the KO/PBS group, but this mouse was still included in the analyses of tumor size and survival. The graph shows tumor volume (in mm^3 ± SD) in mice from the three groups at Day-21 after tumor inoculation.

Figure 20

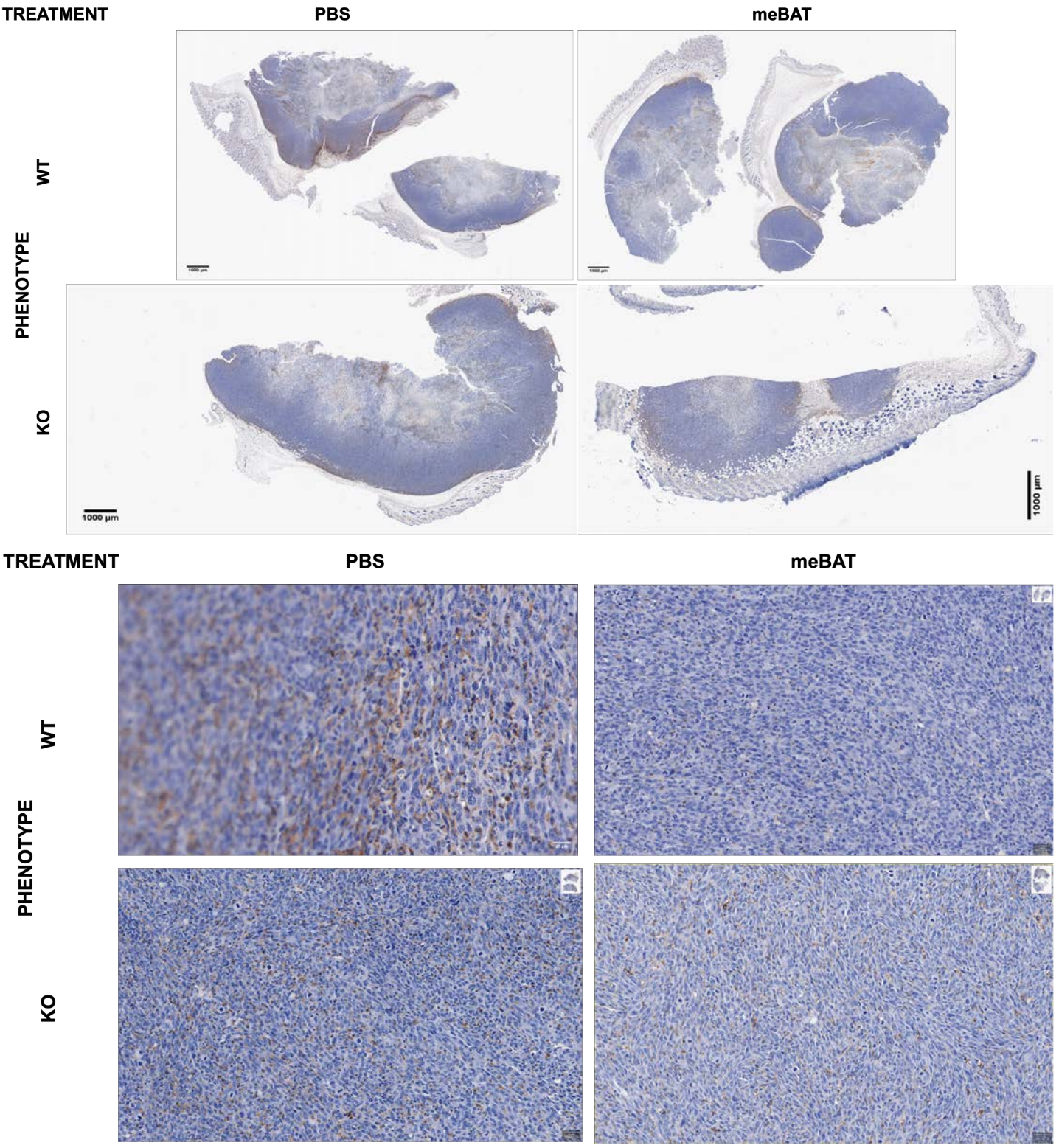

Figure 20. Depletion of TAMS in MC17 tumors by meBAT treatment. Tumors harvested at endpoint from representative mice in the experiment described in Figure 19 were immunostained using antibody F4/80 to quantify infiltrating TAMs. The top four panels in the figure represent low power (40X) images from the tumors. The bottom four panels show higher magnification (200X) images from the tumors stained for F4/80. The quantitative data for the all the tumors and regions analyzed are shown in Table 2.

Figure 21

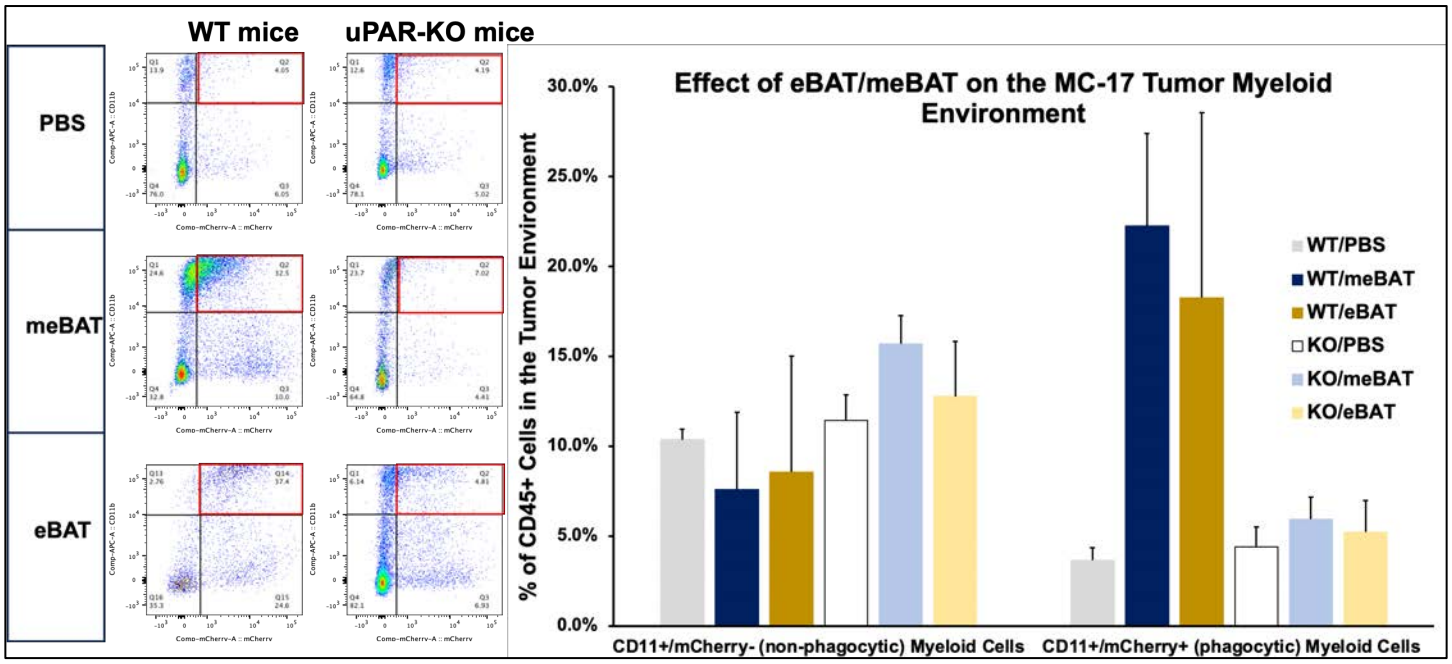

Figure 21. eBAT and meBAT reprogram myeloid cells in the tumor environment to acquire phagocytic phenotypes. Tumors harvested at endpoint from representative mice in the experiment described in Figure 19 were analyzed by flow cytometry to quantify infiltrating $CD11^{+}$ myeloid cells. The panels on the left show representative 2-dimensional flow cytometry dot plots of myeloid cells stained with anti-CD11b and tumor cells expressing mCherry. The red boxes delineate putative phagocytic myeloid cells (CD11b+/mCherry+). The panel on the right shows the quantitative data (% cells in the TME ± SD) for phagocytic (double positive for CD11 and mCherry) and non-phagocytic (single positive for CD11) cells in each group of mice.

Figure 22

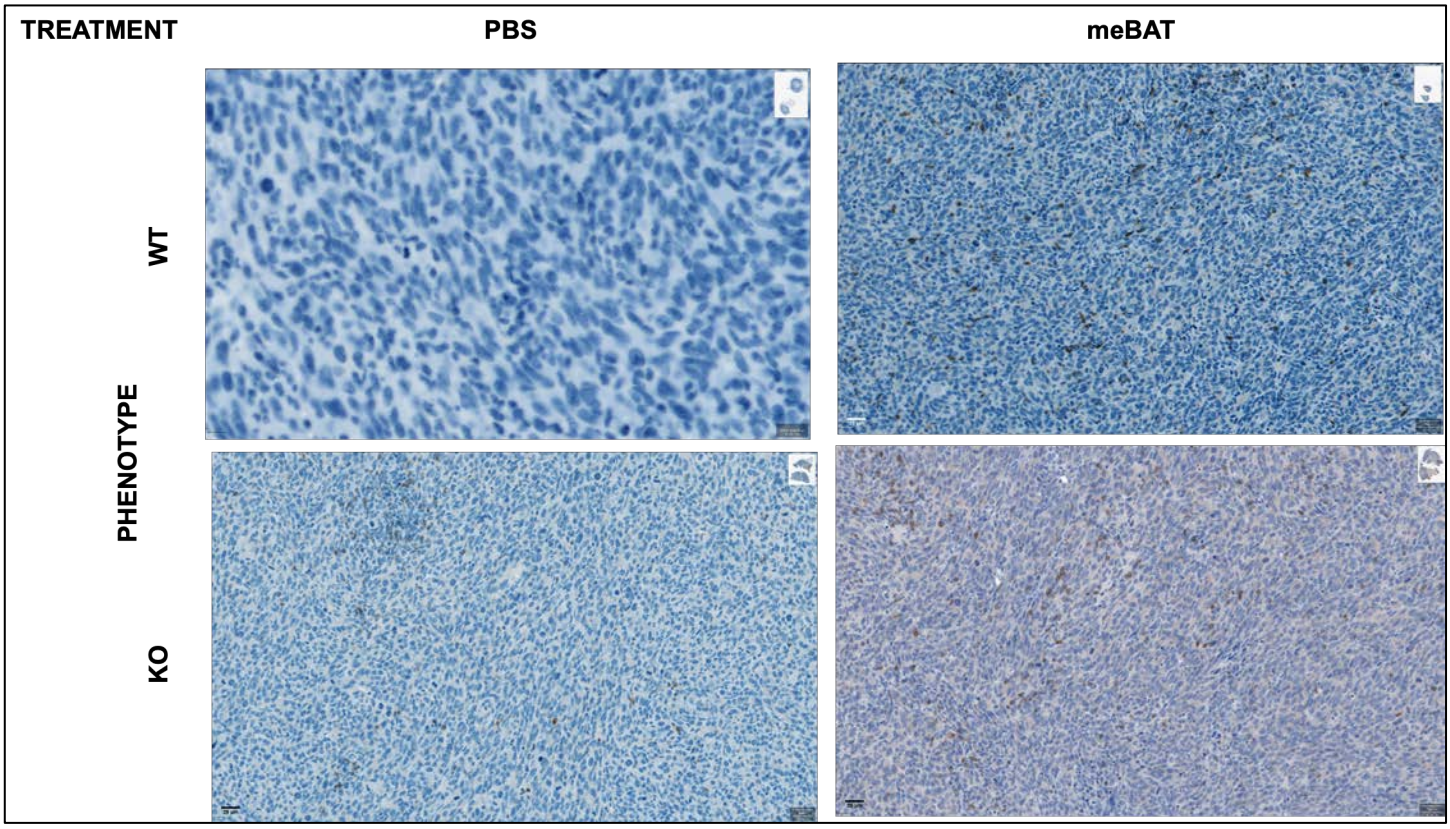

Figure 22. Infiltration of T-cells into MC17 tumors treated with meBAT. Tumors harvested at endpoint from representative mice in the experiment described in Figure 19 were immunostained to assess $CD3^+$ cells in the TME. The panels show high magnification (200X) images from the tumors stained for CD3. Quantitative flow cytometry data are shown in Figure 23.

Figure 23

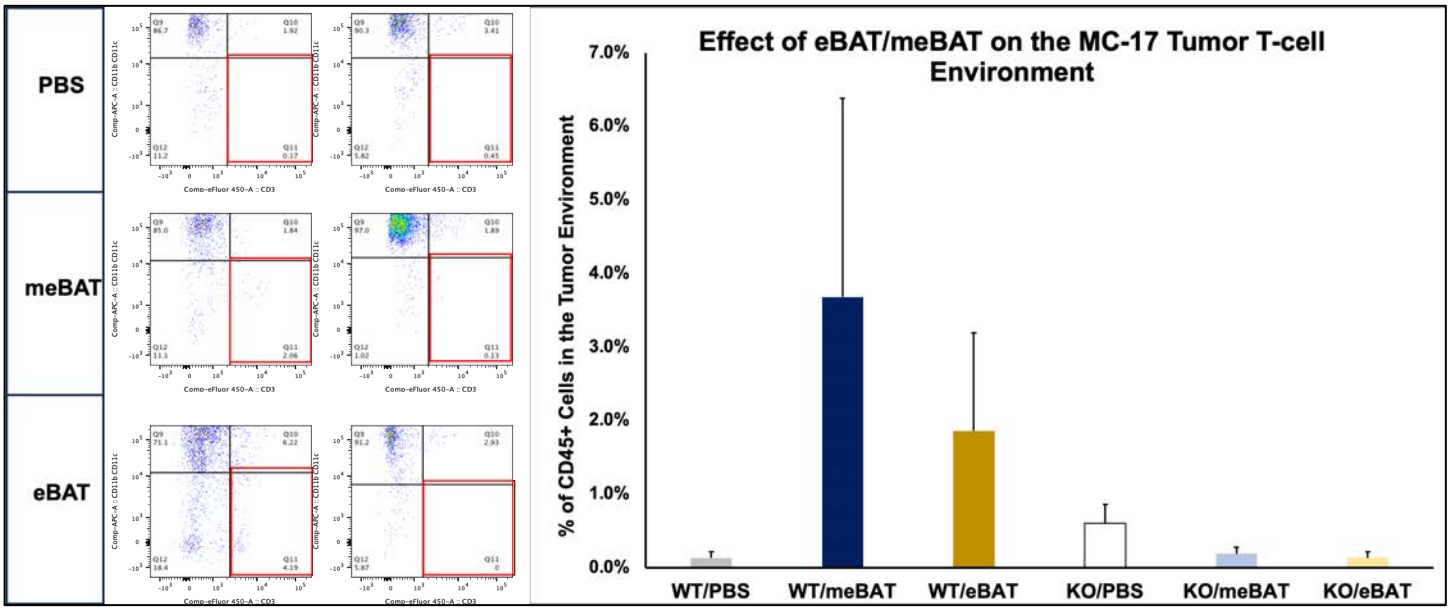

Figure 23. Effect of eBAT and meBAT on the MC17 tumor T-cell environment. Tumors harvested at endpoint from representative mice in the experiment described in Figure 19 were analyzed by flow cytometry to quantify infiltrating T cells. The panels on the left show representative 2-dimensional flow cytometry dot plots of myeloid cells stained with anti-CD11b and anti-CD11c and T cells stained with anti-CD3. The red boxes delineate T cells found in the TME. The panel on the right shows the quantitative data (% cells in the TME ± SD) for $CD3^+$ cells in each group of mice.

Figure 24

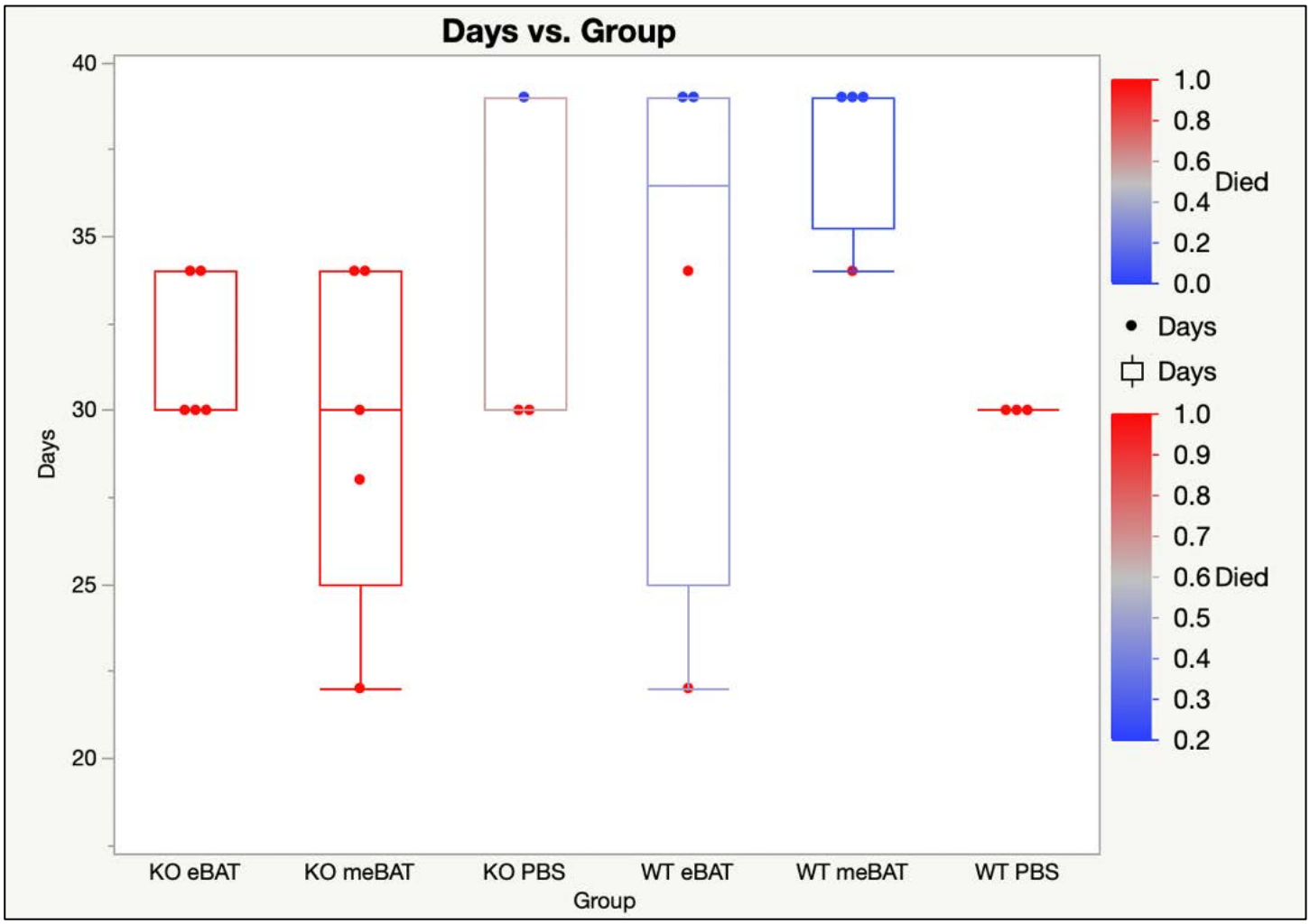

Figure 24. eBAT and meBAT improve survival of mice harboring MC17 tumors. The groups of mice described in Figure 19 were followed to endpoint. This box and whisker plot shows survival outcomes for all groups, with individual animals denoted by red dots (dead) or blue dots (alive at the end of the experiment). Only the mouse that did not engraft with tumor in the KO/PBS group and mice in the WT/meBAT and WT/eBAT groups survived longer than 34 days. The mice were sacrificed at Day-40 to maximize the probability that changes in the TME attributable to meBAT or eBAT treatment would still be detectable.

Figure 25

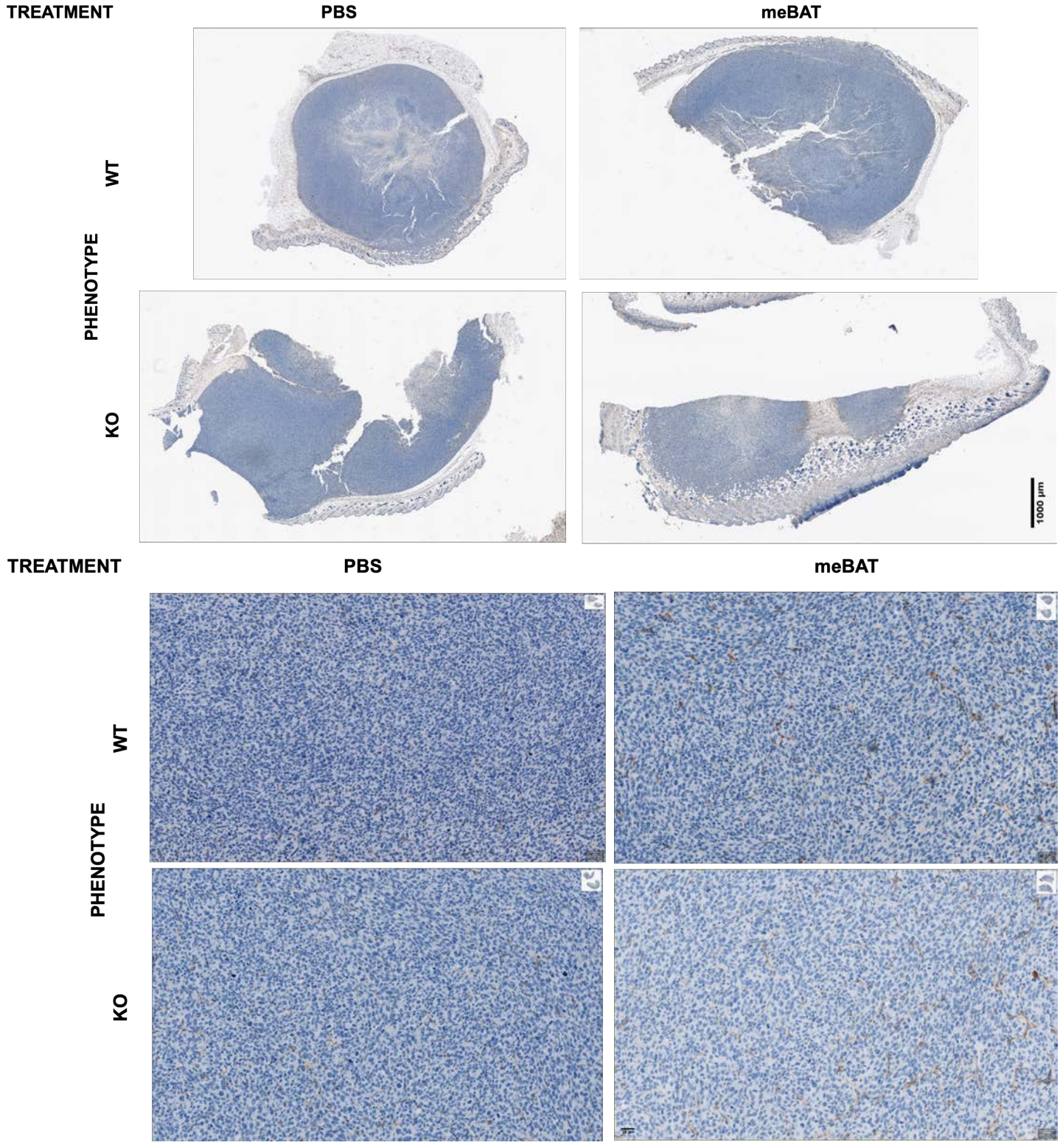

Figure 25. eBAT and meBAT do not affect microvascular density of MC17 tumors. Tumors harvested at endpoint from representative mice in the experiment described in Figure 19 were immunostained using anti-CD31 to quantify microvessel density. The top four panels in the figure represent low power (40X) images from the tumors. The bottom four panels show higher magnification (200X) images from the tumors stained with anti-CD31. The quantitative data for the all the tumors and regions analyzed are shown in Table 3.

Figure 26

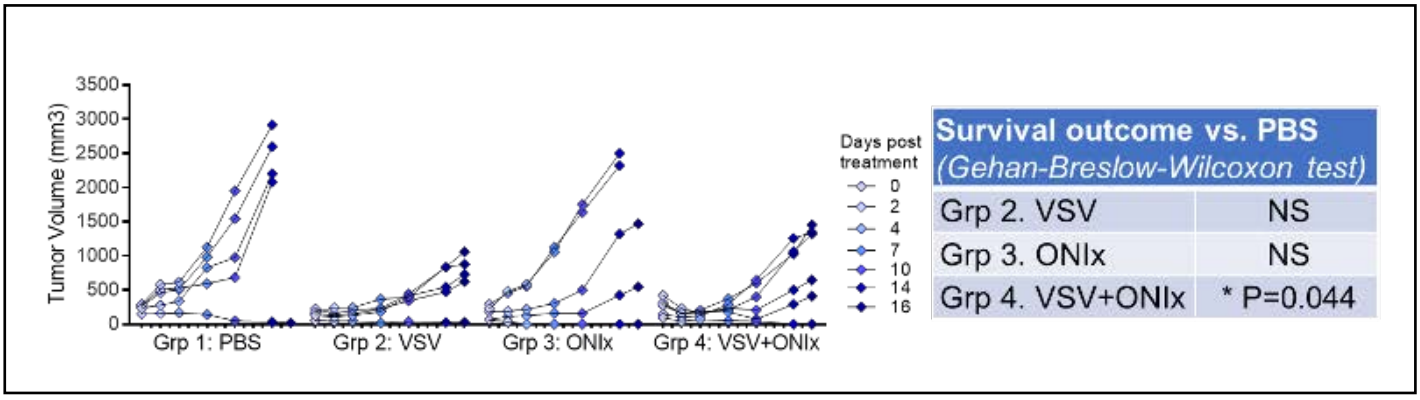

Figure 26. VSV and P-DIC combination treatment induces tumor remission in a Balb/c tumor model. Mice were injected with A20 lymphoma cells, and once visible tumors arose, they were treated with PBC (control), VSV alone, ONIx alone, or VSV + ONIx. The spider plots show tumor growth for individual mice in each group.

Figure 27

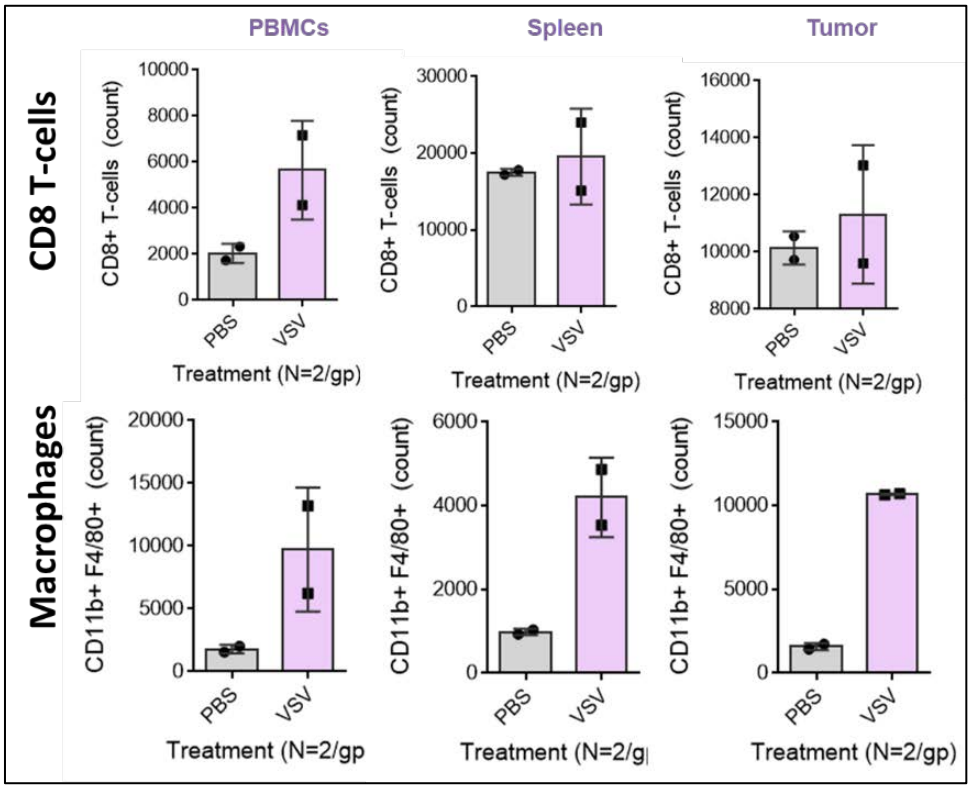

Figure 27. VSV treatment induces and increases presence of immune cells in tumors and systemically. PBMCs, spleens, and tumors were harvested from the mice at the time of sacrifice and the presence of CD8 T-cells and tumor-associated macrophages was established using flow cytometry.

Figure 28

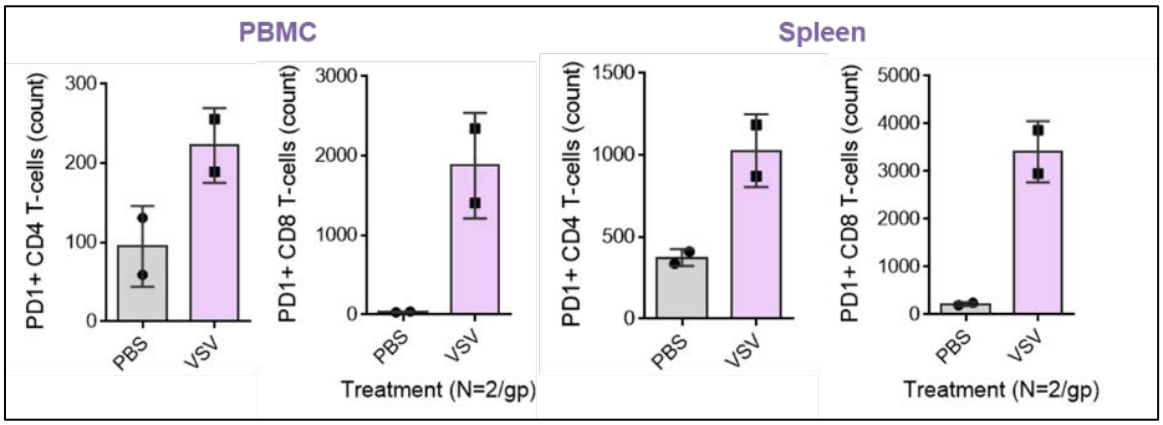

Figure 28. Increased PD-1 expression on T-cells in tumor and spleen following VSV treatment. PBMCs and spleens obtained as in Figure 27 were evaluated for CD4 T-cell activation and potential exhaustion based on expression of PD-1 using flow cytometry.

Figure 29

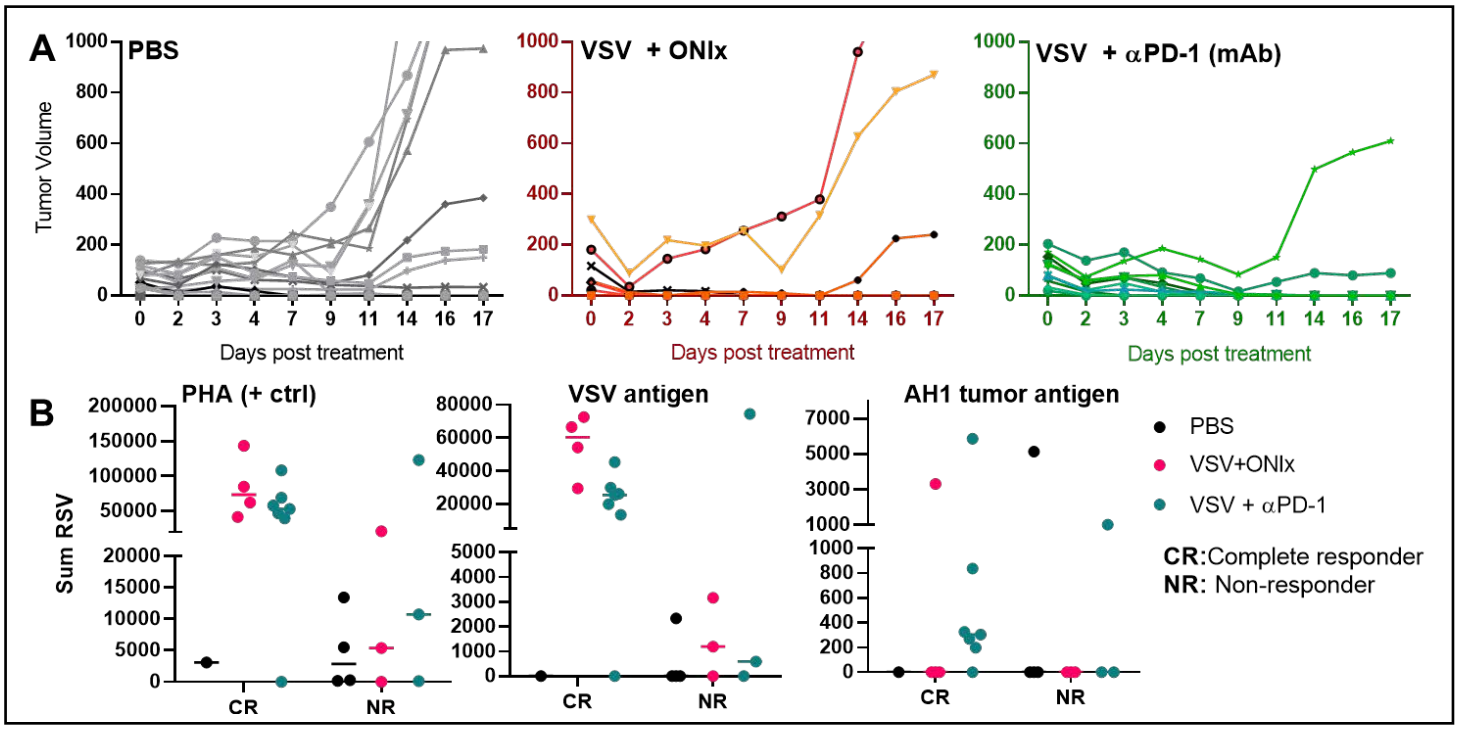

Figure 29. Immunomodulatory effects of VSV and CPI combination therapy in the A20 murine lymphoma model. Mice with established subcutaneous A20 murine lymphoma tumors were treated with $5x10^8$ VSV-mIFN-NIS in combination with 6 doses of 5mg/kg ONIx or 200ug αmPD-1 antibody. (A) Therapeutic response was assessed by measurement of tumor volume by serial caliper measurements. (B) Mice were monitored to designate complete responders (CR) and non-responders (NR). Mice were euthanized and spleens were collected. Splenocytes were analyzed by ELISPOT to detect T-cell response against assessed PHA (Lectin, positive control), VSV antigen peptides, and the MHC-I specific AH1 tumor associate antigen peptide.

Figure 30

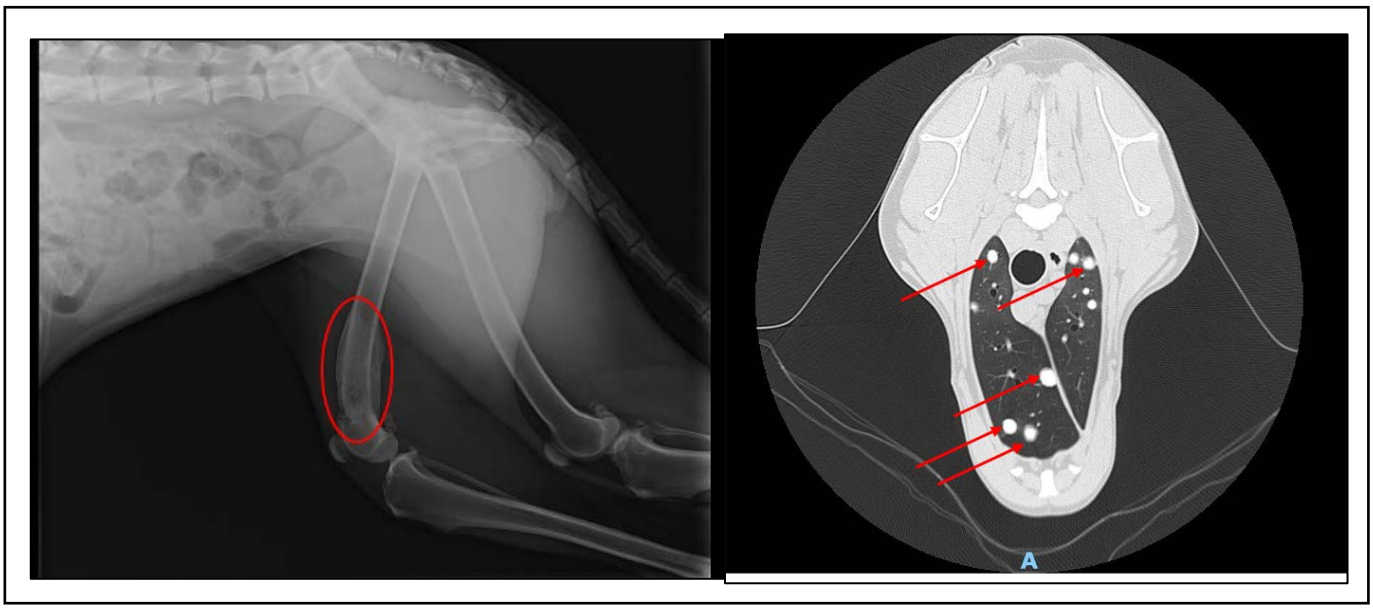

Figure 30. Imaging studies of the index canine patient for the METEOR study. The left panel shows a left lateral radiograph of the hind limbs showing a large area of soft tissue swelling, periosteal reaction, and cortical bony lysis in the distal left femur (red circle). The right panel shows a computed tomography image through the chest, including the lung cavity. Multiple opaque nodules, representing calcified tumor metastasis, are visible in this image (red arrows).

Figure 31

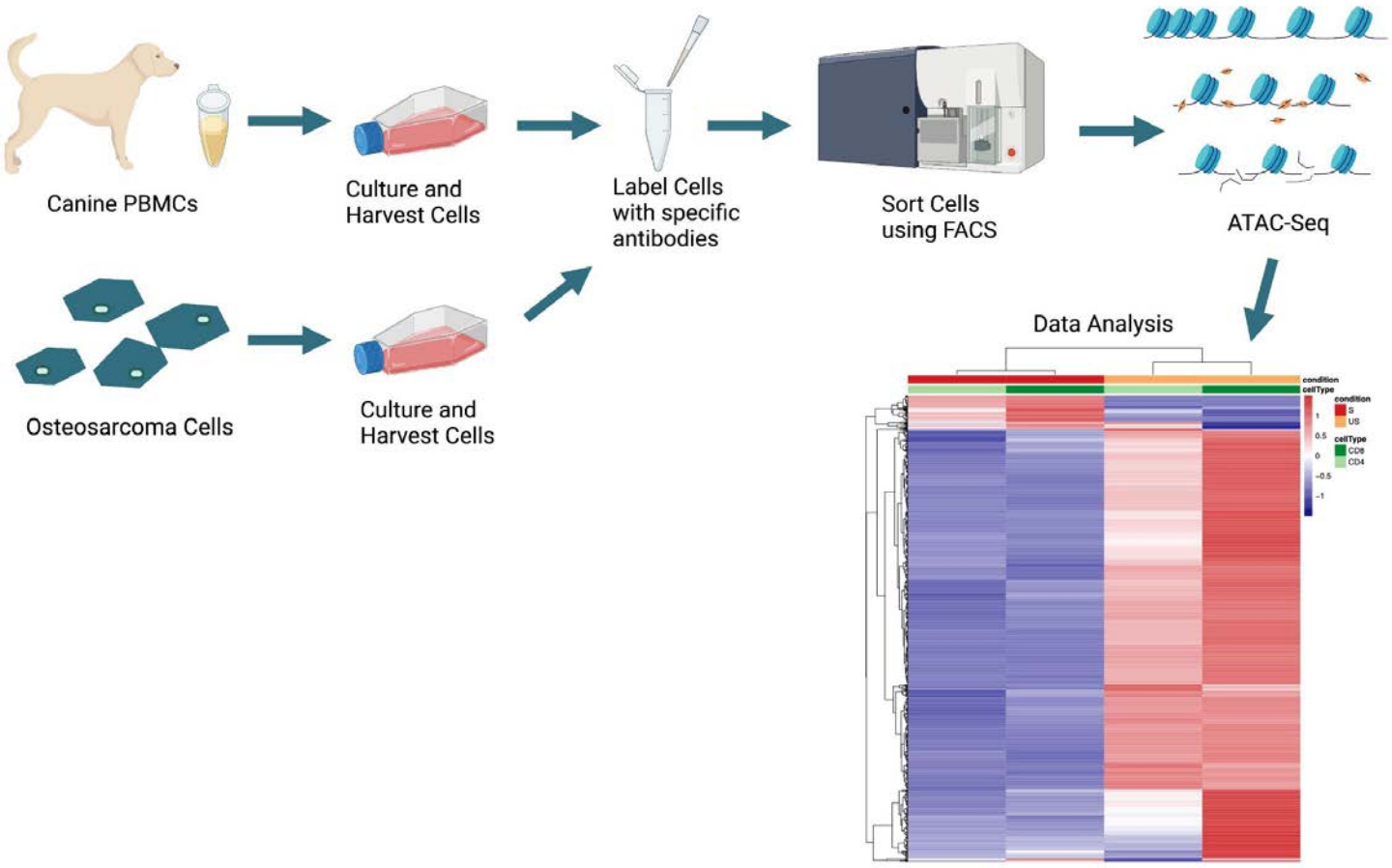

Figure 31. Graphical illustration of experiments designed to evaluate chromatin accessibility in canine T cells and canine osteosarcoma cells. Canine peripheral blood mononuclear cells (PBMCs) and canine osteosarcoma cell lines are being used for these experiments. PBMCs are enriched from peripheral blood, set up in parallel cultures with no stimulation or stimulated by mitogens, and at the peak of activation, CD4 and CD8 T cells are further enriched by fluorescence activated cell sorting (cell purity >98%). These cells, and cultured osteosarcoma cells are subjected to ATAC-seq to assess chromatin accessibility. The heat map illustrates data from our initial experiment, showing that unique patterns of open chromatin are found in both cell types under resting and stimulated conditions.

Figure 32

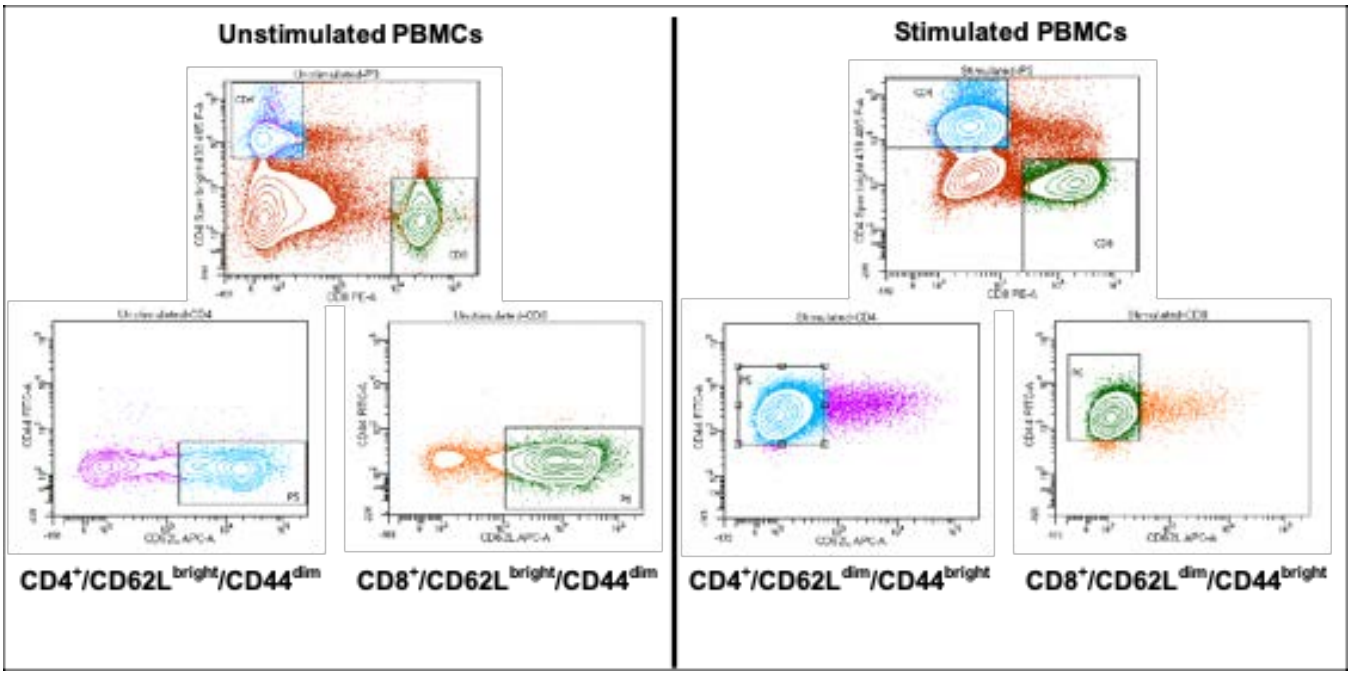

Figure 32. Example of cell sorting for resting (unstimulated) and activated (stimulated) canine $CD4^+$ and $CD8^+$ T cells. A B. PBMCs were isolated from whole blood from a normal healthy dog and cultured without mitogenic stimulation (unstimulated) or in the presence of PMA (10 ng/ml) and ionomycin (500 nM) for 72 hours. At the end of the culture period, cells were stained with antibodies recognizing canine CD4, CD8, CD44, and CD62L. Sorting for resting ($CD44^{dim}/CD62L^{bright}$) and for activated ($CD44^{bright}/CD62L^{dim}$) cells was done using a FACSAria cell sorter. $CD4^+$ cells are tracked in blue color and $CD8^+$ cells are tracked in green color.

Figure 33

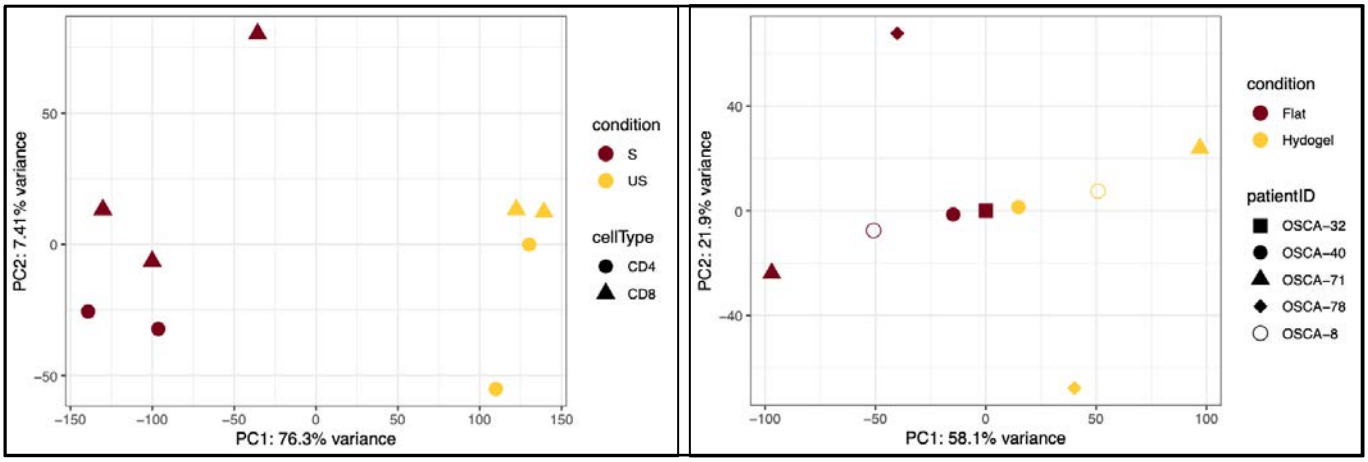

Figure 33. Principal component analysis of ATAC-seq data from sorted canine T-cells and from cultured osteosarcoma cells. ATAC-seq data were analyzed by PCA. The left panel shows PCA data for nine samples of canine T cells obtained from three dogs. Paired, resting (unstimulated, or US) and activated (stimulated of S) $CD4^+$ and $CD8^+$ cells were sorted from two dogs. Only stimulated CD8 cells generated enough material for preparation of high quality DNA for ATAC-seq from the third dog. The data show that the largest separation along the first principal component was dependent on the activation state of the T cells, with some degree of separation occurring along the second component, related to the phenotype of the cells. The right panel shows PCA data for samples of five osteosarcoma cell lines cultured in 2-dimensions using plastic dishes or in 3-dimensions using a hydrogel matrix. The data show that the largest separation along the first principal component was dependent on the culture conditions, but unlike the T cells, where the equivalent CD4 and CD8 cells from different dogs had similar distribution along the PCA plot, the osteosarcoma cells were all distinctly different, indicative of the transcriptional heterogeneity (chromatin states) that characterizes these tumors.

Figure 34

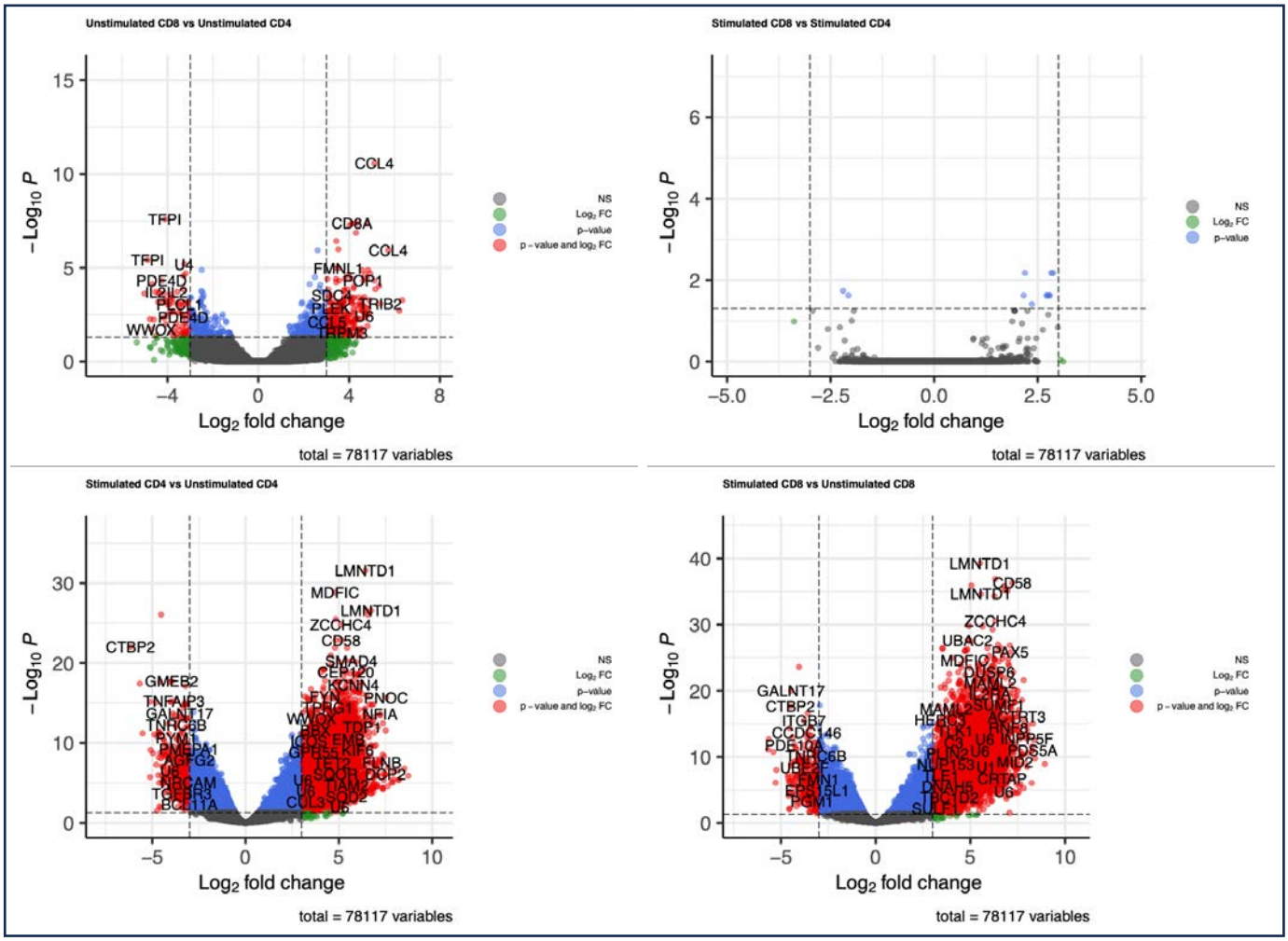

Figure 34. Volcano plots showing enrichment of differentially accessible (open) chromatin regions in resting and activated canine T cells. The top left panel shows enrichment of accessible chromatin regions, labeled using the nearest protein coding gene, between resting (unstimulated) CD4 and CD8 T cells. Dots (DA regions denoted by the closest gene) on the positive X-axis are enriched in $CD8^+$ T cells and dots on the negative X-axis are enriched in $CD4^+$ T cells. The top right panel shows enrichment of accessible chromatin regions, labeled using the nearest protein coding gene, between activated (stimulated) CD4 and CD8 T cells. Dots on the positive X-axis are enriched in $CD8^+$ T cells and dots on the negative X-axis are enriched in $CD4^+$ T cells. The bottom left panel shows enrichment of accessible chromatin regions, labeled using the nearest protein coding gene, between resting (unstimulated) and activated (stimulated) CD4 T cells. Dots on the positive X-axis are enriched in activated $CD4^+$ T cells and dots on the negative X-axis are enriched in resting $CD4^+$ T cells. The bottom right panel shows enrichment of accessible chromatin regions, labeled using the nearest protein coding gene, between resting (unstimulated) and activated (stimulated) CD8 T cells. Dots on the positive X-axis are enriched in activated $CD8^+$ T cells and dots on the negative X-axis are enriched in resting $CD8^+$ T cells.

Figure 35

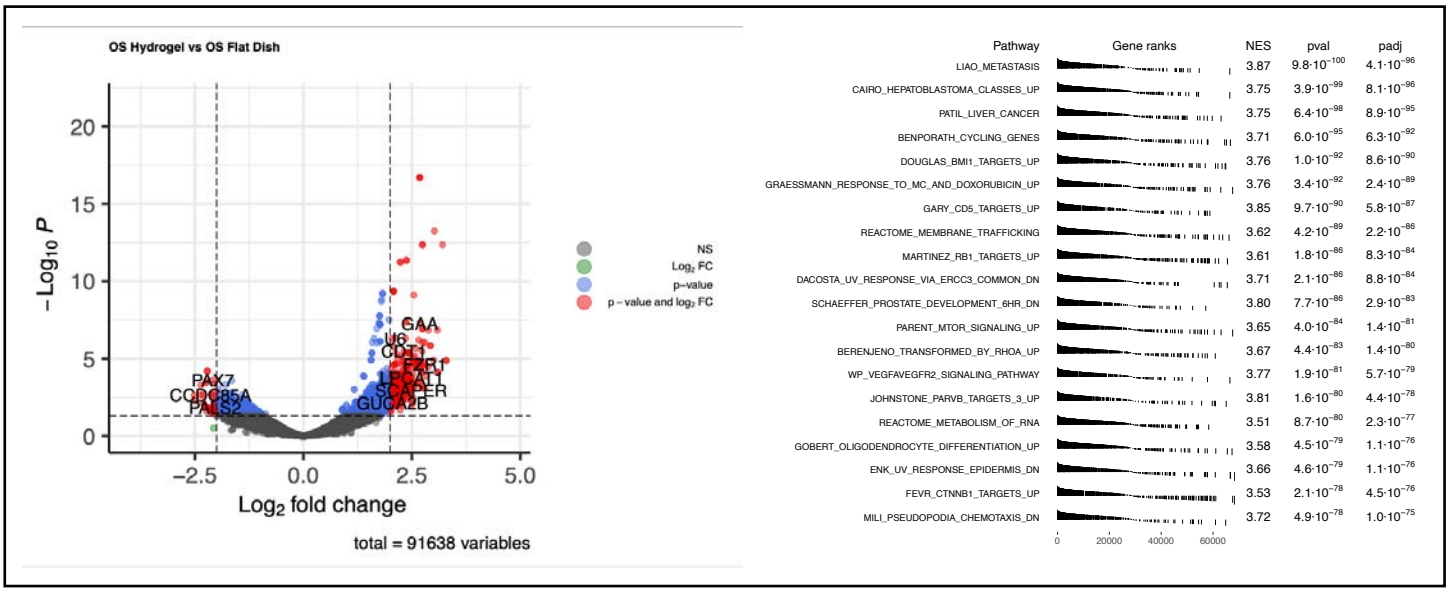

Figure 35. Volcano plots showing enrichment of differentially accessible (open) chromatin regions in osteosarcoma cells grown in 2-dimensional and 3-dimensional culture conditions. The left panel shows enrichment of accessible chromatin regions, labeled using the nearest protein coding gene, between osteosarcoma cells cultured in 3-dimensional hydrogels and in 2-dimensional plastic dishes. Dots (DA regions denoted by the closest gene) on the positive X-axis are enriched in cells grown in 3-dimensional culture and dots on the negative X-axis are enriched in cells grown in 2-dimensional culture. The right panel shows enrichment of functional pathways identified using GSEA.

Figure 36

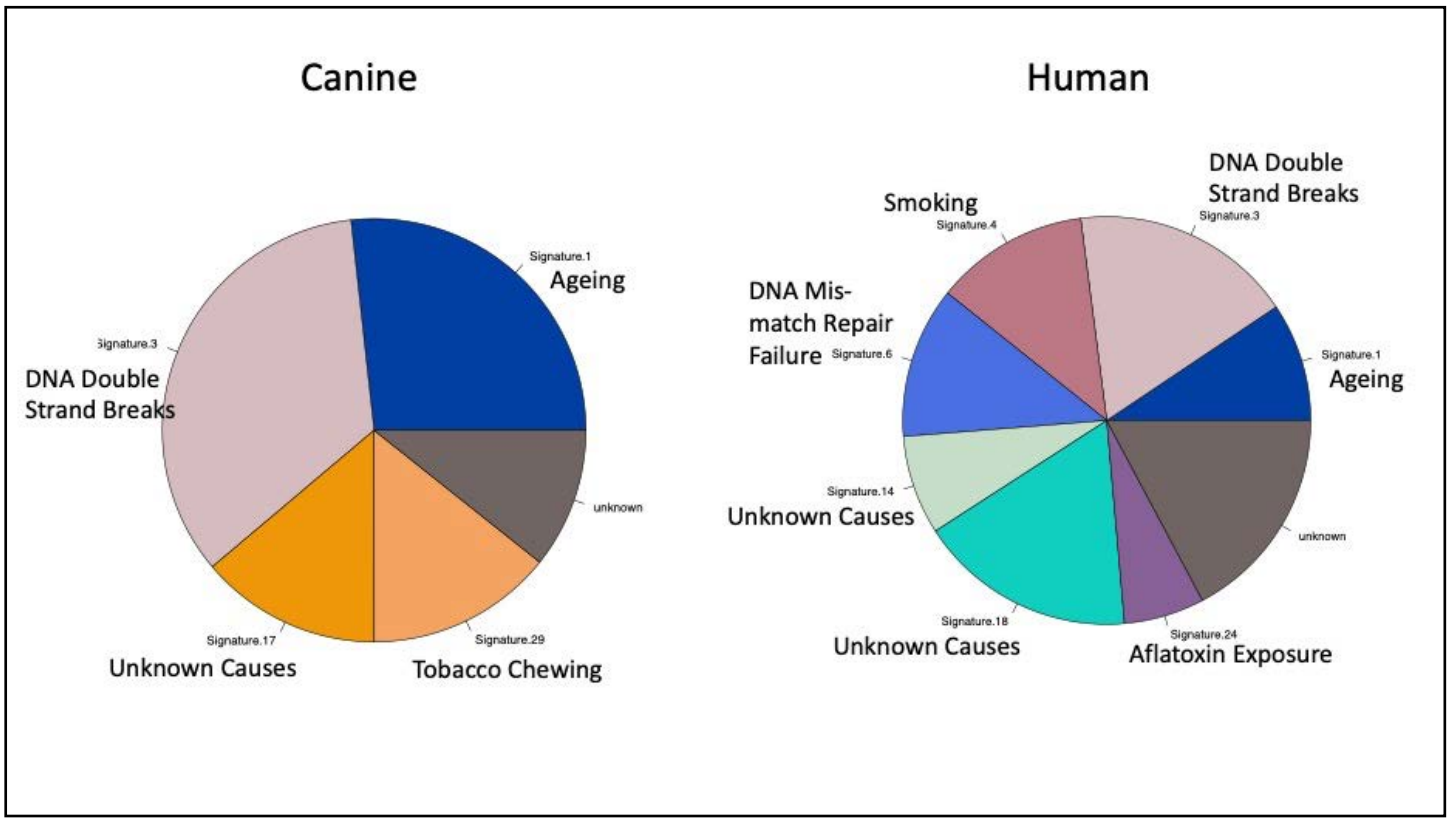

Figure 36. Cosmic signatures describing inferred mutational mechanisms in human and canine osteosarcoma. Whole exome sequencing data were analyzed to uncover the context of recurrent mutations and infer potential mechanisms leading to such mutations in osteosarcoma samples from dogs and humans. The data show that COSMIC signatures 1 (cellular “aging”) and 3 (DNA double strand breaks) putatively account for more than of the mutations seen in canine osteosarcoma, but they only account for about 25% of the mutations in human osteosarcoma. These are also the only COSMIC signatures shared between both species, suggesting that independent, likely unrelated events are responsible for the mutational patterns seen in 75% of human osteosarcomas and about one third of canine osteosarcomas.

Figure 37

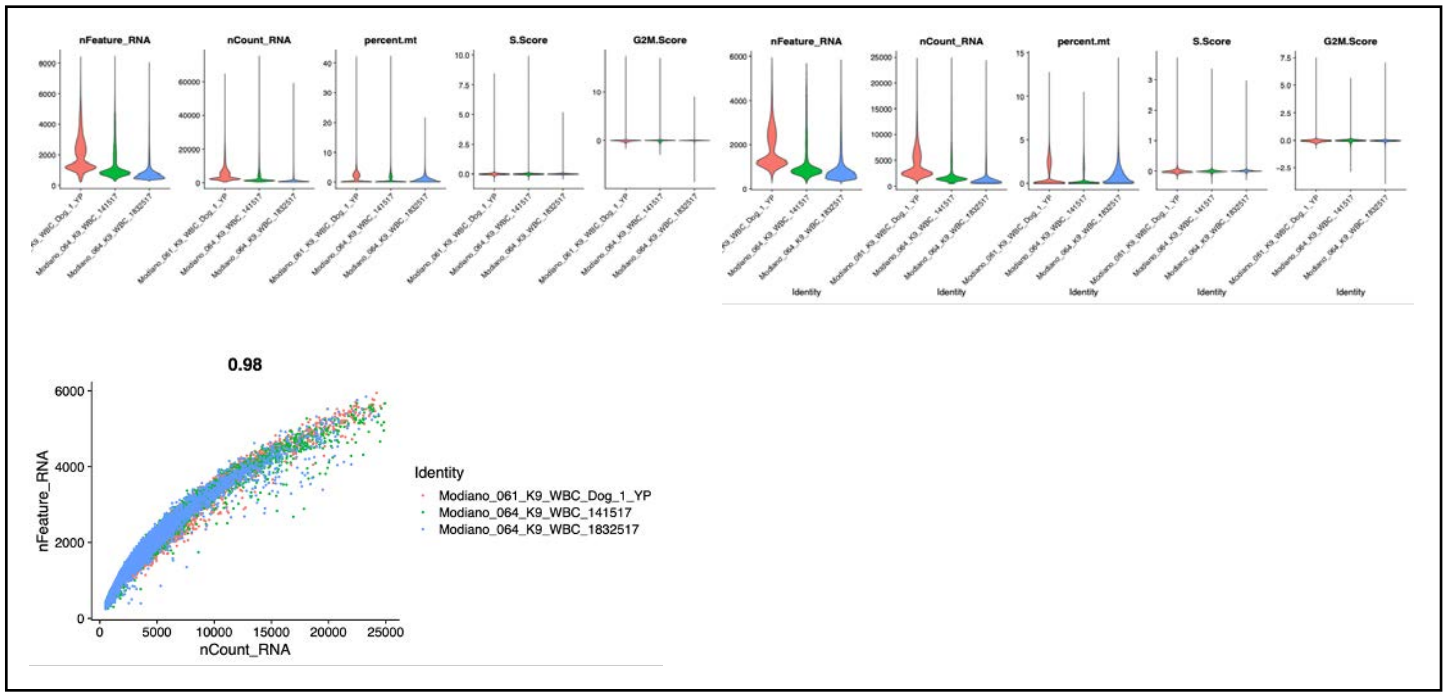

Figure 37. Quality control metrics for peripheral blood leukocyte single cell sequencing data. **Top left panel**: Violin plot showing quality control data prior to filtering dead cells and duplicates in three independent samples of canine peripheral blood leukocytes. The graphs show the distributions of number of genes detected per cell (nFeature_RNA), number of unique transcript molecules detected per cell (nCount_RNA), percent mitochondrial reads per cell (percent.mt), DNA synthesis scores for cells predicted to be in the S phase of the cell cycle ("S.Score"), and G2M phase scores ("G2M.score"), for cells predicted to be in the G2 and M (mitosis) phases of the cell cycle. **Top right panel**: Violin plot showing quality control data after filtering dead cells and duplicates in the same three samples of canine peripheral blood leukocytes. The individual graphs show the same parameters as the top panel. **Bottom left panel**: Scatterplot showing the highly positively correlated relationship between the number of transcripts detected and number of genes detected in the three independent samples.

Figure 38

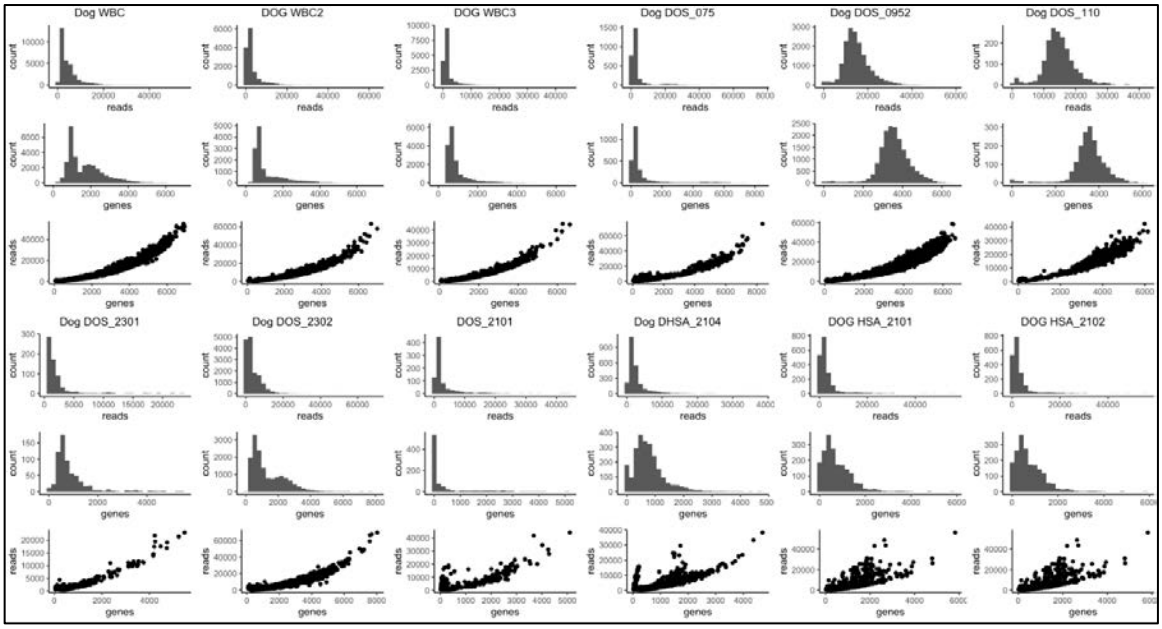

Figure 38. Graphical representation of transcript counts as a function of reads, transcript counts as a function of genes, and reads as a function of genes for the WBC, OS cells, OS tissues, and splenic samples after thresholding to remove dead cells.

Figure 39

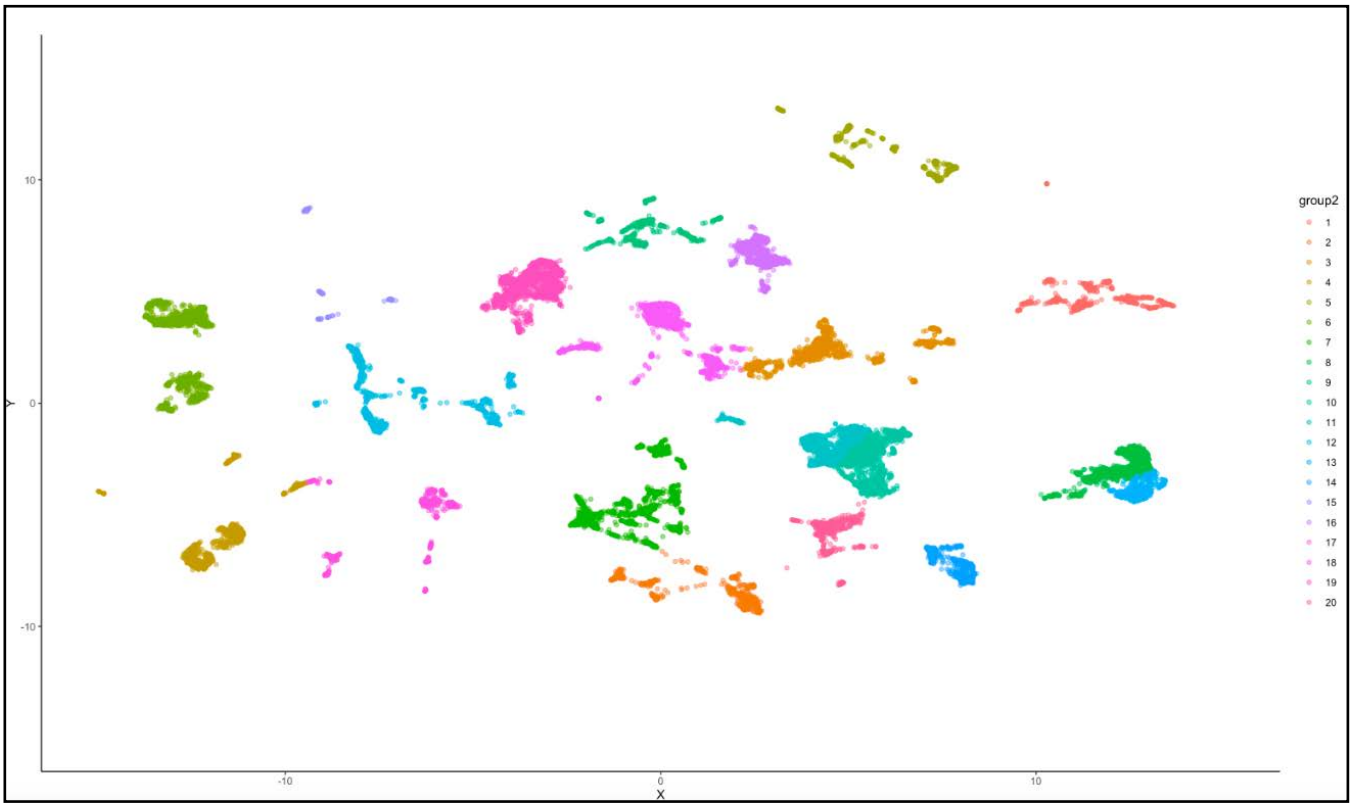

Figure 39. UMAP plot of single-cell data from 12 canine samples. The thresholded data for live cells shown in Figure 35 was used to create this UMAP visualization with 20 clusters, through K-means clustering, for the WBCs, OS cells, OS tissues, and splenic samples.

Figure 40

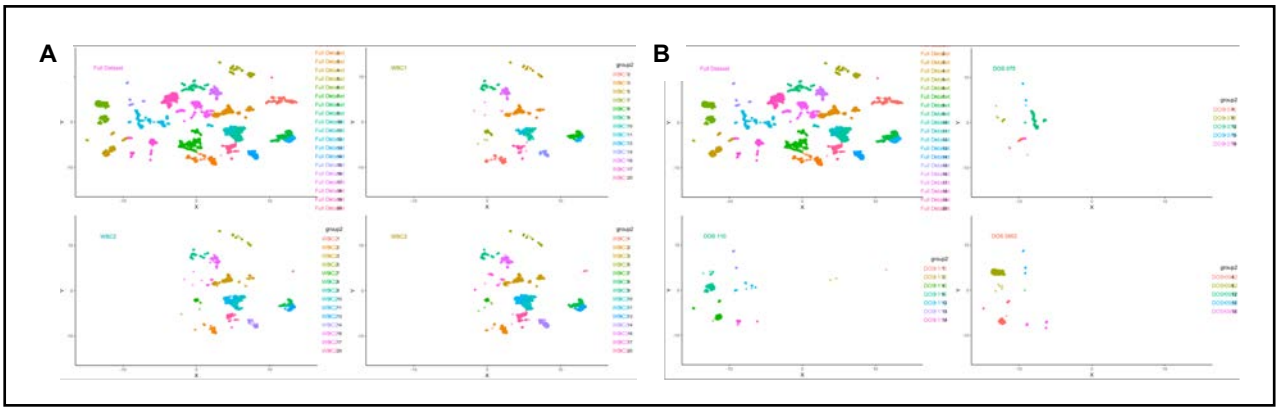

Figure 40. Distribution of clusters from the WBC and the OS cell samples on the UMAP plot. **(**A): Representation of the UMAP plot including all of the samples (top left) next to the three individual WBC samples. Note the similarity in the location of clusters found in each sample. (B): Representation of the UMAP plot including all of the samples (top left) next to the three individual OS cell samples. Note the remarkably dissimilarity in the location of clusters found in each sample.

Figure 41

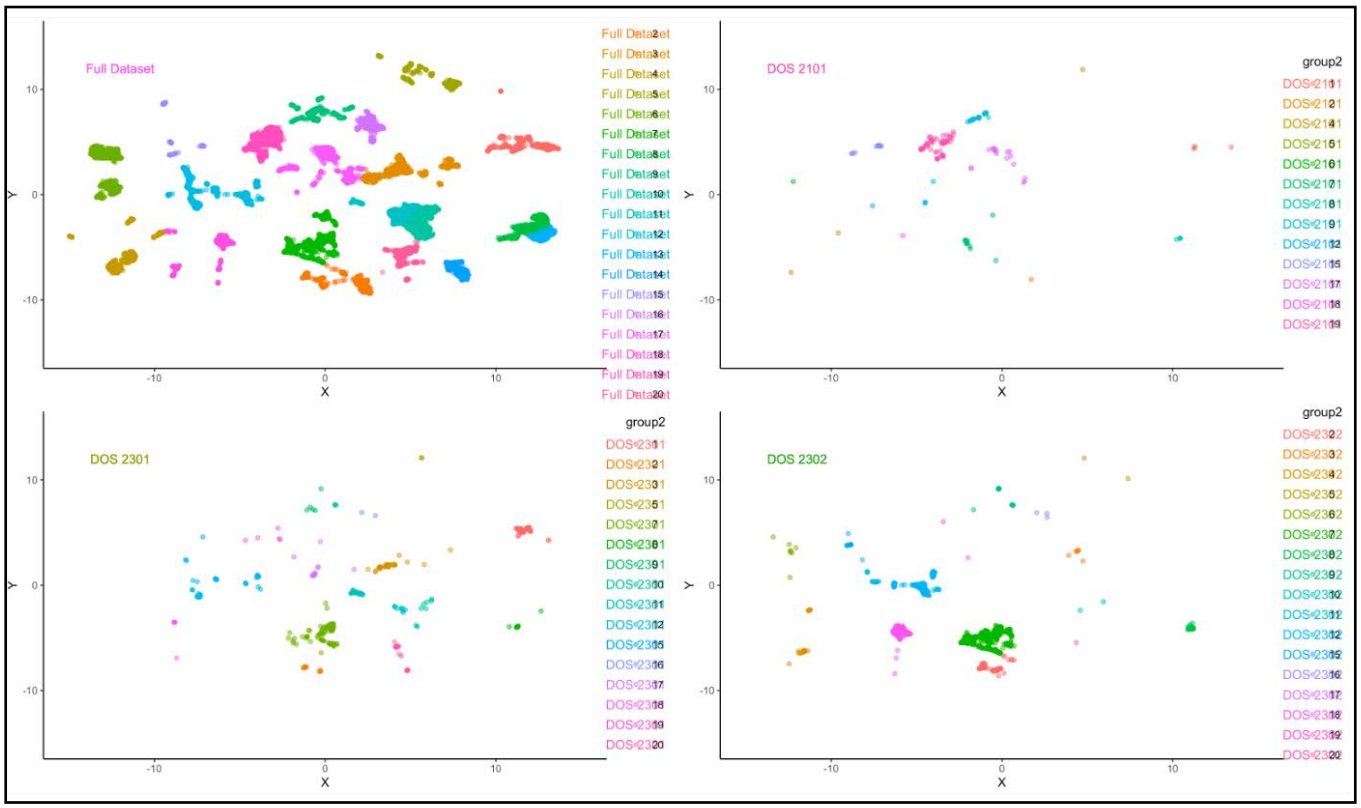

Figure 41. Distribution of clusters the OS tissue samples on the UMAP plot.: Representation of the UMAP plot including all of the samples (top left) next to the three individual OS tissue samples. Note the presence of clusters along the full extent of the plot, including some unique clusters present exclusively in individual samples and some clusters that overlap those seen in the WBC samples.

Figure 42

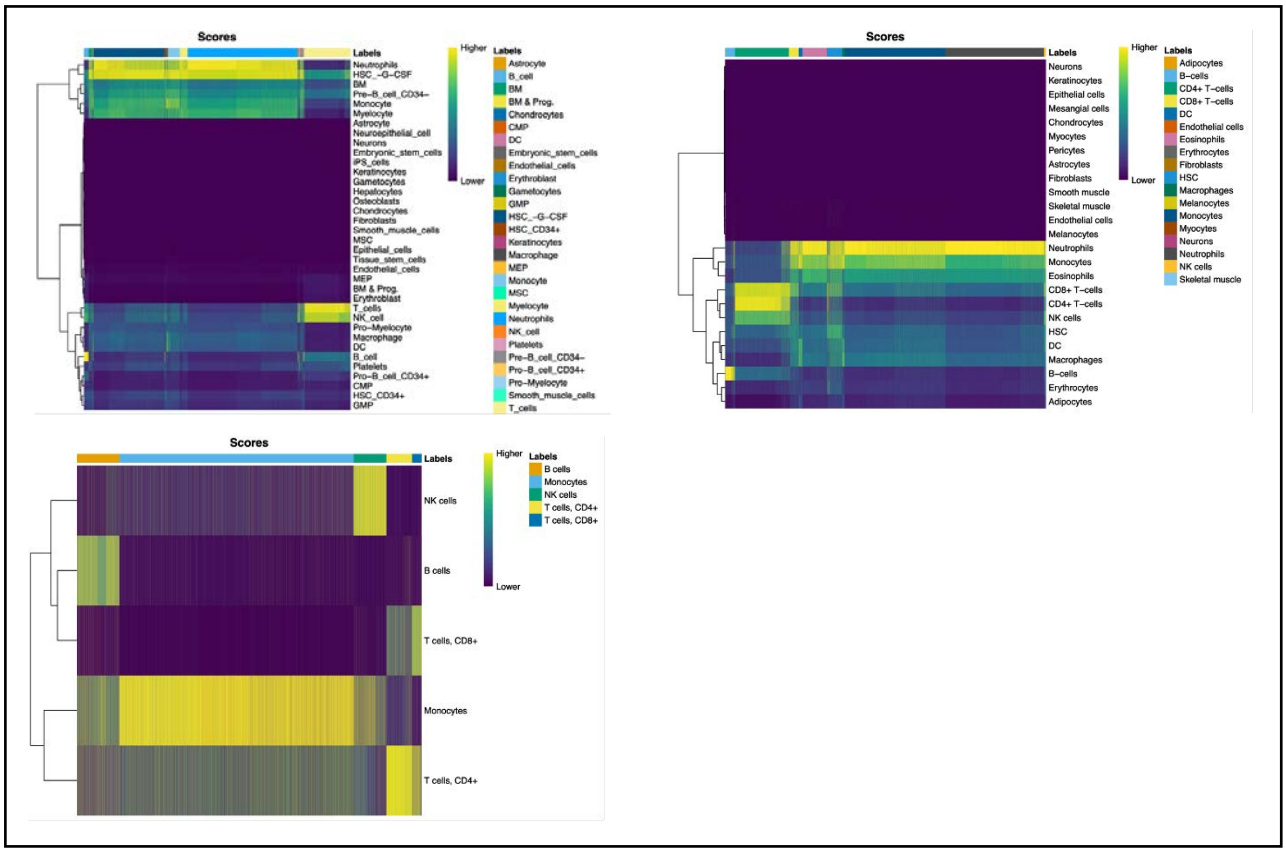

Figure 42. Heatmap of the HPCA, BluePrint ENCODE, and ImmuneCell cell type classification scores for all the dog WBCs. Top left panel: Heatmap shows the alignment of cell types based on the HPCA reference. Note the inferred exclusive presence of leukocytes based on this reference (lime green and yellow alignment with neutrophils, monocytes, myelocytes, T cells, NK cells and B cells). Top right panel: Heatmap shows the alignment of cell types based on the BluePrint ENCODE reference. Note the inferred exclusive presence of leukocytes based on this reference (lime green and yellow alignment with neutrophils, monocytes, eosinophils, CD8+ T-cells, CD4+ T-cells, NK cells, hematopoietic stem cells, dendritic cells, macrophages, and B cells). Bottom left panel: Heatmap shows the alignment of cell types based on the ImmuneCell reference. Note the excellent agreement with this reference set that includes NK cells, B cells, CD8+ T-cells, monocytes, and CD4+ T-cells.

Figure 43

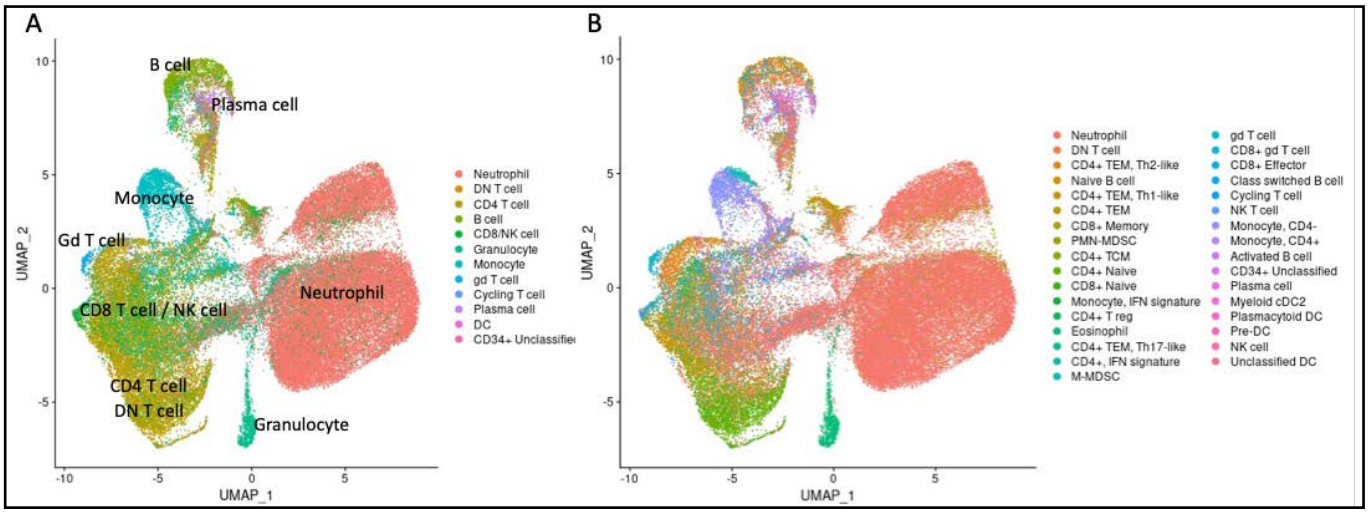

Figure 43. UMAP plots of single-cell data from canine WBC samples with transferred labels from Dog GSE22559 annotations (Ammons et al). A) UMAP plot colored by main cell type labels. B) UMAP plot colored by the fine cell type labels.

Figure 44

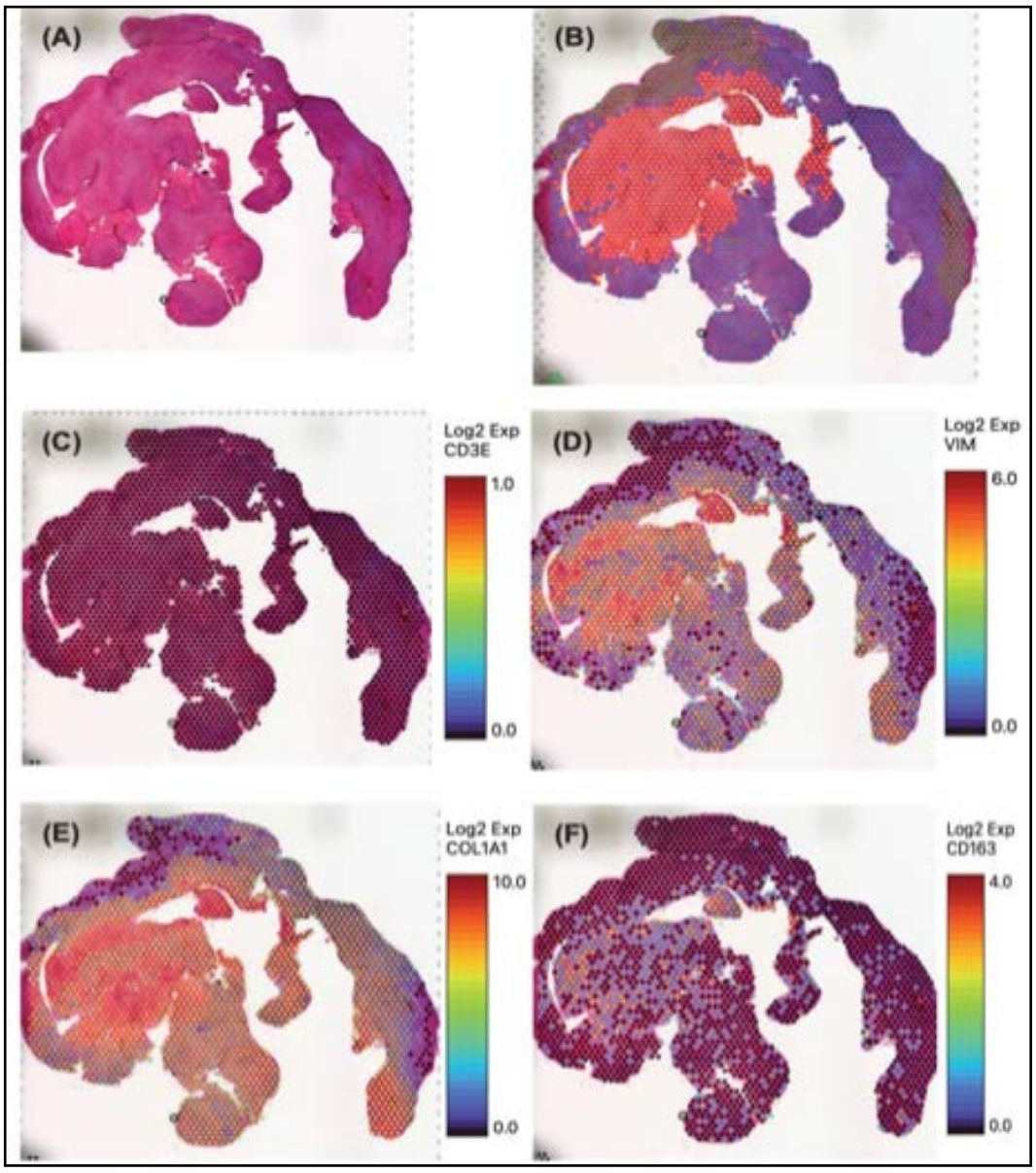

Figure 44. Spatial analysis of FFPE human osteosarcoma sample. (A) H&E stained tissue sample. (B) Clustering analysis from gene expression data. (C-F) Tumors express low levels of CD3E (C) and high levels of VIM (D), COL1A1 (E), and CD163 (F). Note the compartmentalization of cells expressing VIM and COL1A1 (mostly tumor cells) and the diffuse distribution of cells expressing CD163 (macrophages).

10. Appendices

a. Literature Cited

1 Scott, M. C. *et al.* Comparative Transcriptome Analysis Quantifies Immune Cell Transcript Levels, Metastatic Progression, and Survival in Osteosarcoma. *Cancer Res* **78**, 326-337, doi:10.1158/0008-5472.CAN-17-0576 (2018).

2 Naik, S. *et al.* Curative one-shot systemic virotherapy in murine myeloma. *Leukemia* **26**, 1870-1878, doi:10.1038/leu.2012.70 (2012).

3 Shen, W., Patnaik, M. M., Ruiz, A., Russell, S. J. & Peng, K. W. Immunovirotherapy with vesicular stomatitis virus and PD-L1 blockade enhances therapeutic outcome in murine acute myeloid leukemia. *Blood* **127**, 1449-1458, doi:10.1182/blood-2015-06-652503 (2016).

4 Modiano, J. F. *et al.* Inflammation, apoptosis, and necrosis induced by neoadjuvant fas ligand gene therapy improves survival of dogs with spontaneous bone cancer. *Mol Ther* **20**, 2234-2243, doi:10.1038/mt.2012.149 (2012).

5 Chen, S. H. *et al.* Dual checkpoint blockade of CD47 and PD-L1 using an affinity-tuned bispecific antibody maximizes antitumor immunity. *J Immunother Cancer* **9**, doi:10.1136/jitc-2021-003464 (2021).

6 Makielski, K. M. *et al.* Neoadjuvant systemic oncolytic vesicular stomatitis virus is safe and may enhance long-term survivorship in dogs with naturally occurring osteosarcoma. *bioRxiv*, doi:10.1101/2023.04.16.533664 (2023).

7 Weiskopf, K. *et al.* Eradication of Canine Diffuse Large B-Cell Lymphoma in a Murine Xenograft Model with CD47 Blockade and Anti-CD20. *Cancer Immunol Res* **4**, 1072-1087, doi:10.1158/2326-6066.CIR-16-0105 (2016).

8 Anderson, K. L. *et al.* Evolutionarily conserved resistance to phagocytosis observed in melanoma cells is insensitive to upregulation of pro-phagocytic signals and to CD47 blockade. *Melanoma Res* **30**, 147-158, doi:10.1097/CMR.0000000000000629 (2020).

9 Pandey, M. S., Wang, C., Umlauf, S. & Lin, S. Simultaneous Inhibition of PD-1 and Stimulation of CD40 Signaling Pathways by Anti-PD-L1/CD40L Bispecific Fusion Protein Synergistically Activate Target and Effector Cells. *Int J Mol Sci* **22**, doi:10.3390/ijms222111302 (2021).

10 Abraham, R. T. & Weiss, A. Jurkat T cells and development of the T-cell receptor signalling paradigm. *Nat Rev Immunol* **4**, 301-308, doi:10.1038/nri1330 (2004).

11 Modiano, J. F., Kolp, R., Lamb, R. J. & Nowell, P. C. Protein kinase C regulates both production and secretion of interleukin 2. *Journal of Biological Chemistry* **266**, 10552-10561 (1991).

12 Helfand, S. C., Hank, J. A., Gan, J. & Sondel, P. M. Lysis of human tumor cell lines by canine complement plus monoclonal antiganglioside antibodies or natural canine xenoantibodies. *Cell Immunol* **167**, 99-107, doi:10.1006/cimm.1996.0012 (1996).

13 Graef, A. J., Kim, J.-H., Vallera, D. A. & Modiano, J. F. Targeting epidermal growth factor receptors and urokinase-type plasminogen activator receptors for sarcoma therapy (Abstract). *Cancer Research* **78**, 824-824, doi:10.1158/1538-7445.Am2018-824 (2018).

14 Grisez, B. T., Ray, J. J., Bostian, P. A., Markel, J. E. & Lindsey, B. A. Highly metastatic K7M2 cell line: A novel murine model capable of in vivo imaging via luciferase vector transfection. *J Orthop Res*, doi:10.1002/jor.23868 (2018).

15 Khanna, C. *et al.* Metastasis-associated differences in gene expression in a murine model of osteosarcoma. *Cancer Res* **61**, 3750-3759 (2001).

16 Khanna, C. *et al.* An orthotopic model of murine osteosarcoma with clonally related variants differing in pulmonary metastatic potential. *Clin Exp Metastasis* **18**, 261-271, doi:10.1023/a:1006767007547 (2000).

17 Ivanov, II & Littman, D. R. Segmented filamentous bacteria take the stage. *Mucosal Immunol* **3**, 209-212, doi:mi20103 [pii]10.1038/mi.2010.3 (2010).

18 Rasmussen, T. S. *et al.* Mouse Vendor Influence on the Bacterial and Viral Gut Composition Exceeds the Effect of Diet. *Viruses* **11**, doi:10.3390/v11050435 (2019).

19 Loscher, W., Ferland, R. J. & Ferraro, T. N. The relevance of inter- and intrastrain differences in mice and rats and their implications for models of seizures and epilepsy. *Epilepsy Behav* **73**, 214-235, doi:10.1016/j.yebeh.2017.05.040 (2017).
20 Huang, L. *et al.* Expression of tdTomato and luciferase in a murine lung cancer alters the growth and immune microenvironment of the tumor. *PLoS One* **16**, e0254125, doi:10.1371/journal.pone.0254125 (2021).
21 Baklaushev, V. P. *et al.* Luciferase Expression Allows Bioluminescence Imaging But Imposes Limitations on the Orthotopic Mouse (4T1) Model of Breast Cancer. *Sci Rep* **7**, 7715, doi:10.1038/s41598-017-07851-z (2017).
22 Modiano, J. F. *et al.* Mesenchymal stromal cells inhibit murine syngeneic anti-tumor immune responses by attenuating inflammation and reorganizing the tumor microenvironment. *Cancer Immunol Immunother* **64**, 1449-1460, doi:10.1007/s00262-015-1749-6 (2015).
23 Aoyama, N. *et al.* Transgenic mice that accept Luciferase- or GFP-expressing syngeneic tumor cells at high efficiencies. *Genes Cells* **23**, 580-589, doi:10.1111/gtc.12592 (2018).
24 Wedekind, M. F. *et al.* Endogenous retrovirus envelope as a tumor-associated immunotherapeutic target in murine osteosarcoma. *iScience* **24**, 102759, doi:10.1016/j.isci.2021.102759 (2021).
25 Morrow, J. J. *et al.* mTOR Inhibition Mitigates Enhanced mRNA Translation Associated with the Metastatic Phenotype of Osteosarcoma Cells In Vivo. *Clin Cancer Res* **22**, 6129-6141, doi:10.1158/1078-0432.CCR-16-0326 (2016).
26 Rao, P. H. *et al.* Coamplification of Myc/Pvt1 and homozygous deletion of Nlrp1 locus are frequent genetics changes in mouse osteosarcoma. *Genes Chromosomes Cancer* **54**, 796-808, doi:10.1002/gcc.22291 (2015).
27 Schappa, J. T. *et al.* Hemangiosarcoma and its cancer stem cell subpopulation are effectively killed by a toxin targeted through epidermal growth factor and urokinase receptors. *Int J Cancer* **133**, 1936-1944, doi:10.1002/ijc.28187 (2013).
28 Pilbeam, K. *et al.* Targeting pediatric sarcoma with a bispecific ligand immunotoxin targeting urokinase and epidermal growth factor receptors. *Oncotarget* **9**, 11938-11947, doi:10.18632/oncotarget.21187 (2018).
29 Oh, F., Modiano, J. F., Bachanova, V. & Vallera, D. A. Bispecific Targeting of EGFR and Urokinase Receptor (uPAR) Using Ligand-Targeted Toxins in Solid Tumors. *Biomolecules* **10**, doi:10.3390/biom10060956 (2020).
30 Tsai, A. K. *et al.* A novel bispecific ligand-directed toxin designed to simultaneously target EGFR on human glioblastoma cells and uPAR on tumor neovasculature. *J Neurooncol* **103**, 255-266, doi:10.1007/s11060-010-0392-5 (2011).
31 Antignani, A. *et al.* Essential role for Bim in mediating the apoptotic and antitumor activities of immunotoxins. *Oncogene* **36**, 4953-4962, doi:10.1038/onc.2017.111 (2017).
32 Borgatti, A. *et al.* Safe and Effective Sarcoma Therapy through Bispecific Targeting of EGFR and uPAR. *Mol Cancer Ther* **16**, 956-965, doi:10.1158/1535-7163.MCT-16-0637 (2017).
33 Durham, N. M. *et al.* Oncolytic VSV Primes Differential Responses to Immuno-oncology Therapy. *Mol Ther* **25**, 1917-1932, doi:10.1016/j.ymthe.2017.05.006 (2017).
34 Rajha, E. *et al.* Gastrointestinal adverse events associated with immune checkpoint inhibitor therapy. *Gastroenterol Rep (Oxf)* **8**, 25-30, doi:10.1093/gastro/goz065 (2020).
35 Advani, R. *et al.* CD47 Blockade by Hu5F9-G4 and Rituximab in Non-Hodgkin's Lymphoma. *N Engl J Med* **379**, 1711-1721, doi:10.1056/NEJMoa1807315 (2018).
36 Makielski, K. M. *et al.* Risk Factors for Development of Canine and Human Osteosarcoma: A Comparative Review. *Vet Sci* **6**, 48, doi:10.3390/vetsci6020048 (2019).
37 Sarver, A. L., Makielski, K. M., DePauw, T. A., Schulte, A. J. & Modiano, J. F. Increased risk of cancer in dogs and humans: a consequence of recent extension of lifespan beyond evolutionarily-determined limitations? *Aging Cancer* **3**, 3-19, doi:10.1002/aac2.12046 (2022).
38 Diessner, B. J. *et al.* Nearly Half of TP53 Germline Variants Predicted To Be Pathogenic in Patients With Osteosarcoma Are De Novo: A Report From the Children's Oncology Group. *JCO Precis Oncol* **4**, doi:10.1200/PO.20.00087 (2020).

39 Mills, L. J. *et al.* Comparative analysis of genome-wide DNA methylation identifies patterns that associate with conserved transcriptional programs in osteosarcoma. *Bone* **158**, 115716, doi:10.1016/j.bone.2020.115716 (2022).
40 Sakthikumar, S. *et al.* SETD2 Is Recurrently Mutated in Whole-Exome Sequenced Canine Osteosarcoma. *Cancer Res* **78**, 3421-3431, doi:10.1158/0008-5472.CAN-17-3558 (2018).
41 Sarver, A. L. *et al.* Distinct mechanisms of PTEN inactivation in dogs and humans highlight convergent molecular events that drive cell division in the pathogenesis of osteosarcoma. *Cancer genetics* **276-277**, 1-11, doi:10.1016/j.cancergen.2023.05.001 (2023).
42 LeBlanc, A. K. *et al.* Adjuvant Sirolimus Does Not Improve Outcome in Pet Dogs Receiving Standard-of-Care Therapy for Appendicular Osteosarcoma: A Prospective, Randomized Trial of 324 Dogs. *Clin Cancer Res* **27**, 3005-3016, doi:10.1158/1078-0432.CCR-21-0315 (2021).
43 Ammons, D. T. *et al.* A single-cell RNA sequencing atlas of circulating leukocytes from healthy and osteosarcoma affected dogs. *Front Immunol* **14**, 1162700, doi:10.3389/fimmu.2023.1162700 (2023).

b. Abbreviations Used in this Report

ACURO: animal care and use review office
APC: antigen presenting cell
ATAC-seq: assay for transposase-accessible chromatin using sequencing
ATF: amino terminal fragment
AYAs: adolescents and young adults
BM: bone marrow
CD: cluster designation
CDMRP: congressionally directed medical research program
CPIs: checkpoint inhibitors
CRISPR: clustered regularly interspaced short palindromic repeats
COVID: (sudden acute respiratory syndrome) coronavirus-2 (2019) induced disease
DA: differential accessibility (of chromatin)
DOD: (U.S.) Department of Defense
eBAT: EGF bispecific angiotoxin
EGF: epidermal growth factor
EGFR: epidermal growth factor receptor
FDR: false discovery rate
FITC: fluorescein isocyanate
GFP: green fluorescent protein
GSEA: gene set enrichment analysis
EU: endotoxin units
Fluc: firefly luciferase
Gluc: Gaussia luciferase
IACUC: institutional animal care and use committee
IBC: institutional biosafety committee
IFNβ: interferon-beta
IL: interleukin
iv: intravenous
KO: knockout
LTT: ligand targeted toxin
MDSC: myeloid derived suppressor cells
meBAT: Mouse eBAT
METEOR: metastatic experimental osteosarcoma research (study)
NCI: National Cancer Institute (of the National Institutes of Health)
NIS: sodium iodide symporter
ONIx: onco-immune accelerator
OS: osteosarcoma
PBMC: peripheral blood mononuclear cell
PBS: phosphate buffered saline
PD-1: programmed death (receptor)-1
PD-L1: programmed death ligand-1
P-DIC: peptide for dual immune checkpoint blockade (this nomenclature has been replaced with the term onco-immune accelerator or ONIx)
PD: pharmacidynamics
PE: *Pseudomonas* exotoxin
P/I: combination of phorbol myristate acetate and ionomycin
PK: pharmacokinetics
PKC: protein kinase C
PMA: phorbol myristate acetate
PRCRP: peer reviewed cancer research program

PRMRP: peer reviewed medical research program
QA: quality assurance
QC: quality control
RNAseq: next generation ribonucleic acid sequencing
SD: standard deviation
SDS-PAGE: sodium dodecyl sulfate-polyacrylamide gel electrophoresis
SIRP: signal regulatory protein
SOP: standard operating protocol
SOW: statement of work
sq: subcutaneous
TAMs: tumor associated macrophages
$TCID_{50}$: half maximal tissue culture infective dose
TME: tumor microenvironment
UMGC: University of Minnesota Genomics Center
uPA: urokinase type plasminogen activator
uPAR: urokinase type plasminogen activator receptor
VIGOR: VSV immunotherapy and genomics osteosarcoma research (study)
VSV: vesicular stomatitis virus
WBC: white blood cell
WT: wild type

c. Other Reports

i. Pathology Report for Balb/c Mice Injected with K7M2 Cells

(next page)

University of Minnesota Masonic Cancer Center
Comparative Pathology Shared Resource

CPSR Study Number:

22-237

Study Title
Histopathologic Analysis of BALB/c Mice Injected with K7M2 Mouse Osteosarcoma Cells

Author:
Davis M. Seelig, DVM, PhD
Diplomate, A.C.V.P.
&
Emma Torii, BVSc, MANZCVS (Pathobiology),
Postdoctoral associate

Comparative Pathology Shared Resource
Masonic Cancer Center
University of Minnesota
1352 Boyd Ave, St. Paul, MN 55108

Study Sponsor:
N/A

Table of Contents	

1. Regulatory Compliance Statement and Data Integrity

This non-GLP study was conducted for research and development purposes. Sample receipt, processing, analysis and data reporting are performed in alignment with the best practices of The Society of Toxicologic Pathology. Histopathological evaluation was done in the spirit of FDA regulations on good laboratory practices (GLP) for nonclinical laboratory studies CFR title 21 part 58. The chain of custody for tissues analyzed and slides reported was verified by the study pathologist. The undersigned signifies that they approve all pathology-related data within this report, including tables, narrative, and overall summary.

Pathologist's Signature

Study Title: Histopathologic Analysis of BALB/c Mice Injected with K7M2 Mouse Osteosarcoma Cells

CPSR Study Number: 22-237

Sponsor Study Number: N/A

Study Pathologist(s)

Signature:  Date: September 6, 2022

Davis M. Seelig, DVM, PhD
Diplomate, A.C.V.P.

Signature: 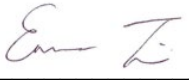 Date: September 06, 2022

Emma Torii, BVSc,
MANZCVS (Pathobiology),

2. Study background and experimental objectives (from submitter)

a. Female BALB/c mice injected with K7M2 mouse osteosarcoma cells on May 10 in different dosages – IV injection of 1E6 K7Me cells in mice numbered 1, 2 and 3; IV injection of 0.5E6 K7Me cells in mice numbered 4,5 and 6; IV injections of 0.25E6 K7Me cells in mice numbered 7, 8 and 9. 1 sample included from the mice numbered 14, received SQ injection of 1E6 K7Me cells.

3. Gross Necropsy Findings:

a. None Provided

4. Clinical Pathology Data:

a. None Provided

5. Methods

a. Received tissues were paraffin-embedded, sectioned, mounted onto slides and stained with Hematoxylin and Eosin (H&E) using standard techniques[1]. See Table 1 (below) for slide annotation information

b. H&E-stained sections were evaluated using light microscopy according to STP guidelines[2]. H&E-stained sections were evaluated.

Table 1. Study groups in histopathologic analysis

CPSR ID	Investigator Animal ID	Genotype	Sex	Treatment	List of tissues
22-237-1	M10K7M2-IV1-1	BALB/c	Female	1E6 K7M2 cells IV	Lung, Spleen
22-237-2	M10K7M2-IV1-2	BALB/c	Female	1E6 K7M2 cells IV	Lung, Spleen
22-237-3	M10K7M2-IV1-3	BALB/c	Female	1E6 K7M2 cells IV	Lung, Spleen, Tail
22-237-4	M10K7M2-IV0.5-4	BALB/c	Female	0.5E6 K7M2 cells IV	Lung, Spleen, Tail
22-237-5	M10K7M2-IV0.5-5	BALB/c	Female	0.5E6 K7M2 cells IV	Lung, Spleen
22-237-6	M10K7M2-IV0.5-6	BALB/c	Female	0.5E6 K7M2 cells IV	Lung, Spleen
22-237-7	M10K7M2-IV0.25-7	BALB/c	Female	0.25E6 K7M2 cells IV	Lung, Spleen
22-237-8	M10K7M2-IV0.25-8	BALB/c	Female	0.25E6 K7M2 cells IV	Lung, Spleen
22-237-9	M10K7M2-IV0.25-9	BALB/c	Female	0.25E6 K7M2 cells IV	Lung, Spleen
22-237-10	M10K7M2-SQ1-14	BALB/c	Female	1E6 K7M2 cells SQ	Skin and subcutaneous fat with possible tumor remnant

6. Results:

a. Descriptive histopathologic analysis of submitted tissues

Table 2. Summary histopathologic findings from submitted tissues.

CPSR ID	Tissue	H&E Findings
22-237-1	Spleen	There is diffuse moderate congestion and extramedullary hematopoieiss (EMH; considered appropriate for species).
	Lung	There is diffuse mild alveolar vascular congestion, and mild increased cellularity of the alveolar septa by owing to increased few large round mononuclear cells (presumed to be macrophages) and few small lymphocytes. Particularly at the edge of the sections, there are small foci of atelectasis.
22-237-2	Spleen	Changes are similar to that described in the spleen of 22-237-1.
	Lung	Changes are similar to that described in the lungs of 22-237-1.
22-237-3	Spleen	Changes are similar to that described in the spleen of 22-237-1.
	Lung	Affecting approximately <5% of the total surface area, predominantly perivascularly and intravascularly, and less frequently randomly, there are small clusters of neoplastic cells similar to that described in the tail below (22-273-3). In a deeper section, multiple cross and tangential sections of large-caliber blood vessels contain tumor emboli. The remainder of the lungs have changes similar to that described in the lungs of 22-237-1.
	Tail	Surrounding, infiltrating, and effacing a vertebra and its marrow cavity and associated skeletal muscle, and elevating the overlying dermis and epidermis is an unencapsulated, moderately well-demarcated, densely cellular mass consistent with a sarcoma. The neoplastic cells are arranged into ill-defined broad sheets to poorly-formed bundles and streams, and are supported by a fine fibrovascular stroma. Rarely, between neoplastic cells are scant amounts of wispy, fibrillary, eosinophilic material (possible osteoid, and/or fibrous tissue). The neoplastic cells are plump spindle shaped with indistinct cell borders, and have a large amount of eosinophilic to amphophilic cytoplasm. The nuclei are round to oval with vesicular chromatin, and have up to 3 prominent, magenta nucleoli. There is marked anisocytosis and anisokaryosis. The mitotic count is 39 in 2.37mm^2 (equivalent to 10 HPF), with frequent atypical mitotic figures. Throughout the mass are individual cell necrosis and/or apoptosis, as well as scattered, low numbers of lymphocytes, and rarely eosinophils.
22-237-4	Spleen	Changes are similar to that described in the spleen of 22-237-1.
	Lung	Within the right caudal lung lobe is an approximately 4 x 3 mm, unencapsulated, well-demarcated sarcoma that moderately compresses the surrounding lungs. The mass is similar to that described in the tail of 22-237-3, although with increased pleomorphism, including increased anisocytosis, anisokaryosis and irregularly indented nuclei. In addition, there are occasional multinucleated cells, and cells with bizarre, karyomegalic nuclei. There are a few medium-sized foci of lytic necrosis. The mitotic count is 17 in 2.37mm^2 (equivalent to 10 HPF) with

		frequent atypical mitotic figures. The remainder of the lung lobes have changes similar to that described in the lungs of 22-237-1.
	Tail	Within the subcutis and dermis, and elevating the overlying epidermis is a moderately well-demarcated, unencapsulated, oval mass composed of neoplastic cells similar to that described in the lungs of 22-237-4, although with fewer cells with bizarre nuclei. The mitotic count is 18 in 2.37mm^2 (equivalent to 10 HPF) with frequent atypical mitotic figures.
22-237-5	Spleen	Changes are similar to that described in the spleen of 22-237-1.
	Lung	In one lung lobe, there is a small subpleural mass consisting of neoplastic cells similar to that described in the tail of 22-237-3, although with increased anisocytosis, anisokaryosis and rare multinucleated cells. The mitotic count is 14 in 2.37mm^2 (equivalent to 10 HPF) with frequent atypical mitotic figures. The remainder of the lung lobes have changes are similar to that described in the lungs of 22-237-1.
22-237-6	Spleen	Changes are similar to that described in the spleen of 22-237-1.
	Lung	Changes are similar to that described in the lungs of 22-237-1.
22-237-7	Spleen	Changes are similar to that described in the spleen of 22-237-1.
	Lung	Changes are similar to that described in the lungs of 22-237-1.
22-237-8	Spleen	Changes are similar to that described in the spleen of 22-237-1.
	Lung	Changes are similar to that described in the lungs of 22-237-1, although the alveolar septal thickening is mild. There are rare medium-caliber blood vessels that are surrounded by moderate numbers of macrophages, eosinophils and fibroblasts. On deeper section, the perivascular inflammation was absent.
22-237-9	Spleen	Changes are similar to that described in the spleen of 22-237-1.
	Lung	Changes are similar to that described in the lungs of 22-237-1, although there is reduced alveolar septal thickening.
22-237-10	Skin and subcutaneous Tissue	The tissue consists of skin, subcutis, multiple small quiescent mammary glands and ducts, abundant adipose tissue and a lymph node. There are no significant abnormalities detected.

Representative Images

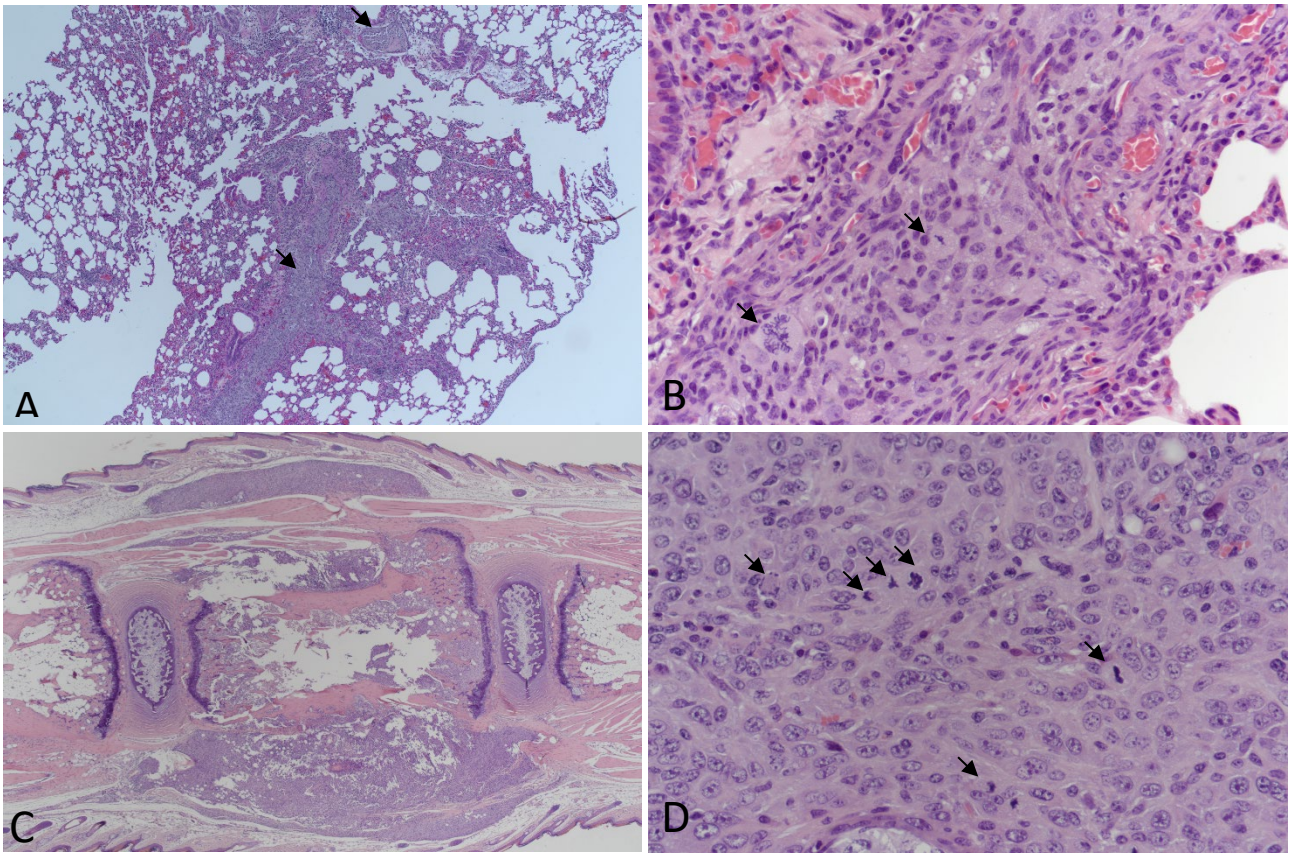

Figure 1 – Mouse 3, lungs (A-B) and tail (C-D), HE. **A. Lungs**, **40x.** Multiple cross sections of vessels have tumor emboli (arrows). **B. Lungs, 400x.** Higher magnification of tumor emboli. Note multiple mitotic figures (arrows), some of which are bizarre (left arrow). **C. Tail, 20x.** Surrounding and infiltrating a vertebra is a sarcoma. **D. Tail, 400x.** Higher magnification of the sarcoma. There are numerous mitotic figures (arrows), many of which are atypical.

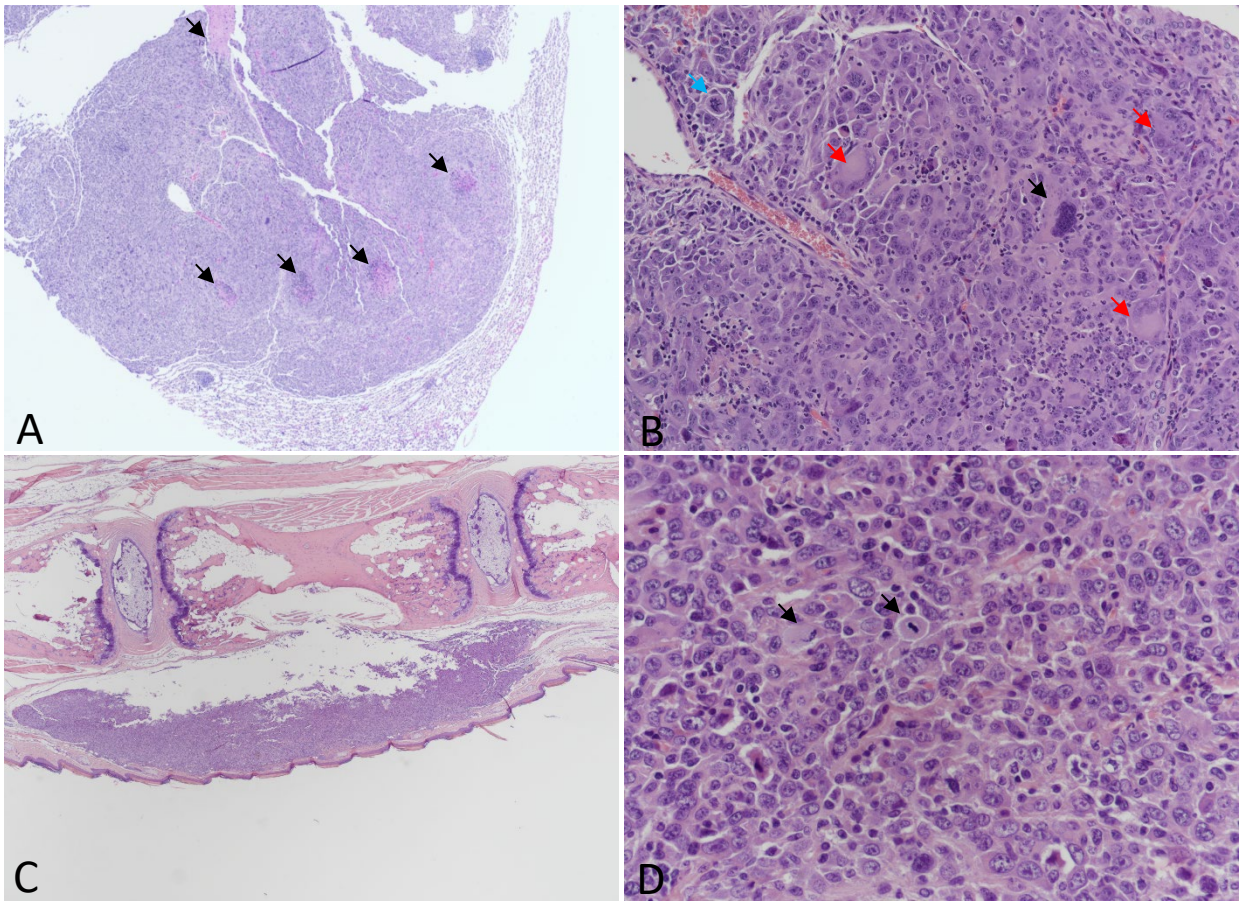

Figure 2 - Mouse 4, lungs (A-B) and tail (C-D), HE. **A. Lungs (right caudal lobe)**, **40x.** Well-demarcated sarcoma metastasis that moderately compresses the adjacent lung. Throughout the tumor are multiple necrosis (arrows). **B. Lungs, 200x.** Higher magnification of the mass. Compared to mouse 3, there is increased pleomorphism with occasional large cells with atypical, large, bizarre nuclei (black arrow) and multinucleated cells (red arrows). There is an atypical mitotic figure (blue arrow). **C. Tail, 20x.** Surrounding a vertebra is a sarcoma. **D. Tail, 400x.** Higher magnification of the sarcoma. There are numerous mitotic figures (arrows), many of which are atypical.

7. Project Summary:

- **a.** Three of nine mice (22-237-3, 22-237-4, and 22-237-5) had sarcoma within the lungs
  - **i.** Two of these mice (22-237-3 and 22-237-4) each had a mass in the submitted tails with similar histological appearance.
  - **ii.** There were rare, scant amounts of wispy material that somewhat resembled osteoid, however pre-existing stroma and/or fibrous tissue could not be excluded. Despite lack of convincing osteoid, osteosarcoma was considered most likely given the treatment history.
  - **iii.** All the masses across the affected mice had similar morphology, albeit 22-237-4 and 22-237-5 were more anaplastic. Differences in morphology of the K7M2 cells have been reported.[4]
  - **iv.** No other mice had evidence of neoplastic cells.
  - **v.** The prevalence of pulmonary metastasis in this study is in contrast to a previous publication, where intravenous injection of K7M2 osteosarcoma cell lines resulted in pulmonary metastasis and subsequent death in all treated mice.[3]
- **b.** Lungs:
  - **i.** All mice had mild diffuse increased cellularity of the alveolar septa.
  - **ii.** Subjectively, this change seemed less severe in the mice given the lower dosages.
  - **iii.** To our knowledge, previous publications using K7M2 cell lines did not provide any descriptions of lung pathology aside from metastasis.[3,4] If further investigation is warranted, examination of age and sex-matched control mice is recommended.
- **c.** Spleen:
  - **i.** None of the mice had gross or histologic evidence of neoplastic cells.

8. Recommendations

- a. There was a lower than expected number of mice with pulmonary metastasis compared to previous publications. It is possible that small metastases may not have been evident in the examined section. Hence, if further investigation is warranted, deeper sections of each blocks can be requested at an additional cost.
  - i. However, it is possible that the differences between previously published work and this study may reflect: different sacrifice time-points, different age at tumor cell injection, and different tumor cell dosages (the cited publication above describes an inoculation dosage of 1e6 cells).
- **b.** Submission of control animals may be warranted to compare the pulmonary alveolar changes. In addition, adequate inflation of the lungs at the time of fixation will reduce the atelectasis, allowing for improved interpretation of the cellularity.

9. References

1. Tucker DK, Foley JF, Hayes-Bouknight SA, Fenton SE. Preparation of High-quality Hematoxylin and Eosin-stained Sections from Rodent Mammary Gland Whole Mounts for Histopathologic Review. Toxicol Pathol. 2016;44(7):1059-64. Epub 20160729. doi: 10.1177/0192623316660769. PubMed PMID: 27474221; PMCID: PMC5035598.

2. Crissman JW, Goodman DG, Hildebrandt PK, Maronpot RR, Prater DA, Riley JH, Seaman WJ, Thake DC. Best practices guideline: toxicologic histopathology. Toxicol Pathol. 2004;32(1):126-31. doi: 10.1080/01926230490268756. PubMed PMID: 14713558.

3. Khanna C, Prehn J, Yeung C, Caylor J, Tsokos M, Helman L. An orthotopic model of murine osteosarcoma with clonally related variants differing in pulmonary metastatic potential. Clin Exp Metastasis. 2000: 18(3):261-71. DOI: 10.1023/a:1006767007547 PubMed PMID: 11315100.

4. Grisez BT, Ray JJ, Bostian PA, Markel JE, Lindsey BA. Highly metastatic K7M2 cell line: A novel murine model capable of in vivo imaging via luciferase vector transfection. 2018. DOI: 10.1002/jor.23868. Pubmed PMID: 29427436; PMCID: PMC6086764

ii. **ONIx Sterility Report**
(next page)

IDEXX BioAnalytics

FINAL REPORT OF LABORATORY EXAMINATION

4011 Discovery Drive, Columbia, MO 65201
1-800-669-0825 1-573-499-5700
idexxbioanalytics@idexx.com www.idexxbioanalytics.com

IDEXX BioAnalytics Case # 114232-2022 **Received Date: 5/20/2022**
Client Case # n/a **Completed: 6/3/2022**

Submitted By

Kathleen Stuebner
University of Minnesota
Clinical Investigation Center
1365 Gortner Ave
B350 VMC
Saint Paul, MN 55108

Phone: 612-624-2485
Email:
stueb005@umn.edu;modiano@umn.edu;prach011@umn.edu

Specimen Description

Species: unspecified
Description: Culture Swab
Number of Specimens/Animals: 12
Building/Facility: VMC
Study: eBAT

Purchase Order #: 000225971

ID	Client ID	Room #	Species
1	Vial1-O	D317	unspecified
2	Vial1-G	D317	unspecified
3	Vial1-R	D317	unspecified
4	Vial1-DR	D317	unspecified
5	Vial2-O	D317	unspecified
6	Vial2-G	D317	unspecified
7	Vial2-R	D317	unspecified
8	Vial2-DR	D317	unspecified
9	Vial3-O	D317	unspecified
10	Vial3-G	D317	unspecified
11	Vial3-R	D317	unspecified
12	Vial3-DR	D317	unspecified

Services/Tests Performed: Aerobic and Anaerobic Culture and ID - bacteria and fungi (1-12)

Microbiologic evaluation for: Aerobic bacterial growth, Anaerobic bacterial growth, Fungal growth

General Comments: Culture Swab - O=outside, G=gray cap, R=inside rim, DR=drug

Summary: All test results were negative.

MICROBIOLOGY

Specimen/Source: culture

Isolate	1	2	3	4	5	6	7	8	9	10
Aerobic bacterial growth	-	-	-	-	-	-	-	-	-	-
Anaerobic bacterial growth	-	-	-	-	-	-	-	-	-	-
Fungal growth	-	-	-	-	-	-	-	-	-	-

Specimen/Source: culture

Isolate	11	12
Aerobic bacterial growth	-	-
Anaerobic bacterial growth	-	-
Fungal growth	-	-

Legend: + = agent recovered - = agent not recovered blank = test not performed n = no growth X = Preliminary

d. Publications

- *Aging and Cancer* manuscript
- *Cancer Genetics* manuscript
- *Molecular Therapy – Oncolytics* manuscript
- *Medical* Research Archives manuscript

(Next page)

Received: 31 March 2021 | Accepted: 21 January 2022

DOI: 10.1002/aac2.12046

Aging and Cancer
Open Access
SAMUEL WAXMAN CANCER RESEARCH FOUNDATION

PERSPECTIVE

Increased risk of cancer in dogs and humans: A consequence of recent extension of lifespan beyond evolutionarily determined limitations?

Aaron L. Sarver[1,2,3] | **Kelly M. Makielski**[1,3,4] | **Taylor A. DePauw**[1,3,4] | **Ashley J. Schulte**[1,3,4] | **Jaime F. Modiano**[1,3,4,5,6,7,8]

[1] Masonic Cancer Center, University of Minnesota, Minneapolis, Minnesota, USA

[2] Institute for Health Informatics, University of Minnesota, Minneapolis, Minnesota, USA

[3] Animal Cancer Care and Research Program, University of Minnesota, St. Paul, Minnesota, USA

[4] Department of Veterinary Clinical Sciences, College of Veterinary Medicine, University of Minnesota, St. Paul, Minnesota, USA

[5] Department of Laboratory Medicine and Pathology, School of Medicine, University of Minnesota, Minneapolis, Minnesota, USA

[6] Center for Immunology, University of Minnesota, Minneapolis, Minnesota, USA

[7] Stem Cell Institute, University of Minnesota, Minneapolis, Minnesota, USA

[8] Institute for Engineering in Medicine, University of Minnesota, Minneapolis, Minnesota, USA

Correspondence
Jaime F. Modiano, Masonic Cancer Center, University of Minnesota, 420 Delaware St. SE, MCRB 560F/MMC806, Minneapolis, MN 55455, USA.
Email: modiano@umn.edu

Present address
Taylor A. DePauw, Microbiology, Immunology, and Cancer Biology Graduate Group, University of Minnesota, Minneapolis, MN, USA

Funding information
National Cancer Institute, Grant/Award Numbers: R50CA211249, R21CA208529; Institutional training grant in Molecular, Genetic, and Cellular Targets of Cancer, Grant/Award Number: T32CA009138; United States Department of Defense Congressionally Designated Medical Research Program, Grant/Award Numbers: CA170218, CA190276; AKC Canine Health Foundation, Grant/Award Numbers: MOU-02234, MOU-02806; Morris Animal Foundation, Grant/Award Number: D18CA-050; Karen Wyckoff Rein

Abstract

Cancer is among the most common causes of death for dogs (and cats) and humans in the developed world, even though it is uncommon in wildlife and other domestic animals. We provide a rationale for this observation based on recent advances in our understanding of the evolutionary basis of cancer. Over the course of evolutionary time, species have acquired and fine-tuned adaptive cancer-protective mechanisms that are intrinsically related to their energy demands, reproductive strategies, and expected lifespan. These cancer-protective mechanisms are general across species and/or specific to each species and their niche, and they do not seem to be limited in diversity. The evolutionarily acquired cancer-free longevity that defines a species' life history can explain why the relative cancer risk, rate, and incidence are largely similar across most species in the animal kingdom despite differences in body size and life expectancy. The molecular, cellular, and metabolic events that promote malignant transformation and cancerous growth can overcome these adaptive, species-specific protective mechanisms in a small proportion of individuals, while independently, some individuals in the population might achieve exceptional longevity. In dogs and humans, recent dramatic alterations in healthcare and social structures have allowed increasing numbers of individuals in both species to far exceed their species-adapted longevities (by two to four times) without allowing the time necessary for compensatory natural selection. In other words, the cancer-protective

in Sarcoma Foundation; Zach Sobiech Osteosarcoma Fund; Team Nat Fund of the Children's Cancer Research Fund; Animal Cancer Care and Research Program of the University of Minnesota

mechanisms that restrain risk at comparable levels to other species for their adapted lifespan are incapable of providing cancer protection over this recent, drastic, and widespread increase in longevity.

KEYWORDS
cancer-protective mechanisms, cancer risk, evolution, longevity

1 | INTRODUCTION: THE EVOLUTIONARY LEGACY OF CANCER

According to the National Cancer Institute's Surveillance, Epidemiology, and End Results (SEER) Program, cancer describes a group of over 100 pathological conditions that are characterized by uncontrolled cellular proliferation.[1] Even including deaths due to COVID-19 in 2020, cancer is the most common or the second most common cause of death for humans in Europe[2] and in the United States,[3–5] and it is believed that cancer is also the leading cause of disease-related death for older companion and working dogs in the developed world.[6–12]

In a remarkable thesis of how cancer was transformed from an obscure and mystical condition to a medical problem,[13] Koblenz notes that the death rate from cancer increased by almost 20-fold from the years 1850 to 2009, although it is apparent that a major portion of the cancer epidemic of the 20th century was driven by tobacco.[14] For humans living in the United States in 2020, the lifetime probability of being diagnosed with an invasive cancer is approximately 40% (an approximate lifetime risk of 1 in 2.5).[15] Tumors of the prostate, lung, and colon account for more than 40% of all cases in men, and tumors of the breast, lung, and colon account for 50% of all cases in women. Cancer also claims a large number of domestic dogs' and cats' lives.[7,11,12,16–20] Even while the frequent occurrence of cancer in both of these domestic species is well recognized, the precise incidence of invasive cancers remains to be established.[21] Registries that systematically account for cancer incidence and mortality of dogs and cats are not standardized, making comparisons among them challenging.[22] Furthermore, many (perhaps most) cases of suspected cancers in animals are not definitively diagnosed histopathologically, and there are considerable referral biases in the hospital databases used to obtain estimates of cancer incidence and cancer mortality.[23]

Despite these limitations, the Veterinary Cancer Society estimates that one in four dogs will be diagnosed with cancer in their lifetime, and that cancer is the leading cause of death in pets that are beyond middle age.[24]

As hard as it is to obtain actuarial estimates in domestic animals, assessment of disease and cause-specific mortality rates in wild animal populations is even more challenging.[25] The available data suggest that animals in the wild have variable incidence rates of specific cancers, although mortality is often due to loss of fitness, competition, predation, accidents, or human-related causes.[26] It is also clear that the overall rate of cancer among species in captivity is variable,[27] but none are as high as those seen in domestic dogs and cats.[28] Cancers in wild animals where the etiology can be determined are often due to infectious agents[28,29] or the tumors themselves are transmissible,[29–31] and it is notable that such infectious and transmissible cancers represent exceptions to the low rates of cancer observed in wild animals. Conversely, cancers associated with infectious agents (such as feline leukemia virus-associated tumors[32]) and transmissible cancers (such as canine transmissible venereal tumors[33]) account for only a small fraction of the rather large number of cancers seen in dogs and cats in the developed world.

Comparative biologists have questioned why cancer is so prevalent in domestic dogs and in humans, what accounts for the difference in cancer risk and incidence seen in dogs and humans as compared to wild populations, and what we can do about it. In this perspective, we propose that the apparent excess incidence of cancer in both of these species is due to the fact that dogs and humans are two species that have benefited from social, medical, and technological advances that allow them to live beyond the age that nature intended, as species-specific cancer-protective mechanisms that evolved over millions of years[34] cannot address the cancer vulnerabilities acquired through the rapid increase in longevity experienced by modern dogs and humans. The observation that there are substantial differences in the incidence of specific cancer types that afflict domestic pet dogs and humans, despite a closely shared environment, suggests that there are fundamental biological risk factors present in both species that are distinct from environmental exposures.[15,21] This different prevalence of cancer types and the rather poor conservation of genomic driver events in histologically similar cancers of both species should raise a note of caution about "the dog as a model" of cancer causation.[35] On the other hand, the shared sensitivity of dogs and humans to age-associated cancers provides unique opportunities to understand the

relationships between organismal aging and cancer risk.[36] Finally, we advance the concept of risk assessment coupled with strategic prevention as a means to reduce cancer mortality in dogs, and eventually, perhaps also in humans.

1.1 | Cancer is an ancient disease

To understand the apparent cancer epidemic, it is essential to understand the foundational pathogenesis of cancer and its relationship to evolution across the animal kingdom. Cancer arises from the malignant transformation of a single cell that undergoes uncontrolled proliferation, but the disease is confined to multicellular animals.[37,38] In single-cell organisms such as yeast, uncontrolled proliferation might lead to exhaustion of resources that will cause some individuals to die, but others can remain dormant until the environment is once again favorable for growth and reproduction.[39,40] In contrast, because multicellular animals rely on specialization of tissues and organs, they cannot tolerate the damage and dysfunction created by excessive, uncontrolled cellular proliferation even in a single organ or tissue. Thus, cancer is not a modern physiological defect, but rather it is a vulnerability that is rooted deeply in vertebrate evolutionary history[41] and nearly every multicellular animal is at risk for developing cancer.[26,37,38,42] The ancient origins of cancer are supported by the increasing examples of cancers identified in the fossil record.[43–47] While a precise estimate of cancer incidence and prevalence in antiquity is impossible, it has mostly been assumed that it was rare.[48,49] This is partly due to the fact that the fossil record is biased toward tumors of bone (primary and metastatic), which overall represent only a fraction of the cancer burden in modern humans.[50] Historians and scientists have offered different interpretations for this assumed rarity, ranging from lack of exposure to carcinogens that are ubiquitous in modern societies to support it, to the technical and methodological pitfalls in the analysis of paleopathological samples to refute it,[48,51] to the focus on literature and paleopathological specimens originating primarily from ancient Egyptian and Greek societies and neglecting the literature from Chinese and other significant ancient societies.[52]

Ewald has also proposed that the rarity of cancer in antiquity (and in wildlife) could be due to increased mortality of individuals with cancer where such evidence of cancer-related mortality or cancer-related morbidity contributing to mortality would disappear due to predation (consumption of the tumorous tissue).[53] The evidence of cancer could also be erased by environmental effects on the cancerous tissues, directly related to the fragility caused by the cancer, or to the lack of specificity of the pathological changes caused by the cancer.[53] Ewald also suggested that parasites that cause cancer (where parasites are defined broadly to include multicellular, cellular, and subcellular replicative agents that live in or on a host organism and negatively affect the evolutionary fitness of the host) have existed in human and animal populations for millennia, but their impact may be underappreciated by the emphasis of mutations as the root cause of cancer.[53] It is interesting that dogs appear to be a privileged species in this regard: with the exception of canine papillomaviruses that cause benign warts, neither DNA nor RNA oncoviruses that fulfill Koch's postulates have been definitively identified in canids, despite sporadic reports of retrovirus or herpes virus particles in dog lymphomas, leukemias, and peripheral blood lymphocytes.

1.2 | Cellular replication and the creation of aged (permissive) microenvironments are major risk factors for cancer

Malignant transformation, an essential step in the pathogenesis of cancer, is caused by mutations that alter the sequence or structure of DNA.[54] Cancer, thus, results in part from a collection of somatic changes leading to inappropriate cell division or survival, coupled with the failure of tumor-suppressive mechanisms, which together provide cells with a clonal growth advantage. Examples of clonal somatic changes include mutations, copy number changes, and epigenetic structural DNA changes that lead to oncogenic activation. A consequence of this paradigm is that anything that increases somatic changes can also lead to increased cancer risk. A further requirement for cancer formation is that the transformed cells must have a permissive environment where they can grow and develop the complex anatomical structures that create tumors.[54–56] Recently, Laconi and colleagues proposed that, "the tumor-suppressive potential of youth is more potent than previously realized, limiting cancers through half a century of human life even in the face of increased DNA mutations and highly perturbed tissue environments,"[57] and much additional work suggests that organismal aging and the associated development of cellular senescence, proinflammation, and waning immunity appear to be major mechanisms that allow for the development of these permissive environments.[58–64]

Pathologically significant mutations are propagated during the process of DNA replication, as nondividing cells will not pass on the cancer phenotype to progeny cells. The earliest examples that cemented the association between mutations, proliferation, and cancer included the increased cancer risk observed in individuals who had occupational exposures to mutagens,[65,66] habitual

tobacco users,[67] or individuals who had mutations in genes involved in DNA damage repair.[68] Similarly, elevated cancer rates can be found in individuals with germline mutations in DNA polymerases (*POLE*/*POLD1*).[69]

Companion dogs generally do not have the same level of exposures to industrial (occupational) or social (tobacco) mutagens as humans, their hair coat protects them from cancer-causing ultraviolet radiation from the sun, and controlled breeding practices help to significantly reduce the likelihood for true heritable cancer syndromes to become established. In a singular situation where a syndromic cancer (canine renal cystadenoma and nodular dermatofibrosis, associated with a mutation in the folliculin gene) arose in a canine pedigree, it was rapidly identified and characterized,[70,71] providing tools to eliminate it from the breeding population. Some studies have identified associations between certain animal cancers and environmental exposures. For example, studies done by Reif and colleagues 30–40 years ago reported associations between exposure to environmental tobacco smoke and cancers of the respiratory tract in dogs.[72,73] However, these findings have not been replicated in more recent studies.[74] Similar lack of replication has confounded definitive associations between other environmental exposures and dog cancers.[75–77]

On the other hand, consistent associations between certain cancer types and dog breeds suggest enrichment of risk alleles that can inform heritable risks associated with cancer.[21,78–87] While there are multiple examples of genomic regions and of coding and regulatory variants associated with canine tumors in specific breeds,[85,86,88–90] virtually all of these cancers occur in dogs that are past middle age, accounting for variations in breed-specific aging. Furthermore, many factors in the germline seem to contribute to breed-specific risk for cancer in dogs,[91,92] underscoring the complexity of the disease, and/or the incomplete penetrance of the putative risk alleles.

Importantly, the association between cellular replication and cancer is not a new concept. As far back as the early 1900s, Theodor Boveri's work on cell division had led to the hypothesis that cell division created cancer risk.[93] Even to this day, one of the most universal prognostic indicators within tumor tissue is the level of Ki-67 protein, which is often used to gauge the proliferation rate, and by extension the aggressiveness of a tumor.[94]

1.3 | Peto's paradox

An implication of the association between replication and cancer is that increased longevity (more cell divisions) and increased size (more cells) should result in elevated cancer risk and greater cancer incidence. From this paradigm, Sir Richard Peto, a statistician well known for helping to uncover the association between lung cancer and smoking, identified a paradox[95] and articulated the problem,[96] which was subsequently named "Peto's paradox" by Nunney.[97] Peto's paradox states that at the species level, the incidence of cancer does not appear to correlate with the number of cells in an organism. In other words, the predicted linear association between large size of an organism (which is partly due to greater numbers of cells, attained by increased cell division) and cancer is inapparent across the multitude of species in the animal kingdom[27]; extremely large animals, especially those with long lifespans, which undergo far more replications (and therefore would be expected to have an excessively high replicative cancer risk) *do not* have higher cancer rates than smaller animals, which need less replication to attain their adult size and that generally have shorter lifespans (Figure 1). As detailed below, various investigators have since proposed that cancer-protective mechanisms acquired over the course of evolution provide satisfactory answers to Peto's paradox.

2 | CANCER-PROTECTIVE MECHANISMS IN LONG-LIVED SPECIES

Several decades passed between Peto's original observation and the initial formulation of a potential solution, which came to light through the study of large and/or long-lived species of animals that have evolved mechanisms allowing for the minimization of cancer risk (see references[26,34,37,58,97–105] for previous, outstanding discussions on this subject).

As species have evolved, unique adaptations that protect them from cancer have arisen multiple times, and often, independently from each other. These cancer-protective mechanisms address different aspects of vulnerability and they become part of each species' evolutionary history. As illustrated below, different species have "attacked" different aspects of tumor formation, including reducing the likelihood that detrimental mutations are incorporated into their genomes, altering their metabolism, making the tissue microenvironment inhospitable to tumor growth, and probably others. These changes have occurred stochastically over millions of years, but they must have been subject to strong positive selection,[106] with the consequent effect of giving rise to adaptive traits that protect species from cancer[97] while allowing them to occupy niches where they can invest energy to become large, have a long lifespan, or both.[107] It is especially intriguing that in their evolutionary history, several tumor suppressor genes in hominoids have been subject to evolutionary selection such that the wild type (reference) alleles are distinct from variants

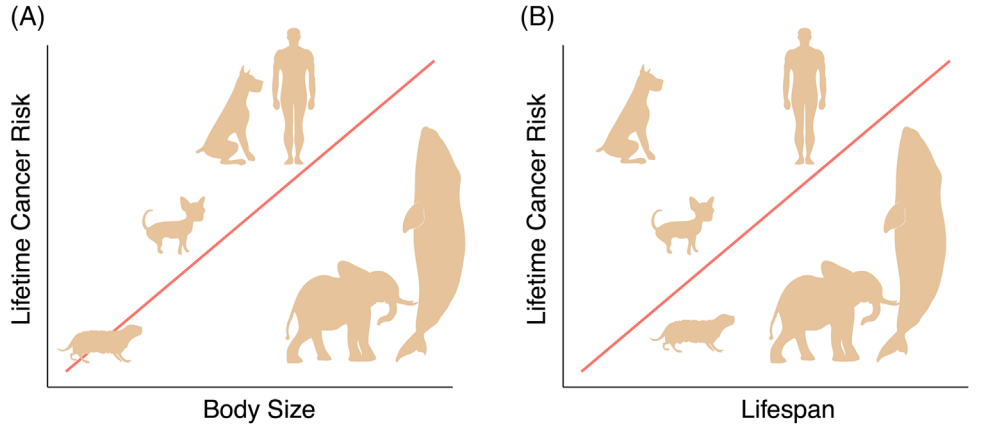

FIGURE 1 Cancer risk and Peto's paradox. Illustration of Peto's paradox, which describes the absence of the predicted relationship between animals' (A) size and (B) longevity relative to their cancer risk

found in apes, and presumably in the common ancestor to these primate species.[106] Indeed, the ancestral wild type alleles for some of these genes such as *APC* and *TP53* (as found in some modern apes), or *BRAF* and *TNFAIP3* (as found in Neanderthals and Denisovans, respectively) are found to be deleterious in modern humans, exclusively as somatic variants, and closely associated with cancer risk.[106]

It is reassuring that many tumor-suppressive mechanisms are highly conserved across vertebrate (and oftentimes invertebrate) species. For example, the products of the *TP53* and the *PTEN* genes, and the enzymes that maintain telomere length, are highly conserved mechanisms that suppress tumor formation across many different species.[108–116] Replicative senescence is another widespread, primordial mechanism that seems to protect animal species against longevity-associated somatic modifications.[117,118] In most cells, senescence programs are activated upon reaching a predetermined number of replication events, as well as by somatic mutation events, and many genes involved in regulation of senescence have been directly implicated in tumor suppression.[119]

Specific examples of species-specific cancer-protective mechanisms have been described in the elephant family, bowhead and other whales, and in different families of long-lived mole rats,[34] while more are being deduced from recently sequenced genomes of other long-lived species such as Amazon parrots,[120] white sharks,[121] and whale sharks.[122] Each of these species appears to have acquired or "fine-tuned" unique mechanisms that allow them to have long and relatively cancer-free lives. For example, the *TP53* gene underwent a series of retrotranspositions in the elephant lineage, after the split from its last common ancestors that in the extreme resulted in more than 20 copies of this gene in modern African elephants.[123,124] While not all of the elephant *TP53* genes are likely to be active, the orthologous elephant p53 protein was shown to be a more potent inducer of the p21cell cycle kinase inhibitor and to have greater pro-apoptotic activity than the human p53 protein. The specific mechanisms of the elephant p53's enhanced apoptotic ability, including it to be delivered as a novel therapeutic for cancer in dogs and humans remains a subject of intense investigation (Dr. Joshua Schiffman, personal communication). The function of the elephant p53 retrogenes remains unclear, but when transfected into human cells, the retrogenes were upregulated and translated upon treatment with chemotherapy and radiation,[123] and in separate experiments, Vazquez and colleagues showed that one or more of the retrotransposons may induce expression of at least one pseudogene (*LIF-6*) that seems to have been refunctionalized to promote apoptosis in elephant cells, but not in those of other mammalian species.[125] And yet, duplication of *TP53* is not unique to elephants, nor does it guarantee long life. Rats, wallabies, and some small bats also have duplicated this gene over the course of evolution without consequent gains in size or longevity.[124]

The bowhead whale genome hints at unique metabolic adaptations, including mutations in *UCP1*, which encodes the mitochondrial uncoupling protein-1 of brown fat, as well as altered insulin signaling. Additionally, the bowhead whale genome includes cancer-protective genes under positive selection, including ERCC1 (excision repair cross-complementing rodent repair deficiency, complementation group-1; a member of the nucleotide excision repair pathway) and duplication of PCNA (proliferating cell nuclear antigen; a gene involved in DNA repair).[126] Other whales, including humpbacks, minkes, and toothed whales seem to have developed segmental duplications in tumor suppressor genes that are species-specific and are also under positive selection,[104,127] consistent with the interpretation that these events occur over long

evolutionary periods and are unique to each species and dictated by their niche.

Rodents show extreme variation in lifespan, which can be used to identify potential cancer-protective mechanisms. Across multiple short- and long-lived rodent species, five amino acid substitutions in *SIRT6* account for most of the variation in DNA double-strand break repair efficacy, with increased *SIRT6* activity also showing a direct correlation with lifespan among these species.[128] Another example comes from mole rats, the longest lived rodents alive today, which can reach 20 to more than 30 years of age. African mole rats of the family Heterocephalidae have developed a series of distinct cancer-protective mechanisms that modify the organization of stromal matrix proteins, making the microenvironment inhospitable to cancer,[129] while the distantly related blind Middle Eastern mole rats of the family Spalacidae have developed a hypersensitive cell-death response to mitigate the excessive drive to proliferate that is associated with events that lead to malignant transformation.[130] Perhaps the most widely recognized cancer-protective mechanism in mole rats is the abundance of high molecular weight hyaluronic acid in the African naked mole rat, possibly due to increased production of hyaluronan by the *HAS2* gene product with concomitant reduced activity of the enzymatic machinery that degrades hyaluronic acid.[129,131] This stands in sharp contrast to the hyaluronic acid content in, for example, human tumors, where hyaluronidases cleave hyaluronic acid into small molecular weight species that promote inflammation and tumor growth.[132]

Together, these examples indicate that large and long-lived animals have evolved diverse and sometimes convergent mechanisms that have enabled large investments in reproduction and high energy requirements over long and relatively noncancer-prone lifespans.[97] These varied solutions to the cancer problem, in turn, create species-specific barriers with limitations on cancer protection determined by the idealized lifespan and body size acquired through these millions of years-long evolutionary processes. And thus, exceeding these barriers through technological innovation to achieve increased lifespans, as is the case with "caninity" and humanity, or via artificial selection (selection for size in the absence of selection for compensatory protective mechanisms), as is the case in dogs, generates conditions that are cancer prone.

We should note that Ujvari and colleagues proposed an alternative hypothesis that, while selective breeding (and inbreeding) and the consequent attenuation of genetic diversity result in the accumulation of deleterious genetic variants in domestic animals, the absence of natural selection could theoretically allow these animals to invest more resources to support existing anticancer mechanisms and potentially develop new ones.[133] While this is an intriguing premise, humans have not significantly increased the lifespan of domestic animals other than dogs and cats, and in our opinion, rare anecdotes of spontaneous cancer regression, for example, in dogs with bone cancer, fail to support strong maintenance or widespread development of novel cancer-protective mechanisms in the accelerated time scale of domestication. On the contrary, the excess of cancers seen in modern dogs (and in humans), and the patterns of their association with age, would strongly suggest that there has been neither sufficient time nor selective pressure to allow for evolution of adaptive mechanisms to reduce the risk of cancer that comes with the creation of aged cellular environments, increased exposures, and the accumulation of somatic mutational events in these populations.

2.1 | Breaking through the evolutionary lifespan adaptation is a major contributor to cancer risk in humans and in dogs

One theme that has been underappreciated, in our opinion, is the dramatic gains in expected lifespan that have occurred in the past 150–200 years in humans and over the past ~50 years in dogs, and the associated risk of cancer that is attributable to aging. According to Finch,[134] life expectancy from birth in humans doubled in the 5–7 million years from the time the hominid lineage split from the common ancestor shared with chimpanzees until modern hunter-gatherers. It is worth noting that the process of speciation in apes and hominoids (presumably similar to the process of speciation in other animals) included unique adaptations in sequence, and perhaps in function of tumor suppressor genes.[106] In their study of 120 oncogenes and tumor suppressor genes in seven hominoid species, including two extinct species, Neanderthal and Denisovan, Kang and Michalak also found opposing selection pressures operating on these two classes of genes, with tumor suppressor genes being under weaker purifying selection than oncogenes.[106] The authors hypothesize that the selective pressures accounting for these differences could come from the activity of oncogenes, where a single variant can be detrimental to the individual, in contrast to tumor suppressor genes, which generally maintain activity even in a state of heterozygosity, and where loss of both alleles is usually necessary for cancer-prone phenotypes to arise.[106]

The precise lifespans of intermediate species during human evolution are unknown, although it is apparent that early modern humans and Neanderthals had a larger proportion of older adults than prior Homo species and Australopithecines.[134] Human life expectancy doubled again in the 150 years between 1860 and 2010 during

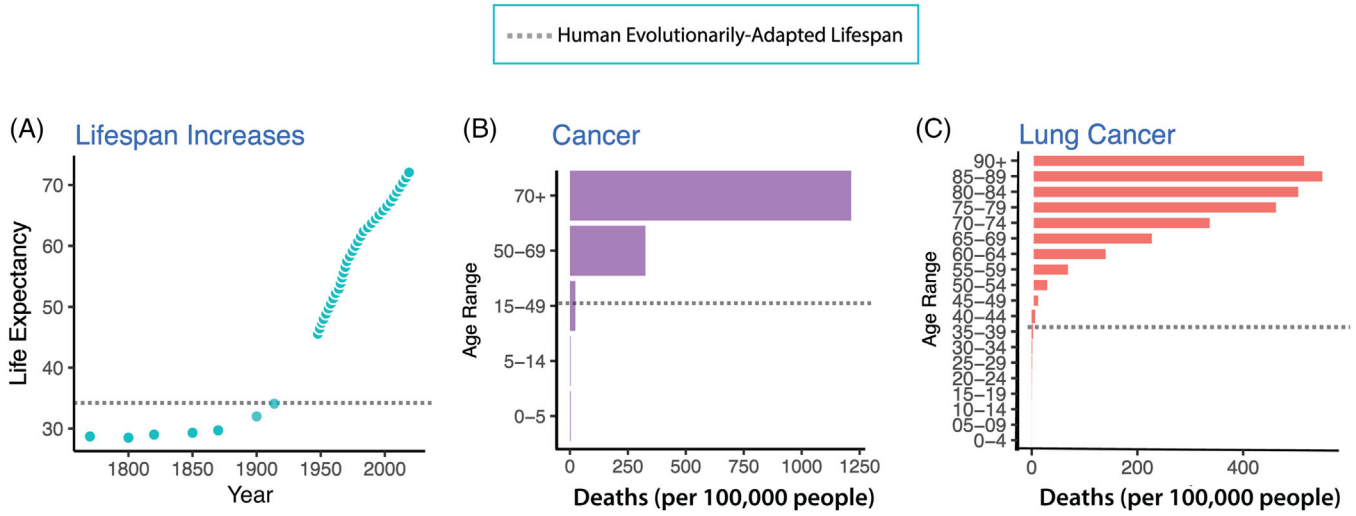

FIGURE 2 Increases in human lifespan overlap with the majority of human cancer deaths. (A) Humans had a relatively stable life expectancy of 30–40 years until the industrial revolution. The upper boundary of this life expectancy represents the ancestral evolved cancer barrier. However, in the 100 years between 1850 and 1950, human life expectancy increased by approximately 50% across the world, and it did so again in the 60 years between 1950 and 2010. That trend continued through the present (latest measurements shown for 2017). (B) The overall cancer death rates per 100,000 people do not have a proportional relationship with age in the United States. Instead, cancer death rates are vanishingly rare, proportionately, in individuals under 15 years of age, they become apparent with a marginal increase between the ages of 40 and 50 after individuals cross the cancer barrier, and then increase dramatically thereafter. Individuals over 60 years of age account for the vast majority of cancer deaths in the United States (United States data from 2017). This is representative for most of the developed world. (C) Lung cancer death rates per 100,000 men also do not have a proportional relationship with age. Despite decades of persistent exposure to myriad potent carcinogens in tobacco products, lung cancer is extremely rare in smokers under the age of 40. Lung cancer becomes more apparent in smokers by the age of 40 after individuals cross the cancer barrier and continues to increase geometrically until the age of 80–85 (United Kingdom data from 2015–2017). This is also representative for most of the developed world

industrialization, and it increased further in the contemporary era with increasing access to hygiene, medical care, and other advantages of complex societies[135] (Figure 2A).

Thus, human lifespan was molded to a niche over a 5–7-million-year period where there were strong evolutionary selective pressures, including selection for cancer-protective mechanisms.[106] Because the niche occupied by our hominid ancestors was different from that occupied by other great apes, we cannot infer their lifespan from that of modern nonhuman great apes. But we can estimate it was shorter than pre-industrial modern humans or 20th century foragers, whose life expectancy was 30–40 years,[134,136] although this was heavily influenced by high infant mortality. Nevertheless, even if we accept an age somewhere between 35 and 45 years as the evolutionarily determined lifespan for humans, fewer than 5% of cancer cases are diagnosed in humans from birth to 35 and less than 10% from birth to 45, making the expected cancer incidence in this population comparable to that seen in apes and monkeys[134] (Figure 2B,C).

Like humans, the lifespan of canids in the wolf family was molded to a niche over a 5–7-million-year period under strong evolutionary selective pressures. We cannot be certain of the expected lifespan of the canid wolf ancestor, but an estimate of approximately 3.5–5 years is possible based on studies of modern wild wolves and feral dog or village dog populations.[106,137,138] And yet, in contrast to what is observed in wolves and in feral dogs and village dogs even today, the expected lifespan of companion pet dogs in much of the developed world has increased by a factor of two to four (to an average of 9–14 years, depending on breed, according to information available from the American Kennel Club[139]) in the ~50 years since dogs were brought into the household and integrated as members of the family in the latter part of the 20th century. Interestingly, the eventual selective breeding for form and function that occurred over the past 15,000 years, and the purposeful derivation of modern dog breeds over the past 100–400 years, might have influenced the canine lifespan through enrichment of alleles that encode for small size.[140,141] But, following the human example, if we accept 3–5 years as the evolutionarily determined lifespan for primordial dogs evolving over a period of *ca.* 6 million years, the available data reproducibly indicate that fewer than 5%–10% of cancer cases are diagnosed in modern dogs from birth to 3–5 years,[12,18,142,143] making the expected cancer incidence in this population comparable to that seen in captive wolves under 5 years of

age[144] (no estimates of cancer exist for wolves or other related canid species in the wild) and to that which has been estimated for most animals in the absence of human influences.[107] It is also worth noting that wolves and other wild canids that are maintained in captivity and that reach advanced ages also exhibit increased susceptibility to some of the most common cancers seen in modern domestic dogs.[144,145]

Hence, we advance the premise that a major component of the elevated cancer risk seen in domestic dogs and in humans when compared to other animals is due to the shattering of the life-expectancy barrier that was evolutionarily determined: essentially "living longer than nature intended." The longevity that both species enjoy at the present time has dramatically increased (two to four times), compared to the lifespan to which each species had adapted over its evolutionarily history (an "evolutionarily determined lifespan"), through social, medical, and technological advancements, over very short periods of time, and with artificial selection playing an increasingly important role, especially in the case of dogs.[58,98]

A recent study of cancer in nondomestic mammals kept in zoological collections is consistent with the interpretation that living longer than nature intended is a major risk factor for cancer. While captivity might introduce its own set of risks for cancer or premature mortality, such as exposure to anthropogenic pollutants, stress, etc., it also removes common causes of mortality for many species, such as competition, predation, accidents, or human-related causes. Consequently, animals in zoos would be expected to outlive some of their counterparts in the wild. Vincze and colleagues did not specifically address gains in longevity in their study, but cancer-related mortality was still lower than 10% for almost 80% of the species in this study (and it was zero for almost 25%).[27] As a group, cancer mortality was highest in carnivores. The authors propose that this might be due to dietary factors (consumption of meat), but it is possible that carnivores are also more amenable than noncarnivores to greater life extension in captivity.

Returning to the dog example, canine osteosarcoma provides a good example to illustrate the association of size and cancer susceptibility, and a solution to Peto's paradox.[98] This disease occurs only rarely in humans, but it is quite common in dogs.[146] Because the natural history of the disease in both species is similar, canine osteosarcoma has been long proposed as a surrogate disease model to better understand its human counterpart.[147,148] In addition to an anatomical predilection for the long bones and shared patterns of metastasis, a few molecular traits are conserved between canine and human osteosarcoma. An initiating event, such as *TP53* mutation, seems to be required, which allows replication of chaotic genomes and clonal outgrowth of tumors with highly disrupted and heterogeneous genomes.[149]

However, important epidemiologic differences coexist with the similarities between human and canine bone tumors. For example, the reported age-adjusted incidence of osteosarcoma in humans is between 0.2 and 4.5 per million, with most affected patients being children, adolescents, and young adults,[150] whereas in dogs, this disease is most commonly observed in adult and elderly individuals from large and giant breeds, with a lifetime risk of approximately one in five at the extreme.[146,148,151–153] The strong association between size and risk of osteosarcoma in dogs illustrates a similar, albeit weaker, association between risk of osteosarcoma and size in humans, where it is more common in males than in females, and in children who are taller and have high birthweights.[154–156]

Of additional interest, larger dogs *age* more rapidly than smaller dogs and have shorter lifespans.[157] This pattern of rapid aging and shorter lifespan also aligns well with the risk for bone cancer (Figure 3), where a high rate of cellular replication is necessary to form large bones (larger than the norm for the species as it evolved), where aged tissues might provide more permissive environments for the development of cancer, and where the protections afforded by modern veterinary healthcare, vaccination against lethal pathogens, appropriate nutrition, and shelter have more than doubled life expectancy for dogs living as companions in the human environment.

The association between increased body size and increased cancer risk is observed, not only with osteosarcoma where the effect manifests in the extreme, but also with other cancers.[7,12,17,19,158] And while the major variant alleles associated with size determination in the dog (including *GHR*, *HMGA2*, *IGF1*, *IGF1R*, *SMAD2*, *STC2*, *LCORL*, and *CDK4*)[159] have not been found to confer independent cancer risk, this may be due to the fact that variants are fixed in purebred dogs. To understand the potential significance of genomic traits that regulate size in dog aging and cancer, future studies should include multiple breeds and/or mixed breed dogs to unmask the potential contribution of fixed alleles.[159,160]

Altogether, these observations suggest that Peto's paradox is no paradox at all, when applied within a single species, and removing the impact of evolution within a niche. That is, Peto's principle (as opposed to Peto's paradox) would predict that increased body size should be associated with increased cancer risk in dogs. Thus, extension of this concept leads to the notion that *longevity is intricately associated with cancer risk, but only when such longevity exceeds the evolutionarily adapted lifespan for that species*. The observation that small dogs live longer than large dogs and have lower cancer rates, thus conforms with Peto's principle.[12,98,161,162]

FIGURE 3 Canine size, lifespan, and osteosarcoma risk. Larger dogs have shorter life expectancy and increased risk for osteosarcoma than smaller dogs. Specifically, using the German shepherd dog breed as the reference, great danes have an odds ratio (OR) of 5 for development of osteosarcoma, whereas miniature schnauzers have an OR of 0.2 for development of osteosarcoma.[153] Overall, the highest risk breed has an OR >200-fold greater than the lowest risk breeds for development of this disease (reproduced from Makielski et al. Risk factors for development of canine and human osteosarcoma: a comparative review. *Vet Sci*. 2019;6(2):48. Copyright: the authors)

Furthermore, these relationships are not completely static, so if replicative senescence is a cancer-protective mechanism, the earlier onset of senescence (as would occur in animals with shorter lifespans) that is observed in large dogs could be related to their increased cancer risk over the same timescale as their smaller counterparts. Untangling the connections between senescence, cancer risk, and lifespan in different dog breeds should generate important insights into how better to understand cancer in humans and identify people with increased risk earlier in their lifetime.[21,36,58,84,162,163]

After considering these concepts, a "simple model" is that, within a given species over the course of a lifetime, cancer-preventive mechanisms may change from protective states ensuring evolutionary fitness to less-protective states once they no longer provide advantage. In other words, anticancer defenses in old animals will be under less selective pressure than in younger animals, and costly defenses are likely to be maintained at a lower level. In reality, this is likely to be far more complicated as progenitor cells need extreme protection from somatic damage, while damage might be tolerated (and is observed) in terminally differentiated cells.[164] This threshold of age-related vulnerability,[58] which is more readily observed after individuals cross cancer-protective barriers for their species, can also explain the prolonged latency seen in humans between carcinogen exposures and the onset of cancer. For example, habitual use of tobacco products usually starts in early adolescence, but the onset of tobacco-related cancers, on average, occurs after the age of 60,[165] which is beyond the predicted cancer-protective barriers for humans (Figure 2C). Intriguingly, the apparent evolution of a permissive environment in the aged lungs may be independent of exposure to tobacco-derived toxicants, although there does appear to be an incontrovertible association between the overall increased frequency of lung cancer and increased mutagenesis mediated by these compounds.[166]

The impact of these ideas is more profound among species. Extension of this concept indicates that small species that are highly vulnerable to predation and rely on explosive growth strategies, such as wild mice, have short lives, and the cost of cancer-protective mechanisms might decrease their overall fitness.[167] The elevated incidence of cancer in laboratory mice, which far exceed the evolutionarily determined lifespan for this species, is consistent with this observation and argues that exceeding this lifespan barrier in any species will probably result in excess cancer when compared to the same population inhabiting within its evolutionary niche. And the opposite may also be true: "ancient" species or species that are less vulnerable to predation and that have had relatively stable body sizes over "long periods" of evolutionary time such as turtles and alligators should have, and likely did evolve, stronger cancer-protective mechanisms,.[34,a] These examples support the ideas that cancer is influenced by evolutionary pressures[58] and that increased risk associated with modern increases in lifespans may be responsible for the observed increased incidence of cancer in human and canine populations. Large dogs are dually affected as artificial selection for large size seems to have had the unintended consequence of increasing cancer risk, perhaps in part by increasing the replicative risk as large stature requires

[a] This concept was also attributed to Dr. Jay Olshansky (University of Chicago) in a Vox article, authored by Joseph Stromberg and published on June 16, 2014 (https://www.vox.com/2014/6/16/5796732/do-naked-mole-rats-have-the-secret-to-long-healthy-lives)

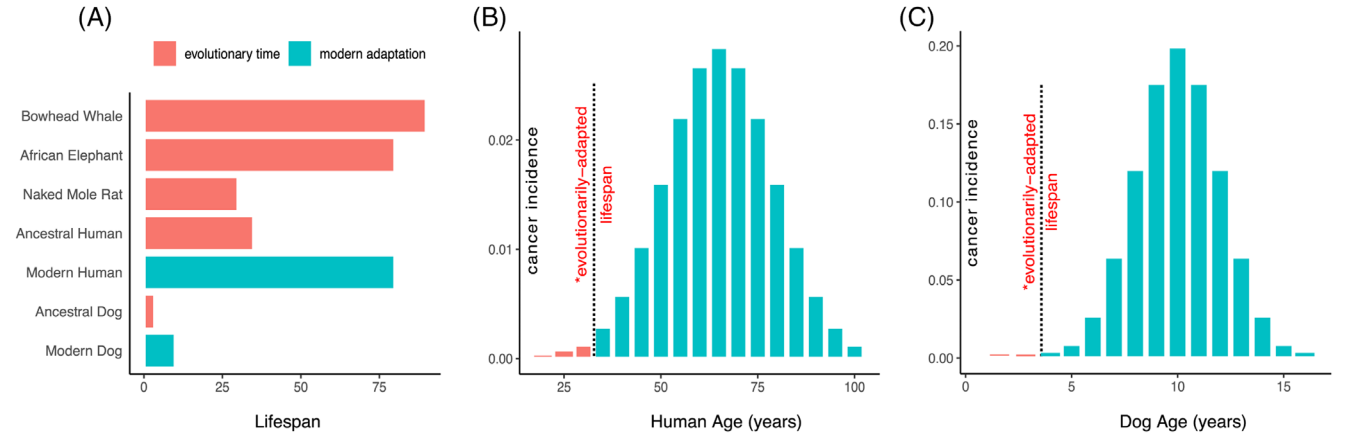

FIGURE 4 Increasing canine and human risk due to surpassing the species' respective evolutionarily determined lifespan barriers. (A) Multicellular species, represented here by bowhead whales, African elephants, African naked mole rats, ancestral humans, modern humans, ancestral dogs, and modern dogs, have achieved an evolutionarily derived balance between tumor-suppressive mechanisms and senescence mechanisms that have selected for lifespans that are consistent with their respective evolutionary pressures. Recent technological advances have led to lifespans in humans and dogs that are more than twice as long as those to which each species had adapted over millions of years of evolution. The vast majority of cancers occur after individuals cross this evolutionarily adapted lifespan (dashed line) for (B) humans and (C) dogs. Neither species has had the time, nor has it been subjected to selective pressures, to establish a new evolutionary balance that resets its cancer barrier

more cells.[12,162] Figure 4 illustrates this concept using bowhead whales, African elephants, African naked mole rats, ancestral humans, modern humans, ancestral dogs, and modern dogs. Each of these species has achieved an evolutionarily derived balance between tumor-suppressive mechanisms and senescence mechanisms that have selected for lifespans that are consistent with their respective evolutionary pressures. Modern humans and modern domestic dogs are outliers in that their expected lifespan now is more than twice as long as that to which each species had adapted over millions of years of evolution, and for both species, the vast majority of cancers occur in individuals that have crossed this evolutionarily adapted lifespan. Neither species has had the time, nor has it been subjected to selective pressures, to establish a new evolutionary balance that resets its cancer barrier.

2.2 | If cancer is virtually inevitable, what is the solution

Cancer is virtually, but not entirely, inevitable. Even with the risks of replication-induced mutations, size, and longevity, only about 25%–40% of all humans and dogs will develop cancer in their lifetime. Incredible breakthroughs have been made in treatments for advanced human cancers, all of which raise hope and might find future applications in dogs.

Nevertheless, the best solution to cancer is to prevent it entirely. Decreasing environmental exposure to carcinogenic agents has been extensively described and pursued in humans.[14] It may be possible to engineer cancer risk out of the genome by increasing endogenous anticancer mechanisms, or potentially by transferring protective strategies utilized by large and long-lived organisms,[168] although this could raise serious ethical dilemmas. In dogs, strategies to decrease environmental exposure to carcinogenic agents are less likely be an effective method to reduce cancer, as the exposure of dogs to such environmental carcinogens is generally quite limited, and at the same time, such exposures might be unavoidable.

In humans, early identification of cancer via screening of at-risk populations has led to effective treatment and decreases in mortality. To extend this approach to dogs, we are developing diagnostic tests to identify canine cancer as early as possible.[169] However, testing for early detection and for risk assessment alone is insufficient. In order to be ethical and valuable, the information from such testing must be actionable. So, our goal is to pair each test with a potential preventive solution that can eliminate the cancer at its earliest stage. One example is the Shine-On project[169,170] (Figure 5), where we have developed a blood test to detect rare events associated with the presence (or risk) of hemangiosarcoma (a malignant tumor of blood vessel-forming cells that is relatively common in dogs), and which is meant to be used once dogs reach an age where risk for this cancer is meaningful (i.e., older than 6 years).[12,142,171,172] Another example from our group is a serum exosomal mRNA signature associated with the presence of osteosarcoma[173] that is currently being investigated for early detection in at-risk breeds of dogs. By design, these early detection and risk assessment tests would be

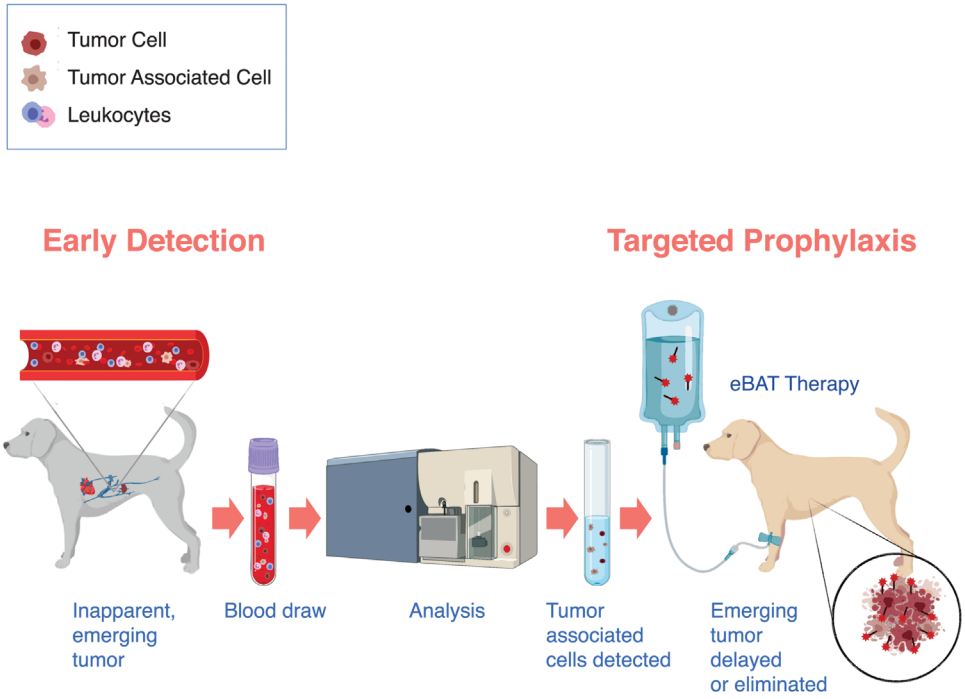

FIGURE 5 The Shine-On concept of paired early detection and strategic prevention. Shine-On illustrates the approach of early detection and strategic cancer prevention. In this case, dogs that reach the age of increased cancer susceptibility are screened for the presence of incipient or emerging hemangiosarcoma (a terminal tumor of blood vessel-forming cells) using the Shine-On suspicion (SOS) test. The SOS test uses flow cytometry and artificial intelligence to enumerate rare hemangiosarcoma-associated cells in blood and to assign a level of risk. Dogs at high risk would be eligible for targeted prophylaxis, for example, using the drug eBAT, with the intent to prevent or delay the development of clinical hemangiosarcoma

paired with a preventive strategy, for example, the targeted drug EGF bispecific angiotoxin (eBAT).[174–176] This preventive solution is based on eBAT's safety profile, which justifies its use in otherwise healthy animals, and on its proposed mechanisms of action to simultaneously eliminate cancer stem cells and disrupt the tumor niche.[174–177] In this way, eBAT may be effective in preventing or delaying the emergence of cancer in healthy dogs determined to be at high risk by eliminating emerging tumors before they ever have a chance to develop. This proof-of-concept in dogs would open the door to develop similar approaches for people.[178] We recognize that these approaches may not be the only or the definitive answer to cancer. But we are convinced that these approaches, and others like them, will be part of the solution. As we tilt the balance toward successful prevention, though, we must remember that it is our duty to support graceful aging. We must resist the siren's song of "longevity at any cost." It is not wise, and it is not evolutionarily sound.

3 | CONCLUSIONS

Our summation of the literature supports the concept that the increased risk of cancer in humans and dogs is a consequence of recent extensions of lifespan and body size beyond evolutionarily determined cancer barriers. In the short-term, we contend that the inevitability of cancer that accompanies these extensions can and should be managed by early detection and risk assessment. For example, screening tests to detect cancer at its inception, before it has become a clinical entity, could be implemented, and paired with rational, strategic interventions such as eBAT that can eliminate the cancer-initiating cell populations and/or make the environment inhospitable for tumor growth. In the long-term, rather than wait for evolutionary innovation, we should carefully consider whether practical and ethical norms would allow engineering of extended cancer-protective mechanisms into at-risk genomes, at least in dog populations that have been rendered highly vulnerable to cancer by artificial selection.

ACKNOWLEDGMENTS

The authors wish to thank Dr. Don Bellgrau and Dr. Logan Spector for their helpful suggestions and critical review of the manuscript, and Curt McAloney (Curt's Media) for assistance with professional illustrations. The work reported in this manuscript was supported in part by the National Cancer Institute of the National Institutes of Health under award numbers R50CA211249 (Aaron L.

Sarver) and R21CA208529 (Jaime F. Modiano) and by the United States Department of Defense Congressionally Designated Medical Research Program under award numbers CA170218 and CA190276 (Jaime F. Modiano). Additional support was provided by grants MOU-02234 and MOU-02806 from the AKC Canine Health Foundation (Jaime F. Modiano) and grant D18CA-050 from Morris Animal Foundation (Jaime F. Modiano). The authors also acknowledge generous support from the Karen Wyckoff Rein in Sarcoma Foundation, the Zach Sobiech Osteosarcoma Fund, and the Team Nat Fund of the Children's Cancer Research Fund, and the Animal Cancer Care and Research Program of the University of Minnesota and its many individual donors. Kelly M. Makielski was supported in part by a postdoctoral fellowship from the institutional NIH training grant in Molecular, Genetic, and Cellular Targets of Cancer (T32CA009138). Jaime F. Modiano was supported in part by the Alvin and June Perlman Endowed Chair in Animal Oncology. The content of this manuscript is solely the responsibility of the authors and does not necessarily represent the official views of the National Institutes of Health, the Public Health Service, the United States Department of Defense, or any of the other agencies that provided support for this work.

CONFLICT OF INTEREST

Jaime F. Modiano is an inventor on U.S. patent 7910315, "Early Detection of Hemangiosarcoma and Angiosarcoma," assigned to the Regents of the University of Colorado. Jaime F. Modiano is an inventor on U.S. patent application, "Reduction of EGFR Therapeutic Toxicity," filed on behalf of the Regents of the University of Minnesota. Jaime F. Modiano and Taylor A. DePauw are inventors on U.S. patent application, "Artificial Intelligence for Early Cancer Detection," filed on behalf of the Regents of the University of Minnesota.

AUTHOR CONTRIBUTIONS

All authors had full access to the data in the study and take responsibility for the integrity of the data and the accuracy of the data analysis. Conceptualization: Aaron L. Sarver and Jaime F. Modiano. Methodology: Aaron L. Sarver, Kelly M. Makielski, Taylor A. DePauw, Ashley J. Schulte, and Jaime F. Modiano. Data curation: Aaron L. Sarver and Jaime F. Modiano. Investigation: Aaron L. Sarver, Kelly M. Makielski, Taylor A. DePauw, Ashley J. Schulte, and Jaime F. Modiano. Formal analysis: Aaron L. Sarver and Jaime F. Modiano. Resources: Aaron L. Sarver, Kelly M. Makielski, Taylor A. DePauw, Ashley J. Schulte, and Jaime F. Modiano. Writing the original draft: Aaron L. Sarver and Jaime F. Modiano. Writing the review and editing: Aaron L. Sarver, Kelly M. Makielski, Taylor A. DePauw, Ashley J. Schulte, and Jaime F. Modiano. Visualization: Aaron L. Sarver, Kelly M. Makielski, Taylor A. DePauw, Ashley J. Schulte, and Jaime F. Modiano. Supervision: Jaime F. Modiano. Funding acquisition: Aaron L. Sarver, Kelly M. Makielski, and Jaime F. Modiano.

DATA AVAILABILITY STATEMENT

The data used to illustrate the premises of this study were derived from the following resources available in the public domain: Life expectancy data (1770–2017) in Figure 2A are from Our World in Data and are available at https://ourworldindata.org/life-expectancy. Cancer death rates by age group in Figure 2B are from Our World in Data and are available at https://ourworldindata.org/cancer. Lung cancer incidence statistics in Figure 2C are from Cancer Research UK and are available at https://www.cancerresearchuk.org/health-professional/cancer-statistics/statistics-by-cancer-type/lung-cancer/incidence#ref-1. Age and cancer risk data in Figure 4B are modeled from the NCI Surveillance Epidemiology and End Results (SEER) Program.[1] Cancer attributed deaths in dogs in Figure 4C are modeled from ref.[142]

ORCID

Jaime F. Modiano https://orcid.org/0000-0001-6398-7648

REFERENCES

1. National Cancer Institute. *SEER Training Modules, What Is Cancer?* U.S. National Institutes of Health, National Cancer Institute. Accessed February 21, 2021. https://training.seer.cancer.gov/
2. Townsend N, Wilson L, Bhatnagar P, Wickramasinghe K, Rayner M, Nichols M. Cardiovascular disease in Europe: epidemiological update 2016. *Eur Heart J*. 2016;37(42):3232-3245.
3. Heron M, Anderson RN. Changes in the leading cause of death: recent patterns in heart disease and cancer mortality. *NCHS Data Brief*. 2016;(254):1-8.
4. Siegel RL, Miller KD, Fuchs HE, Jemal A. Cancer statistics, 2021. *CA Cancer J Clin*. 2021;71(1):7-33.
5. Ahmad FB, Anderson RN. The leading causes of death in the US for 2020. *JAMA*. 2021;325(18):1829-1830.
6. Adams VJ, Evans KM, Sampson J, Wood JL. Methods and mortality results of a health survey of purebred dogs in the UK. *J Small Anim Pract*. 2010;51(10):512-524.
7. Bonnett BN, Egenvall A, Hedhammar A, Olson P. Mortality in over 350,000 insured Swedish dogs from 1995–2000: I. Breed-, gender-, age- and cause-specific rates. *Acta Vet Scand*. 2005;46(3):105-120.
8. Egenvall A, Bonnett BN, Hedhammar A, Olson P. Mortality in over 350,000 insured Swedish dogs from 1995–2000: II. Breed-specific age and survival patterns and relative risk for causes of death. *Acta Vet Scand*. 2005;46(3):121-136.
9. Proschowsky HF, Rugbjerg H, Ersboll AK. Mortality of purebred and mixed-breed dogs in Denmark. *Prev Vet Med*. 2003;58(1-2):63-74.

10. Moore GE, Burkman KD, Carter MN, Peterson MR. Causes of death or reasons for euthanasia in military working dogs: 927 cases (1993–1996). *J Am Vet Med Assoc*. 2001;219(2):209-214.
11. Dobson JM. Breed-predispositions to cancer in pedigree dogs. *ISRN Vet Sci*. 2013;2013:941275.
12. Fleming JM, Creevy KE, Promislow DE. Mortality in North American dogs from 1984 to 2004: an investigation into age-, size-, and breed-related causes of death. *J Vet Intern Med*. 2011;25(2):187-198.
13. Koblenz L. *From Sin to Science: The Cancer Revolution of the Nineteenth Century*. Graduate School of Arts and Sciences, Columbia University; 2013.
14. Jha P. The hazards of smoking and the benefits of cessation: a critical summation of the epidemiological evidence in high-income countries. *Elife*. 2020;9:e49979.
15. Siegel RL, Miller KD, Jemal A. Cancer statistics, 2020. *CA Cancer J Clin*. 2020;70(1):7-30.
16. Graf R, Gruntzig K, Boo G, et al. Swiss feline cancer registry 1965–2008: the influence of sex, breed and age on tumour types and tumour locations. *J Comp Pathol*. 2016;154(2-3):195-210.
17. Gruntzig K, Graf R, Boo G, et al. Swiss canine cancer registry 1955–2008: occurrence of the most common tumour diagnoses and influence of age, breed, body size, sex and neutering status on tumour development. *J Comp Pathol*. 2016;155(2-3):156-170.
18. Dorn CR, Taylor DO, Schneider R, Hibbard HH, Klauber MR. Survey of animal neoplasms in Alameda and Contra Costa Counties, California. II. Cancer morbidity in dogs and cats from Alameda County. *J Natl Cancer Inst*. 1968;40(2):307-318.
19. Bonnett BN, Egenvall A, Olson P, Hedhammar A. Mortality in insured Swedish dogs: rates and causes of death in various breeds. *Vet Rec*. 1997;141(2):40-44.
20. Cannon CM. Cats, cancer and comparative oncology. *Vet Sci*. 2015;2(3):111-126.
21. Davis BW, Ostrander EA. Domestic dogs and cancer research: a breed-based genomics approach. *ILAR J*. 2014;55(1):59-68.
22. Pinello KC, Queiroga F, de Matos A, et al. The Global Initiative for Veterinary Cancer Surveillance (GIVCS): report of the first meeting and future perspectives. *Vet Comp Oncol*. 2020;18(2):141-142.
23. Bartlett PC, Van Buren JW, Neterer M, Zhou C. Disease surveillance and referral bias in the veterinary medical database. *Prev Vet Med*. 2010;94(3-4):264-271.
24. What are the most common types of cancers in dogs? How many dogs typically get cancer? Veterinary Cancer Society; 2021. Accessed December 20, 2021. http://vetcancersociety.org/pet-owners/faqs/
25. Joly DO, Heisey DM, Samuel MD, et al. Estimating cause-specific mortality rates using recovered carcasses. *J Wildl Dis*. 2009;45(1):122-127.
26. Boddy AM, Abegglen LM, Pessier AP, et al. Lifetime cancer prevalence and life history traits in mammals. *Evol Med Public Health*. 2020;2020(1):187-195.
27. Vincze O, Colchero F, Lemaitre JF, et al. Cancer risk across mammals. *Nature*. 2022;601(7892):263-267.
28. Madsen T, Arnal A, Vittecoq M, et al. Cancer prevalence and etiology in wild and captive animals. In: *Ecology and Evolution of Cancer*. 2017:11-46.
29. Ewald PW, Swain Ewald HA. Infection and cancer in multicellular organisms. *Philos Trans R Soc Lond B Biol Sci*. 2015;370(1673):20140224.
30. Pye RJ, Woods GM, Kreiss A. Devil facial tumor disease. *Vet Pathol*. 2016;53(4):726-736.
31. Ujvari B, Papenfuss AT, Belov K. Transmissible cancers in an evolutionary context. *Bioessays*. 2016;38:S14-S23.
32. Sykes JE, Hartmann K. Feline leukemia virus infection. In: *Canine and Feline Infectious Diseases*. 2014:224-238.
33. Strakova A, Murchison EP. The changing global distribution and prevalence of canine transmissible venereal tumour. *BMC Vet Res*. 2014;10:168.
34. Seluanov A, Gladyshev VN, Vijg J, Gorbunova V. Mechanisms of cancer resistance in long-lived mammals. *Nat Rev Cancer*. 2018;18(7):433-441.
35. Modiano JF, Kim JH. The etiology of cancer. Section A: the genetic basis of cancer. In: Vail DM, Thamm DH, Liptak JM, eds. *Withrow & MacEwen's Small Animal Clinical Oncology*. 6th ed. Elsevier; 2020:1-11.
36. Kaeberlein M, Creevy KE, Promislow DE. The dog aging project: translational geroscience in companion animals. *Mamm Genome*. 2016;27(7-8):279-288.
37. Aktipis CA, Boddy AM, Jansen G, et al. Cancer across the tree of life: cooperation and cheating in multicellularity. *Philos Trans R Soc Lond B Biol Sci*. 2015;370(1673):20140219.
38. Domazet-Loso T, Tautz D. Phylostratigraphic tracking of cancer genes suggests a link to the emergence of multicellularity in metazoa. *BMC Biol*. 2010;8:66.
39. Gray JV, Petsko GA, Johnston GC, Ringe D, Singer RA, Werner-Washburne M. "Sleeping beauty": quiescence in *Saccharomyces cerevisiae*. *Microbiol Mol Biol Rev*. 2004;68(2):187-206.
40. Alanio A. Dormancy in *Cryptococcus neoformans*: 60 years of accumulating evidence. *J Clin Invest*. 2020;130(7):3353-3360.
41. Haridy Y, Witzmann F, Asbach P, Schoch RR, Frobisch N, Rothschild BM. Triassic cancer-osteosarcoma in a 240-million-year-old stem-turtle. *JAMA Oncol*. 2019;5(3):425-426.
42. Boddy AM, Harrison TM, Abegglen LM. Comparative oncology: new insights into an ancient disease. *iScience*. 2020;23(8):101373.
43. Czarnetzki A, Schwaderer E, Pusch CM. Fossil record of meningioma. *Lancet*. 2003;362(9381):408.
44. Dumbrava MD, Rothschild BM, Weishampel DB, et al. A dinosaurian facial deformity and the first occurrence of ameloblastoma in the fossil record. *Sci Rep*. 2016;6:29271.
45. Ekhtiari S, Chiba K, Popovic S, et al. First case of osteosarcoma in a dinosaur: a multimodal diagnosis. *Lancet Oncol*. 2020;21(8):1021-1022.
46. Rothschild BM, Tanke DH, Helbling M 2nd, Martin LD. Epidemiologic study of tumors in dinosaurs. *Naturwissenschaften*. 2003;90(11):495-500.
47. Rothschild BM, Witzke BJ, Hershkovitz I. Metastatic cancer in the Jurassic. *Lancet*. 1999;354(9176):398.
48. Faltas B. Cancer is an ancient disease: the case for better palaeoepidemiological and molecular studies. *Nat Rev Cancer*. 2011;11(1):76; author reply 76.
49. Gamba S, Fornaciari G. The problem of cancer in antiquity: brief review of 94 cases. University of Pisa Medical School; 2017. Accessed March 14, 2021. https://www.paleopatologia.it/the-problem-of-cancer-in-antiquity-brief-review-of-94-cases/
50. Binder M, Roberts C, Spencer N, Antoine D, Cartwright C. On the antiquity of cancer: evidence for metastatic carcinoma in a young man from ancient Nubia (c. 1200 BC). *PLoS One*. 2014;9(3):e90924.

51. David AR, Zimmerman MR. Cancer: an old disease, a new disease or something in between? *Nat Rev Cancer*. 2010;10(10):728-733.
52. Wang Y, Zhang T, Wang W. An old disease, a new disease or something in between: evidence from China. *Nat Rev Cancer*. 2011;11(1):76.
53. Ewald PW. Ancient cancers and infection-induced oncogenesis. *Int J Paleopathol*. 2018;21:178-185.
54. Hanahan D, Weinberg RA. Hallmarks of cancer: the next generation. *Cell*. 2011;144(5):646-674.
55. DeGregori J. Connecting cancer to its causes requires incorporation of effects on tissue microenvironments. *Cancer Res*. 2017;77(22):6065-6068.
56. Langsten KL, Kim JH, Sarver AL, Dewhirst M, Modiano JF. Comparative approach to the temporo-spatial organization of the tumor microenvironment. *Front Oncol*. 2019;9:1185.
57. Laconi E, Marongiu F, DeGregori J. Cancer as a disease of old age: changing mutational and microenvironmental landscapes. *Br J Cancer*. 2020;122(7):943-952.
58. Rozhok AI, DeGregori J. The evolution of lifespan and age-dependent cancer risk. *Trends Cancer*. 2016;2(10):552-560.
59. Rozhok AI, DeGregori J. The three dimensions of somatic evolution: integrating the role of genetic damage, life-history traits, and aging in carcinogenesis. *Evol Appl*. 2020;13(7):1569-1580.
60. Rozhok A, DeGregori J. A generalized theory of age-dependent carcinogenesis. *Elife*. 2019;8:e39950.
61. Evans EJ Jr, DeGregori J. Cells with cancer-associated mutations overtake our tissues as we age. *Aging Cancer*. 2021;2(3):82-97.
62. Campisi J. Cancer, aging and cellular senescence. *In Vivo*. 2000;14(1):183-188.
63. Velarde MC, Demaria M, Campisi J. Senescent cells and their secretory phenotype as targets for cancer therapy. *Interdiscip Top Gerontol*. 2013;38:17-27.
64. Ruhland MK, Loza AJ, Capietto AH, et al. Stromal senescence establishes an immunosuppressive microenvironment that drives tumorigenesis. *Nat Commun*. 2016;7:11762.
65. Nicholson WJ. Cancer following occupational exposure to asbestos and vinyl chloride. *Cancer*. 1977;39:1792-1801.
66. Boffetta P, Jourenkova N, Gustavsson P. Cancer risk from occupational and environmental exposure to polycyclic aromatic hydrocarbons. *Cancer Causes Control*. 1997;8(3):444-472.
67. Wogan GN, Hecht SS, Felton JS, Conney AH, Loeb LA. Environmental and chemical carcinogenesis. *Semin Cancer Biol*. 2004;14(6):473-486.
68. Knudson AG. Cancer genetics. *Am J Med Genet*. 2002;111(1):96-102.
69. Robinson PS, Coorens THH, Palles C, et al. Increased somatic mutation burdens in normal human cells due to defective DNA polymerases. *Nat Genet*. 2021;53(10):1434-1442.
70. Lingaas F, Comstock KE, Kirkness EF, et al. A mutation in the canine BHD gene is associated with hereditary multifocal renal cystadenocarcinoma and nodular dermatofibrosis in the German Shepherd dog. *Hum Mol Genet*. 2003;12(23):3043-3053.
71. Jonasdottir TJ, Mellersh CS, Moe L, et al. Genetic mapping of a naturally occurring hereditary renal cancer syndrome in dogs. *Proc Natl Acad Sci U S A*. 2000;97(8):4132-4137.
72. Reif JS, Cohen D. The environmental distribution of canine respiratory tract neoplasms. *Arch Environ Health*. 1971;22(1):136-140.
73. Reif JS, Dunn K, Ogilvie GK, Harris CK. Passive smoking and canine lung cancer risk. *Am J Epidemiol*. 1992;135(3):234-239.
74. Zierenberg-Ripoll A, Pollard RE, Stewart SL, et al. Association between environmental factors including second-hand smoke and primary lung cancer in dogs. *J Small Anim Pract*. 2018;59(6):343-349.
75. Garabrant DH, Philbert MA. Review of 2,4-dichlorophenoxyacetic acid (2,4-D) epidemiology and toxicology. *Crit Rev Toxicol*. 2002;32(4):233-257.
76. Kaneene JB, Miller R. Re-analysis of 2,4-D use and the occurrence of canine malignant lymphoma. *Vet Hum Toxicol*. 1999;41(3):164-170.
77. Hayes HM, Tarone RE, Cantor KP, Jessen CR, McCurnin DM, Richardson RC. Case-control study of canine malignant lymphoma: positive association with dog owner's use of 2,4-dichlorophenoxyacetic acid herbicides. *J Natl Cancer Inst*. 1991;83(17):1226-1231.
78. Sutter NB, Ostrander EA. Dog star rising: the canine genetic system. *Nat Rev Genet*. 2004;5(12):900-910.
79. Khanna C, Lindblad-Toh K, Vail D, et al. The dog as a cancer model. *Nat Biotechnol*. 2006;24(9):1065-1066.
80. Ostrander EA. Canine cancer: mapping complex traits in the domestic dog. In: Genes Dogs and Cancer: Fifth International Cancer Conference; February 13–15, 2009; Orlando, FL.
81. Shearin AL, Ostrander EA. Leading the way: canine models of genomics and disease. *Dis Model Mech*. 2010;3(1-2):27-34.
82. Shearin AL, Hedan B, Cadieu E, et al. The MTAP-CDKN2A locus confers susceptibility to a naturally occurring canine cancer. *Cancer Epidemiol Biomarkers Prev*. 2012;21(7):1019-1027.
83. Truve K, Dickinson P, Xiong A, et al. Utilizing the dog genome in the search for novel candidate genes involved in glioma development-genome wide association mapping followed by targeted massive parallel sequencing identifies a strongly associated locus. *PLoS Genet*. 2016;12(5):e1006000.
84. Ostrander EA, Dreger DL, Evans JM. Canine cancer genomics: lessons for canine and human health. *Annu Rev Anim Biosci*. 2019;7:449-472.
85. Decker B, Parker HG, Dhawan D, et al. Homologous mutation to human BRAF V600E is common in naturally occurring canine bladder cancer–evidence for a relevant model system and urine-based diagnostic test. *Mol Cancer Res*. 2015;13(6):993-1002.
86. Evans JM, Parker HG, Rutteman GR, et al. Multi-omics approach identifies germline regulatory variants associated with hematopoietic malignancies in retriever dog breeds. *PLoS Genet*. 2021;17(5):e1009543.
87. Modiano JF, Breen M, Burnett RC, et al. Distinct B-cell and T-cell lymphoproliferative disease prevalence among dog breeds indicates heritable risk. *Cancer Res*. 2005;65(13):5654-5661.
88. Karyadi DM, Karlins E, Decker B, et al. A copy number variant at the KITLG locus likely confers risk for canine squamous cell carcinoma of the digit. *PLoS Genet*. 2013;9(3):e1003409.
89. Biasoli D, Compston-Garnett L, Ricketts SL, et al. A synonymous germline variant in a gene encoding a cell adhesion molecule is associated with cutaneous mast cell tumour development in Labrador and Golden Retrievers. *PLoS Genet*. 2019;15(3):e1007967.
90. Hedan B, Cadieu E, Rimbault M, et al. Identification of common predisposing loci to hematopoietic cancers in four dog breeds. *PLoS Genet*. 2021;17(4):e1009395.

91. Karlsson EK, Sigurdsson S, Ivansson E, et al. Genome-wide analyses implicate 33 loci in heritable dog osteosarcoma, including regulatory variants near CDKN2A/B. *Genome Biol*. 2013;14(12):R132.
92. Tonomura N, Elvers I, Thomas R, et al. Genome-wide association study identifies shared risk loci common to two malignancies in golden retrievers. *PLoS Genet*. 2015;11(2):e1004922.
93. Boveri T. Concerning the origin of malignant tumors. *J Cell Sci*. 2008;121:1-84.
94. Scholzen T, Gerdes J. The Ki-67 protein: from the known and the unknown. *J Cell Physiol*. 2000;182(3):311-322.
95. Peto R. Quantitative implications of the approximate irrelevance of mammalian body size and lifespan to lifelong cancer risk. *Philos Trans R Soc Lond B Biol Sci*. 2015;370(1673):20150198.
96. Peto R. Epidemiology, multistage models, and short-term mutagenicity tests. In: Hiatt HH, Watson JD, Winsten JA, eds. *Origins of Human Cancer*. Cold Spring Harbor Laboratory; 1977:1403-1428.
97. Nunney L. Lineage selection and the evolution of multistage carcinogenesis. *Proc Biol Sci*. 1999;266(1418):493-498.
98. Nunney L. Resolving Peto's paradox: modeling the potential effects of size-related metabolic changes, and of the evolution of immune policing and cancer suppression. *Evol Appl*. 2020;13(7):1581-1592.
99. Noble R, Kaltz O, Hochberg ME. Peto's paradox and human cancers. *Philos Trans R Soc Lond B Biol Sci*. 2015;370(1673):20150104.
100. Moller AP, Erritzoe J, Soler JJ. Life history, immunity, Peto's paradox and tumours in birds. *J Evol Biol*. 2017;30(5):960-967.
101. Caulin AF, Maley CC. Peto's paradox: evolution's prescription for cancer prevention. *Trends Ecol Evol*. 2011;26(4):175-182.
102. Roche B, Hochberg ME, Caulin AF, et al. Natural resistance to cancers: a Darwinian hypothesis to explain Peto's paradox. *BMC Cancer*. 2012;12:387.
103. Brown JS, Cunningham JJ, Gatenby RA. The multiple facets of Peto's paradox: a life-history model for the evolution of cancer suppression. *Philos Trans R Soc Lond B Biol Sci*. 2015;370(1673):20140221.
104. Tollis M, Robbins J, Webb AE, et al. Return to the sea, get huge, beat cancer: an analysis of cetacean genomes including an assembly for the humpback whale (Megaptera novaeangliae). *Mol Biol Evol*. 2019;36(8):1746-1763.
105. Rozhok AI, DeGregori J. Toward an evolutionary model of cancer: considering the mechanisms that govern the fate of somatic mutations. *Proc Natl Acad Sci U S A*. 2015;112(29):8914-8921.
106. Kang L, Michalak P. The evolution of cancer-related genes in hominoids. *J Mol Evol*. 2015;80(1):37-41.
107. Hochberg ME, Noble RJ. A framework for how environment contributes to cancer risk. *Ecol Lett*. 2017;20(2):117-134.
108. Biscotti MA, Barucca M, Carducci F, Forconi M, Canapa A. The p53 gene family in vertebrates: evolutionary considerations. *J Exp Zool B Mol Dev Evol*. 2019;332(6):171-178.
109. Cayuela ML, Claes KBM, Ferreira MG, et al. The zebrafish as an emerging model to study DNA damage in aging, cancer and other diseases. *Front Cell Dev Biol*. 2018;6:178.
110. Coffill CR, Lee AP, Siau JW, et al. The p53-Mdm2 interaction and the E3 ligase activity of Mdm2/Mdm4 are conserved from lampreys to humans. *Genes Dev*. 2016;30(3):281-292.
111. den Hertog J. Tumor suppressors in zebrafish: from TP53 to PTEN and beyond. *Adv Exp Med Biol*. 2016;916:87-101.
112. Jolliffe AK, Derry WB. The TP53 signaling network in mammals and worms. *Brief Funct Genomics*. 2013;12(2):129-141.
113. Justiniano SE, Mathew A, Mitra S, Manivannan SN, Simcox A. Loss of the tumor suppressor Pten promotes proliferation of Drosophila melanogaster cells in vitro and gives rise to continuous cell lines. *PLoS One*. 2012;7(2):e31417.
114. Nowak K, Seisenbacher G, Hafen E, Stocker H. Nutrient restriction enhances the proliferative potential of cells lacking the tumor suppressor PTEN in mitotic tissues. *Elife*. 2013;2:e00380.
115. Sieren JC, Quelle D, Meyerholz DK, Rogers CS. Porcine cancer models for translational oncology. *Mol Cell Oncol*. 2014;1(4):e969626.
116. Xue B, Brown CJ, Dunker AK, Uversky VN. Intrinsically disordered regions of p53 family are highly diversified in evolution. *Biochim Biophys Acta*. 2013;1834(4):725-738.
117. Tian X, Doerig K, Park R, et al. Evolution of telomere maintenance and tumour suppressor mechanisms across mammals. *Philos Trans R Soc Lond B Biol Sci*. 2018;373(1741):20160443.
118. Risques RA, Promislow DEL. All's well that ends well: why large species have short telomeres. *Philos Trans R Soc Lond B Biol Sci*. 2018;373(1741):20160448.
119. Calcinotto A, Kohli J, Zagato E, Pellegrini L, Demaria M, Alimonti A. Cellular senescence: aging, cancer, and injury. *Physiol Rev*. 2019;99(2):1047-1078.
120. Wirthlin M, Lima NCB, Guedes RLM, et al. Parrot genomes and the evolution of heightened longevity and cognition. *Curr Biol*. 2018;28(24):4001-4008.e7.
121. Marra NJ, Stanhope MJ, Jue NK, et al. White shark genome reveals ancient elasmobranch adaptations associated with wound healing and the maintenance of genome stability. *Proc Natl Acad Sci U S A*. 2019;116(10):4446-4455.
122. Weber JA, Park SG, Luria V, et al. The whale shark genome reveals how genomic and physiological properties scale with body size. *Proc Natl Acad Sci U S A*. 2020;117(34):20662-20671.
123. Abegglen LM, Caulin AF, Chan A, et al. Potential mechanisms for cancer resistance in elephants and comparative cellular response to DNA damage in humans. *JAMA*. 2015;314(17):1850-1860.
124. Sulak M, Fong L, Mika K, et al. TP53 copy number expansion is associated with the evolution of increased body size and an enhanced DNA damage response in elephants. *Elife*. 2016;5:e11994.
125. Vazquez JM, Sulak M, Chigurupati S, Lynch VJ. A zombie LIF gene in elephants is upregulated by TP53 to induce apoptosis in response to DNA damage. *Cell Rep*. 2018;24(7):1765-1776.
126. Keane M, Semeiks J, Webb AE, et al. Insights into the evolution of longevity from the bowhead whale genome. *Cell Rep*. 2015;10(1):112-122.
127. Tejada-Martinez D, de Magalhães JP, Opazo JC. Positive selection and gene duplications in tumour suppressor genes reveal clues about how cetaceans resist cancer. *Proc Biol Sci*. 2021;288(1945):20202592.
128. Tian X, Firsanov D, Zhang Z, et al. SIRT6 is responsible for more efficient DNA double-strand break repair in long-lived species. *Cell*. 2019;177(3):622-638.e22.

129. Tian X, Azpurua J, Hine C, et al. High-molecular-mass hyaluronan mediates the cancer resistance of the naked mole rat. *Nature*. 2013;499(7458):346-349.
130. Gorbunova V, Hine C, Tian X, et al. Cancer resistance in the blind mole rat is mediated by concerted necrotic cell death mechanism. *Proc Natl Acad Sci U S A*. 2012;109(47):19392-19396.
131. Faulkes CG, Davies KT, Rossiter SJ, Bennett NC. Molecular evolution of the hyaluronan synthase 2 gene in mammals: implications for adaptations to the subterranean niche and cancer resistance. *Biol Lett*. 2015;11(5):20150185.
132. Liu M, Tolg C, Turley E. Dissecting the dual nature of hyaluronan in the tumor microenvironment. *Front Immunol*. 2019;10:947.
133. Thomas F, Giraudeau M, Dheilly NM, et al. Rare and unique adaptations to cancer in domesticated species: an untapped resource? *Evol Appl*. 2020;13(7):1605-1614.
134. Finch CE. Evolution in health and medicine Sackler colloquium: evolution of the human lifespan and diseases of aging: roles of infection, inflammation, and nutrition. *Proc Natl Acad Sci U S A*. 2010;107:1718-1724.
135. Life expectancy. OurWorldInData.org; 2013. Accessed April 26, 2021. https://ourworldindata.org/life-expectancy
136. Caspari R, Lee SH. Older age becomes common late in human evolution. *Proc Natl Acad Sci U S A*. 2004;101(30):10895-10900.
137. Basic wolf life history facts. Western Wildlife Outreach; 2021. Accessed December 12, 2021. https://westernwildlife.org/gray-wolf-outreach-project/faqs/
138. Czupryna AM, Brown JS, Bigambo MA, et al. Ecology and demography of free-roaming domestic dogs in rural villages near Serengeti National Park in Tanzania. *PLoS One*. 2016;11(11):e0167092.
139. Burke A. How long do dogs live? American Kennel Club; 2016. Accessed December 12, 2021. https://www.akc.org/expert-advice/health/how-long-do-dogs-live/
140. Rimbault M, Beale HC, Schoenebeck JJ, et al. Derived variants at six genes explain nearly half of size reduction in dog breeds. *Genome Res*. 2013;23(12):1985-1995.
141. Sutter NB, Bustamante CD, Chase K, et al. A single IGF1 allele is a major determinant of small size in dogs. *Science*. 2007;316(5821):112-115.
142. Kent MS, Burton JH, Dank G, Bannasch DL, Rebhun RB. Association of cancer-related mortality, age and gonadectomy in golden retriever dogs at a veterinary academic center (1989–2016). *PLoS One*. 2018;13(2):e0192578.
143. Priester WA, McKay FW. The occurrence of tumors in domestic animals. *Natl Cancer Inst Monogr*. 1980;54:1-210.
144. Acton AE, Munson L, Waddell WT. Survey of necropsy results in captive red wolves (*Canis rufus*), 1992–1996. *J Zoo Wildl Med*. 2000;31(1):2-8.
145. Bernstein KS, Schelling SH. Oral squamous cell carcinoma in a coyote (*Canis latrans*). *J Zoo Wildl Med*. 1999;30(2):305-307.
146. Makielski KM, Mills LJ, Sarver AL, et al. Risk factors for development of canine and human osteosarcoma: a comparative review. *Vet Sci*. 2019;6(2):48.
147. Withrow SJ, Powers BE, Straw RC, Wilkins RM. Comparative aspects of osteosarcoma. Dog versus man. *Clin Orthop Relat Res*. 1991(270):159-168.
148. Fenger JM, London CA, Kisseberth WC. Canine osteosarcoma: a naturally occurring disease to inform pediatric oncology. *ILAR J*. 2014;55(1):69-85.
149. Moriarity BS, Otto GM, Rahrmann EP, et al. A Sleeping Beauty forward genetic screen identifies new genes and pathways driving osteosarcoma development and metastasis. *Nat Genet*. 2015;47(6):615-624.
150. Mirabello L, Troisi RJ, Savage SA. International osteosarcoma incidence patterns in children and adolescents, middle ages and elderly persons. *Int J Cancer*. 2009;125(1):229-234.
151. Phillips JC, Stephenson B, Hauck M, Dillberger J. Heritability and segregation analysis of osteosarcoma in the Scottish deerhound. *Genomics*. 2007;90(3):354-363.
152. Fan TM, Khanna C. Comparative aspects of osteosarcoma pathogenesis in humans and dogs. *Vet Sci*. 2015;2(3):210-230.
153. Ru G, Terracini B, Glickman LT. Host related risk factors for canine osteosarcoma. *Vet J*. 1998;156(1):31-39.
154. Longhi A, Pasini A, Cicognani A, et al. Height as a risk factor for osteosarcoma. *J Pediatr Hematol Oncol*. 2005;27(6):314-318.
155. Troisi R, Masters MN, Joshipura K, Douglass C, Cole BF, Hoover RN. Perinatal factors, growth and development, and osteosarcoma risk. *Br J Cancer*. 2006;95(11):1603-1607.
156. Mirabello L, Pfeiffer R, Murphy G, et al. Height at diagnosis and birth-weight as risk factors for osteosarcoma. *Cancer Causes Control*. 2011;22(6):899-908.
157. Selman C, Nussey DH, Monaghan P. Ageing: it's a dog's life. *Curr Biol*. 2013;23(10):R451-R453.
158. Dobson JM, Samuel S, Milstein H, Rogers K, Wood JL. Canine neoplasia in the UK: estimates of incidence rates from a population of insured dogs. *J Small Anim Pract*. 2002;43(6):240-246.
159. Schoenebeck JJ, Ostrander EA. Insights into morphology and disease from the dog genome project. *Annu Rev Cell Dev Biol*. 2014;30:535-560.
160. Hayward JJ, White ME, Boyle M, et al. Imputation of canine genotype array data using 365 whole-genome sequences improves power of genome-wide association studies. *PLoS Genet*. 2019;15(9):e1008003.
161. Nunney L. Size matters: height, cell number and a person's risk of cancer. *Proc Biol Sci*. 2018;285(1889):20181743.
162. Yordy J, Kraus C, Hayward JJ, et al. Body size, inbreeding, and lifespan in domestic dogs. *Conserv Genet*. 2020;21(1):137-148.
163. Rimbault M, Ostrander EA. So many doggone traits: mapping genetics of multiple phenotypes in the domestic dog. *Hum Mol Genet*. 2012;21(R1):R52-R57.
164. Yizhak K, Aguet F, Kim J, et al. RNA sequence analysis reveals macroscopic somatic clonal expansion across normal tissues. *Science*. 2019;364(6444):eaaw0726.
165. Cancer Research UK. *Lung Cancer Incidence by Age*. Cancer Research UK; 2020. Accessed April 26, 2021. https://www.cancerresearchuk.org/health-professional/cancer-statistics/statistics-by-cancer-type/lung-cancer/incidence#ref-1
166. Samet JM, Avila-Tang E, Boffetta P, et al. Lung cancer in never smokers: clinical epidemiology and environmental risk factors. *Clin Cancer Res*. 2009;15(18):5626-5645.
167. Perret C, Gidoin C, Ujvari B, Thomas F, Roche B. Predation shapes the impact of cancer on population dynamics and the evolution of cancer resistance. *Evol Appl*. 2020;13(7):1733-1744.

168. Ferris E, Abegglen LM, Schiffman JD, Gregg C. Accelerated evolution in distinctive species reveals candidate elements for clinically relevant traits, including mutation and cancer resistance. *Cell Rep*. 2018;22(10):2742-2755.
169. Modiano JF, DePauw TA, Khammanivong A, et al. Early detection for strategic prevention of a terminal canine cancer: a model to reduce the impact of cancer in our society. *Cancer Res*. 2020;80:4592-4592.
170. DePauw TA, Khammanivong A, Modiano JF. A method for early detection of hemangiosarcoma in dogs. *Clin Cancer Res*. 2020;26:B22-B22.
171. Prymak C, McKee LJ, Goldschmidt MH, Glickman LT. Epidemiologic, clinical, pathologic, and prognostic characteristics of splenic hemangiosarcoma and splenic hematoma in dogs: 217 cases (1985). *J Am Vet Med Assoc*. 1988;193(6):706-712.
172. Kim JH, Graef AJ, Dickerson EB, Modiano JF. Pathobiology of hemangiosarcoma in dogs: research advances and future perspectives. *Vet Sci*. 2015;2(4):388-405.
173. Makielski KM, Donnelly AJ, Khammanivong A, et al. Development of an exosomal gene signature to detect residual disease in dogs with osteosarcoma using a novel xenograft platform and machine learning. *Lab Invest*. 2021;101(12):1585-1596.
174. Borgatti A, Koopmeiners JS, Sarver AL, et al. Safe and effective sarcoma therapy through bispecific targeting of EGFR and uPAR. *Mol Cancer Ther*. 2017;16(5):956-965.
175. Oh F, Modiano JF, Bachanova V, Vallera DA. Bispecific targeting of EGFR and urokinase receptor (uPAR) using ligand-targeted toxins in solid tumors. *Biomolecules*. 2020;10(6):956.
176. Oh F, Todhunter D, Taras E, Vallera DA, Borgatti A. Targeting EGFR and uPAR on human rhabdomyosarcoma, osteosarcoma, and ovarian adenocarcinoma with a bispecific ligand-directed toxin. *Clin Pharmacol*. 2018;10:113-121.
177. Tsai AK, Oh S, Chen H, Shu Y, Ohlfest JR, Vallera DA. A novel bispecific ligand-directed toxin designed to simultaneously target EGFR on human glioblastoma cells and uPAR on tumor neovasculature. *J Neurooncol*. 2011;103(2):255-266.
178. Gatenby RA, Brown JS. The evolution and ecology of resistance in cancer therapy. *Cold Spring Harb Perspect Med*. 2020;10(11):a040261.

How to cite this article: Sarver AL, Makielski KM, DePauw TA, Schulte AJ, Modiano JF. Increased risk of cancer in dogs and humans: A consequence of recent extension of lifespan beyond evolutionarily determined limitations? *Aging Cancer*. 2022;3:3–19.
https://doi.org/10.1002/aac2.12046

Cancer Genetics 276–277 (2023) 1–11

Contents lists available at ScienceDirect

Cancer Genetics

journal homepage: www.elsevier.com/locate/cancergen

Original Article

Distinct mechanisms of *PTEN* inactivation in dogs and humans highlight convergent molecular events that drive cell division in the pathogenesis of osteosarcoma

Aaron L. Sarver[a,b,d,*], Lauren J. Mills[a,c], Kelly M. Makielski[a,d,e], Nuri A. Temiz[a,b], Jinhua Wang[a,b], Logan G. Spector[a,c,d], Subbaya Subramanian[a,d,f], Jaime F. Modiano[a,d,e,g,h,i,j]

[a] *Masonic Cancer Center, University of Minnesota, Minneapolis, MN 55455, USA*
[b] *Institute for Health Informatics, University of Minnesota, Minneapolis, MN 55455, USA*
[c] *Department of Pediatrics, University of Minnesota Medical School, Minneapolis, MN 55455, USA*
[d] *Animal Cancer Care and Research Program, University of Minnesota, St. Paul, MN 55108, USA*
[e] *Department of Veterinary Clinical Sciences, University of Minnesota College of Veterinary Medicine, St. Paul, MN 55108, USA*
[f] *Department of Surgery, University of Minnesota School of Medicine, Minneapolis, MN 55455, USA*
[g] *Center for Immunology, University of Minnesota, Minneapolis, MN 55455, USA*
[h] *Stem Cell Institute, University of Minnesota, Minneapolis, MN 55455, USA*
[i] *Center for Engineering and Medicine, University of Minnesota, Minneapolis, MN 55455, USA*
[j] *Department of Laboratory Medicine and Pathology, University of Minnesota Medical School, Minneapolis, MN 55455, USA*

ARTICLE INFO

Article history:
Received 28 October 2022
Revised 2 March 2023
Accepted 19 May 2023

Keywords:
Comparative genomics
Osteosarcoma
Genomics
Bioinformatics
Cancer

ABSTRACT

A hallmark of osteosarcoma in both human and canine tumors is somatic fragmentation and rearrangement of chromosome structure which leads to recurrent increases and decreases in DNA copy number. The *PTEN* gene has been implicated as an important tumor suppressor in osteosarcoma via forward genetic screens. Here, we analyzed copy number changes, promoter methylation and transcriptomes to better understand the role of *PTEN* in canine and human osteosarcoma. Reduction in *PTEN* copy number was observed in 23 of 95 (25%) of the canine tumors examined leading to corresponding decreases in *PTEN* transcript levels from RNA-Seq samples. Unexpectedly, canine tumors with an intact *PTEN* locus had higher levels of *PTEN* transcripts than human tumors. This variation in transcript abundance was used to evaluate the role of *PTEN* in osteosarcoma biology. Decreased *PTEN* copy number and transcript level was observed in - and likely an important driver of - increases in cell cycle transcripts in four independent canine transcriptional datasets. In human osteosarcoma, homozygous copy number loss was not observed, instead increased methylation of the *PTEN* promoter was associated with increased cell cycle transcripts. Somatic modification of *PTEN*, either by homozygous deletion in dogs or by promoter methylation in humans, is clinically relevant to osteosarcoma, because the cell cycle related transcripts are associated with patient outcomes. The *PTEN* gene is part of a syntenic rearrangement unique to the canine genome, making it susceptible to somatic loss of both copies of distal chromosome 26 which also includes the *FAS* death receptor.

Significance Statement: PTEN function is abrogated by different mechanisms in canine and human osteosarcoma tumors leading to uncontrolled cell cycling. Somatic loss of this canine specific syntenic region may help explain why the canine genome appears to be uniquely susceptible to osteosarcoma. Syntenic arrangement, in the context of copy number change, may lead to synergistic interactions that in turn modify species specific cancer risk. Comparative models of tumorigenesis may utilize different driver mechanisms.

Introduction

Osteosarcoma, the most common primary tumor of bone, is very rare in humans, but is commonly observed in large and giant dogs [1]. Human and canine osteosarcoma share many driver events including mutation of the *TP53* tumor suppressor gene

* Corresponding author at: Masonic Cancer Center, University of Minnesota, Minneapolis, MN 55455, USA.
E-mail address: sarver@umn.edu (A.L. Sarver).

https://doi.org/10.1016/j.cancergen.2023.05.001
2210-7762/

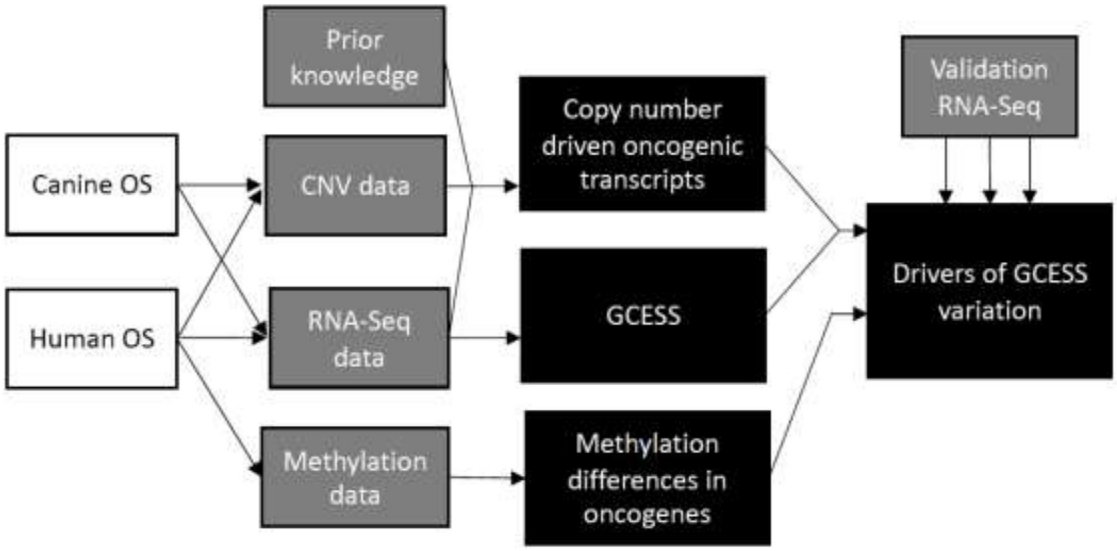

Fig. 1. Study Design identification of copy number and methylation driven transcriptional phenotypes in human and canine osteosarcoma.

[2–4], and somatic fragmentation and rearrangement of chromosome structure which leads to recurrent increases and decreases in DNA copy number [5,6]. As a result, canine osteosarcoma is considered an excellent model for studying the genomic and biochemical events that govern disease progression. PI3K signaling has been shown to be important for the development or progression of human osteosarcoma [7] and decreases in *PTEN* transcript are associated with poor outcomes in human patients in a variety of cancers [8]. Despite differences in chromosome number (human=23, canine=39) and syntenic alignment, many common somatic copy number changes can be observed between human and canine tumors (i.e., *MYC* amplification; loss of *RB, DLG2, LSAMP*) [5,9–11]. Loss of *PTEN*, a negative regulator of PI3K signaling, has been postulated as an important driver event in canine osteosarcoma. Several independent studies have documented loss or reduction of *PTEN* mRNA and protein expression, and DNA copy number loss at the terminal end of canine chromosome 26 (CFA26) [12,6]. *Pten* also contributes to osteosarcomagenesis in mice. We identified disruption of *Pten* as a recurrent event in forward genetic screens for osteosarcoma [13,14]. However, neither mutation of *PTEN*, nor homozygous DNA copy number loss of the p arm of chr10 are reported as strongly recurrent occurrences in human osteosarcoma, suggesting that *PTEN*-deleted osteosarcomas of dogs and *PTEN*-intact but "silenced" osteosarcomas of humans could represent convergent tumor evolutionary mechanisms in histologically similar cancers.

Transcriptional variation has been observed in osteosarcoma, with increased levels of cell cycle transcripts being associated with poor outcomes [15–17]. In prior work we used Gene Cluster Expression Summary Score (GCESS) based dimensional reduction analysis of transcriptomic data to make statistical associations between driver events and transcriptional patterns with datasets of limited power, many of which have been validated externally [17]. In this work we hypothesized that copy number changes and or promoter methylation could be important drivers of conserved transcriptional variation in osteosarcoma (Fig. 1). We show a clear association between genomic loss of *PTEN*, reduced transcriptional expression of *PTEN* and increased cell cycle transcripts in canine tumors. Using a similar approach, we show that increased methylation of a specific region of the *PTEN* promoter is similarly associated with increases in cell cycle transcripts in human tumors. Our results indicate that disruption of *PTEN* mediated tumor suppression is primarily occurring by different mechanisms in canine and human osteosarcoma tumors, and this knowledge is essential to the use of canine tumors as a model system for understanding the etiology of osteosarcoma.

Results

Homozygous deletion of the terminal end of CFA26 containing PTEN *in canine osteosarcoma*

To investigate the significance of CFA26 deletions, and of *PTEN* in particular, we investigated the peri–*PTEN* region in CFA26 in two independent canine osteosarcoma whole exome sequencing (WES) datasets (total $n = 95$) for which matched normal blood was available. The *PTEN* gene showed the largest decrease of any region on CFA26 in both canine osteosarcoma datasets, but it was not observed to be distinctly lost on human Chr 10 in a human osteosarcoma dataset ($n = 59$) (Supplemental Fig. 1). The *PTEN* locus suffered prominent copy number decreases (less than 50% of that observed in normal tissue) in 23/95 (25%) tumors. Both copies of *PTEN* were lost in 18/95 (20%) tumors. The specific region of loss of CFA26 was variable. Four tumors showed a focal deletion of the *PTEN* gene, while 11 tumors showed patterns consistent with loss of the entire distal end of both copies of CFA26 with a conserved break point between the *ZWINT* gene (never lost) and the *PCDH15* (first gene lost). The remaining eight tumors showed smaller regions of contiguous deletion, including the *PTEN* gene (Fig. 2A). The region lost in canines maps to 3 syntenic sequences in humans, including 2 distant regions on Chr 10 as well as a region of Chr 22 (Fig. 2B). Loss of *PTEN* was observed in all breeds examined, in both sexes and was independent of neuter status.

To compare loss of *PTEN* in canine and human disease we plotted the CNV changes for *PTEN* in the 95 canine tumors and compared them to the values observed in a set of 59 human tumors. While *PTEN* copy-number changes have been reported sporadically in human osteosarcoma [3], deep (homozygous) *PTEN* copy number loss is far more common in canine tumors (T-test $P = 0.00082$) (Fig. 2C). To ensure that the differences observed were not an artifact of data quality among the datasets, the recurrently gained gene *MYC*(8) and recurrently lost genes *RB1*(9), *DLG2*(10) and *LSAMP*(11) were plotted. Similar copy number changes, both gains and losses were observed in the human and canine datasets for *MYC* (T-test Pval=0.68), *RB1* (T-test $P = 0.78$), *DLG2* (T-test Pval=0.38), while for *LSAMP* more loss was observed in the human

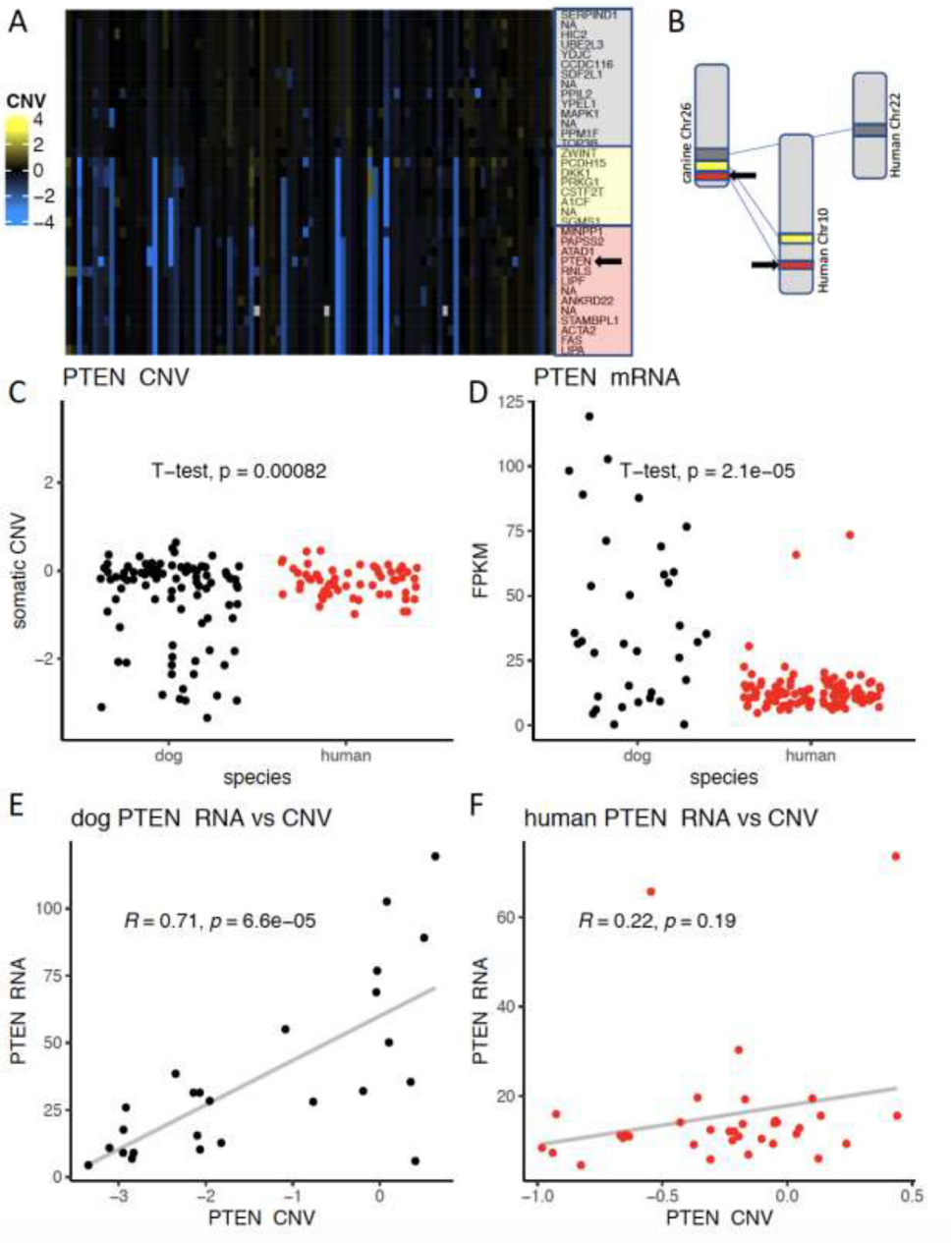

Fig. 2. Loss of distal CFA26 region containing *PTEN* in canine osteosarcoma.
A) Somatic changes observed between normal tissue and canine osteosarcoma tumors are shown for the distal end of CFA26. The data has been log base [2] transformed and genes shown in bright blue represent somatic loss, genes shown in black are unchanged between tumor and control, and genes that show somatic gain are shown in yellow. B) The syntenic alignment between CFA26 and the human genome is shown. The canine lost region is orthologous to two distant separate regions on human chr10 and one region on human chr22. C)Values for tumor *PTEN* copy number are shown for canine samples in black and human samples shown in red. Values are log base 2 transformed and show the change observed in tumors relative to the copy number observed in blood from the patient. The T-test P-Value is shown for the comparison of dog samples to human samples. D) The FPKM transcript level of *PTEN* observed in RNA-Seq samples derived from canine osteosarcoma is shown in black and from human osteosarcoma is shown in red. The T-test P-Value is shown for the comparison of dog samples to human samples. E-F) For 25 of the canine and 34 of the human exome samples we also had RNA-Seq data derived from sections of the same tumor. The CNV for *PTEN* is plotted on the X-axis and the FPKM level for *PTEN* is plotted on the y axis. A high and significant correlation was observed for the canine samples which was not observed the human samples. The Pearson correlation coefficient and the P-value are shown for the human and canine data.

samples (T-test Pval=0.000035) (Supplemental Fig. 2). We compared the *PTEN* RNA transcript levels in human and canine bone tumors. *PTEN* transcripts were uniformly low in human osteosarcomas even though the available WES data suggests that most tumors contained one or more copies of *PTEN*, suggesting that other mechanisms silencing *PTEN* are operative and widespread in human osteosarcoma (methylation and/or miRNA mediated mechanisms) (reviewed in 5). Somewhat surprisingly, while some canine tumors showed low levels of *PTEN* transcript similar to those observed in human tumors, many of the canine tumors showed higher *PTEN* transcript levels (T-test $P = 0.000021$) (Fig. 2D)

RNAseq data were available for 25 of the canine samples which also had WES data allowing us to directly examine the transcript levels of *PTEN* as a function of the number of copies of the gene. Tumors that had lost both copies of *PTEN* had very low *PTEN* transcript levels, while tumors which retained both copies of *PTEN* had higher *PTEN* transcript levels (Fig. 2E). A strong Pearson correla-

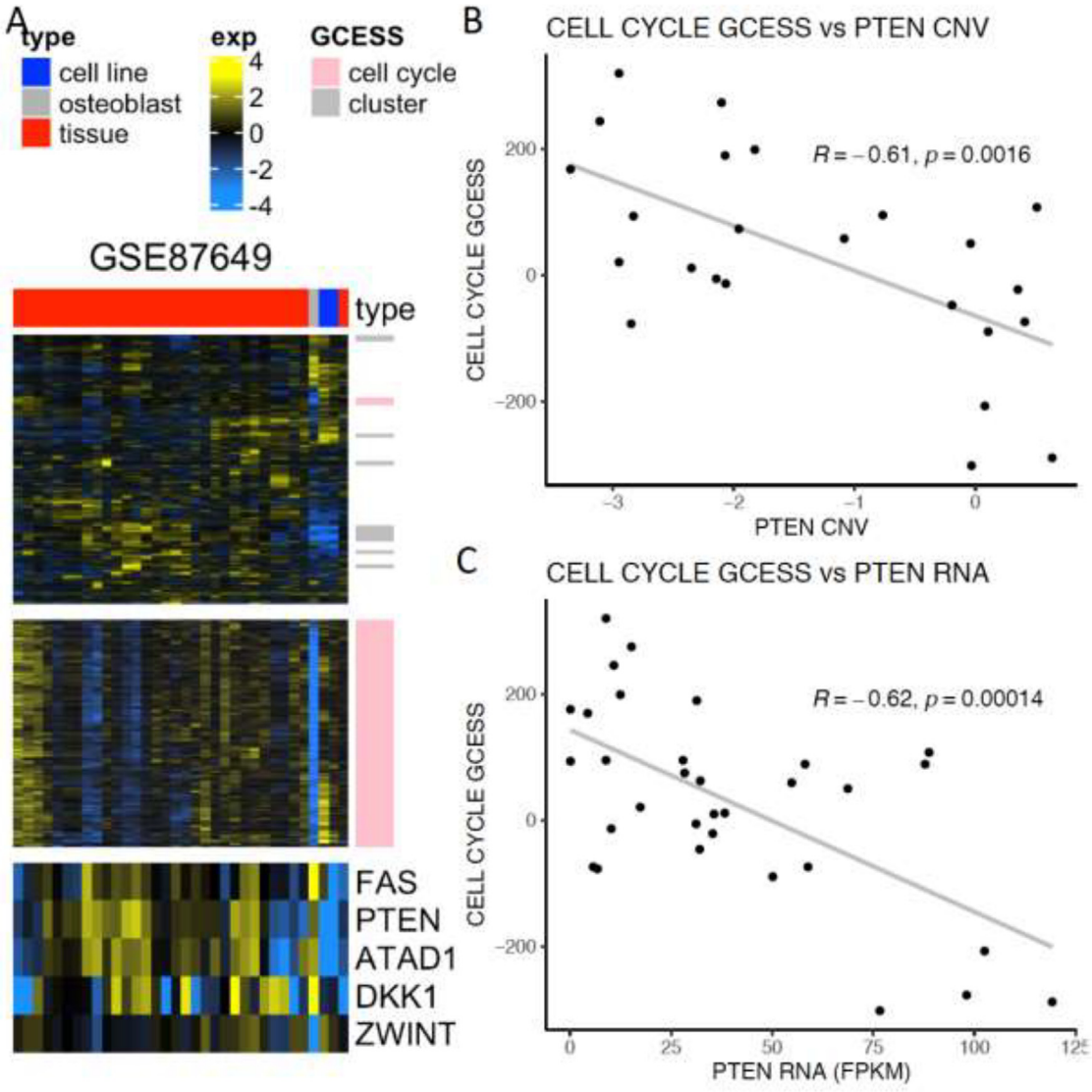

Fig. 3. *PTEN* copy number and transcript level drives cell cycle signature in canine tumors.
A)Heatmap of GSE87469 RNA-Seq data which contains osteosarcoma tumors, cell lines and osteoblasts quantified in FPKM units (n = 35) The dataset is normalized, log transformed, mean centered and analyzed using GCESS analyses to define and score clusters of genes that covary, which are marked in the row annotation of each dataset. The second inset contains a blowup of the heatmap containing the cell cycle cluster. The third inset contains the transcript levels of genes near and including the *PTEN* gene. B) The *PTEN* copy number is plotted against the cell cycle GCESS score. C) The *PTEN* FPKM level is plotted against the cell cycle GCESS score. The Pearson correlation coefficient and the P-value are shown for each of the plots.

tion R^2 value (R^2=0.71, P = 0.000066) for *PTEN* copy number vs. *PTEN* transcripts indicates that the association between copy number and transcript level was quite robust in the canine tumors. A similar result was present for the FAS gene which is also found in the distal region of CFA26 near PTEN but was not observed for ZWINT which is located just outside the lost region (Supplemental Fig. 3). The two samples with the lowest *PTEN* transcript levels were canine osteosarcoma cell lines, supporting the notion that stromal cells (not derived from the tumor clone) contribute to the overall levels of *PTEN* expression in bulk RNA-Seq from osteosarcoma tissues. For the tumors that retained two copies of *PTEN*, the number of transcripts was variable (Fig. 2E), suggesting that other mechanisms that suppress *PTEN* mRNA expression are operative in canine osteosarcoma, and these could be similar to those that repress *PTEN* expression in human tumors. In human samples direct correlation was not observed between copy number and transcript level (R^2=0.22, P = 0.19), likely because deep deletions in *PTEN* were not observed (Fig. 2F).

PTEN *loss is associated with upregulation of transcriptional programs that drive cell cycle progression and DNA damage repair in canine osteosarcoma*

PTEN is a well-known tumor suppressor and regulator of the cell cycle that counterbalances the activity of PI3K and suppresses the AKT signaling pathway. We thus hypothesized that the strong variation present in the transcript levels of *PTEN* in canine osteosarcoma might be responsible for regulating the transcriptional signature for cell cycle progression that is associated with poor outcomes in canine disease [15,17]. Genes like *MKI67* and others are coregulated and make up the cell cycle transcriptional programs. We used the GCESS dimensional reduction technique [17] to identify and score strong and conserved transcriptional patterns, and to identify and quantify a cell cycle (G2/M transition and DNA damage repair checkpoint) signature across the canine osteosarcoma samples (Fig. 3A). We reasoned that if a pattern of association between *PTEN* copy

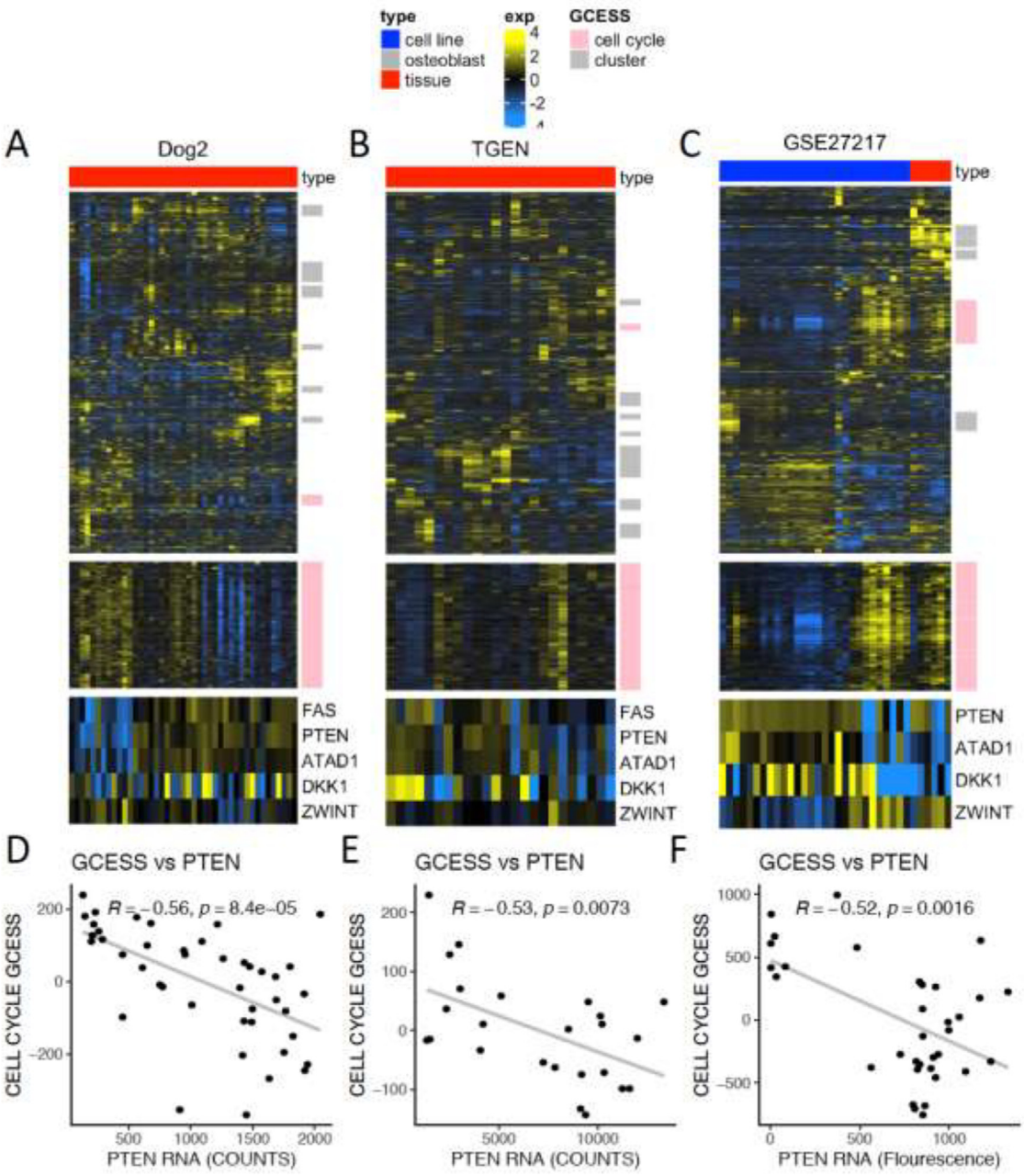

Fig. 4. Validation of *PTEN* transcript levels driving cell cycle signature in canine tumors.
Heatmaps are shown for genome-wide mRNA transcript levels for 3 additional canine osteosarcoma datasets A) CCOGC canine OS tumor tissue RNA-Seq dataset quantified in read counts and quantile normalized generated for this publication (n = 44). B) TGEN tumor tissue dataset tissue RNA-Seq dataset quantified in counts and quantile normalized (n = 24) C) GSE27217 a cell line and tumor tissue dataset generated using Affymetrix arrays. Each dataset was individually normalized, log transformed, mean centered and analyzed using GCESS analyses to define and score clusters of genes that covary, which are marked in the row annotation of each dataset. On the basis of conserved gene membership with previously defined cell cycle transcripts, the cell cycle cluster is marked in pink while the other defined clusters are shown in gray using the threshold of Pearson correlation > 0.5 and more than 100 individual transcripts present. In the second panel of the heatmap the cell cycle cluster is blown up so that it is clearly visible in each of the 3 datasets. In the third panel the levels of select genes from distal chr26 are shown including the *PTEN* tumor suppressor transcript. D-F) The *PTEN* transcript level is plotted on the x axis while the cell cycle GCESS score is plotted on the Y axis for each dataset. The Pearson correlation coefficient and the P-value are shown for each of the plots.

number abundance and the cell cycle signature were robust, a negative correlation would be apparent. A strong negative correlation is present between the *PTEN* copy number and the GCESS cell cycle score (R^2=−0.61, P = 0.0016; Fig. 3B). FAS and DKK1 also show negative correlation to the GCESS cell cycle score but they are not as strong as what is observed with PTEN (Supplemental Fig. 4). Due to the correlation between copy number and transcript level for *PTEN*, we further reasoned that the transcript level of *PTEN* could serve as a surrogate marker for *PTEN* loss and a negative correlation would exist between the GCESS cell cycle score and the *PTEN* transcript level. A strong negative correlation was also observed between the cell cycle GCESS scores and the *PTEN* transcript levels (R^2=−0.62, P = 0.00014; Fig. 3C) indicating that the decrease in *PTEN* transcripts due to loss of *PTEN* copy number, is an important driver of the cell cycle transcripts in canine osteosarcoma.

To independently validate this finding, we examined 3 additional canine osteosarcoma datasets. We generated a new RNAseq dataset for canine osteosarcoma samples obtained from the Canine Comparative Oncology and Genomics Consortium, Inc. [18]

(CCOGC, $n = 44$) and quantified it to read counts per gene. We obtained a recently published dataset from Gardner and colleagues [3] and used samples with read depths of ~100 million ($n = 24$) for our analysis. We also utilized GSE27217($n = 34$) [15] a canine Affymetrix array gene expression dataset of cell lines and tumor tissue. We used the GCESS approach to identify gene clusters with correlation greater than 0.5 and more than 100 members. In each dataset, the cell cycle cluster was clearly apparent (Supplemental Table S1). Comparison of GCESS cell cycle scores to *PTEN* transcript levels show strong negative correlation in each of the three independent canine validation datasets (R^2=−0.56, −0.53, −0.52 and $P = 0.000084$, 0.0073, 0.0016), even though the data was generated by different technologies and gene summarization approaches (Fig. 4). These results are consistent with deletion of *PTEN* and resulting loss of transcript being a driver of the increased cell cycle signature in canine osteosarcoma. Other potential copy number-regulated drivers, including *MYC, RB1*, and *LSAMP* did not show consistent negative correlation with the cell cycle gene cluster as we observed for *PTEN* at the copy number (Supplemental Fig. 4) or at the transcript level (Supplemental Fig. 5) with the exception of *DLG2. DLG2* showed negative correlation at the CNV(R^2=−0.58, $P = 0.0022$) and transcript level (R^2=−0.48, $P = 0.0043$) to the cell cycle GCESS in our discovery dataset but did not replicate in the three validation datasets. As a positive control and as a measure of the power available, *ZWINT* (an essential mitotic gene never lost on CFA26 and member of the cell cycle cluster [19]) transcript levels were shown to be highly positively correlated to the cell cycle score in all 4 canine datasets (R^2=0.69, 0.61, 0.60, 0.77, and $P = 0.00001$, 0.000015, 0.0021, 1.20e-07) (Supplemental Fig. 6). While many factors likely influence the cell cycle status in canine osteosarcoma cells including occasional loss of *DLG2*, abrogated *PTEN* function due to somatic copy number loss appears to be principal among them. While many transcripts are positively and negatively correlated to the cell cycle signature, these results are stronger than observational correlations between transcript expression patterns, and they approach the definition of causality due to the connection between somatic copy number loss and transcript level decreases.

To determine if comparable results to what we saw in dogs could be observed in human osteosarcoma samples, we evaluated the correlation between *PTEN* copy number as well as mRNA transcript level and the GCESS cell cycle transcripts in a dataset composed of 105 samples from 3 datasets [7,17]. The negative correlation was present using both copy number (R^2=−0.34, $P = 0.043$; Fig. 5A and B) and transcript level (R^2=−0.37, $P = 0.000054$; Fig. 5A and C), but the correlations were not as strong as what was observed in dogs (Fig. 4A–C). We examined the other potential driver (*MYC, RB1, LSAMP, DLG1*) and canine chr26 lost genes (*FAS, DKK1*) for correlation to the cell cycle score. None of these showed negative correlation to the GCESS cell cycle score as strong as what was observed for *PTEN* in the human data (Supplemental Fig. 4–5). As expected, *ZWINT* showed strong correlation to the cell cycle score (R^2=0.78, P = 8.6e-24; Supplemental Fig. 6) indicating that sufficient power was available to detect functional relationships within transcriptional programs in this dataset. These results led us to hypothesize that *PTEN* promoter methylation may be driving *PTEN* silencing and the reduced cell cycle signature in human osteosarcoma tumors.

PTEN *promoter methylation is associated with upregulation of transcriptional programs that drive cell cycle progression and DNA damage repair in human osteosarcoma*

To determine whether *PTEN* promoter methylation had a role in cell cycle progression we examined DNA methylation data for a set of human tumors [20] for which we also had RNA-Seq transcriptional data. Examination of the *PTEN* promoter region between chr10:89,621,000–89,624,000 identified an unmethylated region corresponding to the CpG island as well as a variably methylated region on the 5′ edge of the CpG island (5′ shore) (examples in Fig. 5D and full data in Supplemental Fig. 7 and 8). In the 5′ shore methylated region between 89,621,400–89,621,700 methylated CpG values were averaged. A wide range of average methylation values (1–80%) was obtained (Fig. 5D) corresponding to the values present in Supplemental Fig. 8. We initially hypothesized that the 5′ shore methylation pattern might be directly correlated to the *PTEN* transcript level observed. While increased methylation of the *PTEN* promoter 5′ shore was somewhat associated with decreased *PTEN* transcript levels (R^2=0.38, $P = 0.15$) (Fig. 5E) this result was still less explanatory than what was observed in dogs. We further hypothesized that the variable *PTEN* promoter methylation pattern might lead to decreased ability for *PTEN* transcript response (i.e., inducibility) as a result of tumorigenic cell division. If this was the case, tumors with increased *PTEN* 5′ shore promoter methylation would be associated with higher cell cycle scores due to their inability to respond transcriptionally to signals that would lead to increased *PTEN* transcripts beyond basal homeostasis. We observed a strong correlation for the comparison of the human *PTEN* promoter 5′ shore methylation pattern to the cell cycle GCESS score (R^2=0.56, $P = 0.026$) (Fig. 5F). Together, our data indicate that in human osteosarcoma *PTEN* promoter methylation is associated with uncontrolled cell division, while in canine tumors deletion of the *PTEN* gene is associated with uncontrolled cell division.

Discussion

The importance of *PTEN* loss as a driver of human cancer is well recognized [21], although its relevance has not been firmly established in osteosarcoma. Here, we show that reduction or loss of *PTEN* expression is a common event in canine and human osteosarcomas, and more specifically, that *PTEN* transcript abundance is strongly negatively correlated with a transcriptional program that is activated during cell cycle progression. Our data also corroborate that the genomic integrity and/or expression of *FAS, DKK1, ZWINT, MYC, RB1*, and *DLG2* play important roles in osteosarcoma proliferation.

For this study, GCESS-based scoring was used to clearly identify associations between copy number variation/gene transcript abundance and transcriptional programs that are activated during cell cycle progression. Furthermore, GCESS-based scoring has been used to identify associations with outcome [17,22], tumor subtypes [23,24] and driver events [25] in comparative oncology studies. GCESS scoring was originally derived to minimize problems associated with multiple testing and provide a single value to represent a group of highly correlated genes. Comparing the correlations between *PTEN* and GCESS cell cycle scores to the correlation between *PTEN* and all individual transcripts (which are combined to generate the GCESS cell cycle score) indicates that GCESS score correlations are stronger than the vast majority of individual transcripts (Fig. 6). Further, the few individual transcripts which perform better than the GCESS scores are not consistent across each of the experiments. We believe that the GCESS scores measure the transcriptional state found within the tumor better than individual transcripts due to highly individually variable epigenetic and/or transcript stability differences which are averaged out during the creation of the GCESS score. Regardless of the rationale, these results strongly suggest that the GCESS scores have utility beyond reduction of the multiple testing problem associated with genome-wide transcriptional analyses and provide a direct route to identifying the correct granularity for statistical analyses of gene expression data.

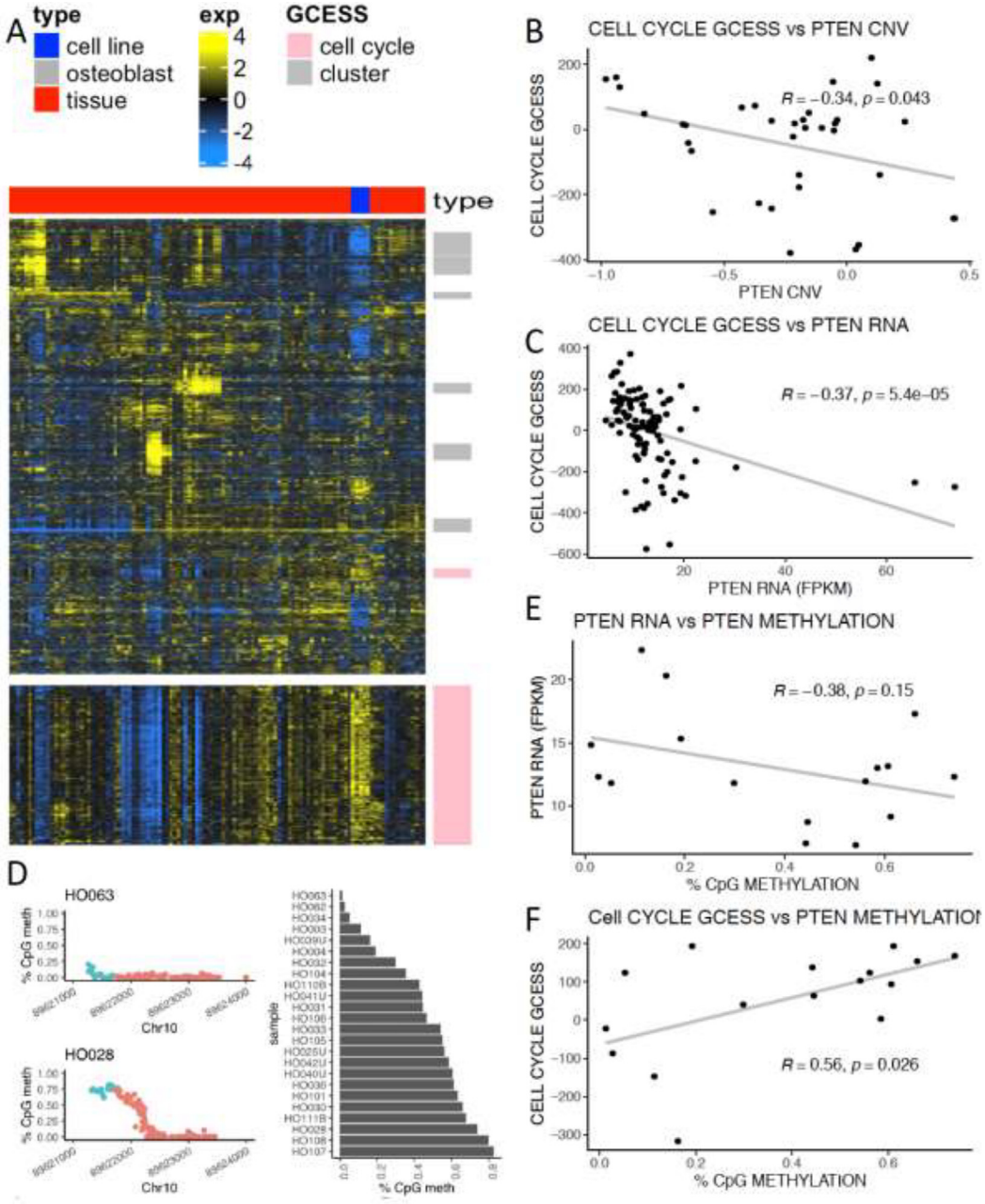

Fig. 5. *PTEN* promoter methylation drives cell cycle signature in human tumors.
A)Heatmap generated from the combination of 3 human osteosarcoma datasets including both tumors and cell lines. The dataset is normalized, log transformed, mean centered and analyzed using GCESS analyses to define and score clusters of genes that covary, which are marked in the row annotation of each dataset. The second inset contains a blowup of the heatmap containing the cell cycle cluster. B) The *PTEN* copy number is plotted against the cell cycle GCESS score. C) The *PTEN* FPKM level is plotted against the cell cycle GCESS score. D) Methylation levels were obtained for CpGs in the promoter of *PTEN* in human tumors where RNA-Seq data was also available. Two representative plots (one with low and one with high methylation) are shown of the observed genomic positions plotted relative to the percent methylation observed at specific positions. A variably methylated region was identified (shown in blue) and the average methylation of the variable region was plotted for each tumor. E) Correlation between the variably methylated region and the *PTEN* transcript level in 16 samples where both RNA-SEQ and CNV data was available from the same tumor. F) Correlation between the variably methylated region and GCESS cell cycle score level in 16 samples where both RNA-SEQ and CNV data was available from the same tumor. Tumors with increased methylation also showed increased cell cycle scores. The Pearson correlation coefficient and the P-value are shown for each of the plots.

While osteosarcoma is observed at significantly higher rates in dogs than in humans, other *PTEN*-driven tumors do not show similar incidence increases in canine tumors relative to human tumors. Examination of the canine-human gene synteny (gene order) may shed light on this observation. Our results indicate that two syntenic blocks in the distal region of CFA26 are commonly lost together in canine osteosarcomas. The first region maps to a 10 Mb region on human chr10, which contains *PTEN* (at 87.86 Mb) and *FAS* (at 88.9 Mb). The second region also maps to chr10 and contains *DKK1* (at 52.31 Mb) and *ZWINT* (at 56.26 Mb). There is a third synteny block immediately proximal to *ZWINT* that maps to human chr22 (Fig. 2B). None of the genes in the *ZWINT*/chr22 synteny block of CFA26 were lost in any of the canine osteosarcoma samples analyzed in this study. As was true for *PTEN*, we also observed strong copy number decreases of *FAS* and *DKK1* (Supplementary Fig. 3) consistent with loss of both copies in approximately 15–20% of the canine osteosarcomas analyzed; however, like *PTEN*, neither gene showed strong copy number loss in any

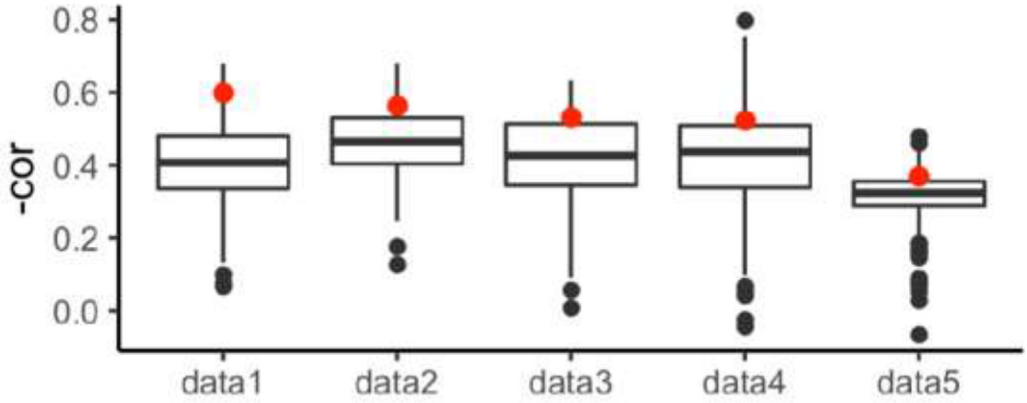

Fig. 6. *PTEN* transcript correlation to GCESS score consistently stronger than to individual transcripts that make up the GCESS score.
The negative correlation coefficient for the correlation between transcript level and the GCESS score is shown with a red dot for each dataset. Correlation was also calculated between *PTEN* and each individual transcript that makes up the GCESS score for each dataset and the negative correlation is plotted. In all cases examined, the correlation between PTEN transcript to the GCESS score is stronger than the vast majority of individual correlations between PTEN transcript and transcripts used to generate the GCESS score. The label data1 indicates that the correlation was derived from GSE87649, data2 is from the CCOGC samples, data3 is from the TGEN samples, data4 is from GSE27217 and data5 is from the human samples.

human sample. In contrast, copy number aberrations were undetectable in the *ZWINT* gene in either canine or human osteosarcomas (Supplementary Figure 3). *ZWINT* is an essential gene that has a critical role in mitosis [19]. *ZWINT* is also a member of the cell cycle gene cluster, so by definition, it is highly correlated with the cell cycle signature in all the datasets examined. As an essential mitotic gene, it is likely that loss of *ZWINT* is not tolerated by tumors, generating a recurrent breakpoint that is under strong selection and allows tumors to continue to produce *ZWINT*, while at the same time eliminating *PTEN*.

FAS and *DKK1* copy number variation could independently contribute to osteosarcoma progression. The *FAS* death receptor is inversely associated with human osteosarcoma metastasis; specifically, decreased levels of FAS protein were associated with metastasis to the lung, whereas increased levels of FAS were protective [26,27]. Tumors with focal deletions of *FAS* were also associated with worse outcomes. In our analysis, *FAS* transcript levels were directly correlated with *FAS* copy number, and negatively correlated to cell cycle signature, although less so than *PTEN*. Loss of *FAS* may contribute to tumorigenesis via removing an apoptic pathway leading to increased likelihood of cell division or alternatively may be associated with high cell cycle scores via close genetic linkage to *PTEN*. *DKK1* is a potent inhibitor of osteoblast proliferation. Specifically, increased levels of *DKK1* protein suppress osteoblast proliferation while the absence of *DKK1* leads to increases in the numbers of osteoblasts [28,29]. Intriguingly, a negative correlation between *DKK1* copy number variation and cell cycle GCESS could be appreciated in the canine tumors, but such a correlation was not present for *DKK1* transcript abundance and cell cycle GCESS in all of the canine datasets. While the presence of a correlation with copy number variation makes reduced effect of *PTEN* linkage over a larger chromosomal distance unlikely, the lack of correlation with transcript abundance could be due to lower strength of selection seen with loss of *DKK1*, or it could be due to the differences in resolution provided by variable depth of sequencing. In support of this idea, the association between cell cycle GCESS score and the *DKK1* transcript level was observable in the TGEN dataset which also had the deepest sequencing.

Overall, this allows us to begin to generate a model for osteosarcoma tumorigenesis in the dog, where mutation of *TP53* is an initial (or the critical) event in an osteosarcoma precursor cell, which allows for genome degradation and homozygous loss of distal chr26. Copy number loss of *PTEN* may mechanistically be occurring by two mechanisms, telomeric degradation or chromothrypsis. The large number of copy number changes (both gains and losses) observed in OS outside of telomeric regions suggest that chromothrypsis is a more likely mechanistic rational for the loss of *PTEN* in canines. Alternatively, acquisition of telomerase activity as has been reported in canine OS [30] may also stabilize telomeric degradation following loss of *PTEN*. Loss of *PTEN* leads to increased cell division; loss of *FAS* decreases apoptosis; and loss of *DKK1* may lead to increased proliferation of the tumor cell within the osteoblast lineage. We propose that the organization of the canine genome following syntenic rearrangements during speciation left dogs (and possibly other canids) uniquely vulnerable to osteosarcoma due to the colocalization of several genes that can be lost together with *PTEN* in a subtelomeric region, creating a perfect storm for bone tumorigenesis. While these changes can provide the recipe for bone cancer, it is apparent that two other requirements are excessive proliferation (to create the bone mass of large and giant dogs), as well as longevity with its consequent increase in cell division events, potential genotoxic exposures, and development of a permissive environment for oncogenesis [31], since osteosarcoma does not appear to be a common cancer in large wild canids that have shorter lifespans than most domestic companion dogs.

These events do not happen in humans because the loci encoding these genes are not in the distal area of a small chromosome, but rather they exist in less vulnerable regions of the genome and are susceptible to regulation via methylation. The *PTEN* 5′ shore promoter methylation region in human tumors does not show a strong association with the transcript level of *PTEN*. Rather, the 5′ shore methylated region may control a number of cell cycle-responsive binding sites, including transcriptional response elements that regulate the *PTEN* transcript, which then may be unable to be induced in response to stimuli that demand cell cycle control or cell cycle arrest. In support of this concept, binding sites for *GATA, ZIC* and *KLF* family transcription factors are within the differentially methylated region [32]. Alternatively, the methylated region may regulate expression of the *KLLN* gene, which is transcribed in the opposite direction from *PTEN* and has been shown to be a tumor suppressor [33]. *H3F3A* mutations have been reported to lead to increased methylation of the *KLLN/PTEN* promoter region in human osteosarcoma [34]. Further, KLLN promoter methylation can be observed in the germline DNA of Cowden syndrome patients [35]. Cowden syndrome is a rare disease associated with increased risk of tumor formation as well as benign hamartomatous overgrowth and is associated with mutations of the *PTEN* gene [36].

Our results unify a number of outcome associations [15,17,37–39] and suggest that they are all based on a common pattern of tumor behavior: variation in *PTEN* transcript levels allowed us to directly elucidate the likely function of the Pten tumor suppressor protein in canine osteosarcoma, presumably due to the decreased genetic heterogeneity present in dog breeds (as compared to humans). In this regard, the utility of canine osteosarcoma as a model for human osteosarcoma may be limited, as one must rectify the different, albeit convergent driver mechanisms of tumorigenesis in both species. Specifically, treatments intended to restore *PTEN* function, such as through epigenetic recovery of *PTEN* transcript expression, would be ineffective in many dogs but could be highly effective for most humans. Conversely, dogs can provide outstanding models to develop treatments that leverage the common absence of a gene and/or its corresponding protein product, for example, *FAS* (Fas), where we previously demonstrated that dogs whose tumors were Fas-deficient were able to generate strong immunity to neoadjuvant therapy with adenovirus-Fas ligand [40,41].

And while our results provide a working hypothesis for the observed increased rate of osteosarcoma in dogs, they also suggest a potential solution. Engineering an essential gene to a location on distal chr26 or alternatively identifying a synthetic lethal drug interaction with a gene lost on distal chr26 (as has been proposed for the *MTAP* gene near *CDKN2A* deletions [42]) may lead to decreased incidence and improved treatment of canine osteosarcoma. Understanding how changes in gene order and chromosomal location contribute to cancer risk may also allow for better understanding and decreasing cancer risks inherent in the human genome.

In summary, our work shows that distinct mechanisms of *PTEN* inactivation occur in dogs and in humans, and they highlight convergent molecular events that drive cell division in the pathogenesis of osteosarcoma. Awareness of these differences is critical to utilization of the dog as a model for human disease.

Methods

This work aimed to use informatic analyses to understand how molecular drivers of tumorigenesis impact transcriptional variation in osteosarcoma. Genomic regions implicated in osteosarcoma via forward genetic screens and prior biological knowledge were examined to identify where copy number changes were associated directly with transcriptional patterns. Associations between oncogene/tumor suppressor transcript levels and transcriptional patterns were then identified and validated in 3 additional datasets. Knowing that somatic copy number change was responsible for the variation observed at the transcript level allows the inference that oncogene/tumor suppressor transcript level changes are likely causal for the associations observed. Genome-wide methylation data was then used to look for associations between promoter methylation status, transcript level and GCESS patterns in human data. (Fig. 1)

Canine tumor samples used for exome analyses

Twenty-seven samples representing six golden retrievers, 12 rottweilers, one greyhound and eight dogs from six other breeds were selected from the Animal Cancer Care and Research Program (ACCRP) tumor biorepository. These specimens were obtained under protocols approved by either the University of Minnesota's Institutional Review Board or Institutional Animal Care and Use Committee (protocol numbers 0802A27363, 1101A94713, 1312–31131A) or the University of Colorado Institutional Review Board or Institutional Animal Care and Use Committee (AMC 635,040,202, AMC 200201jm, AMC 2002141jm, 02,905,603(01)1F, and COMIRB 06–1008). Additionally, 70 samples representing 23 golden retrievers, 23 rottweilers, and 24 greyhounds were retrieved from a previously published study [2]. These 70 samples were provided by the Pfizer Canine Comparative Oncology and Genomics Consortium (CCOGC) Biospecimen Repository and were collected according to protocols approved by the seven institutions participating in CCOGC sample collection. Selection from both sources (CCOGC and ACCRP) included a purposeful over-representation of three breeds to increase the likelihood of detecting recurrent somatic changes, and it added representation of additional breeds to assess the potential for wider distribution of somatic changes across breeds. For inclusion, cases needed to include fresh frozen tumor samples with a definitive, histological diagnosis of osteosarcoma that were collected as part of a medically necessary procedure (biopsy, amputation for local tumor control, or necropsy), and also have a paired EDTA-anticoagulated peripheral blood sample collected at the same time as the tumor. ACCRP samples were further selected to represent diversity of age (seven dogs younger than 3 years old, 13 dogs aged between 3.1 and 8.9 years old, and seven dogs older than 9 nears old). As expected, based on the anatomical distribution of canine osteosarcomas, 13 tumors originated in the forelimbs and eight tumors originated in the hindlimbs. Tumor location was not specified for six tumors.

Canine tumor samples used for RNA-Seq analyses

One hundred and six samples were provided by the Pfizer CCOGC Biospecimen Repository. Sixty-two samples with a definitive, histological diagnosis of osteosarcoma were selected for RNA sequencing based on the availability of sufficient frozen tissue (>50 mg), treatment information, and follow-up data. RNA from 43 of the 62 samples had RNA integrity numbers (RIN) >6, and these were included in the final selection for next-generation RNA sequencing.

Sample preparation

DNA was extracted using either the QIAGEN QIAamp DNA mini kit or the QIAGEN DNeasy® Blood and Tissue kit. RNA was extracted using the Ambion miRvana kit.

Exome capture

The Roche Nimblegen SeqCap-EZ capture canine exome kit was used for exome capture, following the manufacturer's protocol.

Sequencing

Sequencing libraries for tumor, normal DNA,and from tumor RNA were prepared as previously described [2,17]. The barcoded exome-captured libraries were multiplexed in pools of eight and sequenced on the Illumina HiSeq 2500 to a target depth of 60× for tumor DNA and 30× for normal germline DNA. RNA libraries were similarly multiplexed and sequenced on the Illumina NovaSeq to a depth >30 million reads per sample.

Human exome datasets

Human exome sequencing data was obtained from dbGap:phs000699.v1.p1(5).

Exome data read alignment

Reads were aligned to the human or CanFam3.1 reference genome via the SpeedSeq pipeline [43]. Somatic copy number changes were calculated between canine and human normal

(PBMC) tumor pairs using Varscan v2.4.3 [44]. Varscan copynumber was run on pileup data generated by samtools mpileup [45] to generate raw copy number ratios and GC content. Copy number ratios are log2 ratios of tumor depth compared to normal depth. Varscan copyCaller was used to make final copy number calls normalized for GC content. These copy number changes were then collapsed into larger segments using CNA.smoothed from the bioconductor R library DNAcopy. Bedtools intersectBed was used to assign copy number ratios to each protein coding gene from the ensembl annotation for each genome.

Transcriptome data read alignment

CCOGC RNA-Seq was mapped to the CanFam3.1 genome with Hisat2 [46] and FeatureCounts [47] was used to generate raw counts per gene.

Additional canine RNA-Seq datasets

TGEN RNA-Seq data was obtained from the authors in counts for 24 samples with read depths of ~100 million data [3]. Additionally, RNA-seq dataset GSE87649 and array data GSE27217 were downloaded from GEO.

Human RNA-Seq datasets

Human OS RNA-Seq datasets GSE87624 [17], dbGap:phs000699.v1.p1 [7] and additional datasets(17) were analyzed as previously described [17] generating FPKM based summarizations of the transcript levels.

RNA-Seq analyses

For the FPKM summarized RNA-Seq data the value of 0.1 was added to all values to minimize the effects of dividing by very small numbers. For the count summarized data the value of 3 was added to the CCOGC data and the values of 30 was added to the TGEN data for the same rational. Datasets summarized to FPKM values were used without additional normalization. Count based datasets were additionally normalized using quantile normalization. Cluster 3.0 (C Clustering Library 1.52) was used to $\log_2$ transform and gene-mean-center the data, select genes with SD $>$ 0.8 and then perform hierarchical average linkage clustering using the Pearson similarity metric. Gene clusters with a dendrogram node correlation $>$ 0.50 and at least 100 individual genes were identified in each of the datasets. The GCESS is defined as the sum of expression values ($\log_2$-transformed and mean centered) of all genes in a particular defined cluster for a single sample. The GCESS quantifies transcriptional variation between tumors. It takes many correlated individual transcript data points and condenses them into a single value [17].

Bisulfite-seq data

Bisulfite conversion, library preparation and target region capture were carried out using SeqCap Epi on DNA extracted from human OS samples (n = 24) [20]. On average 48 million Paired end 125 base Illumina reads were generated, aligned to a bisulfite converted human (hg19) genome and methylation frequencies were calculated at CpG sequences across the dataset as previously described [20]. CpG sequence methylation frequencies corresponding to the *PTEN* promoter region were extracted from the dataset for tumors(n = 24). Promoter methylation frequencies were further analyzed in tumors (n = 16) from GSE87624 where RNA-Seq data was also available derived from the same tumor.

Data analyses and figure generation

The R programming language [48] was used to analyze all data, carry out statistical analyses, and generate all figures.

Declaration of Competing Interest

None.

CRediT authorship contribution statement

Aaron L. Sarver: Investigation, Visualization, Resources, Data curation, Formal analysis, Writing – review & editing. **Lauren J. Mills:** Visualization, Resources, Data curation, Formal analysis, Writing – review & editing. **Kelly M. Makielski:** Visualization, Writing – review & editing. **Nuri A. Temiz:** Visualization, Resources, Writing – review & editing. **Jinhua Wang:** Visualization, Writing – review & editing. **Logan G. Spector:** Investigation, Writing – review & editing. **Subbaya Subramanian:** Investigation, Writing – review & editing. **Jaime F. Modiano:** Investigation, Writing – review & editing.

Data availability

Data will be made available on request.

Acknowledgments

The authors would like to thank both David Largaespada and Mathew Breen for insightful discussions regarding *PTEN* deletion and *PTEN* silencing.

Grant Support

This work was generously supported by the Zach Sobiech Osteosarcoma Fund and the Team Nat Fund of the Children's Cancer Research Fund (CCRF), the Karen Wyckoff Rein in Sarcoma Foundation, GREYlong, and the Van Sloun Foundation; by grants R50 CA211249 (ALS), P30 CA077598 (Masonic Cancer Center Comprehensive Cancer Center Support Grant), and R21 CA208529 (JFM) from the National Cancer Institute of the National Institutes of Health (NCI); and by grants CA170218 and CA190276 (JFM) from the United States Department of Defense Congressionally Directed Peer Reviewed Cancer Research Program. KMM was supported in part by an institutional training grant in Molecular, Genetic, and Cellular Targets of Cancer (Grant T32CA009138) from the NCI. JFM is supported in part by the Alvin and June Perlman Endowed Chair in Animal Oncology. The authors acknowledge support from individual donors to the Animal Cancer Care and Research Program, University of Minnesota. The content of this manuscript is solely the responsibility of the authors and does not necessarily represent the official views of any of the funding agencies listed above.

Supplementary materials

Supplementary material associated with this article can be found, in the online version, at doi:10.1016/j.cancergen.2023.05.001.

References

[1] Makielski KM, Mills LJ, Sarver AL, Henson MS, Spector LG, Naik S, Modiano JF. Risk factors for development of canine and human osteosarcoma: a comparative review. Vet Sci 2019;6(2):48.
[2] Sakthikumar S, Elvers I, Kim J, Arendt ML, Thomas R, Turner-Maier J, Lindblad-Toh K. SETD2 is recurrently mutated in whole-exome sequenced canine osteosarcoma. Cancer Res 2018;78(13):3421–31.

[3] Gardner HL, Sivaprakasam K, Briones N, Zismann V, Perdigones N, Drenner K, Facista S, et al. "Canine osteosarcoma genome sequencing identifies recurrent mutations in DMD and the histone methyltransferase gene SETD2". Commun Biol 2019;2:1–13 no. 1.
[4] Chen X, Bahrami A, Pappo A, Easton J, Dalton J, Hedlund E, Dyer MA. Recurrent somatic structural variations contribute to tumorigenesis in pediatric osteosarcoma. Cell Rep 2014;7(1):104–12.
[5] Angstadt AY, Motsinger-Reif A, Thomas R, Kisseberth WC, Guillermo Couto C, Duval DL, Breen M. Characterization of canine osteosarcoma by array comparative genomic hybridization and RT-qPCR: signatures of genomic imbalance in canine osteosarcoma parallel the human counterpart. Genes Chromosom Cancer 2011;50(11):859–74.
[6] Thomas R, Wang HJ, Tsai PC, Langford CF, Fosmire SP, Jubala CM, Breen M. Influence of genetic background on tumor karyotypes: evidence for breed-associated cytogenetic aberrations in canine appendicular osteosarcoma. Chromosome Res 2009;17(3):365–77.
[7] Perry JA, Kiezun A, Tonzi P, Van Allen EM, Carter SL, Baca SC, Janeway KA. Complementary genomic approaches highlight the PI3K/mTOR pathway as a common vulnerability in osteosarcoma. Proc Natl Acad Sci 2014;111(51):E5564–73.
[8] Zheng C, Tang F, Li M, Hornicek F, Duan Z, Tu C. PTEN in osteosarcoma: recent advances and the therapeutic potential. Biochim Biophys Acta BBA Rev Cancer 2020;1874(2):188405.
[9] Scott MC, Sarver AL, Tomiyasu H, Cornax I, Van Etten J, Varshney J, Modiano JF. Aberrant retinoblastoma (RB)-E2F transcriptional regulation defines molecular phenotypes of osteosarcoma. J Biol Chem 2015;290(47):28070–83.
[10] Shao YW, Wood GA, Lu J, Tang QL, Liu J, Molyneux S, Khokha R. Cross-species genomics identifies DLG2 as a tumor suppressor in osteosarcoma. Oncogene 2019;38(2):291–8.
[11] Kresse SH, Ohnstad HO, Paulsen EB, Bjerkehagen B, Szuhai K, Serra M, Meza-Zepeda LA. LSAMP, a novel candidate tumor suppressor gene in human osteosarcomas, identified by array comparative genomic hybridization. Genes Chromosom Cancer 2009;48(8):679–93.
[12] Levine RA, Forest T, Smith C. Tumor suppressor PTEN is mutated in canine osteosarcoma cell lines and tumors. Vet Pathol 2002;39(3):372–8.
[13] Moriarity BS, Otto GM, Rahrmann EP, Rathe SK, Wolf NK, Weg MT, Largaespada DA. A Sleeping Beauty forward genetic screen identifies new genes and pathways driving osteosarcoma development and metastasis. Nat Genet 2015;47(6):615–24.
[14] Temiz NA, Moriarity BS, Wolf NK, Riordan JD, Dupuy AJ, Largaespada DA, Sarver AL. RNA sequencing of Sleeping Beauty transposon-induced tumors detects transposon-RNA fusions in forward genetic cancer screens. Genome Res 2016;26(1):119–29.
[15] Scott MC, Sarver AL, Gavin KJ, Thayanithy V, Getzy DM, Newman RA, Modiano JF. Molecular subtypes of osteosarcoma identified by reducing tumor heterogeneity through an interspecies comparative approach. Bone 2011;49(3):356–67.
[16] Chibon F, Lagarde P, Salas S, Pérot G, Brouste V, Tirode F, Lucchesi C, et al. "Validated prediction of clinical outcome in sarcomas and multiple types of cancer on the basis of a gene expression signature related to genome complexity". Nat Med 2010;16(7):781–7 no.
[17] Scott MC, Temiz NA, Sarver AE, LaRue RS, Rathe SK, Varshney J, Sarver AL. Comparative transcriptome analysis quantifies immune cell transcript levels, metastatic progression, and survival in osteosarcoma. Cancer Res 2018;78(2):326–37.
[18] Mazcko C, Thomas R. The establishment of the Pfizer-canine comparative oncology and genomics consortium biospecimen repository. Vet Sci 2015;2(3):127–30.
[19] Wang H, Hu X, Ding X, Dou Z, Yang Z, Shaw AW, Yao X. Human Zwint-1 specifies localization of Zeste White 10 to kinetochores and is essential for mitotic checkpoint signaling. J Biol Chem 2004;279(52):54590–8.
[20] Mills LJ, Scott MC, Shah P, Cunanan AR, Deshpande A, Auch B, Modiano JF. Comparative analysis of genome-wide DNA methylation identifies patterns that associate with conserved transcriptional programs in osteosarcoma. Bone 2020;158:115716.
[21] Álvarez-Garcia V, Tawil Y, Wise HM, Leslie NR. Mechanisms of PTEN loss in cancer: it's all about diversity. In: Seminars in cancer biology, 59. Academic Press; 2019. p. 66–79. Volpp.
[22] Li J, Kaneda MM, Ma J, Li M, Shepard RM, Patel K, Koga T, et al. PI3Kγ inhibition suppresses microglia/TAM accumulation in glioblastoma microenvironment to promote exceptional temozolomide response. Proc Natl Acad Sci 2021;118(16):e2009290118 no.
[23] Beckmann PJ, Larson JD, Larsson AT, Ostergaard JP, Wagner S, Rahrmann EP, Largaespada DA. Sleeping Beauty Insertional Mutagenesis Reveals Important Genetic Drivers of Central Nervous System Embryonal TumorsSB Identifies Novel Drivers in Medulloblastoma and CNS-PNET. Cancer Res 2019;79(5):905–17 .
[24] Sarver AL, Xie C, Riddle MJ, Forster CL, Wang X, Lu H, Wagner W, Tolar J, Hallstrom TC. "Retinoblastoma tumor cell proliferation is negatively associated with an immune gene expression signature and increased immune cells". Lab Invest 2021;101(6):701–18.
[25] Heltemes-Harris LM, Hubbard GK, LaRue RS, Munro SA, Yang R, Henzler CM, Farrar MA. Identification of mutations that cooperate with defects in B cell transcription factors to initiate leukemia. Oncogene 2021;40(43):6166–79.
[26] Koshkina NV, Khanna C, Mendoza A, Guan H, DeLauter L, Kleinerman ES. Fas-negative osteosarcoma tumor cells are selected during metastasis to the lungs: the role of the Fas pathway in the metastatic process of osteosarcoma. Mol Cancer Res 2007;5(10):991–9.
[27] Worth LL, Lafleur EA, Jia SF, Kleinerman ES. Fas expression inversely correlates with metastatic potential in osteosarcoma cells. Oncol Rep 2002;9(4):823–7.
[28] Li J, Sarosi I, Cattley RC, Pretorius J, Asuncion F, Grisanti M, Richards WG. Dkk1-mediated inhibition of Wnt signaling in bone results in osteopenia. Bone 2006;39(4):754–66.
[29] Morvan F, Boulukos K, Clément-Lacroix P, Roman SR, Suc-Royer I, Vayssière B, Rawadi G. Deletion of a single allele of the Dkk1 gene leads to an increase in bone formation and bone mass. J Bone Miner Res 2006;21(6):934–45.
[30] Kow K, Thamm DH, Terry J, Grunerud K, Bailey SM, Withrow SJ, Lana SE. Impact of telomerase status on canine osteosarcoma patients. J Vet Intern Med 2008;22(6):1366–72.
[31] Sarver AL, Makielski KM, DePauw TA, Schulte AJ, Modiano JF. Increased risk of cancer in dogs and humans: a consequence of recent extension of lifespan beyond evolutionarily determined limitations? Aging and Cancer 2022;3(1):3–19.
[32] Castro-Mondragon JA, Riudavets-Puig R, Rauluseviciute I, Berhanu Lemma R, Turchi L, Blanc-Mathieu R, Mathelier A. JASPAR 2022: the 9th release of the open-access database of transcription factor binding profiles. Nucleic Acids Res 2022;50(D1):D165–73.
[33] Cho YJ, Liang P. Killin is a p53-regulated nuclear inhibitor of DNA synthesis. Proc Natl Acad Sci 2008;105(14):5396–401.
[34] Koelsche C, Schrimpf D, Tharun L, Roth E, Sturm D, Jones DT, Mechtersheimer G. Histone 3.3 hotspot mutations in conventional osteosarcomas: a comprehensive clinical and molecular characterization of six H3F3A mutated cases. Clin Sarcoma Res 2017;7(1):1–11.
[35] Nizialek EA, Mester JL, Dhiman VK, Smiraglia DJ, Eng C. KLLN epigenotype–phenotype associations in Cowden syndrome. Eur J Hum Genet 2015;23(11):1538–43.
[36] Pilarski R, Burt R, Kohlman W, Pho L, Shannon KM, Swisher E. Cowden syndrome and the PTEN hamartoma tumor syndrome: systematic review and revised diagnostic criteria. J Natl Cancer Inst 2013;105(21):1607–16.
[37] Zhou J, Xiao X, Wang W, Luo Y. Association between PTEN and clinical-pathological features of osteosarcoma. Biosci Rep 2019;39(7):BSR20190954.
[38] Scotlandi K, Serra M, Manara MC, Maurici D, Benini S, Nini G, Baldini N. Clinical relevance of Ki-67 expression in bone tumors. Cancer 1995;75(3):806–14.
[39] Zeng M, et al. "The relationship between the expression of Ki-67 and the prognosis of osteosarcoma". BMC Cancer 2021;21(1):1–9.
[40] Modiano JF, Bellgrau D, Cutter GR, Lana SE, Ehrhart NP, Ehrhart EJ, Duke RC. Inflammation, apoptosis, and necrosis induced by neoadjuvant fas ligand gene therapy improves survival of dogs with spontaneous bone cancer. Mol Ther 2012;20(12):2234–43.
[41] Modiano JF, Bellgrau D. Fas ligand based immunotherapy: a potent and effective neoadjuvant with checkpoint inhibitor properties, or a systemically toxic promoter of tumor growth? Discov Med 2016;21(114):109–16.
[42] Marjon K, Cameron MJ, Quang P, Clasquin MF, Mandley E, Kunii K, Marks KM. MTAP deletions in cancer create vulnerability to targeting of the MAT2A/PRMT5/RIOK1 axis. Cell Rep 2016;15(3):574–87.
[43] Chiang C, Layer RM, Faust GG, Lindberg MR, Rose DB, Garrison EP, Hall IM. SpeedSeq: ultra-fast personal genome analysis and interpretation. Nat Methods 2015;12(10):966–8.
[44] Koboldt DC, Zhang Q, Larson DE, Shen D, McLellan MD, Lin L, Wilson RK. VarScan 2: somatic mutation and copy number alteration discovery in cancer by exome sequencing. Genome Res 2012;22(3):568–76.
[45] Li H, Handsaker B, Wysoker A, Fennell T, Ruan J, Homer N, Durbin R. The sequence alignment/map format and SAMtools. Bioinformatics 2009;25(16):2078–9.
[46] Kim D, Paggi JM, Park C, Bennett C, Salzberg SL. Graph-based genome alignment and genotyping with HISAT2 and HISAT-genotype. Nat Biotechnol 2019;37(8):907–15.
[47] Liao Y, Smyth GK, Shi W. "featureCounts: an efficient general purpose program for assigning sequence reads to genomic features". Bioinformatics 2014;30(7):923–30 no.
[48] Ihaka R, Gentleman R. R: a language for data analysis and graphics. J Comput Graph Statist 1996;5(3):299–314.

Molecular Therapy - Oncolytics

Neoadjuvant systemic oncolytic vesicular stomatitis virus is safe and may enhance long-term survivorship in dogs with naturally occurring osteosarcoma.

--Manuscript Draft--

Manuscript Number:	MTO-D-23-00140R1
Full Title:	Neoadjuvant systemic oncolytic vesicular stomatitis virus is safe and may enhance long-term survivorship in dogs with naturally occurring osteosarcoma.
Article Type:	Research Article
Section/Category:	Regular Issue
Keywords:	oncolytic virus, osteosarcoma, neoadjuvant, immunotherapy, tumor microenvironment
Corresponding Author:	Shruthi Naik, PhD UNITED STATES
First Author:	Kelly M Makielski, DVM, MS
Order of Authors:	Kelly M Makielski, DVM, MS
	Aaron L Sarver, PhD
	Michael S Henson, DVM, PhD
	Kathleen M Stuebner, BS
	Antonella Borgatti, DVM, MS
	Lukkana Suksanpaisan, PhD
	Caitlin Preusser, BA
	Alexandru-Flaviu Tabaran, DVM, PhD
	Ingrid Cornax, DVM, PhD, MS
	M. Gerard O'Sullivan, MVB, MSc, PhD
	Andrea Chehadeh, BS
	Donna Groschen, BS
	Kelly Bergsrud, Assoc.
	Sara Pracht, BA
	Amber Winter, BS
	Lauren J Mills, PhD
	Marc D Schwabenlander, MPH
	Melissa Wolfe, B.S.
	Michael A Farrar, PhD
	Gary R Cutter, PhD
	Joseph S Koopmeiners, PhD, MS, BA
	Stephen J Russell, MD PhD
	Jaime F Modiano, VMD, PhD
	Shruthi Naik, PhD
Abstract:	Osteosarcoma is a devastating bone cancer that disproportionally afflicts children, adolescents, and young adults. Standard therapy includes surgical tumor resection combined with multiagent chemotherapy, but many patients still suffer from metastatic disease progression. Neoadjuvant systemic oncolytic virus (OV) therapy has the

	potential to improve clinical outcomes by targeting primary and metastatic tumor sites and inducing durable antitumor immune responses. Here we described the first evaluation of neoadjuvant systemic therapy with a clinical-stage recombinant oncolytic Vesicular stomatitis virus (VSV), VSV-IFNβ-NIS, in naturally occurring cancer, specifically appendicular osteosarcoma in companion dogs. Canine osteosarcoma has a similar natural disease history as its human counterpart. VSV-IFNβ-NIS was administered prior to standard of care surgical resection, permitting microscopic and genomic analysis of tumors. Treatment was well-tolerated and a “tail” of long-term survivors (~35%) was apparent in the VSV-treated group, a greater proportion than observed in two contemporary control cohorts. An increase in tumor inflammation was observed in VSV-treated tumors and RNAseq analysis showed that all the long-term responders had increased expression of a T-cell anchored immune gene cluster. We conclude that neoadjuvant VSV-IFNβ-NIS is safe and may increase long-term survivorship in dogs with naturally occurring osteosarcoma, particularly those that exhibit pre-existing antitumor immunity.

Neoadjuvant systemic oncolytic vesicular stomatitis virus is safe and may enhance long-term survivorship in dogs with naturally occurring osteosarcoma.

Kelly M. Makielski[1-3], Aaron L. Sarver[1,2,4], Michael S. Henson[3], Kathleen M. Stuebner[3], Antonella Borgatti[3], Lukkana Suksanpaisan[5], Caitlin Preusser[6], Alexandru-Flaviu Tabaran[7], Ingrid Cornax[7], M. Gerard O'Sullivan[7], Andrea Chehadeh[3], Donna Groschen[3], Kelly Bergsrud[3], Sara Pracht[3], Amber Winter[3], Lauren J. Mills[1,8], Marc D. Schwabenlander[9], Melissa Wolfe[9], Michael A. Farrar[10,11], Gary R. Cutter[12], Joseph S. Koopmeiners[1,13], Stephen J. Russell[6,14], Jaime F. Modiano[1-3,10,15,16], Shruthi Naik[6,14]

[1]Masonic Cancer Center, University of Minnesota, Minneapolis, Minnesota 55455, USA

[2]Animal Cancer Care and Research Program, University of Minnesota, St. Paul, Minnesota 55108, USA

[3]Department of Veterinary Clinical Sciences, University of Minnesota College of Veterinary Medicine, St. Paul, Minnesota 55108, USA

[4]Institute for Health Informatics, University of Minnesota, Minneapolis, Minnesota 55455, USA

[5]Imanis Life Sciences, LLC, Rochester MN

[6]Department of Molecular Medicine, Mayo Clinic, 200 First street SW, Rochester, MN, 55905

[7]Department of Veterinary Population Medicine, St. Paul, Minnesota 55108, USA

[8]Department of Pediatrics, University of Minnesota School of Medicine, Minneapolis, Minnesota 55455, USA

[9]Veterinary Diagnostic Laboratory, University of Minnesota College of Veterinary Medicine, St. Paul, Minnesota 55108, USA

[10]Center for Immunology, University of Minnesota, Minneapolis, Minnesota 55455, USA

[11]Department of Laboratory Medicine and Pathology, University of Minnesota Medical School, Minneapolis, Minnesota 55455, USA

[12]University of Alabama at Birmingham, Birmingham, AL, USA

[13]Division of Biostatistics, University of Minnesota Medical School, Minneapolis, Minnesota 55455, USA

[14]Vyriad, Inc. Rochester MN, 2900 37th St NW, Rochester MN 55901

[15]Stem Cell Institute, University of Minnesota, Minneapolis, Minnesota 55455, USA

[16]Center for Engineering and Medicine, University of Minnesota, Minneapolis, Minnesota 55455, USA

Dr. Tabaran's present address is: Department of Pathology, University of Agricultural Science and Veterinary Medicine, Cluj- Napoca, Romania.

Dr. Cornax's present address is: The Janssen Pharmaceutical Companies of Johnson & Johnson, San Diego, California, United States.

Mr. Schwabenlander's present address is Department of Veterinary and Biological Sciences, University of Minnesota College of Veterinary Medicine, St. Paul, Minnesota 55108, USA.

Abstract

Osteosarcoma is a devastating bone cancer that disproportionally afflicts children, adolescents, and young adults. Standard therapy includes surgical tumor resection combined with multiagent chemotherapy, but many patients still suffer from metastatic disease progression. Neoadjuvant systemic oncolytic virus (OV) therapy has the potential to improve clinical outcomes by targeting primary and metastatic tumor sites and inducing durable antitumor immune responses. Here we described the first evaluation of neoadjuvant systemic therapy with a clinical-stage recombinant oncolytic Vesicular stomatitis virus (VSV), VSV-IFNβ-NIS, in naturally occurring cancer, specifically appendicular osteosarcoma in companion dogs. Canine osteosarcoma has a similar natural disease history as its human counterpart. VSV-IFNβ-NIS was administered prior to standard of care surgical resection, permitting microscopic and genomic analysis of tumors. Treatment was well-tolerated and a "tail" of long-term survivors (~35%) was apparent in the VSV-treated group, a greater proportion than observed in two contemporary control cohorts. An increase in tumor inflammation was observed in VSV-treated tumors and RNAseq analysis showed that all the long-term responders had increased expression of a T-cell anchored immune gene cluster. We conclude that neoadjuvant VSV-IFNβ-NIS is safe and may increase long-term survivorship in dogs with naturally occurring osteosarcoma, particularly those that exhibit pre-existing antitumor immunity.

Introduction

Osteosarcoma is a devastating bone cancer that primarily affects children, adolescents, and young adults, occurring most commonly in the long bones of the limbs.[1] Standard treatment for patients diagnosed with osteosarcoma is definitive tumor resection with limb-sparing surgery elected where possible, combined with multi-agent chemotherapy administered in the neoadjuvant and adjuvant settings. These protocols were developed over 40 years ago, achieving a 5-year survival rate of approximately 60%.[1,2] Many patients have inoperable metastases (commonly in the lung) and mortality is often due to progression of pre-existing or new sites of metastatic disease. Patients who are refractory to frontline treatment or are diagnosed with metastatic osteosarcoma have a very poor prognosis.[3] Treatment modifications tested to date have failed to have a major impact on clinical outcomes. Thus, there is an unmet clinical need for treatments that improve outcomes for osteosarcoma patients. Development of new treatments is hampered by the rarity of this malignancy. Naturally occurring canine cancer represents a clinically relevant model that can recapitulate the spontaneous development and heterogeneity present in human cancer.[4] Osteosarcoma is a common malignancy in dogs with similar clinical presentation and natural history as in humans. Osteosarcoma treatment in dogs includes surgical amputation of the affected limb and adjuvant chemotherapy.[5] Also as in humans, despite removal of the primary tumor, most dogs develop pulmonary metastases and succumb to the disease; however, in dogs this typically occurs in less than 1 year.[6]

Oncolytic viruses (OVs) are engineered to selectively kill tumor cells and recruit immune cells to tumor sites.[7] Vesicular stomatitis virus (VSV) expressing interferon-beta (IFNβ) and the sodium iodide symporter (NIS), referred to henceforth as VSV-IFNβ-NIS, is a clinical-stage recombinant OV that is currently being tested as a systemic therapy for patients with advanced solid tumors

and hematologic malignancies both as a monotherapy and in combination with immune checkpoint inhibitors.[8,9] Preclinical studies showed that systemically administered VSV infected and amplified selectively in tumor cells inducing tumor cell death, antitumor immune responses, and durable tumor remission in murine tumor models.[10-13] Antitumor activity of systemic VSV therapy was also demonstrated in naturally occurring cancer in dogs. Single dose systemic VSV-IFNβ-NIS therapy was well tolerated with clinical remissions of disseminated lesions observed in two dogs with lymphoma and disease stabilization in a dog with metastatic osteosarcoma.[14] These early clinical responses were also notable because most of the dogs had received prior treatments (mainly chemotherapy) and were enrolled after diagnosis with advanced refractory or relapsed disease. Our goal in this study was to evaluate the use of systemic VSV-IFNβ-NIS therapy in the neoadjuvant setting in dogs with newly diagnosed, localized osteosarcoma. Systemic OV therapy administered in the neoadjuvant setting has the potential to target and kill malignant cells in primary and metastatic tumor sites, inducing inflammation in intact tumors to generate antitumor immune responses that persist after surgical interventions to improve clinical outcomes following standard of care treatment.[15] Due to the prevalence of metastatic pulmonary recurrence in canine (and human) osteosarcoma, we hypothesized that systemic VSV therapy administered in the neoadjuvant setting has the potential to improve clinical outcomes following standard therapy for osteosarcoma. We launched the VIGOR study (VSV Immunotherapy and Genomics of Osteosarcoma Research) to test the safety, efficacy, and immunomodulatory effects of neoadjuvant intravenous VSV-IFNβ-NIS therapy in dogs with localized appendicular osteosarcoma.

Results

Oncolytic VSV kills canine osteosarcoma cells *in vitro*

Type I interferons, including IFNβ, activates antiviral innate immune responses in normal cells. Oncolytic VSV expressing IFNβ has been shown to selectively replicate within and kill a variety of tumor cells due to impaired innate immune responses.[16-18] We previously generated and characterized a recombinant VSV expressing canine IFNβ and NIS (VSV-cIFNβ-NIS) for use in veterinary clinical trials in dogs.[14] We evaluated the replication and oncolytic activity of recombinant VSV vectors, VSV-GFP, VSV-hIFNβ-NIS (VSV expressing human IFNβ), and VSV-cIFNβ-NIS in canine osteosarcoma cell lines (OSCA-78, OSCA-08, and OSCA-40) *in vitro*. Evaluation of VSV expressing canine and human IFNβ in canine osteosarcoma cells permits comparison of the effect of VSV expressing active canine IFNβ in canine cells. The VSV vectors replicated in all three canine osteosarcoma cell lines, with VSV-IFNβ-NIS vectors having ~1-log lower maximal titer compared to VSV-GFP. VSV-IFNβ-NIS (expressing both human and canine IFNβ) replication resulted in tumor cell killing with similar potency as VSV-GFP resulting in <50% viability ~48 hours post infection (Figure 1). These data confirm that canine osteosarcoma cell lines are susceptible to VSV infection and oncolysis and expression of canine IFNβ does not attenuate VSV replication and oncolysis in canine osteosarcoma cell lines.

Screening and enrollment to the VIGOR study

The VIGOR (**V**SV **I**mmunotherapy and **G**enomics for **O**steosarcoma **R**esearch) study outline is shown in Figure 2. A total of 41 dogs were fully screened for enrollment in the VIGOR study of the 144 inquiries received (Supplemental Figure S1). Of the dogs screened, 13 were excluded. Twelve of these did not meet eligibility criteria due to documentation of metastatic disease on

screening diagnostics (n=4), clinical suspicion or diagnosis of a different cancer (n=4), evidence of a pathologic fracture (n=3), or concurrent metastatic disease and pathologic fracture (n=1). One screened dog was not enrolled because the owner declined to participate. The study enrolled a total of 28 dogs over a period of 30 months (June 2016 to January 2019) with demographic characteristics of the dogs enrolled in the VIGOR study, as well as the contemporary control comparison populations, shown in Table 1. All dogs had an initial diagnosis of sarcoma of an appendicular bone based on a pre-treatment bone biopsy. This was a fixed-dose study with the first 15 dogs receiving one dose of $1x10^9$ $TCID_{50}$/kg neoadjuvant VSV-cIFNβ-NIS under an open label design. After the safety of systemic neoadjuvant VSV-cIFNβ-NIS was documented, the next 13 dogs were randomized in a double-blinded fashion to receive a single dose of either intravenous VSV-cIFNβ-NIS (n=7) or placebo (PBS, n=6). All dogs were subsequently treated with standard of care and underwent amputation of the affected limb and removal of the associated lymph node(s) 10 days after receiving VSV-cIFNβ-NIS or placebo. Faxitron imaging was performed on the amputated limb to guide sample collection (Supplemental Figure S2). Pathological analysis of resected tumors confirmed primary osteosarcoma in 26 dogs, but the diagnoses in two dogs were subsequently revised: one (treated with VSV in the open label portion of the study) was diagnosed with intramedullary hemangiosarcoma at amputation, and the other (randomized to receive placebo) was diagnosed with intramedullary rhabdomyosarcoma at necropsy.

VSV-cIFNB-NIS treatment is safe and is associated with prolonged survival in a subset of dogs with non-metastatic appendicular osteosarcoma

No clinically significant laboratory abnormalities were observed following VSV administration. About half the treated dogs developed a transient fever (> 1.5°C increase in body temperature) that resolved without intervention within 72 hours post infusion (not shown). Transient hepatotoxicity and lymphopenia are commonly observed following intravenous VSV infusion.[8,14] As expected, mild lymphopenia was observed in some dogs following VSV infusion that resolved spontaneously (Supplemental Figure 3). There were no severe adverse events (AEs) directly attributable to VSV-cIFNβ-NIS. Three dogs that were treated with VSV (two open-label and one randomized to receive VSV) had reportable AEs that were considered independent from the expected side effects of chemotherapy (Supplemental Table S1), including one case each of pneumonia, facial nerve paralysis, and hypovolemic shock after amputation. The latter were post-surgical complications that resulted in death of the dog and likely not related to VSV-cIFNβ-NIS administration.

Clinical efficacy endpoints evaluated included event free survival (EFS) and overall survival. Overall survival for dogs in the VIGOR study roughly segregated into 3 populations with a "tail" of 7 dogs that were "long-term" survivors. The group of long-term survivors includes 4 dogs that are still alive at the time of this report including three dogs with osteosarcoma (two treated with VSV and one randomized to receive placebo) and one with hemangiosarcoma of bone (treated with VSV). Three dogs were excluded from the survival analysis: two dogs that eventually received a histopathologic diagnosis other than osteosarcoma (one rhabdomyosarcoma of bone (placebo-treated) and one hemangiosarcoma of bone (VSV-treated)) and one dog that died immediately after surgery due to hypovolemic shock (VSV-treated), yielding a cohort of 20 evaluable VSV-cIFNβ-NIS treated dogs. The clinical information, treatment categories, and survival data for each individual dog enrolled in VIGOR are shown in Supplementary Table S2.

EFS and overall survival for these evaluable dogs were compared to two contemporary control cohorts of dogs with appendicular osteosarcoma with no evidence of metastasis. The first cohort (n = 57) included dogs seen at the University of Minnesota (UMN) VMC between July 2011 and July 2018, where there was intent to treat with standard-of-care surgery and adjuvant carboplatin chemotherapy, and that had a successful limb amputation and completed at least one cycle of adjuvant chemotherapy. The second control cohort was from a study recently published by the National Cancer Institute's Comparative Oncology Trial Consortium (NCI-COTC) and included 157 dogs between November 2015 and February 2018 enrolled at 18 sites around the United States that were treated with standard-of-care surgery and adjuvant carboplatin chemotherapy.[19] The NCI-COTC national multicenter comparison cohort was made available as a control dataset for evaluation of novel neoadjuvant or adjuvant treatments for osteosarcoma. Comparison to control cohorts showed that neoadjuvant VSV-cIFNβ-NIS therapy did not markedly improve EFS or overall survival (Figure 3A), but importantly did not worsen survival outcomes. Based on the NCI-COTC control cohort, "long-term" survivorship was defined as overall survival that exceeded the 75th percentile value of the NCI-COTC cohort (479 days). The UMN VMC control cohort had, as expected, 26% of dogs that exceeded an overall survival of 479 days. The VIGOR cohort had a higher-than-expected proportion of long-term survivorship with 35% of dogs exceeding an overall survival of 479 days (Figure 3B), though the sample size lacked the power to establish that this difference was not due to random chance with a high level of confidence.

Histopathological assessment of osteosarcoma tumors shows an increase in tumor inflammation following VSV treatment

Pre-treatment tumor biopsies and post-treatment amputation-resected tumor samples were scored based on tumor necrosis, inflammation, and fibrosis (supplemental table S3). Tumor

histopathologic evaluation showed areas of moderate to severe ischemic necrosis, as is typically observed in rapidly growing osteosarcoma lesions, in both VSV-cIFNβ-NIS-treated and placebo-treated cases; however, the tumors of 10 of 22 VSV-cIFNβ-NIS-treated dogs had distinctive areas of micronecrosis that were not consistently present in placebo-treated tumors (Supplemental Figure S4). Inflammatory infiltrates were scored in pre-treatment and post-treatment tumor specimens. Higher tumor infiltration score (TIS) was observed in post-treatment tumor specimens from VSV treated dogs compared to pre-treatment tumor biopsies, while similar increases were not observed in tumor specimens from placebo treated dogs (Figure 4A). Matched pre- vs post-treatment tumor specimens were available for assessment of intratumoral inflammatory infiltrate for half of the enrolled dogs showing a significant increase in TIS in post-treatment tumors compared to baseline (Figure 4B, P=0.0027). These results are encouraging but must be interpreted with caution given the small cohort size and the small number of dogs enrolled in the placebo group.

Regional lymph nodes were evaluated in 27/28 dogs; the associated lymph node could not be found after amputation in one case (from a dog randomized to receive VSV). Two of the 27 cases evaluated had evidence of osteosarcoma metastasis in the lymph node, and the remaining 25 were negative for metastasis. One of the two dogs with lymph node metastasis at the time of amputation had shortened survival and was euthanized 64 days after surgery, with metastasis present throughout the abdomen and thorax on necropsy. Interestingly, the other dog with lymph node metastasis had prolonged survival and was still alive at the time of this report. Both cases with documented lymph node metastasis were treated with VSV.

Virus pharmacokinetics

Monitoring viremia, virus shedding, and antiviral antibodies showed similar trends to previous studies evaluating intravenous VSV therapy in dogs.[14] Viral RNA was detectable in whole blood samples at high quantities for the first 24 hours following infusion, with virus localizing primarily to PBMCs (Figure 5). Decay of viral RNA in blood coincided with an increase in detection of anti-VSV neutralizing antibodies, indicative of antibody-mediated virus clearance (Supplemental Figure S5). Infectious virus was detectable in PBMC samples at low quantities (below the limit of quantification) only at 1 hour post systemic VSV administration and no infectious virus was detected in PBMC samples collected after the 1h timepoint (data not shown). Virus shedding studies showed no detectable infectious virus in urine, rectal swab, or buccal swab samples, though viral RNA was detectable at low levels in some samples as shown (Supplemental Figure S6). Viremia, virus shedding, and neutralizing antibodies were measured in samples from two placebo-treated dogs showing no detectable viral RNA in blood or shedding samples, and no antiviral antibodies providing relevant negative controls in our pharmacokinetic analyses (data not shown). RNA from tumor specimens collected 10 days following VSV or placebo treatment showed detection of VSV RNA in bone tumor specimens from 2 of 22 VSV-treated dogs (supplemental table S4). The dose dependent efficacy of systemic VSV therapy[11], the low amount and brief period that infectious virus was detectable, and the excellent safety of VSV infusion in this fixed-dose study collectively suggest higher doses of VSV-IFNβ-NIS can be safely administered in this treatment setting to potentially improve clinical response.

Pre-treatment immune infiltration is associated with longer overall survival

Acute cytokine responses were measured in the first 15 dogs enrolled and showed a transient elevation in several pro-inflammatory cytokines between 3 and 6 hours following VSV administration (Supplemental Figure S7). Three dogs that were long-term responders to VSV treatment, including the one diagnosed with hemangiosarcoma of bone, had high GM-CSF, IL-2, IL-7, and IL-15 levels at baseline.

Samples were examined for evidence of an immune component in the tumor response using next-generation RNA sequencing. Specifically, we used the gene cluster expression summary score (GCESS) method to summarize co-regulated gene clusters in tumor samples and their association with outcome.[20] Pre- and post-treatment samples from primary osteosarcoma and metastatic osteosarcoma tumors grouped together, separate from both the cell lines derived from the pre-treatment tumors as well as from normal skin biopsy samples obtained from the same dogs at the time of amputation. Fourteen gene clusters were identified and were apparent in unsupervised hierarchical clustering heatmaps (Figure 6A-B), including a skin specific cluster (Figure 6C), as well as immune 1 (Figure 6D), immune 2 (Figure 6E), and cell cycle (Figure 6F) gene clusters previously identified in canine and human osteosarcoma.[20] The distributions of cell cycle and immune GCESS across tumor samples, cell lines, and skin biopsy samples were as predicted, with no immune transcripts identified in osteosarcoma cell lines. VSV treatment did not notably impact the GCESS score of pre- versus post-treatment tumor specimens (Figure 6G-J). When we analyzed the association between GCESS and survival, we observed that the dogs with the highest pre-treatment immune 2 (T-cell) GCESS had longer survival times (Figure 7). This relationship was not observed for the CD37-positive monocyte-related GCESS, and somewhat surprisingly, it was also not evident for the cell cycle GCESS (Figure 7B-D). Upon comparison of the VIGOR cohort to a contemporary CCOGC cohort with available canine osteosarcoma RNAseq data (n=23, Supplemental Figure S8)[21], we noted that a higher immune

GCESS was associated with a longer progression-free survival in both groups, but that this effect was larger in the VSV-treated group. In the CCOGC cohort, all the dogs with longer survival had a higher T-cell anchored GCESS, but not all the dogs with higher CD8 GCESS had longer survival (Supplemental Figure S8C – see overlapping box plots); in the VIGOR group, all of the dogs with higher T-cell GCESS had longer survival (Figure 7E – see non-overlapping VSV high and VSV low box plots). The Kaplan-Meier Survival curve, showing increased overall survival in the VSV-treated dogs in the VIGOR group when compared with CCOGC cohort where RNA sequencing was available, is shown in Supplemental Figure S9.

Discussion

Oncolytic viruses, including VSV, can selectively infect, replicate within, and kill tumor cells, promoting release of tumor associated antigens to drive robust anti-tumor immune responses.[7,22] This approach is of particular interest in osteosarcoma, a genomically chaotic cancer, albeit with a low overall mutational burden and where recurrent mutations across the patient population are uncommon.[23-25] Clinical studies evaluating oncolytic viruses to date have limited evaluation of the immune responses following treatment and highlight the need to identify and investigate biomarkers of clinical response.[26] Here we describe the safety and efficacy of intravenous VSV-IFNβ-NIS therapy in naturally occurring canine appendicular osteosarcoma, a model utilized to inform development of new treatments for human osteosarcoma.[5] Studies in spontaneous canine cancer supported clinical translation of VSV-IFNβ-NIS, a clinical-stage oncolytic virus that is being evaluated for the treatment of both solid tumors and hematologic malignancies.[8,9] The major goals of this study were to establish the safety and clinical utility of VSV-IFNβ-NIS administered in the neoadjuvant setting in dogs with osteosarcoma, and to utilize correlatives

studies in this spontaneous model to identify potential biomarkers of efficacy to oncolytic VSV therapy. Previous studies indicate that both safety and therapeutic response following systemic VSV therapy is dose dependent.[11,27] In this study, we documented the safety profile of systemic therapy with VSV-cIFNβ-NIS in canine osteosarcoma. Intravenous VSV-cIFNβ-NIS, administered at $1x10^9$ $TCID_{50}$/kg, was remarkably well-tolerated, with no clinically significant changes in any of the monitored parameters. Systemic viral distribution was documented with live virus detected (below the limit of quantification) in PBMCs within one-hour post-infusion, but not at later timepoints. Evidence of a systemic response was noted, as a subset of dogs examined showed acute elevations of inflammatory cytokines. No clinically significant adverse events were documented that were attributable to VSV therapy. The absence of adverse events paired with the low quantities and short duration of infectious virus detected in blood, suggest that the dose of systemic VSV therapy can be safely increased to potentially improve clinical outcomes.

We evaluated changes in GCESS and tumor inflammation scores on histopathology before and after treatment with VSV-IFNβ-NIS in this study. An increased tumor inflammation score (based on pathology assessment) was noted in tumor samples collected 10 days post VSV treatment compared to baseline samples. Clinical outcomes with neoadjuvant VSV therapy added to standard treatments for dogs with osteosarcoma were compared with two published control cohorts with dogs treated with only standard of care, including the NCI-COTC osteosarcoma cohort, a prospectively enrolled cohort designed to enable assessment and comparison of new osteosarcoma therapies in this clinically relevant model.[19] While we did not observe a significant difference in survival between the groups, there was a tail of long-term survivors, defined as 75th percentile overall survival from the NCI-COTC osteosarcoma cohort (479 days), noted in each

population. In the VIGOR cohort, 35% of the dogs were considered long-term survivors compared to 25% and 26% in the NCI-COTC and UMN VMC control cohorts respectively. When we evaluated the association between immune GCESS and survival in the VIGOR cohort and CCOGC comparison group that had available RNAseq data, a higher T-cell anchored immune GCESS was associated with prolonged survival in both groups. However, this effect was more pronounced in the VSV-treated dogs. Our interpretation of these data is that the presence of a T-cell signature in osteosarcoma tumors prior to treatment increases the probability of longer survival, and the addition of VSV in the neoadjuvant setting enhances this effect.

In conclusion, these results show that systemically administered VSV-IFNβ-NIS can be used safely in the neoadjuvant setting to treat canine osteosarcoma. Systemic VSV-IFNβ-NIS is biologically active and can target the tumor microenvironment with evidence of increased tumor inflammation in VSV-treated osteosarcoma specimens. The intrinsic tumor immune status at baseline appears to influence the activity and therapeutic benefit of VSV, as dogs with higher immune 2 or T-cell anchored GCESS at baseline had prolonged survivals. The clinical safety and PK data, when viewed in the context of previous findings indicating dose dependent efficacy of systemic VSV therapy,[20] suggest that there is scope to increase the systemic dose to improve clinical outcomes. Additionally, the observed therapeutic benefit in dogs with a pro-immune environment suggests that combinations with agents that promote immune infiltration or that amplify the immune response, such as immune checkpoint inhibitors, may further enhance the therapeutic benefits of VSV-IFNβ-NIS. The observed exceptional safety and immunological activity of VSV-IFNβ-NIS support further evaluation of neoadjuvant systemic VSV therapy including dose modification and combination therapy strategies for the treatment of sarcomas and translation to human cancer patients.

Materials & Methods

Manufacturing of VSV

Vesicular stomatitis virus (VSV) expressing canine interferon-beta (IFNβ) and the sodium iodide symporter (NIS), VSV-cIFNβ-NIS, was constructed as previously described.[10] The VSV-cIFNβ-NIS lot used in veterinary studies was provided by the Mayo Clinic Viral Vector Production laboratory (VVPL). Virus product is stored at ≤ -65°C. Virus titers were determined by 50% tissue culture infective dose ($TCID_{50}$) assays on Vero cells. The virus product was tested to confirm sterility (Mayo Clinic Department of Laboratory Medicine and Pathology) and absence of endotoxin using the LAL-Kinetic QCL Kit (Lonza). Whole genome sequencing was performed by utilizing reverse transcription of purified viral RNA to cDNA, polymerase chain reaction (PCR) of overlapping regions of viral genome, sequencing of PCR fragments (Eurofins Genomics), and assembly of sequencing results.

In vitro efficacy of oncolytic VSV in canine osteosarcoma

Recombinant VSV vectors, including VSV expressing green fluorescent protein (GFP) or VSV expressing canine or human IFNβ and NIS (hIFNβ-NIS or cIFNβ-NIS), were used to infect three canine osteosarcoma cell lines, OSCA-78, OSCA-08, and OSCA-40, to evaluate *in vitro* efficacy of oncolytic VSV in canine osteosarcoma. Cells were grown in DMEM media containing 5% glucose and L-glutamine supplemented with 10% fetal bovine serum (FBS), 10mM HEPES buffer, and 0.1% Primocin, and cultured at 37°C in a humidified atmosphere of 5% CO_2. Cell lines were authenticated based on short tandem repeats at regular intervals (IDEXX BioAnalytics). Virus titers were determined by $TCID_{50}$ assay on BHK-21 cells at several timepoints after infection (12h, 24h, 36h, 48h, 60h, and 72h). Cell viability, as a percent of

366 control, was determined by flow cytometry using a live/dead marker (Invitrogen) at several
367 timepoints after infection (12h, 24h, 36h, 48h, 72h, and 96h). Cell lines are available through
368 Kerafast, Inc (Boston, MA).

369

370 **Enrollment and eligibility criteria**

371 Dogs with a diagnosis of appendicular bone sarcoma, based on radiographic appearance of the
372 lesion and results of bone aspirate or biopsy, were considered for enrollment in the study (see
373 CONSORT diagram, Supplementary Figure S1). All cases were enrolled at the University of
374 Minnesota (UMN) College of Veterinary Medicine between June 2016 and January 2019.
375 Screening diagnostics were performed prior to inclusion in the study, including physical
376 examination, radiographs of the affected limb and thorax, general blood work (complete blood
377 count, serum chemistry profile), computed tomography of the thorax and abdomen, and biopsy
378 of the bone lesion. Inclusion criteria included cytologic or histologic diagnosis of sarcoma in an
379 appendicular bone and body weight greater than 20kg (to facilitate safe collection of blood for
380 the study). Exclusion criteria included evidence of metastatic lesions, evidence of pathologic
381 fracture, intact reproductive status, clinically significant co-morbidities, treatment with other
382 medications, and residence on a farm or other contact with farm animals (to reduce risk of VSV
383 transmission to susceptible hosts).

384

385 **VSV dosing**

386 Previous studies have demonstrated the safety of intravenous VSV-hIFNβ-NIS and VSV-cIFNβ-
387 NIS therapy in dogs with cancer at doses up to 10^{10} $TCID_{50}/0.5m^2$, which converts to

approximately $1x10^9$/kg.[14,27] The VIGOR study enrolled a total of 28 dogs over 30 months (June 2016 to January 2019). The first 15 dogs received a single dose ($1x10^9$ $TCID_{50}$/kg) of neoadjuvant VSV-cIFNβ-NIS under an open label design. Because VSV at this dose was not associated with clinically significant adverse events and a preliminary survival benefit was noted, the next 13 dogs were randomized in a double-blinded fashion to receive a single dose of either intravenous VSV-cIFNβ-NIS or placebo (phosphate buffered saline solution (PBS)). The virus was diluted in sterile PBS to a volume of 10.5ml, which was administered by intravenous infusion over a period of 2-5 minutes. Dogs were housed for up to 24 hours in a BSL-2 housing facility. All procedures were carried out with approval of the University of Minnesota Institutional Animal Care and Use Committee (IACUC #1504-32486A and #1803-35759A) and Institutional Biosafety Committee (IBC #1504-32487H and # 1805-35967H).

Standard of care therapy

All enrolled dogs were treated with standard of care therapy after treatment with intravenous VSV-cIFNβ-NIS or placebo. This consisted of amputation of the affected limb and removal of the associated lymph node(s), which occurred at day 10 following treatment, and initiation of chemotherapy approximately 14 days after amputation. Chemotherapy consisted of six cycles of carboplatin at a dose of 300 mg/m^2, administered intravenously every 3 weeks, with standard monitoring for adverse chemotherapy effects.

Biopsy procedures

Pre-treatment biopsies were obtained from the lesion using 4mm Michele trephine bone biopsy instruments. One pre-treatment tumor biopsy section was placed in 10% neutral buffered formalin for histopathology. A second pre-treatment section was further divided, with one piece used to establish a cancer cell line and a second piece frozen at -80°C for later RNA extraction. Ten days post-treatment with VSV-cIFNβ-NIS, dogs underwent surgical amputation of the affected limb and removal of the associated lymph node(s). A skin punch biopsy was performed, and the tissue frozen at -80°C for later RNA extraction. After amputation, the soft tissues of the limb were removed, and imaging of the affected bone was performed using a Faxitron (Supplementary Figure S2). The amputated limbs were sectioned longitudinally and tumor sections of approximately 5mm thickness were obtained and placed in 10% neutral buffered formalin. Tumor sections were placed in 10% ethanol for slow decalcification, or in acid for rapid decalcification. Separate sections of the tumor were frozen at -80°C for later RNA extraction. Cell lines derived as part of this study can be made available to the scientific community for research purposes under materials transfer agreements negotiated by the Regents of the University of Minnesota and Mayo Clinic.

Monitoring virus pharmacokinetics

Assays to monitor viremia, virus shedding, and antiviral antibodies following intravenous VSV infusion were performed by Imanis Life Sciences using previously described protocols.[13,14,27] Briefly, viremia was monitored by detection of infectious virus and viral RNA in blood samples collected at baseline and at specific time points after VSV treatment. For detection of viral RNA, whole blood was collected in RNAprotect animal blood tubes (Qiagen). For detection of infectious virus, peripheral blood mononuclear cells (PBMCs) were isolated from whole blood.

Urine samples, fecal samples, and buccal swabs were collected after treatment with VSV-cIFNβ-NIS to test for presence of live infectious virus and viral RNA. Detection of infectious virus was performed by overlay of sample supernatants on susceptible BHK-21 cells. Viral RNA was detected in shedding and blood samples by quantitative reverse transcription-polymerase chain reaction (qRT-PCR) as previously described. Tumor specimens were stored at < -65°C at the time of surgical tumor resection (10 days post VSV therapy) for subsequent processing to isolate RNA and detect VSV RNA by qRT-PCR. Serum samples were obtained at baseline, and 3, 7, 14, 21, and 28 days post VSV infusion for detection of anti-VSV neutralizing antibodies.

Serum cytokine monitoring

Serum samples were collected at baseline, 1, 3, 6 hours and 1-, 3-, 7- and 14-days post VSV infusion. Acute cytokine responses were determined as previously described by the COTC Pharmacodynamic Core at Colorado State University (CSU).[22] The acute cytokines evaluated were: GM-CSF, IL-6, MCP-1, KC, IL-2, IP-10, IL-8, TNF-alpha, IL-10, IL-7, IL-1, and IL-18, all of the canine species.

Clinical monitoring

Body temperature was monitored after treatment with VSV-cIFNβ-NIS, every 3 hours for the first 24 hours following treatment, then daily. Blood work to evaluate alanine aminotransferase (ALT), aspartate aminotransferase (AST), total white blood cell count, lymphocyte count, and clotting times (PT and aPTT) was completed at baseline, and at days 3, 7, 14, 21, and 28 after treatment.

Histopathology

Pre-treatment core tumor biopsies and post-treatment amputation-resected tumor samples were evaluated with H&E staining to obtain a definitive histologic diagnosis. Samples were also scored based on tumor inflammation, fibrosis, and necrosis. Inflammation was graded on a 4-point scale, where 0 = absence of inflammation, 1 = minimal inflammation, 2 = mild inflammation, 3 = moderate inflammation, and 4 = marked inflammation. Fibrosis was graded on a 4-point scale, where 0 = absence of fibrosis, 1 = minimal fibrosis, 2 = mild fibrosis, 3 = moderate fibrosis, and 4 = marked fibrosis. Necrosis was graded on a 3-point scale, where 0 = no necrosis, 1 = < 15%, 2 = 15 - 50%, and 3 = > 50% of the section had apparent necrosis. The draining lymph node was evaluated for presence or absence of metastatic osteosarcoma cells. During the placebo-arm of the study, the pathologist was blinded to the treatment assignment of cases (VSV or placebo).

Collection of PBMCs for immune monitoring

Blood samples were obtained for isolation of PBMCs and plasma for immune monitoring. Blood was collected in a commercially available tube for PBMC isolation (BD Mononuclear Cell Preparation Tube), and the manufacturer's protocol was followed. PBMCs were frozen in FBS with 10% DMSO and stored in liquid nitrogen until use.

Diagnostic imaging

Cases were monitored with diagnostic imaging to evaluate for metastatic disease throughout the study period. Thoracic radiographs were performed at study evaluation (d-1), and on days 60,

120, 180, and 360 post-treatment. Computed tomography (CT) was performed at study evaluation (d-1) and at day 90 post-treatment.

RNA extraction from tumor specimens

VIGOR: RNA was extracted from tumor tissue at baseline, and from tumor tissue samples obtained at amputation, post-treatment. RNA was also extracted from cell lines that were established pre-treatment from each case, and from normal skin tissue from each case as a non-malignant control. When available, RNA was also extracted from lung metastases. Tissue samples were disrupted with a tissue homogenizer, and RNA was extracted using a commercially available kit (QIAGEN RNeasy mini kit). RNA was stored at -80°C until submission to the University of Minnesota Genomics Center (UMGC).

CCOGC: A comparison population (n = 23), consisted of tissue samples provided by the Pfizer CCOGC Biospecimen Repository. Samples with a definitive, histological diagnosis of osteosarcoma were selected for RNA sequencing based on the availability of sufficient frozen tissue (>50 mg), treatment information, RNA integrity numbers (RIN) >6, and available follow-up information. These were included in the final selection for next-generation RNA sequencing.

Library preparation and next-generation sequencing

Unique dual-indexed sequencing libraries were prepared using the Clontech Stranded Total RNA-Seq Kit v2 - Pico Input Mammalian kit. RNA sequencing (2x50-bp paired-end, on a NovaSeq S2) was performed at the UMGC. Approximately 3,100M pass filter reads were generated for the run. Mean quality scores were above Q30 for all libraries. Successful libraries

were generated from 64 samples (15 pre-treatment tumors, 20 post-treatment tumors, 18 cancer cell lines generated from pre-treatment tumors, and 11 skin samples) from 24 dogs. Additionally, two dogs had pulmonary metastatic lesions obtained at necropsy from which libraries were generated from tissue and from cell lines. A total of 23 osteosarcoma tissue samples were included in the CCOGC dataset.[21]

Gene cluster expression summary score (GCESS) and Bioinformatics analysis

Initial quality control analysis of RNA sequencing FASTQ data was performed using FastQC software (v0.11.5). FASTQ data were trimmed with Trimmomatic (v0.33.0). Kallisto (v0.43.0) was used for pseudoalignment and quantifying transcript abundance. Sequencing reads were aligned to the canine reference genome (CanFam3.1). Transcript abundance counts were generated, and quantile normalized to correct for differences in sequence counts. Gene cluster expression summary score, or GCESS, analyses were performed as previously described on average linkage hierarchical clustered data.[20] Briefly, clusters of genes are identified based on patterns of correlated expression, such as those associated with immune cell infiltration or cell cycling. After mean-centering and $\log_2$-transformation, individual gene values in each cluster are added together resulting in a single summary score for the cluster that is reflective of the overall degree of gene expression. UMAP was used to generate a 2-dimensional representation of the transcriptional patterns present in the dataset.[28]

Outcome assessment

Formal clinical follow up, including physical examinations, blood work, and diagnostic imaging, occurred for one year after treatment with VSV-cIFNβ-NIS. Thereafter, informal follow up occurred until relapse or death. Necropsies were obtained, when possible, with owner consent. Outcomes assessed included event-free survival (EFS, time to relapse) and overall survival (time to death). The dogs enrolled in the VIGOR study (n = 28) were compared with three control populations. The first population consisted of dogs with appendicular osteosarcoma treated at the same institution (UMN, n = 57) between January 2006 and December 2018. The second population consisted of the control arm of an NCI Comparative Oncology Trials Consortium multicenter clinical trial in dogs with appendicular osteosarcoma (COTC, n = 157) enrolled between November 2015 and February 2018.[13] Both comparison populations were treated with standard of care therapy, consisting of amputation of the affected limb and carboplatin chemotherapy administered every 21 days at 300mg/m^2. A third comparison population (CCOGC, n = 23), consisted of dogs treated with standard of care (chemotherapy and amputation) with known outcome data, enrolled in a multicenter study between April 2008 and March 2011 for which samples were available for tumor next-generation RNA sequencing.[21] This population was used for comparison of survival and tumor gene expression.

Statistical analyses

Tumor inflammation scores were compared between pre-treatment and post-treatment tumor samples using paired student's t-test. P-values are reported without inference to significance, as recommended by the American Statistical Association.[23]

Kaplan-Meier survival curves were generated for the dogs treated with VSV-cIFNβ-NIS in the VIGOR study and the comparison populations. The EFS was calculated as the time between limb

amputation and the first detection of metastasis. Dogs were censored if they did not have metastatic disease at the time of last follow-up. Overall survival was calculated as the time between limb amputation and death. Dogs were censored from survival analyses if they were found to have tumors of bone that were not osteosarcoma, if they died of non-osteosarcoma related causes, or if they were alive at last follow up.

Author contributions

SN, SJR, KMS, and JFM were involved in overall study design and execution including obtaining regulatory approvals and funding to implement the described studies. AC, DG, KB, SP, AW, and KMM were responsible for sample collection and processing. AC, KMS, AB, and MSH were responsible for clinical follow-up. LS and SN oversaw and executed correlative pharmacokinetic studies (assays to measure viremia, virus shedding, antibodies, etc.). CP assisted in data processing and analysis. ALS and LJM analyzed sequencing data. MDS and MW completed methodological design for gross sample collection, imaging with the Faxitron, and gross lesion identification, assessment, and sampling for optimal downstream analysis. MW organized pathological images, maintained supplies, and facilitated communication regarding samples. IC, AFT, and MGOS were responsible for analyzing histopathology specimens. SN, ALS, LJM, JFM, and KMM were responsible for additional data analysis. GRC and JSK were responsible for statistical design and analysis. SN, KMM, ALS, and JFM were responsible for data compilation and manuscript preparation. All authors were responsible for manuscript review and revision.

Keywords

Oncolytic virus, osteosarcoma, neoadjuvant, immunotherapy, virotherapy, tumor microenvironment, antitumor immunity

Data availability statement

RNA-Seq expression profiling data from canine osteosarcoma tumor samples obtained from Canine Comparative Oncology and Genomics Consortium (CCOGC) and VIGOR cohorts are submitted and available to the public via Gene Expression Omnibus (GEO), a public functional genomics data repository. CCOGC dataset GEO accession number: GSE239948. VIGOR dataset GEO accession number: GSE240033.

Acknowledgements

The authors would like to acknowledge Milcah Scott for assistance in training, including cell culture and sequencing techniques. The authors would like to acknowledge Mitzi Lewellen for oversight of sample databases. The authors would also like to acknowledge Katalin Kovacs and Paula Overn for their assistance in preparation of histology specimens. The authors acknowledge the Clinical Investigation Center (CIC) of the University of Minnesota College of Veterinary Medicine, the Veterinary Diagnostic Laboratory (VDL) of the University of Minnesota, the University of Minnesota Genomics Center (UMGC), and the Minnesota Supercomputing Institute (MSI) at the University of Minnesota for providing resources that contributed to the research results reported within this paper. The authors wish to thank the VDL Pathologists for their assistance in sample preparation, including Dr. Arno Wuenschmann, Dr. Erik Olson, and Dr. Jaclyn Dykstra. The authors also wish to thank the CCOGC, Inc. for providing a set of

control tumor samples for this study, as well as Dr. Subbaya Subramanian for help with procuring the CCOGC samples. Additionally, the authors wish to thank Dr. Amy LeBlanc and Christina Mazcko from the NCI COTC for providing the raw survival data for the control cohort treated with the standard of care.

The authors wish to thank the clinical teams at the University of Minnesota College of Veterinary Medicine Lewis Small Animal Teaching Hospital for the clinical care of enrolled dogs, including Oncology, Soft Tissue Surgery, Diagnostic Imaging, the Veterinary Diagnostic Laboratory, Clinical Pathology, and associated support staff.

Funding

The work described in this manuscript was supported by grant MNP #15.25 from the Minnesota Partnership for Biotechnology and Medical Genomics, sponsored research from Vyriad, Inc. (Rochester MN), grant R21 CA208529 from the National Cancer Institute (NCI) of the National Institutes of Health (NIH), United States Public Health Service, and grants CA170218 and CA190276 from the US Department of Defense Peer Reviewed Cancer Research Program. NCI Comprehensive Cancer Center Support Grant P30 CA077598, to the Masonic Cancer Center, University of Minnesota, provided support for genomics and bioinformatics. Tumor samples and relevant metadata from the CCOGC cohort were provided *pro bono* by the CCOGC, Inc. KMM was supported in part by institutional training grant in Molecular, Genetic, and Cellular Targets of Cancer T32 CA009138 from the NCI. ALS was supported in part by grant R50 CA211249 from the NCI. JFM is supported in part by the Alvin and June Perlman Endowed Chair in Animal Oncology. The authors acknowledge support from individual donors to the Animal Cancer Care and Research Program, University of Minnesota. The content of this manuscript is

solely the responsibility of the authors and does not necessarily represent the official views of any of the funding agencies listed above.

Conflict of Interest

Drs S. Naik, S.J. Russell, and Mayo Clinic have a financial conflict of interested related to this research. S. Naik and SJ Russell are inventors on patents related to oncolytic Vesicular stomatitis virus that has been licensed by Mayo Clinic to Vyriad. S. Naik and S.J. Russell have equity interests in Vyriad, and S.J. Russell is the CEO of Vyriad. The research has been reviewed by the Mayo Clinic Conflict of Interest Review Board and is being conducted in compliance with Mayo Conflict of Interest policies.

Table 1. The clinical characteristics of the dogs enrolled in the VIGOR study are similar to contemporary comparison cohorts with appendicular osteosarcoma.

Dogs with osteosarcoma tumors in the appendicular skeleton were enrolled in VIGOR. The demographic characteristics of the dogs enrolled in the VIGOR cohort were generally large breed middle-aged dogs. VIGOR: test population; UMN VMC: comparison cohort at same site (University of Minnesota Veterinary Medical Center); COTC: national multicenter comparison cohort overseen by the Comparative Oncology Network at the NCI. VIGOR, UMN, and COTC were all treated with the same standard of care chemotherapy. All cases were treated with amputation.

* One Mastiff in VIGOR was diagnosed with intramedullary rhabdomyosarcoma.

** One mixed breed enrolled in VIGOR was diagnosed with intramedullary hemangiosarcoma.

*** Body weight was not available for 5 of the dogs in the UMN comparison group.

† **All dogs were neutered and weighed > 20kg as conditions of enrollment in VIGOR.**

		VIGOR (n = 28)	UMN VMC (n = 57)	NCI-COTC (n = 157)
Breed n (%)	Golden retriever	5 (17.9)	12 (21.2)	7 (4.5)
	Labrador retriever	3 (10.7)	7 (12.3)	23 (14.6)
	Mastiff	2 (7.1) *	2 (3.5)	4 (2.5)
	Rottweiler	1 (3.6)	2 (3.5)	12 (7.6)
	Great Dane	1 (3.6)	3 (5.3)	12 (7.6)
	Greyhound	1 (3.6)	1 (1.8)	10 (6.4)
	Great Pyrenees	1 (3.6)	0 (0)	8 (5.1)
	Other purebreed	6 (21.4)	15 (26.3)	40 (30.6)
	Mixed breed	8 (28.6) **	15 (26.3)	33 (21.0)
Age (years)	Mean (± SD)	7.7 (± 2.5)	8.8 (± 2.5)	8.1 (± 2.4)
	Median	8.1	9.0	8.3
	Range	2.1 - 11.7	2.0 - 16.0	(1.4 - 15.6)
Body weight (kg)	Mean (± SD)	38.3 (± 15.5)	37.9 (± 11.3)	41.2 (± 12.3)
	Median	32.7	37.1	38.8
	Range	20 - 81.6	15.3 - 70.3 ***	25 - 94.5
Sex	Spayed female	16 (57) †	28	64
	Intact female	0	2	3
	Neutered male	12 (43) †	25	83
	Intact male	0	2	7
Tumor location n (%)	Left proximal humerus	3 (10.7)	6 (10.5)	17 (10.8)
	Left distal radius	5 (17.9)	6 (10.5)	34 (21.7)
	Other Left forelimb	3 (10.7)	1 (1.8)	5 (3.2)
	Right proximal humerus	7 (25)	4 (7)	16 (10.2)
	Right distal radius	2 (7.1)	12 (21.1)	23 (14.6)
	Other Right forelimb	0 (0)	3 (5.3)	4 (2.5)
	Left distal femur	1 (3.6)	1 (1.8)	8 (5.1)
	Left proximal tibia	2 (7.1)	2 (3.5)	4 (2.5)
	Left distal tibia	1 (3.6)	6 (10.5)	16 (10.2)
	Other Left hindlimb	0 (0)	2 (3.5)	2 (1.3)
	Right distal femur	1 (3.6)	5 (8.8)	11 (7)
	Right proximal tibia	0 (0)	3 (5.3)	4 (2.5)
	Right distal tibia	3 (10.7)	5 (8.8)	11 (7)
	Other R hindlimb	0 (0)	1 (1.8)	2 (1.3)

632

References

1. Mirabello, L., Troisi, R.J. & Savage, S.A. Osteosarcoma incidence and survival rates from 1973 to 2004: data from the Surveillance, Epidemiology, and End Results Program. *Cancer* **115**, 1531-1543 (2009).
2. Cole, S., Gianferante, D.M., Zhu, B. & Mirabello, L. Osteosarcoma: A Surveillance, Epidemiology, and End Results program-based analysis from 1975 to 2017. *Cancer* **128**, 2107-2118 (2022).
3. Smeland, S., Bielack, S.S., Whelan, J., Bernstein, M., Hogendoorn, P., Krailo, M.D., Gorlick, R., Janeway, K.A., Ingleby, F.C., Anninga, J*., et al.* Survival and prognosis with osteosarcoma: outcomes in more than 2000 patients in the EURAMOS-1 (European and American Osteosarcoma Study) cohort. *Eur J Cancer* **109**, 36-50 (2019).
4. Weiss, M.C., Eulo, V. & Van Tine, B.A. Truly Man's Best Friend: Canine Cancers Drive Drug Repurposing in Osteosarcoma. *Clin Cancer Res* **28**, 571-572 (2022).
5. Makielski, K.M., Mills, L.J., Sarver, A.L., Henson, M.S., Spector, L.G., Naik, S. & Modiano, J.F. Risk Factors for Development of Canine and Human Osteosarcoma: A Comparative Review. *Vet Sci* **6**(2019).
6. Poon, A.C., Matsuyama, A. & Mutsaers, A.J. Recent and current clinical trials in canine appendicular osteosarcoma. *Can Vet J* **61**, 301-308 (2020).
7. Russell, S.J. & Barber, G.N. Oncolytic Viruses as Antigen-Agnostic Cancer Vaccines. *Cancer Cell* **33**, 599-605 (2018).
8. Cook, J., Peng, K.W., Witzig, T.E., Broski, S.M., Villasboas, J.C., Paludo, J., Patnaik, M., Rajkumar, V., Dispenzieri, A., Leung, N*., et al.* Clinical activity of single-dose systemic oncolytic VSV virotherapy in patients with relapsed refractory T-cell lymphoma. *Blood Adv* **6**, 3268-3279 (2022).
9. Lutzky, J., Marron, T.U., Powell, S.F., Johnson, D.H., Patel, M., El-Khoueiry, A.B., Sarantopoulos, J., Dadi-Mehmetaj, S., Russell, L., Russell, S.J*., et al.* Optimization of Voyager V1 (VV1) oncolytic virus systemic delivery in combination with cemiplimab and ipilimumab in patients with melanoma and non–small cell lung cancer (NSCLC). *Journal of Clinical Oncology* **40**, TPS9595-TPS9595 (2022).
10. Naik, S., Nace, R., Federspiel, M.J., Barber, G.N., Peng, K.W. & Russell, S.J. Curative one-shot systemic virotherapy in murine myeloma. *Leukemia* **26**, 1870-1878 (2012).
11. Bailey, K., Kirk, A., Naik, S., Nace, R., Steele, M.B., Suksanpaisan, L., Li, X., Federspiel, M.J., Peng, K.W., Kirk, D*., et al.* Mathematical model for radial expansion and conflation of intratumoral infectious centers predicts curative oncolytic virotherapy parameters. *PLoS One* **8**, e73759 (2013).
12. Naik, S., Nace, R., Barber, G.N. & Russell, S.J. Potent systemic therapy of multiple myeloma utilizing oncolytic vesicular stomatitis virus coding for interferon-beta. *Cancer Gene Ther* **19**, 443-450 (2012).
13. Zhang, L., Steele, M.B., Jenks, N., Grell, J., Suksanpaisan, L., Naik, S., Federspiel, M.J., Lacy, M.Q., Russell, S.J. & Peng, K.W. Safety Studies in Tumor and Non-Tumor-Bearing Mice in Support of Clinical Trials Using Oncolytic VSV-IFNbeta-NIS. *Hum Gene Ther Clin Dev* **27**, 111-122 (2016).

14. Naik, S., Galyon, G.D., Jenks, N.J., Steele, M.B., Miller, A.C., Allstadt, S.D., Suksanpaisan, L., Peng, K.W., Federspiel, M.J., Russell, S.J*., et al.* Comparative Oncology Evaluation of Intravenous Recombinant Oncolytic Vesicular Stomatitis Virus Therapy in Spontaneous Canine Cancer. *Mol Cancer Ther* **17**, 316-326 (2018).

15. Thomas, R.J. & Bartee, E. The use of oncolytic virotherapy in the neoadjuvant setting. *J Immunother Cancer* **10**(2022).

16. Naik, S. & Russell, S.J. Engineering oncolytic viruses to exploit tumor specific defects in innate immune signaling pathways. *Expert Opin Biol Ther* **9**, 1163-1176 (2009).

17. Stojdl, D.F., Lichty, B., Knowles, S., Marius, R., Atkins, H., Sonenberg, N. & Bell, J.C. Exploiting tumor-specific defects in the interferon pathway with a previously unknown oncolytic virus. *Nat Med* **6**, 821-825 (2000).

18. Obuchi, M., Fernandez, M. & Barber, G.N. Development of recombinant vesicular stomatitis viruses that exploit defects in host defense to augment specific oncolytic activity. *J Virol* **77**, 8843-8856 (2003).

19. LeBlanc, A.K., Mazcko, C.N., Cherukuri, A., Berger, E.P., Kisseberth, W.C., Brown, M.E., Lana, S.E., Weishaar, K., Flesner, B.K., Bryan, J.N*., et al.* Adjuvant Sirolimus Does Not Improve Outcome in Pet Dogs Receiving Standard-of-Care Therapy for Appendicular Osteosarcoma: A Prospective, Randomized Trial of 324 Dogs. *Clin Cancer Res* **27**, 3005-3016 (2021).

20. Scott, M.C., Temiz, N.A., Sarver, A.E., LaRue, R.S., Rathe, S.K., Varshney, J., Wolf, N.K., Moriarity, B.S., O'Brien, T.D., Spector, L.G*., et al.* Comparative Transcriptome Analysis Quantifies Immune Cell Transcript Levels, Metastatic Progression, and Survival in Osteosarcoma. *Cancer Res* **78**, 326-337 (2018).

21. Sarver, A.L., Mills, L.J., Makielski, K.M., Temiz, N.A., Wang, J., Spector, L.G., Subramanian, S. & Modiano, J.F. Distinct mechanisms of PTEN inactivation in dogs and humans highlight convergent molecular events that drive cell division in the pathogenesis of osteosarcoma. *Cancer Genet* **276-277**, 1-11 (2023).

22. Durham, N.M., Mulgrew, K., McGlinchey, K., Monks, N.R., Ji, H., Herbst, R., Suzich, J., Hammond, S.A. & Kelly, E.J. Oncolytic VSV Primes Differential Responses to Immuno-oncology Therapy. *Mol Ther* **25**, 1917-1932 (2017).

23. Sakthikumar, S., Elvers, I., Kim, J., Arendt, M.L., Thomas, R., Turner-Maier, J., Swofford, R., Johnson, J., Schumacher, S.E., Alfoldi, J*., et al.* SETD2 Is Recurrently Mutated in Whole-Exome Sequenced Canine Osteosarcoma. *Cancer Res* **78**, 3421-3431 (2018).

24. Sayles, L.C., Breese, M.R., Koehne, A.L., Leung, S.G., Lee, A.G., Liu, H.Y., Spillinger, A., Shah, A.T., Tanasa, B., Straessler, K*., et al.* Genome-Informed Targeted Therapy for Osteosarcoma. *Cancer Discov* **9**, 46-63 (2019).

25. Xie, L., Yang, Y., Guo, W., Che, D., Xu, J., Sun, X., Liu, K., Ren, T., Liu, X., Yang, Y*., et al.* The Clinical Implications of Tumor Mutational Burden in Osteosarcoma. *Front Oncol* **10**, 595527 (2020).

26. Kaufman, H.L. Can Biomarkers Guide Oncolytic Virus Immunotherapy? *Clin Cancer Res* **27**, 3278-3279 (2021).

27. LeBlanc, A.K., Naik, S., Galyon, G.D., Jenks, N., Steele, M., Peng, K.W., Federspiel, M.J., Donnell, R. & Russell, S.J. Safety studies on intravenous administration of oncolytic recombinant vesicular stomatitis virus in purpose-bred beagle dogs. *Hum Gene Ther Clin Dev* **24**, 174-181 (2013).

28. McInnes, L.H., J; Melville, J. UMAP: Uniform Manifold Approximation and Projection for Dimension Reduction. in *arXiv:1802.03426* (2018).

Figure Legends

Figure 1. Vesicular stomatitis virus replicates in and kills three established canine osteosarcoma cell lines.

Virus titers and cell viability following infection of canine osteosarcoma cell lines: (A) OSCA-8, (B) OSCA-40, and (C) OSCA-78 with recombinant VSVs: VSV-GFP (green), VSV-hIFNβ-NIS (blue), or VSV-cIFNβ-NIS (pink) at an MOI of 0.03.

Figure 2. Design schematic of the VIGOR study

Clinical procedures following enrollment of dogs with appendicular osteosarcoma are shown. This includes diagnostic imaging to evaluate for pulmonary metastases with either computed tomography (CT) or thoracic radiographs (CXR); pre-treatment biopsy; VSV (or placebo) treatment (study day 1); and standard of care amputation and chemotherapy (consisting of intravenous carboplatin every 3 weeks for 6 doses) that was started on study day 21.

Figure 3. Intravenous VSV therapy is safe, and a subset of VSV-treated dogs with osteosarcoma are long term responders.

(A) Kaplan-Meier survival curve with event free survival (EFS) of dogs treated with systemic VSV in the VIGOR study, compared to two contemporary control cohorts: NCI-COTC and UMN VMC cohorts. (B) Long-term response was defined as overall survival greater then 75th percentile of survival from the COTC cohort (479 days). Similar proportion (26%) of dogs from

the UMN VMC cohort were long-term responders. 35% of dogs from the VSV-treated dogs from the VIGOR cohort were long term responders (overall survival > 479 days).

Figure 4. Increased tumor inflammation following VSV treatment in resected osteosarcoma tissues.

Inflammatory infiltrates were scored by a pathologist in baseline pre-treatment tumor biopsies and post-treatment amputation-resected tumor samples (collected on study day 10). (A) Comparison of Tumor Inflammation Score (TIS) showed higher TIS in post-treatment samples from VSV-treated dogs. (B) Where matched paired pre- and post-treatment tumor samples were available for assessment, we observed a significant increase in TIS in tissues from VSV-treated dogs between baseline and 10 days post treatment (P=0.0027, paired t-test).

Figure 5. Acute viremia following systemic VSV infusion.

Detection of VSV-N RNA copies in whole blood, PBMCs, and plasma samples collected at indicated time points following VSV infusion shows detection of viral RNA in blood and viral localization primarily to PBMCs.

Figure 6. RNAseq analysis of canine tissues does not show significant changes immune gene signatures.

(A) VIGOR RNAseq analysis of osteosarcoma tumor samples (pre- and post-treatment), lung metastases (where available from necropsy samples), skin biopsy, and osteosarcoma cell lines (derived from osteosarcoma tumors) clustered by tissue type. Data is log base 2 transformed mean centered and filtered for genes with high Standard deviation. Unsupervised hierarchical clustering resulted in 14 gene clusters including cell cycle, immune clusters and cluster composed primarily of genes expressed in skin samples. (B) UMAP projection of samples present in VIGOR dataset. Clear separation of OS tumors, skin and cell lines is apparently consistent with heatmap representation of the data. Samples are labeled with colors present in Figure 6A legend. (C-F) Zoomed in regions showing the C) skin specific cluster, D) immune 1 cluster composed of genes enriched in macrophage lineage immune genes, E) immune 2 cluster composed of genes enriched in T cell lineage immune genes and G) cell cycle enriched genes. (H-J) GCESS values generated by summing the genes present in each cluster for each sample are plotted in box plots representing samples grouped by sample type, treatment, and timepoint for H) skin specific GCESS, I) immune 1 GCESS, J) immune 2 GCESS, and F) Cell cycle GCESS. Unsupervised hierarchical clustering resulted in 14 gene clusters including cell cycle and immune clusters. GCESS scores were not significantly different in pre- vs. post-treatment VSV- and placebo treated tumor samples.

Figure 7. Survival outcomes correlate with pre-treatment T-cell GCESS.

(A) Survival outcomes in placebo versus VSV treated dogs; (B-D) Plot of survival outcomes with (B) cell cycle GCESS, (C) immune 1 GCESS (macrophage/monocyte) (D), immune 2 GCESS (T-cell), indicates a correlation between survival and T-cell GCESS in pre-treatment tumor biopsy samples (E). The two dogs with non-osteosarcoma tumors of bone

782 (hemangiosarcoma and rhabdomyosarcoma) and the dog that died of post-operative

783 complications after the amputation surgery were excluded in this analysis.

Figure 1

Click here to access/download;Figure (high resolution without caption);VIGOR_Fig1.pdf

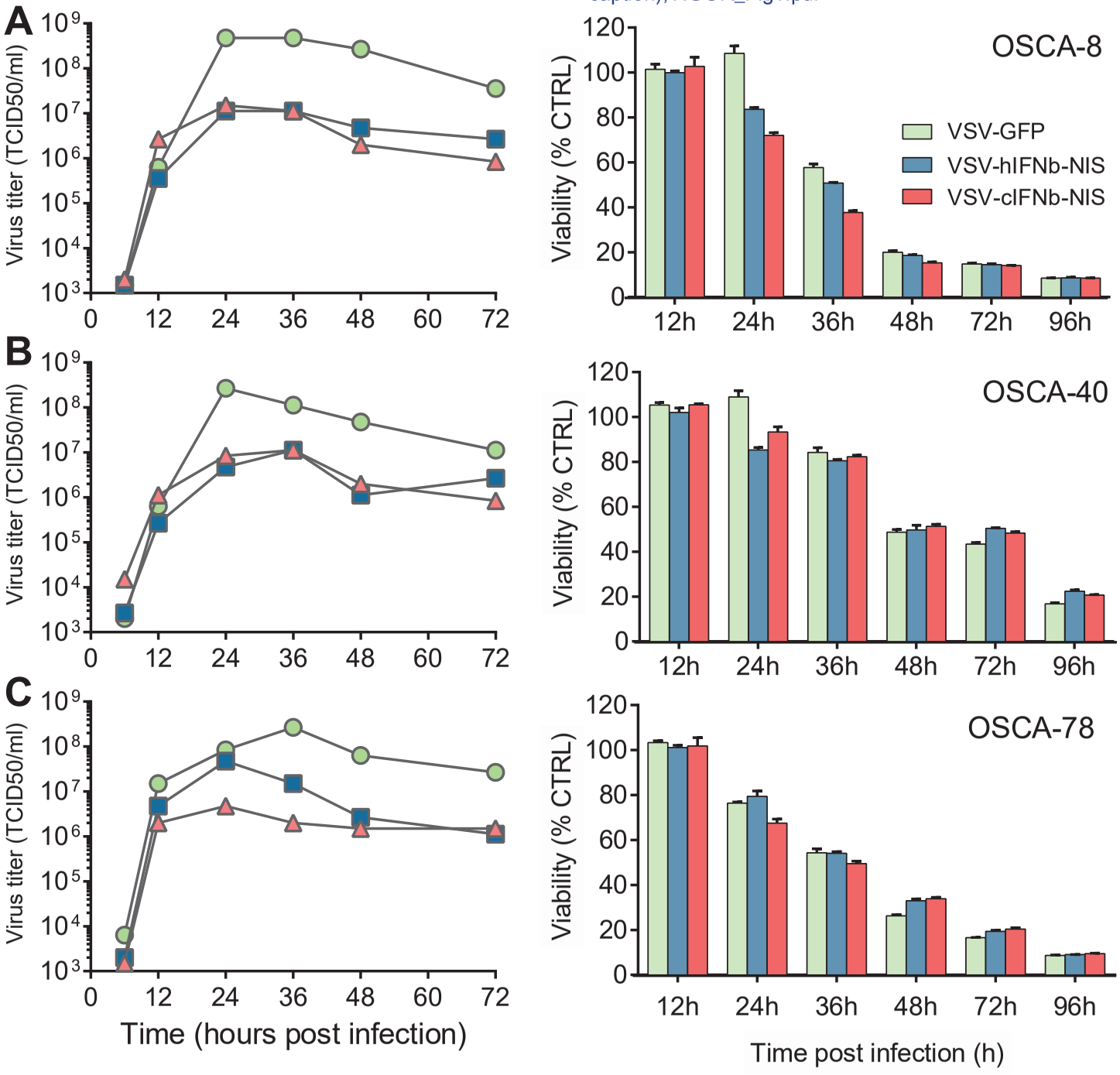

Figure 2

Click here to access/download;Figure (high resolution without caption);VIGOR_Fig2_Schema.pdf

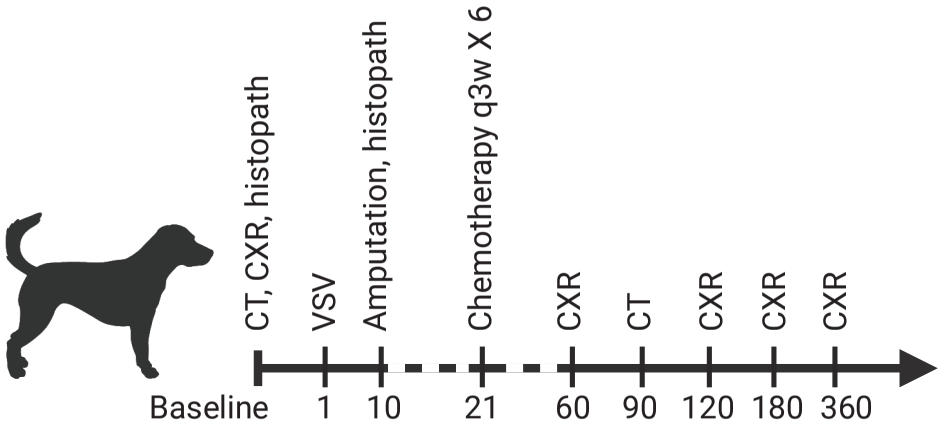

Figure 3

Click here to access/download;Figure (high resolution without caption);VIGOR_Fig3_Survival.pdf

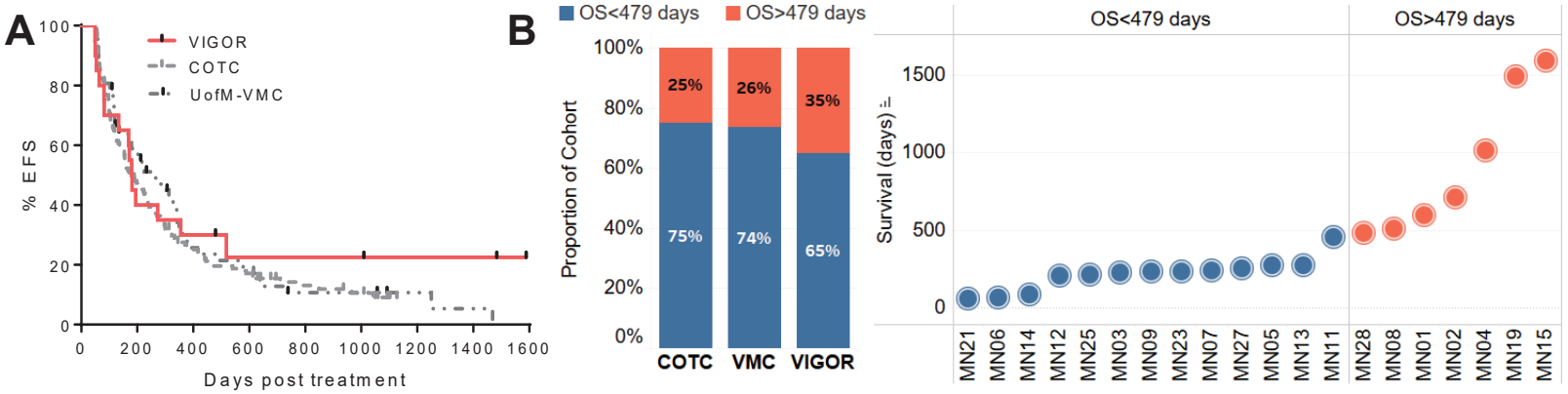

Figure 4

Click here to access/download;Figure (high

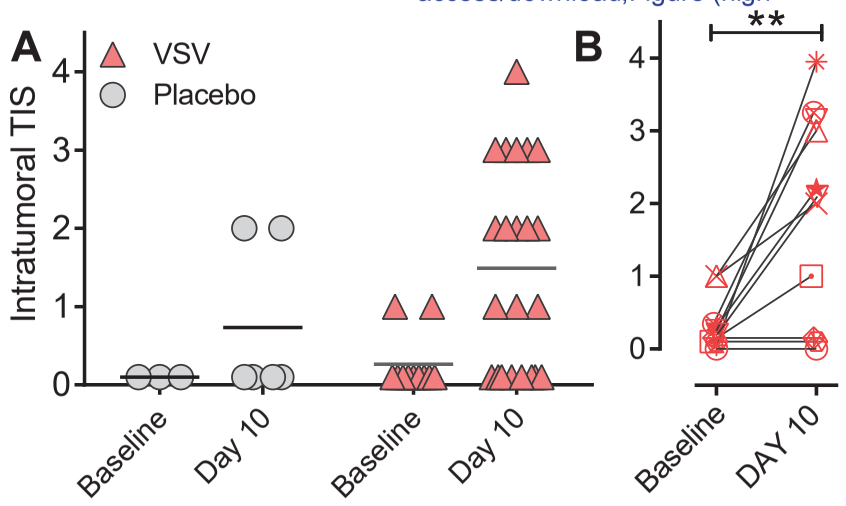

Figure 5

Click here to access/download;Figure (high resolution without caption);VIGOR_Viremia_Jul2023.pdf

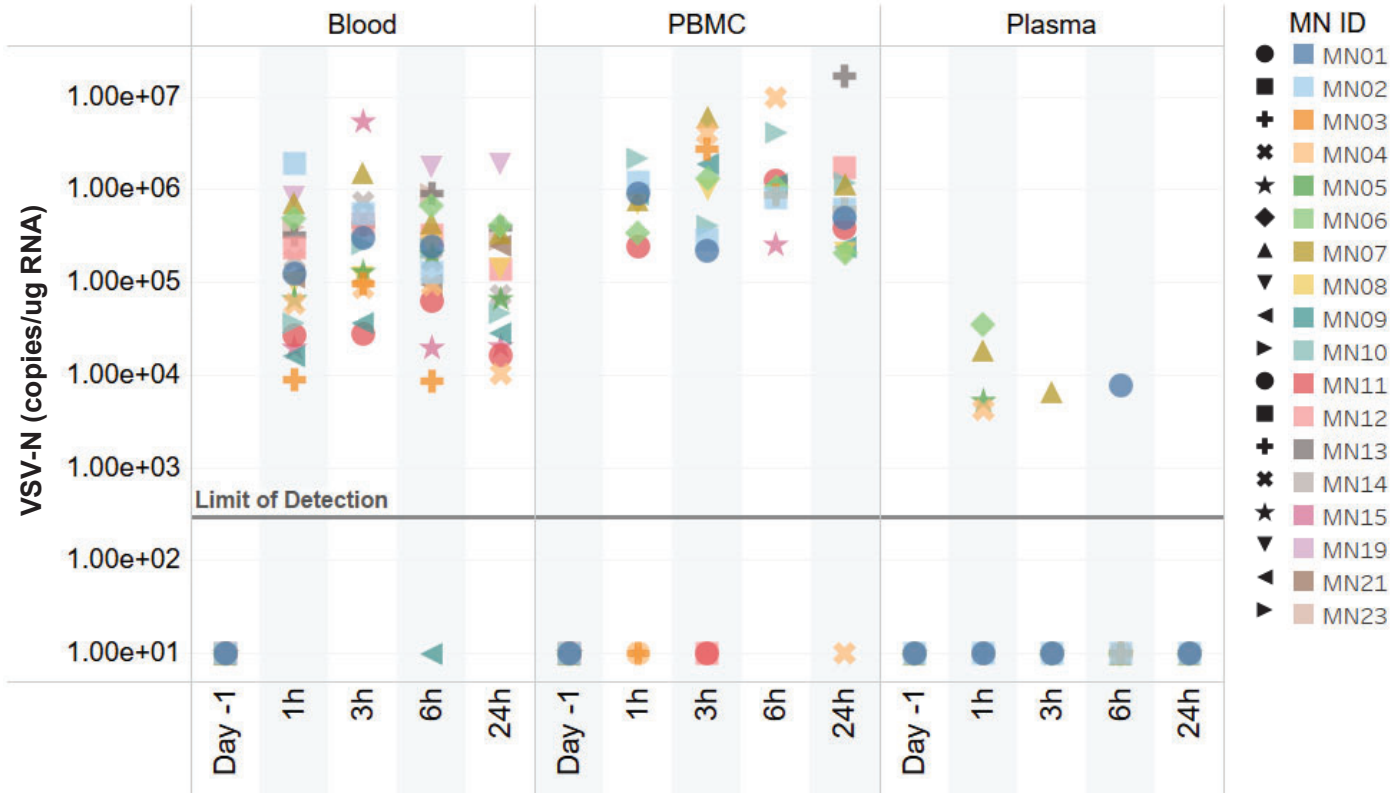

Figure 6

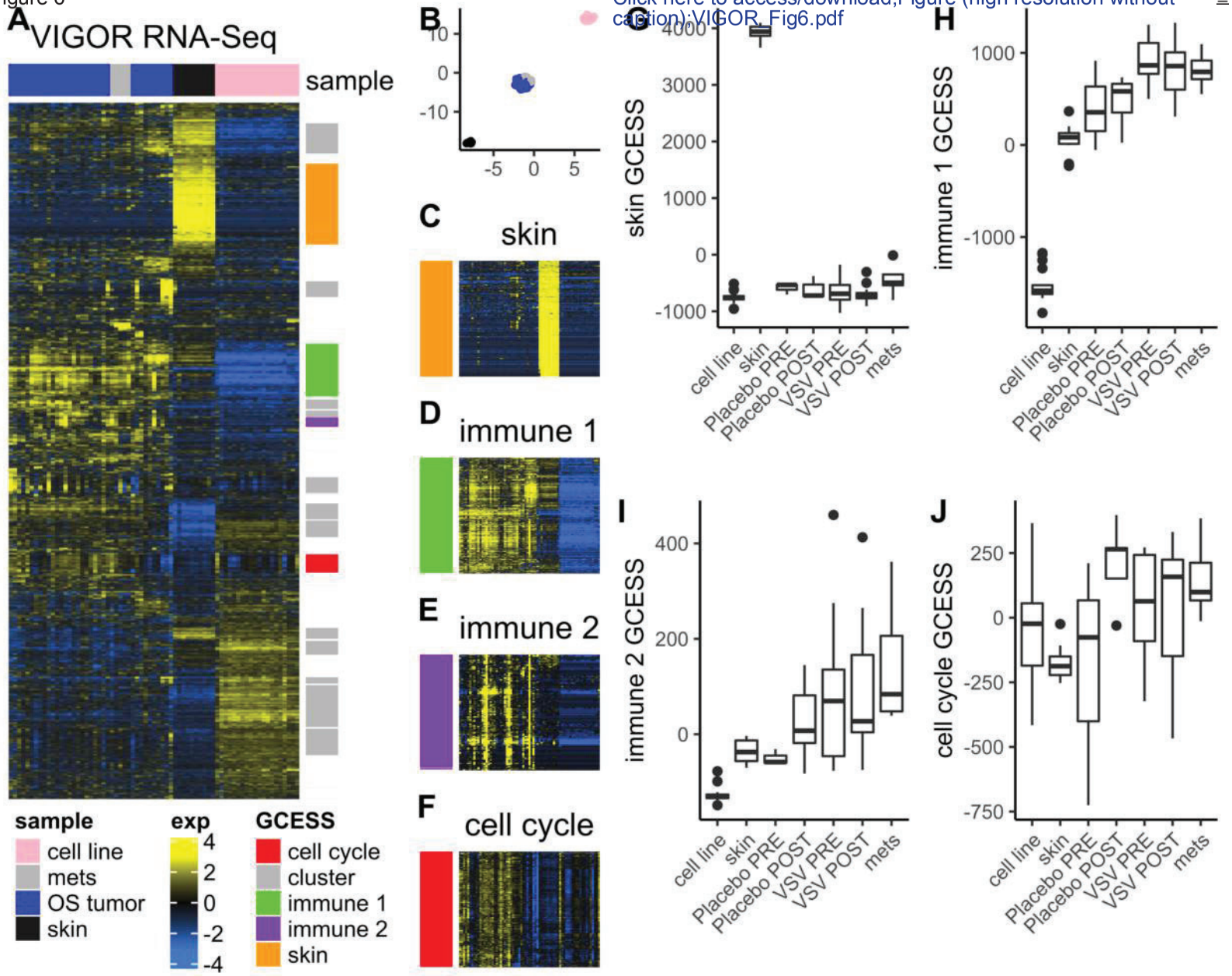

Figure 7

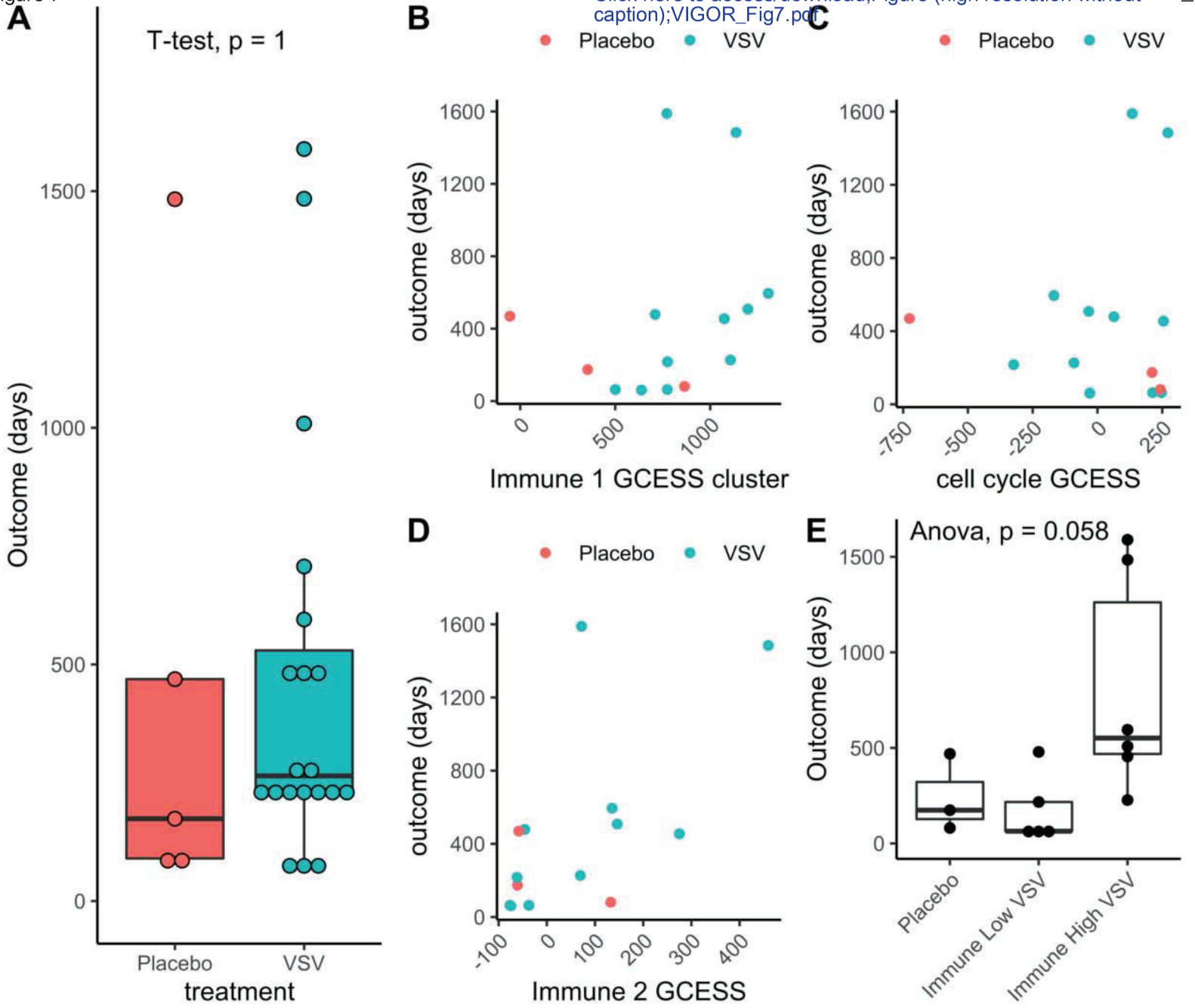

Table S1. List of adverse events that occurred following VSV administration were uncommon and considered unlikely to be related to treatment.

Dogs were monitored closely for AEs following systemic VSV administration. AEs were uncommon and those that occurred were considered unlikely to be related to VSV treatment.

Dog ID	Adverse Events (AEs)	Interval (days) from VSV infusion to AE	AE grade	AE related to VSV?	AE related to disease?	AE outcome
MN01	Facial nerve paralysis	106	1	Unlikely	Unlikely	Not recovered
MN03	Pneuomonia/ intrapulmonary hemorrhage	142	1	Unlikely	Likely[1]	Recovered
MN17	Hypovolemic shock after surgery	5	5	Unlikely	Possible	Death

[1]Although aspiration pneumonia was the presumptive diagnosis, the sum of the data from this case suggests that the dog had intrapulmonary hemorrhage from one of its many pulmonary nodules, and not pneumonia. The hemorrhage resolved, but the nodules did not, and the dog eventually died from progressive disease. While the cause of hemorrhage cannot be clearly ascertained, it was most likely due to disease progression.

Table S2. Clinical information and survival data for enrolled dogs. Censored events due to death from other causes are noted in red font, and animals that are still alive at the time of analysis are noted in blue font.

Case #	Breed	Weight (kg)	Age (years)	Tumor location	TX	Status at study end	Presumed cause of death	EFS (days)	Overall survival (days)
MN01	Golden Retriever	30	6	L proximal humerus	VSV	Dead	Disease	518	595
MN02	Rottweiler	59	7	L distal radius	VSV	Dead	Other cause	356	707
MN03	Boxer	25.7	7	L distal radius	VSV	Dead	Disease	133	227
MN04	Mixed Breed	35	11	L carpus	VSV	Dead	Other cause	1009	1009
MN05	Australian Shepherd	20.2	7	R proximal humerus	VSV	Dead	Disease	273	275
MN06	Mixed Breed	50	5	R distial tibia	VSV	Dead	Disease	64	64
MN07	Mixed Breed	42	2	L proximal humerus	VSV	Dead	Disease	180	243
MN08	Labrador Retriever	52	9.5	L proximal humerus	VSV	Dead	Disease	355	508
MN09	Golden Retriever	33.7	8	L distal radius	VSV	Dead	Disease	181	237
MN10	Mixed Breed	31.2	3	R distal radius *	VSV	**Alive**		1683	1683
MN11	Golden Retriever	29.9	9.5	R proximal humerus	VSV	Dead	Disease	194	455
MN12	Old English Sheepdog	34.7	9	L distal femur	VSV	Dead	Disease	82	205
MN13	Golden Retriever	33.8	9.5	R distal tibia	VSV	Dead	Disease	169	277
MN14	German Shorthair Pointer	30	8	L distal ulna	VSV	Dead	Disease	50	88
MN15	Greyhound	29.7	8	L proximal tibia	VSV	**Alive**		1589	1589
MN16	Labrador Retriever	30.5	8.5	L distal radius	Placebo	Dead	Disease	60	81
MN17	Irish Wolfhound	37.4	6	L distal tibia	VSV	Dead	Surgical complications	0	0
MN18	Mixed Breed	26.3	9	R femoral diaphysis	Placebo	**Alive**		1483	1483
MN19	Mixed Breed	26.9	9	R proximal humerus	VSV	**Alive**		1484	1484
MN20	Mastiff	81.6	2	R proximal humerus **	Placebo	Dead	Disease	53	74
MN21	St. Bernard	50.6	7	L radius	VSV	Dead	Disease	49	61
MN22	Great Pyrenees	39.3	5.5	L distal radius	Placebo	Dead	Disease	63	174
MN23	Labrador Retriever	26.3	12.5	R proximal humerus	VSV	Dead	Disease	81	237
MN24	German Shepherd	48.4	9	R proximal humerus	Placebo	Dead	Disease	56	90
MN25	Mixed Breed	30.8	5	L proximal tibia	VSV	Dead	Disease	171	217
MN26	Mastiff	73.4	8	R proximal humerus	Placebo	Dead	Disease	377	476
MN27	Vizsla	24.8	8	R distal tibia	VSV	Dead	Disease	54	254
MN28	Golden Retriever	23.6	12	R distal radius	VSV	Dead	Other cause	479	479

Table S3. Pathology assessment of pre- and post-treatment tumor specimens

FFPE tissues from pre-treatment (pre-tx) tumor biopsies and tumors resected 10 days after VSV or placebo administration (post-tx) were assessed by a veterinary pathologist who was blinded to treatment group. Tumors were score for inflammation, fibrosis, and necrosis. N/E indicates non-evaluable specimens.

		Intratumoral Inflammation (Grade)		Intratumoral Fibrosis (Grade)		Intratumoral Necrosis (Grade)			
Case #	**TX**	**Pre-tx**	**Post-tx**	**Pre-tx**	**Post-tx**	**Pre-tx**	**Post-tx**	**Micro-necrosis Present**	**Tumor Grade**
MN01	VSV	0	0	0	0	n/e	1	No	3
MN02	VSV	n/e	3	0	4	n/e	4	Yes	3
MN03	VSV	1	3	1	0	2	4	No	3
MN04	VSV	0	2	0	3	0	4	No	3
MN05	VSV	n/e	2	0	3	n/e	4	Yes	3
MN06	VSV	n/e	0	n/e	3	n/e	4	No	3
MN07	VSV	n/e	1	n/e	3	n/e	3	Yes	3
MN08	VSV	n/e	0	2	4	n/e	4	No	2
MN09	VSV	n/e	0	n/e	3	n/e	3	No	3
MN10	VSV	0	3	2	3	n/e	n/e	No	N/A
MN11	VSV	0	4	0	0	0	4	No	3
MN12	VSV	0	2	2	3	n/e	4	Yes	3
MN13	VSV	n/e	2	n/e	2	n/e	4	No	3
MN14	VSV	1	2	3	3	n/e	4	Yes	3
MN15	VSV	n/e	1	0	0	n/e	4	Yes	3
MN16	Placebo	0	0	0	1	n/e	4	Yes	3
MN17	VSV	0	1	0	3	0	0	Yes	1
MN18	Placebo	0	2	0	0	n/e	3	Yes	3
MN19	VSV	0	3	0	3	n/e	3	Yes	3
MN20	Placebo	0	0	0	2	n/e	4	No	3
MN21	VSV	n/e	3	0	3	n/e	2	Yes	2
MN22	Placebo	0	2	1	0	3	4	No	3
MN23	VSV	n/e	0	0	2	n/e	3	Yes	3
MN24	Placebo	n/e	0	0	2	n/e	3	No	3
MN25	VSV	0	0	1	0	n/e	4	No	3
MN26	Placebo	n/e	0	0	0	n/e	4	No	2
MN27	VSV	0	0	0	2	n/e	4	No	3
MN28	VSV	0	0	2	2	0	2	No	2

Table S4. Detection of VSV RNA in tumor specimens.

Detection of VSV-N RNA copies in RNA isolated from resected bone tumor specimens collected 10 days following VSV or placebo administration. Lung metastasis specimens during a necropsy was performed on one dog (MN25) that was humanely euthanized due to disease progression and similarly analyzed for detection of VSV RNA.

Dog ID	Treatment group	Tumor specimen	VSV-N (copies/ug RNA)
MN01	VSV	Bone tissue RNA (Day 10 specimen)	BLD
MN02	VSV	Bone tissue RNA (Day 10 specimen)	BLD
MN03	VSV	Bone tissue RNA (Day 10 specimen)	BLD
MN04	VSV	Bone tissue RNA (Day 10 specimen)	BLD
MN05	VSV	Bone tissue RNA (Day 10 specimen)	BLD
MN06	VSV	Bone tissue RNA (Day 10 specimen)	BLD
MN07	VSV	Bone tissue RNA (Day 10 specimen)	BLD
MN08	VSV	Bone tissue RNA (Day 10 specimen)	BLD
MN09	VSV	Bone tissue RNA (Day 10 specimen)	BLD
MN10	VSV	Bone tissue RNA (Day 10 specimen)	BLD
MN11	VSV	Bone tissue RNA (Day 10 specimen)	BLD
MN12	VSV	Bone tissue RNA (Day 10 specimen)	BLD
MN13	VSV	Bone tissue RNA (Day 10 specimen)	BLD
MN14	**VSV**	**Bone tissue RNA (Day 10 specimen)**	**2.74E+03**
MN15	VSV	Bone tissue RNA (Day 10 specimen)	BLD
MN17	VSV	Bone tissue RNA (Day 10 specimen)	BLD
MN19	VSV	Bone tissue RNA (Day 10 specimen)	BLD
MN21	VSV	Bone tissue RNA (Day 10 specimen)	BLD
MN23	VSV	Bone tissue RNA (Day 10 specimen)	BLD
MN25	**VSV**	**Bone tissue RNA (Day 10 specimen)**	**2.62E+05**
MN25	VSV	Lung metastasis #1 (necropsy specimen)	BLD
MN25	VSV	Lung metastasis #2 (necropsy specimen)	BLD
MN27	VSV	Bone tissue RNA (Day 10 specimen)	BLD
MN28	VSV	Bone tissue RNA (Day 10 specimen)	BLD
MN16	Placebo	Bone tissue RNA (Day 10 specimen)	BLD
MN18	Placebo	Bone tissue RNA (Day 10 specimen)	BLD
MN20	Placebo	Bone tissue RNA (Day 10 specimen)	BLD
MN22	Placebo	Bone tissue RNA (Day 10 specimen)	BLD
MN24	Placebo	Bone tissue RNA (Day 10 specimen)	NA
MN26	Placebo	Bone tissue RNA (Day 10 specimen)	BLD

Figure S1. VIGOR study CONSORT diagram showing screening, enrollment, treatment, and follow-up assessments.

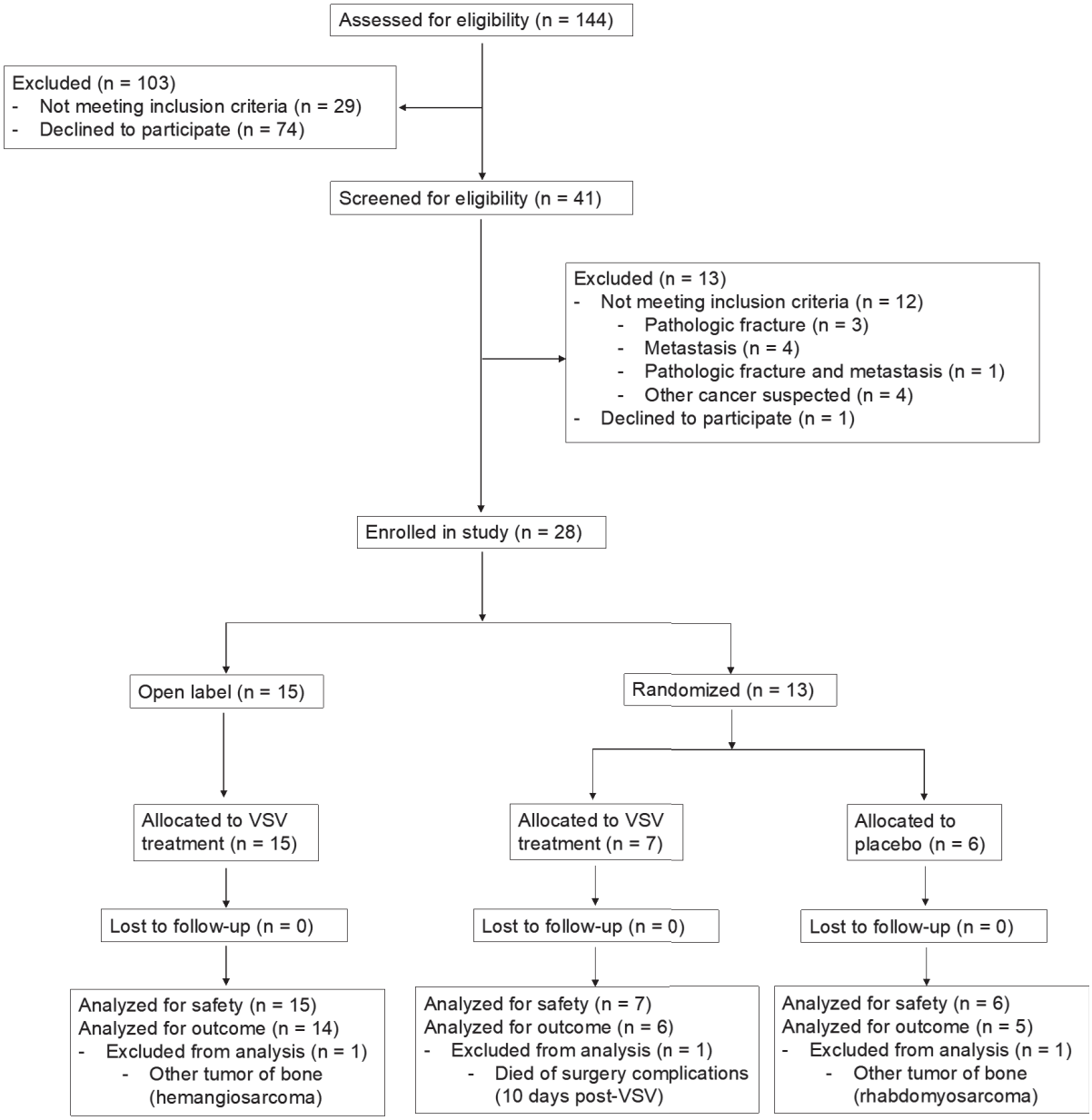

Figure S2. Faxitron imaging after amputation allows for more accurate tumor size determination and guides tumor sample collection. (A) Radiographic image of a left proximal humeral osteosarcoma lesion, and (B) Faxitron image and gross pathology evaluation of the same lesion. White dashed lines indicate tumor borders on visual inspection.

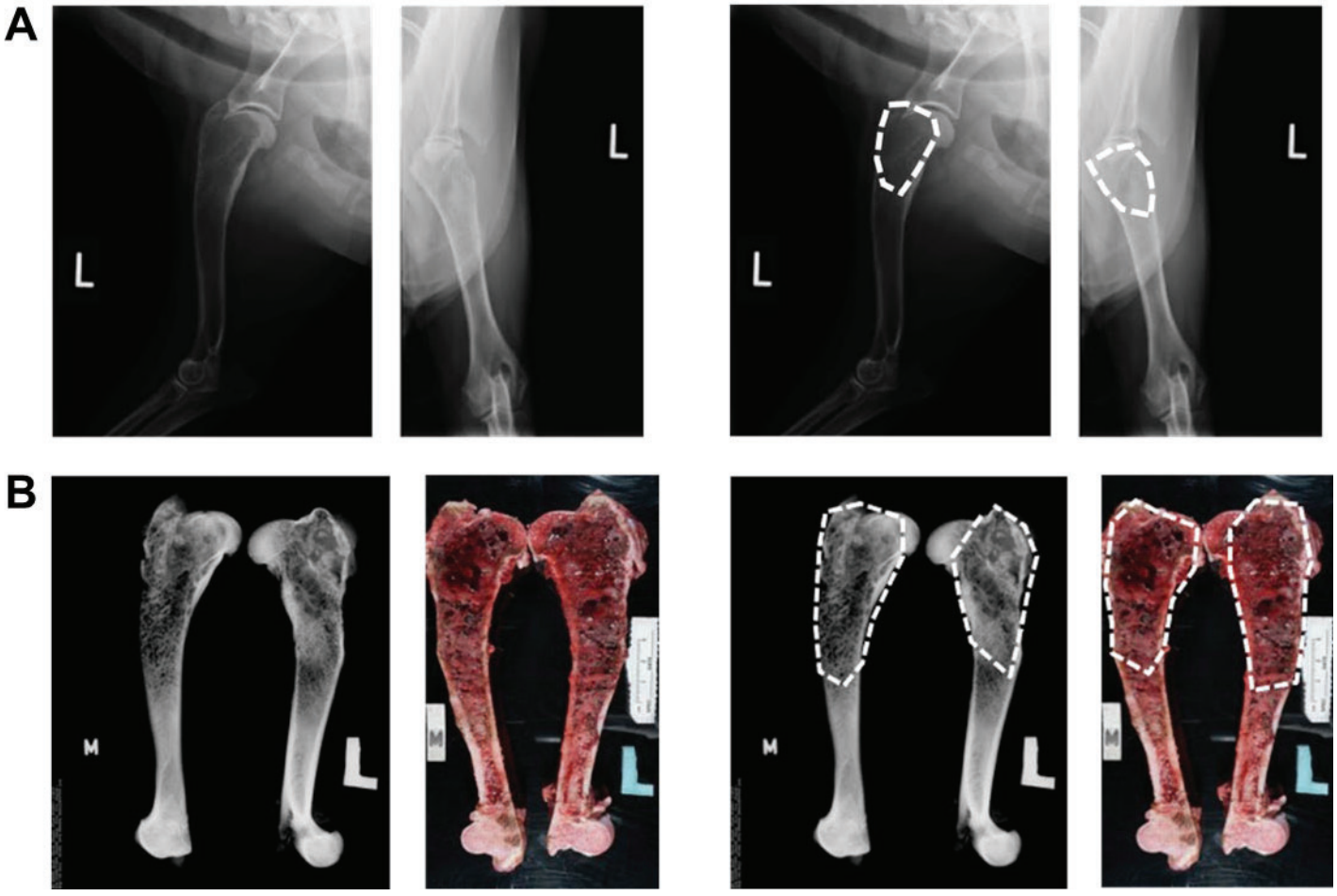

Figure S3. Administration of systemic vesicular stomatitis virus (VSV) in dogs with osteosarcoma did not cause any clinically significant laboratory abnormalities. Common laboratory tests including blood chemistry and complete blood count (CBC) were used to monitor clinical safety following VSV infusion showing no significant abnormalities relative to baseline. Blood test results from the first 11 enrolled dogs are shown indicating no significant changes in (A) liver function testes including alanine aminotransferase (ALT) and aspartate aminotransferase (AST); and (B) lymphocytes (LYMPH) and total white blood cell count (WBC).

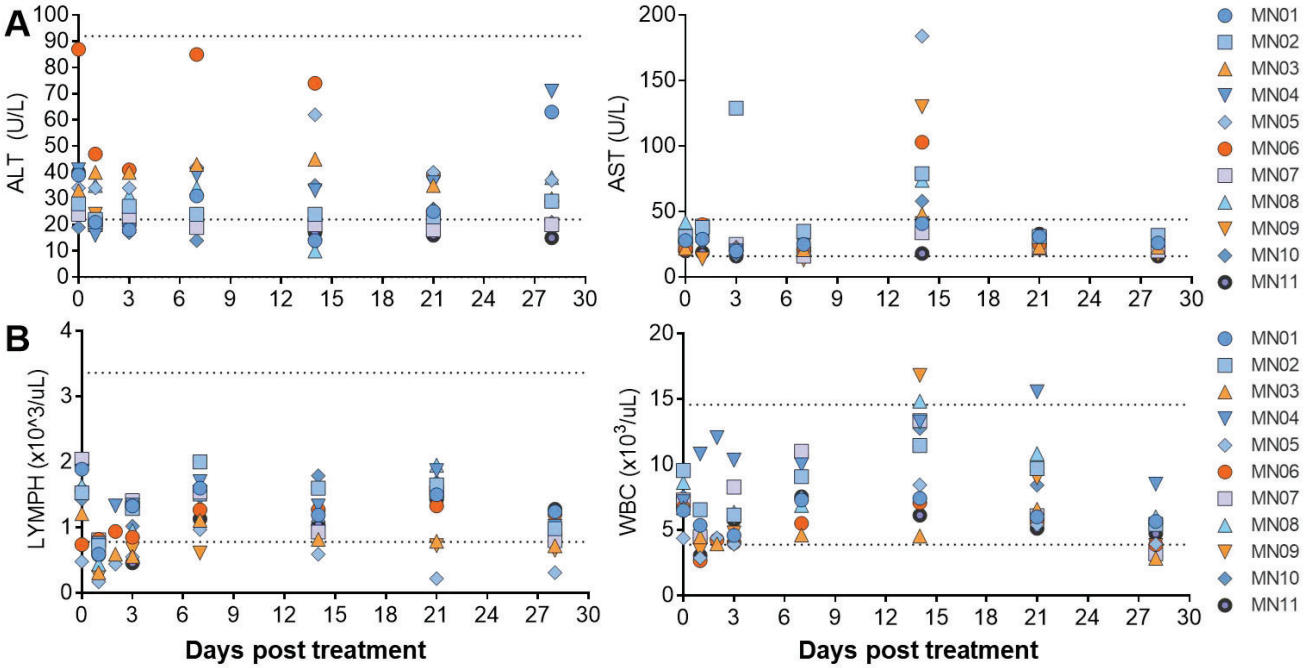

Figure S4. Small foci of micronecrosis seen in a subset of cases treated with systemic VSV may indicate areas of viral oncolysis. H&E histopathology of amputation samples obtained 10 days after treatment with systemic VSV. (A) Large areas of necrosis commonly associated with ischemia observed in resected osteosarcoma specimens. (B) Small focal areas of micronecrosis were seen in a subset of treated cases, potentially due to viral infection of tumor cells and subsequent cell lysis.

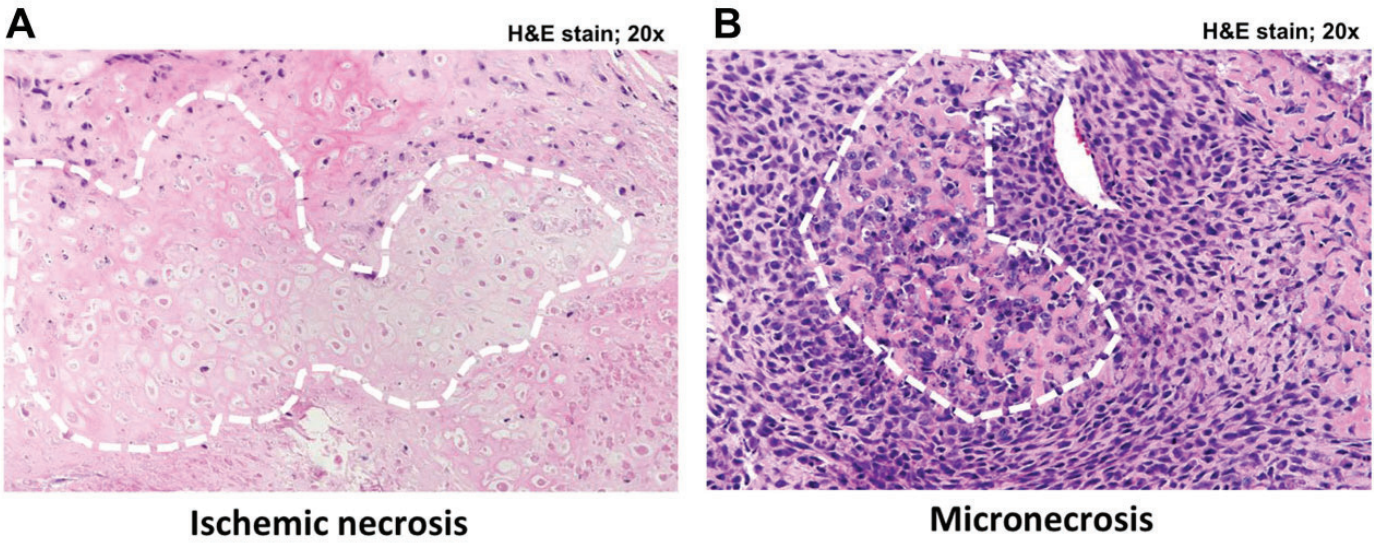

Figure S5. Virus clearance from blood corresponds with generation of anti-VSV neutralizing antibodies

(A) qRT-PCR detection of VSV-N copies in PBMC samples and (B) Neutralizing antibody titers in serum samples collected from a subset of dogs that received systemic VSV therapy. All evaluated dogs developed neutralizing antibodies at or above the limit of detection (LOD) within approximately 7 days after VSV administration.

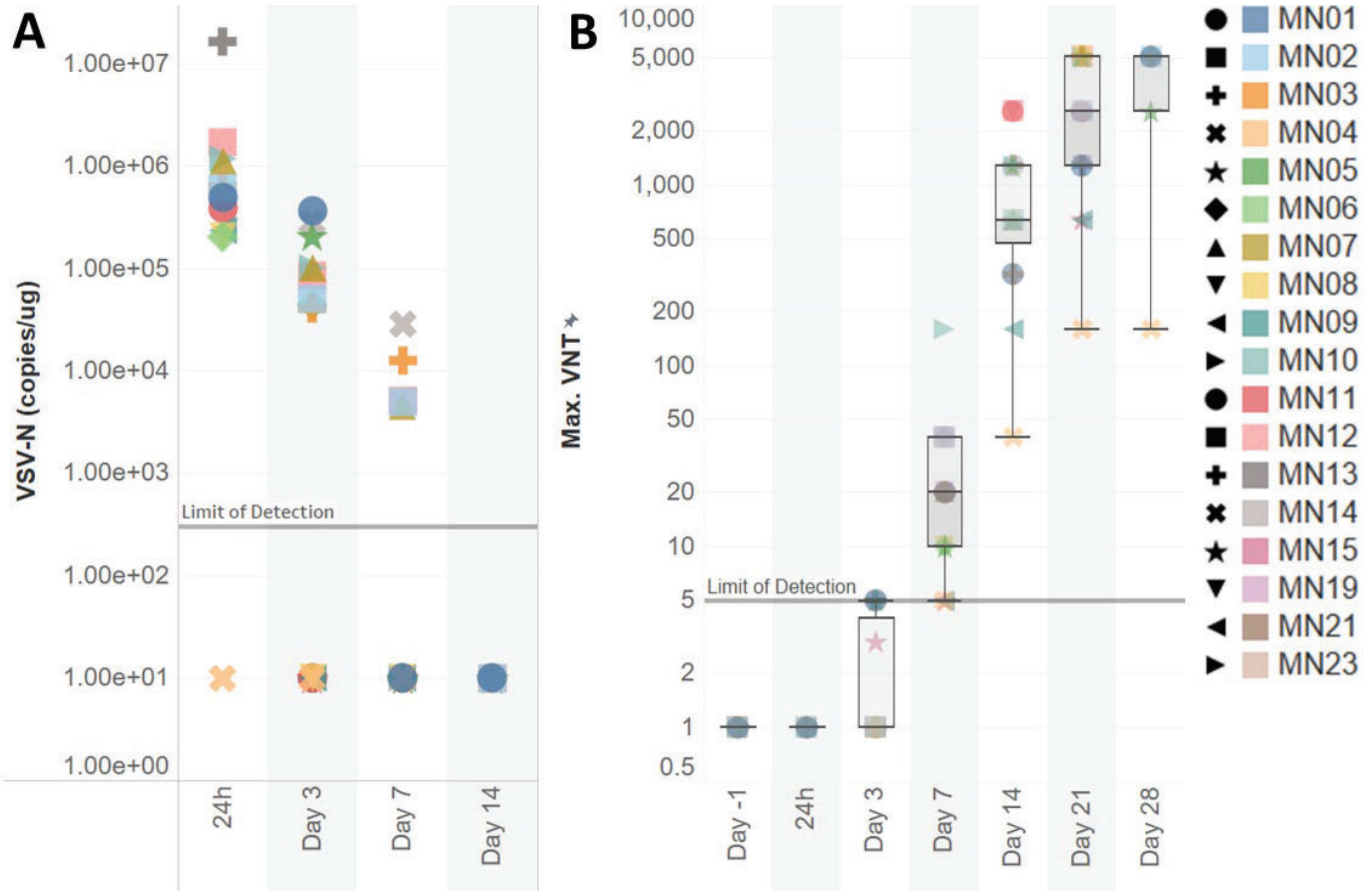

Figure S6. Detection of virus shedding. Detection of VSV-N RNA copies in RNA isolated from buccal swab, urine (separated into urine cells and supernatant), rectal swabs, and feces samples (from a subset of dogs).

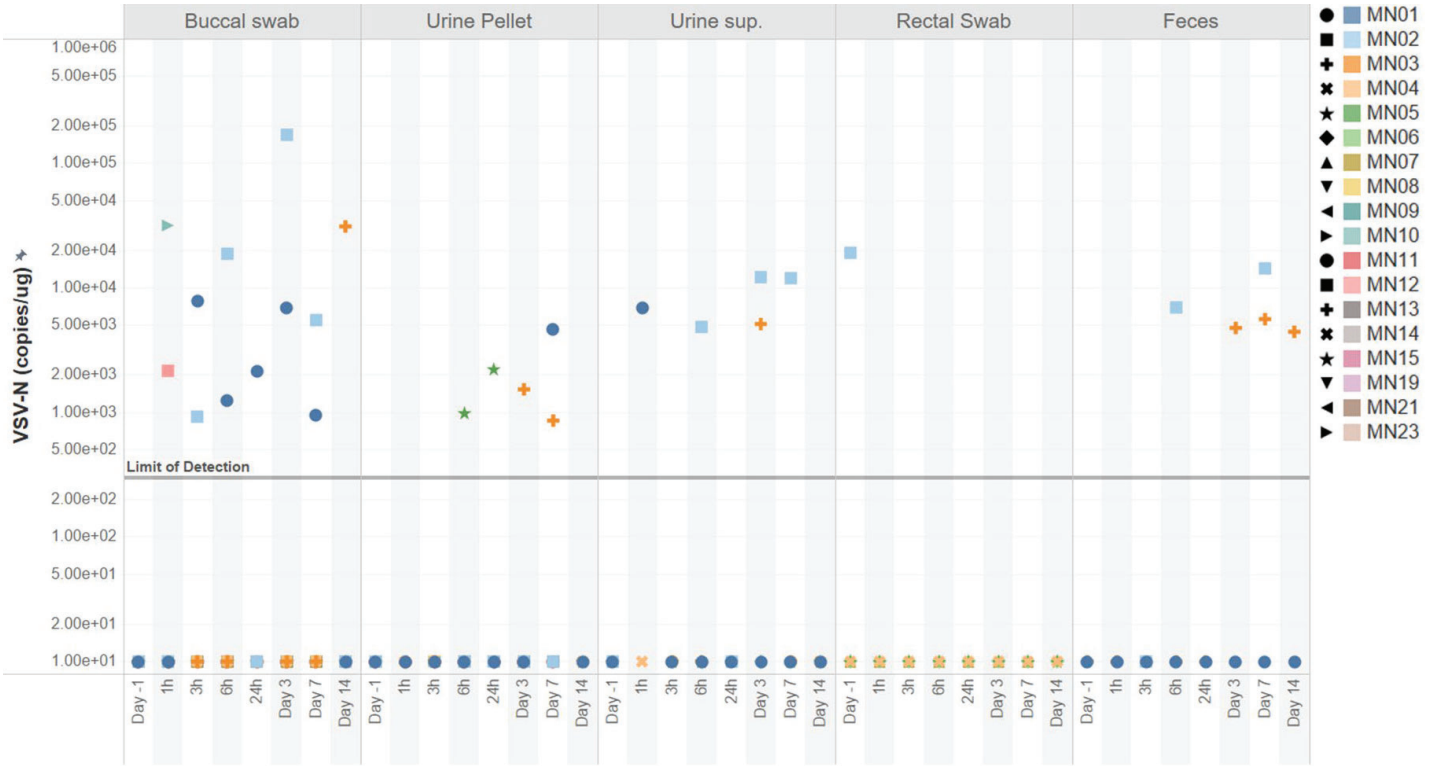

Figure S7. Acute cytokine/chemokine responses after intravenous VSV treatment.

Quantification of canine cytokines and chemokines (Granulocyte-macrophage colony-stimulating factor [GM-CSF], IL-6, monocyte chemoattractant protein-1 [MCP-1], keratinocyte-derived cytokine [KC], IL-2, IP-10, IL-8, TNF-α, IL-10, IL-7, IL-15, IL-18) in serum samples collected at baseline, 1, 3, and 6 hours post VSV infusion in the first 11 enrolled dogs.

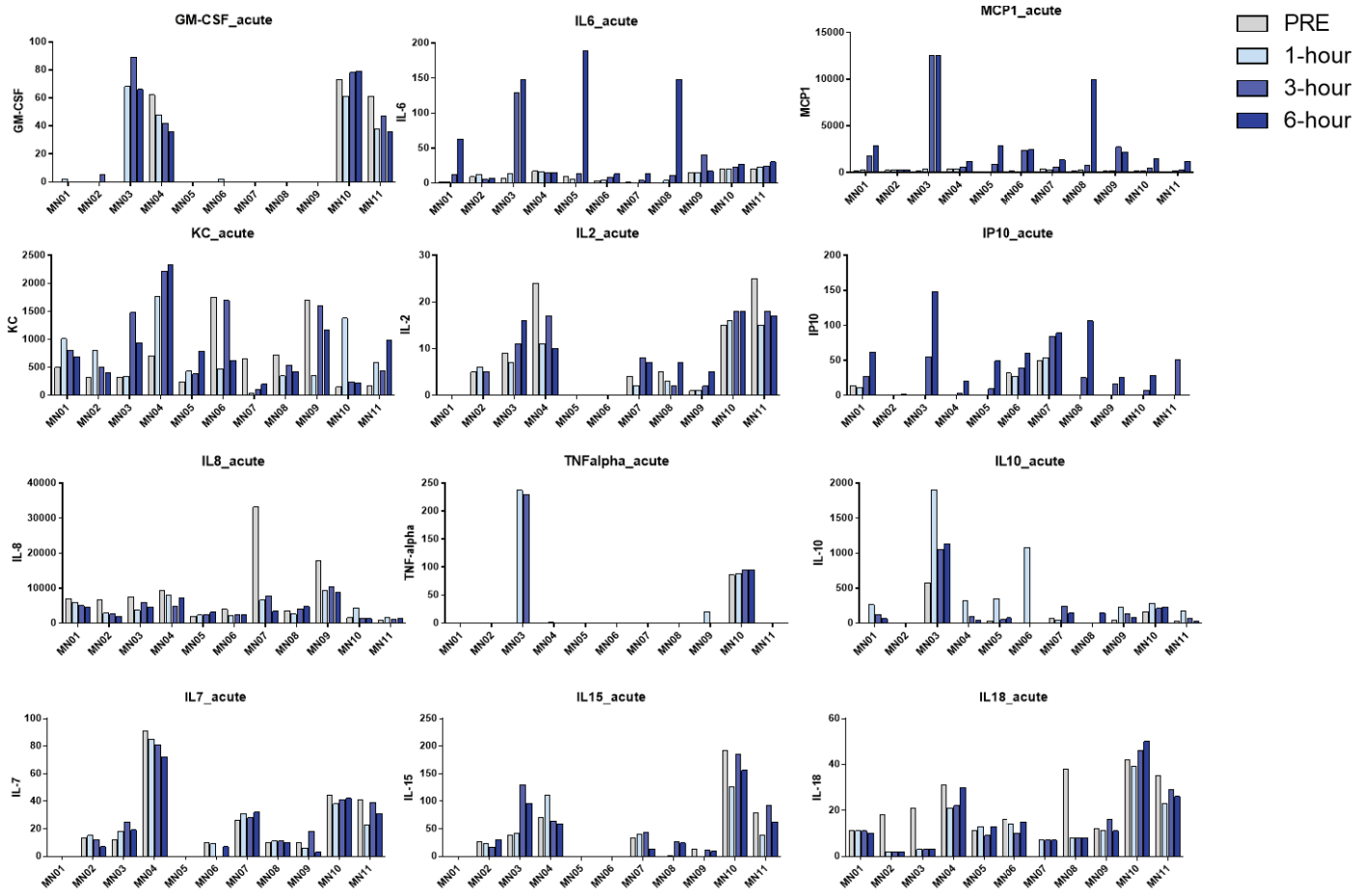

Figure S8. RNAseq analysis of CCOGC control cohort. (A) Unsupervised hierarchical clustering of RNAseq analysis data of available osteosarcoma tumor samples from the CCOGC control cohort. (B) Gene cluster expression summary score (GCESS) of osteosarcoma tumors. (C) Correlation of survival outcomes with CD37 monocyte (i), CD8 T-cell (ii), and cell cycle GCESS (iii), does not indicate a correlation between survival and CD8 T-cell GCESS in pre-treatment tumor biopsy samples (iv) in the CCOGC cohort.

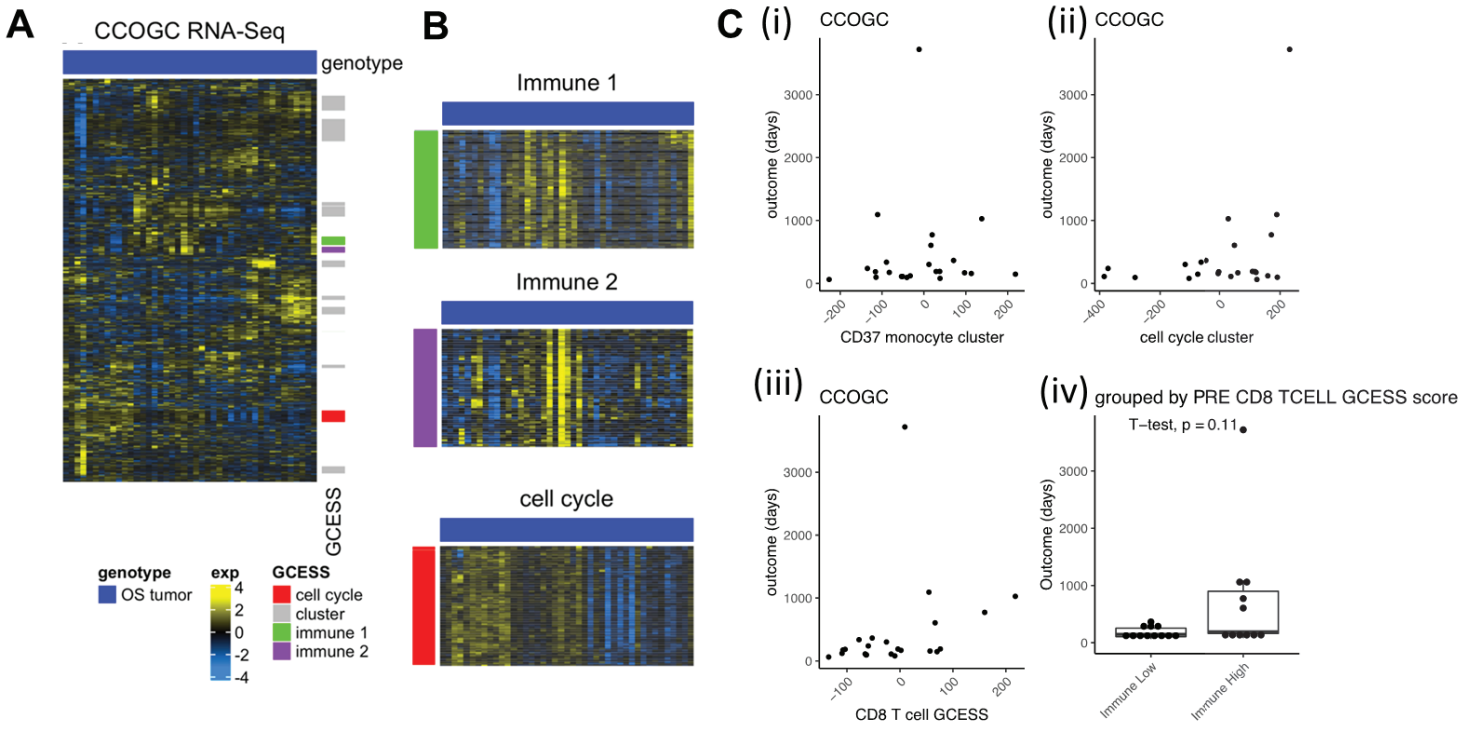

Figure S9. Survival analyses comparing CCOGC and VIGOR cohorts.

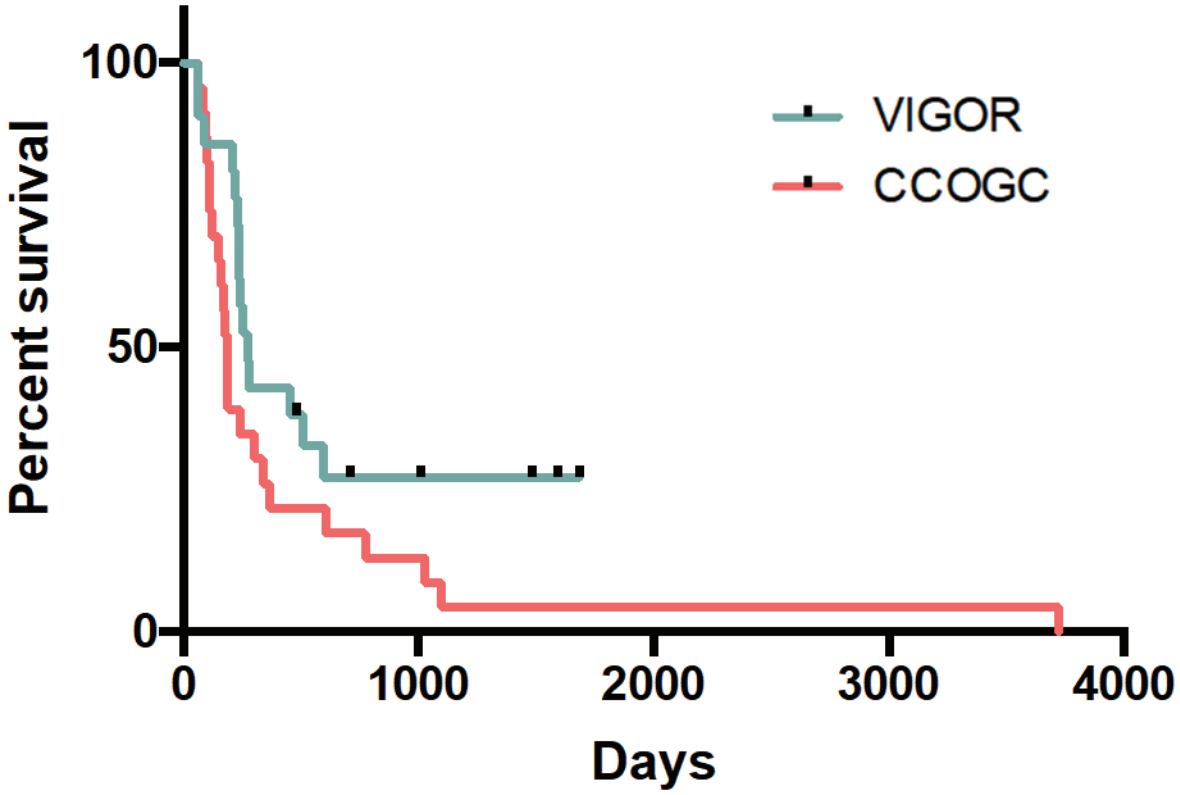

Neoadjuvant systemic oncolytic vesicular stomatitis virus is safe and may enhance long-term survivorship in dogs with naturally occurring osteosarcoma.

eTOC synopsis:

Systemic oncolytic Vesicular stomatitis virus (VSV) can be used safely in the neoadjuvant setting to treat naturally occurring canine osteosarcoma. Long-term survivorship was more frequent in the VSV-treated study cohort compared to control cohorts supporting future clinical advancement of systemic VSV therapy as a neoadjuvant therapy.

Graphical Abstract

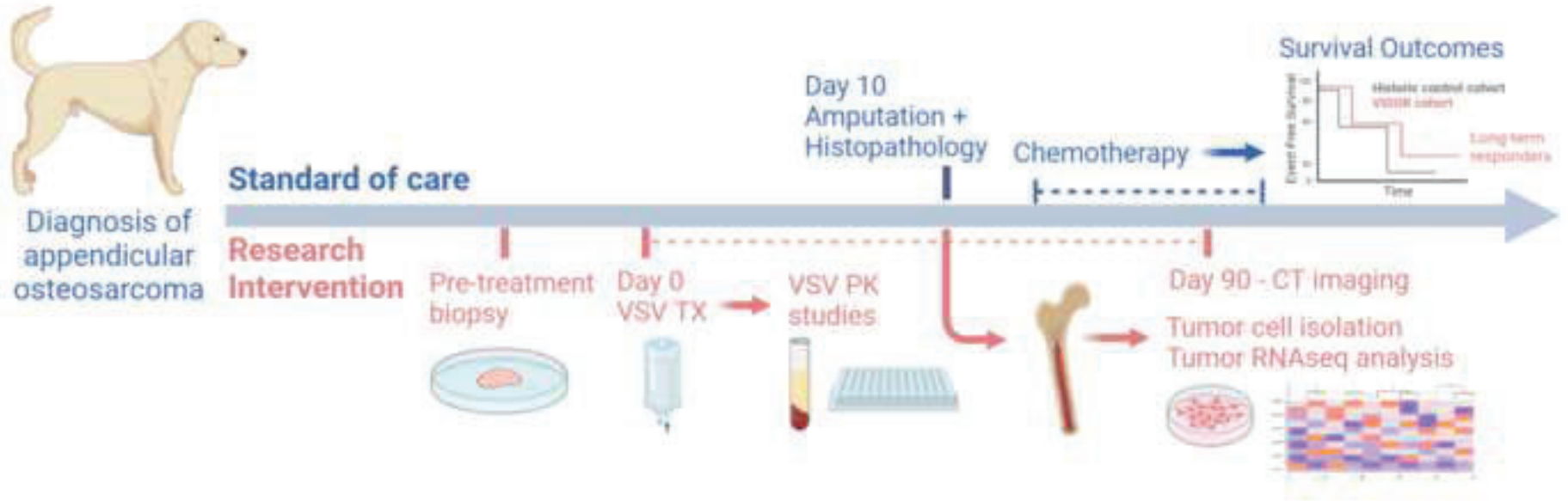

Medical Research Archives

ESMED
European Society of Medicine

OPEN ACCESS

Published: November 30, 2022

Citation: Sarver A. L., Makielski K. M., Modiano J. F., 2022. A Contemporary Assessment of Osteosarcoma: Lessons from a Comparative Approach, Medical Research Archives, [online] 10(11). https://doi.org/10.18103/mra.v10i11.3339

DOI: https://doi.org/10.18103/mra.v10i11.3339

ISSN: 2375-1924

REVIEW ARTICLE

A Contemporary Assessment of Osteosarcoma: Lessons from a Comparative Approach

Aaron L. Sarver[1-3], Kelly M. Makielski[1,3,4], Jaime F. Modiano[1,3-8,*]

[1]Masonic Cancer Center, University of Minnesota, Minneapolis, Minnesota 55455, USA
[2]Institute for Health Informatics, University of Minnesota, Minneapolis, Minnesota 55455, USA
[3]Animal Cancer Care and Research Program, University of Minnesota, St. Paul, Minnesota 55108, USA
[4]Department of Veterinary Clinical Sciences, University of Minnesota College of Veterinary Medicine, St. Paul, Minnesota 55108, USA
[5]Center for Immunology, University of Minnesota, Minneapolis, Minnesota 55455, USA
[6]Stem Cell Institute, University of Minnesota, Minneapolis, Minnesota 55455, USA
[7]Center for Engineering and Medicine, University of Minnesota, Minneapolis, Minnesota 55455, USA
[8]Department of Laboratory Medicine and Pathology, University of Minnesota Medical School, Minneapolis, Minnesota 55455, USA

*modiano@umn.edu

ABSTRACT

This review will describe more than two decades of comparative research on primary bone cancer (osteosarcoma). Osteosarcoma is a chaotic disease present in a complex and variable microenvironment composed of many different cell types which interact with each other and lead to high transcriptional heterogeneity. Despite this heterogeneity, common transcriptional patterns can be observed in the bulk transcriptomes of these tumors; additionally, these patterns are associated with outcome, indicating their importance to the molecular biology of the disease. Work from our group and others has led to our current understanding of osteosarcoma as a disease where multiple pathological processes appear to converge into a limited array of tissue organizations with distinct biology. Recurrent as well as distinct events can lead to these states of tissue organization, explaining the heterogeneity of osteosarcoma that is observed among and within species. Yet, despite their chaotic genomes, osteosarcomas seem to be (relatively) genetically stable, with persistent maintenance of essentially the same chromothriptic karyotype throughout the developmental lifetime of the tumor. Importantly, the transcriptional variance between tumors can highlight the underlying biology of the malignant cells themselves, as well as the composition of the osteosarcoma microenvironment and the host response, both of which are prognostically significant for this disease. Initial single cell RNA-seq reports provide further evidence of the importance of the osteosarcoma microenvironment for tumor characterization. Our data suggest that improving patient outcomes in immunologically barren or "cold" osteosarcomas, necessitates generating immune permissive or "warmer" microenvironments within the tumor. Furthermore, the aging bone microenvironment may create specific niches that predispose to cancer, and identification of the drivers that lead to these variable transcriptional patterns will be essential to identify personalized, effective genomic therapy for osteosarcoma.

1. Introduction

Osteosarcoma is the most common primary tumor of bone, and it has been observed in skeletal remains across the tree of life[1,2]. Just as the maintenance of a hematopoietic progenitor population exposes weaknesses associated with impaired differentiation of blood cells leading to the occurrence of leukemias and lymphomas, maintenance of the mesenchymal stem cell population appears to present vulnerabilities leading to sarcomas including osteosarcoma. The difference is that bone precursors must be much more tightly regulated both spatially and temporally than blood precursors due to their roles in the formation of connective tissues.

Osteosarcoma is characterized by large chromosomal rearrangements. Even in more commonly occurring tumors, somatic driver events are obfuscated by the occurrence of large copy number changes, which can contain many individual genes in addition to the primary cancer driver(s). Using a comparative oncology approach, it has been proposed that the study of orthologous canine tumors can be used to isolate driver events to increase resolution due to syntenic differences between canine and human tumors. This approach is predicated on the idea that copy number change of regions containing specific driver genes is occurring under similar evolutionary conditions within the tumor despite the syntenic differences across species. However, we have recently recognized that different species have evolved different levels of cancer protective mechanisms[1], suggesting that tumor evolution may be occurring under different conditions in different species.

Despite significant efforts in the genomic era to understand osteosarcoma, minimal progress has been made in improving patient outcomes[3]. The following sections of this review will describe strengths and weaknesses of dog and mouse models osteosarcoma and how each has helped to improve our understanding of the molecular etiology this disease. It also raises a cautionary note by highlighting divergent features that suggest osteosarcomas in different species are convergent diseases that achieve common patterns of organization.

2. Comparative approach to the identification of the molecular etiology of osteosarcoma

2a. Animal models of osteosarcoma

By definition, osteosarcoma only occurs in vertebrate animals with ossified skeletons. This cancer is an ancient pathological entity: it has been found in a variety of animals that lived hundreds of millions of years ago, although it is almost certainly overrepresented in the fossil record because soft tissues decay more readily than bones. In the current era, osteosarcoma has been reported in individuals representing every vertebrate class. But overall, this tumor occurs only rarely across the whole of the vertebrate animal kingdom with the notable exception of domestic dogs where it is seen commonly, and especially among individuals from large and giant breeds[2].

As in most other vertebrates, osteosarcoma is a rare disease in humans with a peak incidence in adolescence. In dogs, the peak incidence is usually observed in adults comprising the oldest 25% of the population. Despite these different incidence patterns, the canine disease has been proposed as an ideal model to understand the human disease. The natural history of the canine disease is very similar to that seen in humans; the frequency with which osteosarcoma occurs in dogs provides ready access to samples for molecular and pathological studies and to canine patients for interventional studies; the tumors in dogs arise spontaneously (they are not induced), in an immunocompetent environment; and the treatment intensity and innovation applied to dogs with osteosarcoma are second only to humans[4].

As is true for many other tumors, mouse models have been foundational to our understanding of osteosarcoma biology[5-12]. These models are exceptionally tractable, but some do not recreate the anatomical distribution and metastatic patterns of human disease. One recent comparative approach that utilizes forward genetic screens in mice has been more successful in recreating the conditions observed in humans and has served to identify driver events associated with osteosarcoma[12]. In this model, osteosarcomas develop upon *Sleeping Beauty (SB)* mutagenesis of osteoblasts (**Figure 1**). These mouse tumors do not show the copy number changes observed in human and canine tumors; instead they are driven by mobilization of the *T2/Onc* transposon, allowing specific identification of driver genes. Genes identified by mutagenesis are often found in regions where somatic copy number changes are identified in naturally occurring tumors[12].

FIGURE 1

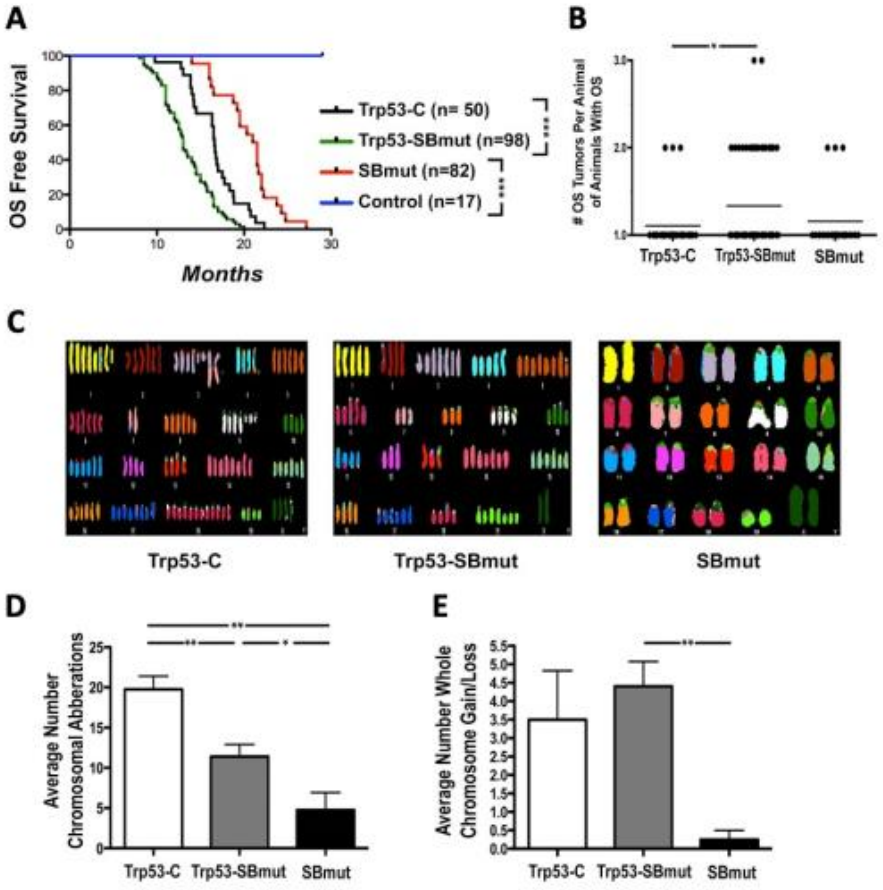

Figure 1. SB mutagenesis can accelerate or induce osteosarcoma development in cells with Sp7-cre expression. (A) Osteosarcoma-free survival curve depicting time to osteosarcoma development and survival endpoints in all cohorts. Control mice contained Sp7-cre with either SB11 or T2/Onc. ***P < 0.0001, log-rank test. (B) Histogram displaying the number of osteosarcomas per mouse. *P = 0.0159, Student's t test. (C) Representative SKY results from analysis of osteosarcoma tumor cells that developed in Trp53-C, Trp53-SBmut and SBmut mice. (D and E) Histograms demonstrating the number of chromosomal aberrations (E) and whole-chromosome gains and/or losses (E) identified by array CGH performed on Trp53-C (n = 4), Trp53-SBmut (n = 5) and SBmut (n = 4) osteosarcoma tumor DNA with matched normal tail DNA. *P < 0.05, **P < 0.001, Student's t test. Error bars, ± s.d. Adapted from ref[12].

Other animal models have been developed to study osteosarcoma, including zebrafish and pigs[13,14]. These models have unique strengths and open new avenues of investigation. But these alternative models have yet to achieve comparable abundance and maturity of data as mouse and canine models of osteosarcoma. And even as mice, dogs, and humans might share certain risk factors for osteosarcoma, there may be as many or more that are species specific (reviewed in[1,2,15]). A comparative approach has allowed us to recognize that the bone microenvironment is a highly complex tissue

and contains a variety of cells with complex cross talk and biological niches[16]. Species-specific differences have led us to conclude that there are multiple overlapping and distinct routes to osteosarcoma tumor formation and progression, and that osteosarcomas of humans, mice, dogs, and other animals are convergent diseases with complex etiologies that achieve comparable patterns of gross and histological organization.

It is thus clear that we must be diligent, deliberate, and vigilant to appreciate that animal models can be good or ideal in certain circumstances, while they may not be models at all in others.

2b. Disruption of *TP53*

Genomic efforts to understand cancer were initially focused on identifying somatic events that are recurrently observed in cancer tissue. In human osteosarcoma, the *TP53* gene has been observed to be recurrently disrupted using whole genome and exome sequencing of tumor tissue[17-20]. It seems apparent that loss of *TP53* function is associated with, and probably might be a major cause of the chaotic karyotypes seen in osteosarcomas[12]. Interestingly, it seems that once the chromothriptic event(s) have taken place, the tumor genomes can remain stable *in vivo*, even as they remain under strong selective pressure during progression and metastasis[21].

Highly recurrent disruption of *TP53* has also been reported in canine osteosarcoma[22-26]. Generally, higher rates of mutation have been reported in canine tumors than in human tumors, where structural variation is more commonly observed (**Figure 2**).

FIGURE 2

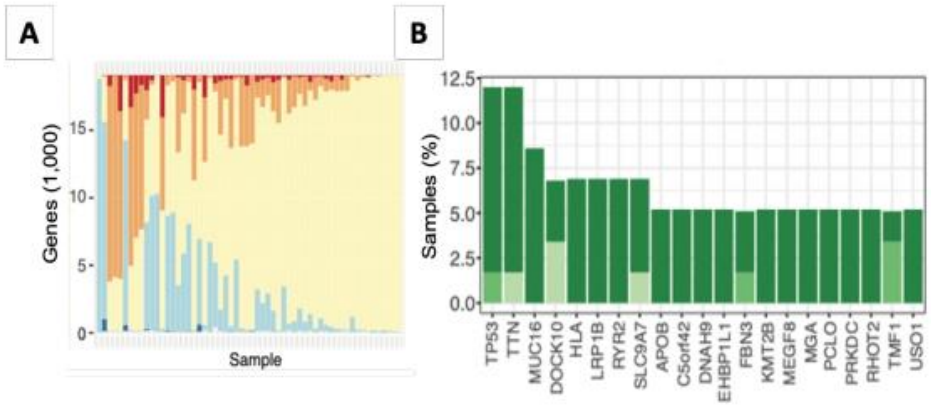

Figure 2. The mutational landscape of human osteosarcoma. We obtained tumor/normal exome sequence data for human osteosarcoma tumors (n=59) from GEO. (A) To examine copy number changes, we summarized the tumor normal reads obtained from the sequence capture to window segments and looked at the copy number changes within these windows. Expected copy number changes were observed on chrX and chrY. These serve as internal controls to show what loss of a single copy would look like (chrX) and also what complete loss of a region would look like (chrY). High level copy number gains were observed in MYC and RUNX2, and micro-deletions were present in regions containing CDKN2A, RB1, PTEN and TP53 corresponding to loss of either 1 or both copies of the chromosomal region. (B) Somatic mutations were identified utilizing a pipeline we designed to call mutations at specific locations based on the signal to noise ratios at each given position. Somatic mutations were observed in every tumor, although recurrence was low. Data are shown for the top-20 genes showing non-synonymous somatic mutations at any site as a proportion of all the samples analyzed. Many additional events were recurrently observed in a low percentage of tumors, but the majority were associated with very large genes that are mutated in many tumors without clear oncogenic functions.

Consistent with an important role for *TP53* in osteosarcoma, Li-Fraumeni syndrome predisposes carriers to osteosarcoma[27]. Germline variants in *TP53* have also been observed to be present in human osteosarcoma[28]. Recent work with human germline trios of affected progeny has shown that at least some of the germline mutations observed in human osteosarcoma cases are generated de novo, including mutations in *TP53*. That is, they are not present in the parents but are present in the germline of the affected patient[29]. While an analogous genetic disease to Li-Fraumeni has not been identified in dogs, a germline variant *TP53*

was reported in a dog that would be predicted to generate a frame shift variant[20].

2c. Loss of *CDKN2A*

The genomic region containing *CDKN2A* appears to be commonly lost in both human[20,30] and canine[31,32] osteosarcoma. Consistent with an important role for *CDKN2A* in osteosarcoma tumorigenesis, 2 independent case control studies identified markers near *CDKN2A* as the most significantly enriched region of the canine genome in dogs that developed osteosarcoma compared to dogs that did not[33,34]. Two distinct proteins with tumor suppressor function are generated from the *CDKN2A* locus, p16 and p14ARF. P16 regulates entry into G1 phase of the cell cycle through its interactions with CDK4/6 and *RB1*. P14ARF induces cell cycle arrest in G2 phase via binding the p53-stabilizing protein MDM2. Loss of *CDKN2A* has been shown to be an important event for malignant transformation of mesenchymal stem cells into osteosarcoma[35].

2d. Loss of *PTEN*

PTEN has been shown to be lost in human[20,36] and canine[32,37] osteosarcoma. Bi-allelic loss of *PTEN* occurs more commonly in the canine than in the human form of the disease (**Figure 3**)[i]. *PTEN* is a tumor suppressor that negatively regulates *PI3k* signaling. Meta-analyses of PTEN transcript levels show that increased levels of *PTEN* in tumors are associated with better outcomes[38].

[i] Sarver et al. Distinct mechanisms of PTEN inactivation in dogs and humans highlight convergent molecular events that drive cell division in the pathogenesis of osteosarcoma. Manuscript submitted.

FIGURE 3

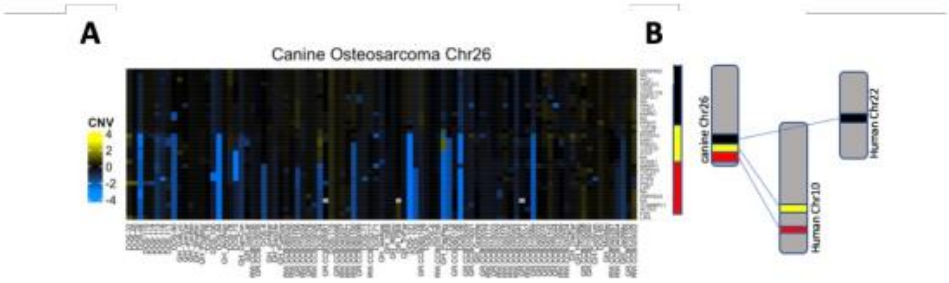

Figure 3. Loss of Distal Chr26 region containing PTEN in canine osteosarcoma. (**A**) Somatic changes observed between normal tissue and canine osteosarcoma tumors are shown for the distal end of canine chromosome 26. The data has been log_2 transformed and genes shown in bright blue represent somatic loss, genes shown in black are unchanged between tumor and control, and genes that show somatic gain are shown in yellow. (**B**) The syntenic alignment between canine chromosome 26 and the human genome is shown. The canine lost region is orthologous to two separate regions on human chr10 and one region on human chr22. Adapted from Sarver et al. Distinct mechanisms of PTEN inactivation in dogs and humans highlight convergent molecular events that drive cell division in the pathogenesis of osteosarcoma (manuscript submitted).

2e. Loss of *RB1, DLG2, and FAS*

RB1 is a tumor suppressor that negatively regulates the cell cycle via its interactions with multiple members of the network comprised by cyclin dependent kinase, (CDK), CDK inhibitors, and E2F transcription factors. *RB1* has been reported to be disrupted and lost in both human[20,39] and canine[32] osteosarcoma.

DLG2 is a tumor suppressor that has been reported to be mutated in human osteosarcoma[17] and to be lost in human and canine tumors[31].

FAS is a cell death receptor which is activated by *FASL*, leading to programmed cell death. Loss of *FAS* expression is one mechanism by which osteosarcoma cells may evade host resistance mechanisms in the lung, increasing metastatic potential[40-42]. In canine tumors loss of *FAS* occurs commonly due to homozygous deletion of the distal end of chr26, which also contains the *PTEN* gene[a].

Dogs that had lost Fas in their tumors showed improved therapeutic benefit from intratumorally delivered Fas ligand (FasL) under the control of a ubiquitin promoter and

encoded in an adenovirus vector[43]. The presumed mechanism of action was that FasL could interact with Fas on inflammatory cells without tumor cell apoptosis (as Fas-deficient cells do not undergo apoptosis in response to FasL). The subsequent death of these Fas-sensitive inflammatory cells established an environment that, somewhat paradoxically, promoted a self-amplifying cycle of inflammation and which led to innate and adaptive anti-tumor immunity[44].

2f. Gain of MYC

MYC is a prototypical oncogene involved in proliferation and growth. On its own in normal cells, *MYC* is tightly regulated, but in a permissive environment *MYC* is highly tumorigenic. Amplifications in the *MYC* region have been consistently reported in human[17,20] and in canine bone tumors[32,37].

3. Genetically engineered mouse models of osteosarcoma

Mice have been genetically engineered to generate osteosarcoma tumors. Germline mutation of *TP53* in mice leads to the generation of osteosarcoma tumors if they don't succumb to other tumors first. Targeting the *TP53* mutation to the osteoblast lineage drastically increases the frequency of osteosarcomas, and co-targeting *RB1* and *TP53* mutations within the osteoblast lineage accelerates tumor formation[9,10]. Targeting of *DLG2* in a *P53, RB1* background in the osteoblast lineage further accelerates tumor formation[31]. Conditionally targeting *PTEN* mutations with a *TP53* mutation in the osteoblast lineage also accelerates tumor formation[12]. But somewhat surprisingly, targeting *RB1* and *PTEN* together in the osteoblast lineage does not lead to osteosarcoma tumors, but instead leads to lipoma formation[45]. A number of other engineered mice develop osteosarcomas, including mice with *MYC* overexpression and *CDK2NA* loss (reviewed in[46]). These results consistently show that transformation of osteoblasts is a key step in the formation of osteosarcoma.

3a. Genetically engineered mice have been used to identify oncogenes and tumor suppressors in osteosarcoma

Forward genetic screens to accelerate tumor formation have been carried out in osteoblast lineage cells using the *Sleeping Beauty* transposon to mobilize a *T2/ONC* transposon (**Figure 1**)[12,47]. These screens have identified important roles for *RB1*, *MYC*, *PTEN*, and *CDKN2A* in osteosarcoma, genes which have been shown to be modified by copy number change or mutation in human and canine tumors.

4. Comparative analysis identifies disruption of the *PI3K* signaling pathway in osteosarcoma

Enrichment analyses of the universe of somatic events observed in human patients point to disruptions of the *PI3K/mTOR* pathways in osteosarcoma[19]. An siRNA screen for essential genes in a mouse osteosarcoma cell line also identified key roles for cell cycle genes, as well as *PI3K/mTOR* pathway genes[19]. Analyses of the combined set of genes identified by forward genetic screens

for osteosarcoma showed pathway enrichment for the *PI3K* signaling pathway[12] as well as cell cycle genes. These independent observations support the importance of the *PI3K* signaling pathway in osteosarcoma tumorigenesis.

5. Syntenic synergy in osteosarcoma

Colocalization of genes within oncogenic risk neighborhoods may play an important role in osteosarcoma and other tumors when they are commonly lost. *PTEN* and *FAS* are commonly lost in canine osteosarcomas, leading to a tumor with diminished suppression of PI3K signaling and decreased apoptotic capability in the presence of *FASL*. The genomic susceptibility to biallelic loss of these two genes, found on the distal end of chr26 within the canine genome, may partially explain the increased risk as well as the shorter survival times associated with canine osteosarcoma[ii].

Other regions of the genome may also carry syntenic synergistic risk and vulnerabilities. For example, *MTAP* is located near *CDKN2A* and is commonly lost leading to tumorigenic changes in metabolism that may provide competitive advantages to tumor clones beyond loss of *CDKN2A* derived protein products. Cells that have lost *MTAP* require *PRMT5*[48] and are sensitive to treatment using *PRMT5* inhibitors[49]. *MYC* and *PVT1* are also commonly amplified together leading to synergistic interactions and increased transformation relative to the individual components[50]. Synergistic interactions based on gene synteny may be important to understanding species specific cancer risk as well as defining weaknesses specific to cancer cells.

6. Comparative genomic studies of osteosarcoma transcriptional patterns

In contrast to other tumors like colon, breast, or blood tumors, inter-tumor transcriptional heterogeneity is extremely high in osteosarcoma tumors. Recent work using single cell analyses of osteosarcoma tumor cells suggests that the expression differences observed between osteosarcoma tumors are likely due to the presence of different populations of tumor and stromal cells at different differentiation states within the bulk microenvironment[51]. Recent work utilizing spatial transcriptomics suggest that multiple distinct cytokine mediated microenvironment niches exist within the bone and bone marrow which allow for the mesenchymal stem cell lineage cells to interact with and regulate the hematopoietic stem cell system[52]. Osteosarcoma may arise from deregulation of these niches and cellular imbalances may be generating the high level of variance observed with bulk osteosarcoma sequencing. This, coupled with difficulties in extracting RNA from bone tissues, has slowed advances in understanding transcriptional heterogeneity in osteosarcoma. Despite these

[ii]Sarver et al. Distinct mechanisms of PTEN inactivation in dogs and humans highlight convergent molecular events that drive cell division in the pathogenesis of osteosarcoma. Manuscript submitted.

complications, a number of landmark studies have identified conserved transcriptional patterns in mRNA and miRNA to be present across sets of osteosarcoma tumors derived from humans, mice and canines and these conserved patterns have been associated with patient outcome.

The gene cluster expression summary score (GCESS) has been used to systematically independently identify and quantify sets of coregulated genes in human, canine and murine tumors[53]. The GCESS is defined as the sum of expression values (log_2-transformed and mean centered) of all genes in a particular defined cluster for a single sample. Clusters of genes are defined by a minimum average linkage hierarchical clustering threshold and a minimum gene number in order to identify strong patterns in the data. Essentially, the GCESS method carries out dimensional reduction of many correlated individual transcript data points and condenses them into a single value. The GCESS method can then be used for statistical analyses of the gene expression patterns with reduced noise relative to individual transcripts. Cluster membership can then be compared across datasets and across species identifying orthologous transcriptional patterns (**Figure 4**).

FIGURE 4

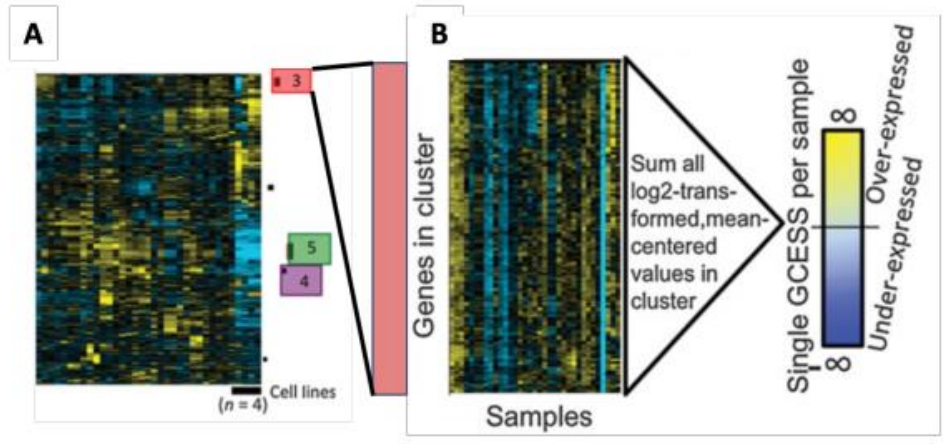

Figure 4. Schematic illustration of the GCESS method. The GCESS method was developed to reduce the high dimensionality of expression profiles generating a normalized and easily comparable value per sample for use in further association analyses. The GCESS is defined as the sum of expression values (log 2 -transformed and mean centered) of all genes in a particular gene cluster for a single sample. A negative GCESS indicates relative under-expression of the group of genes in that sample compared with all of the samples in the analysis set, a positive GCESS indicates overexpression, and a GCESS close to 0 (zero) indicates mean expression. The

GCESS summarizes the relative transcript levels of many correlated genes into a single value. This value is calculated for each cluster in each tumor. This allows for tumors to be rank ordered by summary score, which is based on the observed transcriptional data. Multiple summary scores were generated for each tumor sample, allowing for the independent comparison of the impact of each identified gene cluster, thereby achieving an unbiased dimensional reduction. Adapted from ref[53].

Using the GCESS approach, conserved transcriptional variation has been observed in human, mouse, and canine osteosarcomas in a cluster of genes associated with cell cycle progression[53,54], a cluster of genes associated with immune cell infiltration[53] and a set of miRNA present at the 14q32 human locus[55]. Increased transcription associated with cell cycling has consistently been associated with poor outcome in human and canine osteosarcoma[53,54,56] as well as other tumor types[53,56]. Variable expression of components of the immune system were identified in human mouse and canine samples[53]. Decreased expression of transcripts associated with immune infiltration has been associated with poor patient outcomes[53]. Decreased expression of a set of co-clustered miRNA at the 14q32 locus was observed in human, canine, and mouse samples[57] and was also associated with poor outcome in human and mouse samples[58]. These results have been validated in additional sets of human tumors[59].

7. Linkage of driver events to transcriptional patterns

Identification of driver events responsible for transcriptional heterogeneity of tumors has been difficult in osteosarcoma for a number of reasons. First, driver events outside of *TP53* are highly heterogenous in osteosarcoma. Second, osteosarcoma RNA-seq datasets are generally relatively small compared to other tumors studied. Third, RNA-seq dataset quality is also influenced by difficulties in the extraction of mRNA from bone samples. Fourth, each tumor likely has a distinct background of additional somatic events and germline variants that are likely to modify the transcriptional response of a given driver event. Despite these difficulties, using comparative approaches, driver events can be linked to the observed transcriptional patterns using GCESS based analyses.

As noted above, much higher rates of bi-allelic *PTEN* loss have been reported in canine than in human osteosarcoma. This has allowed us to elucidate the role of *PTEN* in tumor transcriptional heterogeneity. In canine tumors, loss of *PTEN* DNA can be directly correlated to loss of *PTEN* transcript. *PTEN* transcript levels are highly negatively correlated with the cell cycle GCESS in four independent RNA-seq datasets. Taken together these results strongly suggest that *PTEN* loss is a cause of increased cell division in canine osteosarcoma. In human osteosarcoma, increased methylation of the 5' shoulder region of the CPG island in the *PTEN* promoter is associated with increased cell cycle scores. Rather than directly controlling

the basal transcript level of *PTEN*, methylation in human and DNA loss in canines likely inhibits the inducibility of *PTEN* in response to inappropriate cell division. Distinct mechanisms of *PTEN* inactivation in dogs and humans highlight convergent molecular events that drive cell division in the pathogenesis of osteosarcoma[iii].

Mechanisms by which immune infiltration is controlled in osteosarcoma also remain murky. Microenvironment niches have been described within the bone marrow environment for the regulated proliferation and differentiation of hematopoietic stem cells[52,60]. Loss of immune infiltration within the tumor microenvironment suggests that mechanisms exist for maintaining immune cell presence in normal bone, which are compromised in osteosarcoma. Evidence for crosstalk between tumor cells and the immune system also exists in retinoblastoma, where a normally immune privileged environment generates an immune response following inappropriate proliferation. This immune response is negatively correlated to cell cycling in human tumors as well as genetically engineered mouse tumors[61].

RNA-seq analyses of SB mutagenized screens provide clues to how the immune system is deregulated in osteosarcoma. Tumors that overexpress *CSF1R* have very low levels of immune infiltrate. The addition of *CSF1R* overexpression in *TP53* mutant osteoblasts accelerates tumorigenesis in genetically engineered mice and the resulting tumors show lower levels of immune infiltrate relative to *TP53* mutation alone. It is likely that *CSF1R* is hijacking the *CSF1* cytokine creating niches that do not support proliferation of the immune system[iv].

Evidence also exists that an increased immune response due to infection is associated with better outcomes in osteosarcoma. Dogs with post-operative wound infections after limb-salvage surgery for osteosarcoma have improved survival[62]. In human patients, deep post-operative infections also lead to better outcomes[63]. These results suggest that mechanisms that recruit additional immune cells may be beneficial to osteosarcoma.

8. Immunotherapy for osteosarcoma

Dogs as a model have their own limitations[2]; however, we and others have identified instances where the biology allows us to utilize dogs to advance immunotherapy for this disease (reviewed in ref.[64]). The canine trials conducted to date have had mixed results, but a consistent conclusion from these studies is that immunotherapies that activate innate immunity improve survival for dogs with non-metastatic appendicular osteosarcoma[43,65,66]; this has also been

[iii] Sarver et al. Distinct mechanisms of PTEN inactivation in dogs and humans highlight convergent molecular events that drive cell division in the pathogenesis of osteosarcoma. Manuscript submitted.

[iv] Sarver et al. CSF1R regulates immune infiltration in the pathogenesis of osteosarcoma. Manuscript submitted.

observed in humans[67]. Less work has been done in the metastatic setting, where the benefits remain unclear[68]. A recently published study showed benefit of inhaled IL-15 in dogs with advanced metastatic osteosarcoma[69], and a new study combining an oncolytic vesicular stomatitis virus (VSV)[70] and a novel peptide designed to simultaneously block the CD47/SIRPα myeloid checkpoint and the PD-1/PD-L1 immune exhaustion checkpoint, is underway at our institution (z.umn.edu/METEOR). Conventional strategies using antibodies to achieve blockade of the CTLA4 and/or the PD-1/PD-L1 immune exhaustion checkpoints have yet to be completed in canine osteosarcoma. But studies incorporating PD-1/PD-L1 checkpoint blockade have shown no (or very limited) success in human osteosarcoma[71,72].

9. Conclusions

Osteosarcoma is a chaotic disease present in a complex and variable microenvironment composed of many different cell types which can interact with each other leading to high transcriptional heterogeneity. Despite this heterogeneity, common transcriptional patterns can be observed in the bulk transcriptomes of these tumors; additionally, these patterns are associated with outcome, indicating their importance to the molecular biology of the disease. Deconvolution of the cell types present in osteosarcoma will be important to identifying compounds that modify bone marrow niches. While there are clear similarities between highly conserved driver events (*e.g.*, *TP53* mutation across species) conservation of molecular etiology is not absolute across species as is exemplified by PTEN (silenced via methylation in humans vs biallelic loss in dogs). Despite these potential pitfalls a comparative oncology approach has high value to the study of osteosarcoma. Naturally occurring canine tumors and genetically engineered mouse models allow opportunities to study osteosarcoma in the presence of a functional immune system which are not possible with the commonly used osteosarcoma cell line models. We suspect that targeting specific therapies to specific combinations of transcriptional patterns may improve outcomes. For example, the comparative study of human and canine tumors suggests that to improve patient outcomes in immune "cold" osteosarcomas we should be focusing therapeutic strategies on approaches that generate immune "warmer" microenvironments. We suspect that the aging bone microenvironment may create specific niches that predispose to cancer, perhaps through loss of immune monitoring, changes to the immune system as a result of aging, niche modification leading to changes in cellular composition, or by combination of these events. Identification of the molecular drivers that lead to these variable tumor specific transcriptional patterns will be essential to develop more personalized genomic therapy for osteosarcoma. Identification and remedy of factors that lead to immune deficiency in individual tumors may also lead to principles that guide general one-size-fits-all pharmaceutical intervention to activate and improve tumor immune response in osteosarcoma.

Corresponding author:

Jaime F. Modiano
Masonic Cancer Center
University of Minnesota
Minneapolis, Minnesota 55455, USA
Email: modiano@umn.edu

Acknowledgements:

The authors would like to thank Dr. Lauren Mills for her assistance with data management and analysis, and for generating Figure 2. The authors would similarly like to thank Dr. Matthew Breen (North Carolina State University), Dr. Kerstin Lindblad Toh (the Broad Institute of Harvard and MIT) and all of our colleagues in the Sarcoma Research Program and the Sarcoma Translational Working Group of the Masonic Cancer Center, University of Minnesota, for their efforts to advance our collective work over the past 15 years.

Grant Support:

The work described in this review was supported in part by the Zach Sobiech Osteosarcoma Fund of the Children's Cancer Research Fund (CCRF), the Karen Wyckoff Rein-in Sarcoma Foundation, GREYlong, and the Van Sloun Foundation; by grants R50 CA211249, P30 CA077598, and R21 CA208529 from the National Cancer Institute of the National Institutes of Health (NCI), CA170218 and CA190276 from the United States Department of Defense Congressionally Directed Peer Reviewed Cancer Research Program, D13CA-032 and D15CA-047 from Morris Animal Foundation, CHF947 and CHF3015 from the AKC Canine Health Foundation, and T2018-018 from the V Foundation for Cancer Research. KMM was supported in part by an institutional training grant in Molecular, Genetic, and Cellular Targets of Cancer (Grant T32CA009138) from the NCI. JFM is supported in part by the Alvin and June Perlman Endowed Chair in Animal Oncology. The authors acknowledge support from individual donors to the Animal Cancer Care and Research Program, University of Minnesota. The content of this manuscript is solely the responsibility of the authors and does not necessarily represent the official views of any of the funding agencies listed above.

Conflict of Interest Statement:

The authors declare no conflict of interest.

Funding Statement

None

References

1. Sarver AL, Makielski KM, DePauw TA, Schulte AJ, Modiano JF. Increased risk of cancer in dogs and humans: a consequence of recent extension of lifespan beyond evolutionarily-determined limitations? *Aging Cancer.* 2022;3(1):3-19.
2. Makielski KM, Mills LJ, Sarver AL, et al. Risk Factors for Development of Canine and Human Osteosarcoma: A Comparative Review. *Vet Sci.* 2019;6(2):48.
3. Smeland S, Bielack SS, Whelan J, et al. Survival and prognosis with osteosarcoma: outcomes in more than 2000 patients in the EURAMOS-1 (European and American Osteosarcoma Study) cohort. *Eur J Cancer.* 2019;109:36-50.
4. Fenger JM, London CA, Kisseberth WC. Canine osteosarcoma: a naturally occurring disease to inform pediatric oncology. *ILAR journal / National Research Council, Institute of Laboratory Animal Resources.* 2014;55(1):69-85.
5. Beck J, Ren L, Huang S, et al. Canine and murine models of osteosarcoma. *Vet Pathol.* 2022;59(3):399-414.
6. Ek ET, Dass CR, Choong PF. Commonly used mouse models of osteosarcoma. *Crit Rev Oncol Hematol.* 2006;60(1):1-8.
7. Scott MC, Sarver AL, Tomiyasu H, et al. Aberrant Retinoblastoma (RB)-E2F Transcriptional Regulation Defines Molecular Phenotypes of Osteosarcoma. *J Biol Chem.* 2015;290(47):28070-28083.
8. Scott MC, Tomiyasu H, Garbe JR, et al. Heterotypic mouse models of canine osteosarcoma recapitulate tumor heterogeneity and biological behavior. *Dis Model Mech.* 2016;9(12):1435-1444.
9. Berman SD, Calo E, Landman AS, et al. Metastatic osteosarcoma induced by inactivation of Rb and p53 in the osteoblast lineage. *Proc Natl Acad Sci U S A.* 2008;105(33):11851-11856.
10. Walkley CR, Qudsi R, Sankaran VG, et al. Conditional mouse osteosarcoma, dependent on p53 loss and potentiated by loss of Rb, mimics the human disease. *Genes Dev.* 2008;22(12):1662-1676.
11. Calo E, Quintero-Estades JA, Danielian PS, Nedelcu S, Berman SD, Lees JA. Rb regulates fate choice and lineage commitment in vivo. *Nature.* 2010;466(7310):1110-1114.
12. Moriarity BS, Otto GM, Rahrmann EP, et al. A Sleeping Beauty forward genetic screen identifies new genes and pathways driving osteosarcoma development and metastasis. *Nature genetics.* 2015;47(6):615-624.
13. Perleberg C, Kind A, Schnieke A. Genetically engineered pigs as models for human disease. *Dis Model Mech.* 2018;11(1).

14. Mohseny AB, Hogendoorn PC. Zebrafish as a model for human osteosarcoma. *Adv Exp Med Biol.* 2014;804:221-236.
15. Guijarro MV, Ghivizzani SC, Gibbs CP. Animal models in osteosarcoma. *Frontiers in oncology.* 2014;4:189.
16. Langsten KL, Kim JH, Sarver AL, Dewhirst M, Modiano JF. Comparative Approach to the Temporo-Spatial Organization of the Tumor Microenvironment. *Front Oncol.* 2019;9:1185.
17. Chen X, Bahrami A, Pappo A, et al. Recurrent somatic structural variations contribute to tumorigenesis in pediatric osteosarcoma. *Cell Rep.* 2014;7(1):104-112.
18. Kovac M, Blattmann C, Ribi S, et al. Exome sequencing of osteosarcoma reveals mutation signatures reminiscent of BRCA deficiency. *Nature communications.* 2015;6:8940.
19. Perry JA, Kiezun A, Tonzi P, et al. Complementary genomic approaches highlight the PI3K/mTOR pathway as a common vulnerability in osteosarcoma. *Proc Natl Acad Sci U S A.* 2014;111(51):E5564-5573.
20. Sayles LC, Breese MR, Koehne AL, et al. Genome-Informed Targeted Therapy for Osteosarcoma. *Cancer Discov.* 2019;9(1):46-63.
21. Rajan S, Zaccaria S, Cannon MV, et al. Structurally complex osteosarcoma genomes exhibit limited heterogeneity within individual tumors and across evolutionary time. *bioRxiv.* 2022:2021.2008.2030.458268.
22. Sakthikumar S, Elvers I, Kim J, et al. SETD2 Is Recurrently Mutated in Whole-Exome Sequenced Canine Osteosarcoma. *Cancer Res.* 2018;78(13):3421-3431.
23. Gardner HL, Sivaprakasam K, Briones N, et al. Canine osteosarcoma genome sequencing identifies recurrent mutations in DMD and the histone methyltransferase gene SETD2. *Commun Biol.* 2019;2:266.
24. Alsaihati BA, Ho KL, Watson J, et al. Canine tumor mutational burden is correlated with TP53 mutation across tumor types and breeds. *Nature communications.* 2021;12(1):4670.
25. Das S, Idate R, Regan D, et al. Whole exome sequencing and gene expression analysis of canine osteosarcomas identify mutant TP53 and enriched immune pathways associated with longer survival. *Research Square.* 2021;PREPRINT (Version 1) - This preprint has not been peer reviewed.
26. Chu S, Skidmore ZL, Kunisaki J, et al. Unraveling the chaotic genomic landscape of primary and metastatic canine appendicular osteosarcoma with current sequencing technologies and bioinformatic approaches. *PloS one.* 2021;16(2):e0246443.
27. Hameed M, Mandelker D. Tumor Syndromes Predisposing to Osteosarcoma. *Adv Anat Pathol.* 2018;25(4):217-222.

28. Ribi S, Baumhoer D, Lee K, et al. TP53 intron 1 hotspot rearrangements are specific to sporadic osteosarcoma and can cause Li-Fraumeni syndrome. *Oncotarget.* 2015;6(10):7727-7740.

29. Diessner BJ, Pankratz N, Hooten AJ, et al. Nearly Half of TP53 Germline Variants Predicted To Be Pathogenic in Patients With Osteosarcoma Are De Novo: A Report From the Children's Oncology Group. *JCO Precis Oncol.* 2020;4.

30. Mohseny AB, Tieken C, van der Velden PA, et al. Small deletions but not methylation underlie CDKN2A/p16 loss of expression in conventional osteosarcoma. *Genes, Chromosomes and Cancer.* 2010;49(12):1095-1103.

31. Shao YW, Wood GA, Lu J, et al. Cross-species genomics identifies DLG2 as a tumor suppressor in osteosarcoma. *Oncogene.* 2019;38(2):291-298.

32. Thomas R, Wang HJ, Tsai PC, et al. Influence of genetic background on tumor karyotypes: evidence for breed-associated cytogenetic aberrations in canine appendicular osteosarcoma. *Chromosome Res.* 2009;17(3):365-377.

33. Karlsson EK, Sigurdsson S, Ivansson E, et al. Genome-wide analyses implicate 33 loci in heritable dog osteosarcoma, including regulatory variants near CDKN2A/B. *Genome biology.* 2013;14(12):R132.

34. Letko A, Minor KM, Norton EM, et al. Genome-Wide Analyses for Osteosarcoma in Leonberger Dogs Reveal the CDKN2A/B Gene Locus as a Major Risk Locus. *Genes (Basel).* 2021;12(12).

35. Mohseny AB, Szuhai K, Romeo S, et al. Osteosarcoma originates from mesenchymal stem cells in consequence of aneuploidization and genomic loss of Cdkn2. *J Pathol.* 2009;219(3):294-305.

36. Freeman SS, Allen SW, Ganti R, et al. Copy number gains in EGFR and copy number losses in PTEN are common events in osteosarcoma tumors. *Cancer.* 2008;113(6):1453-1461.

37. Angstadt AY, Motsinger-Reif A, Thomas R, et al. Characterization of canine osteosarcoma by array comparative genomic hybridization and RT-qPCR: signatures of genomic imbalance in canine osteosarcoma parallel the human counterpart. *Genes Chromosomes Cancer.* 2011;50(11):859-874.

38. Zhou J, Xiao X, Wang W, Luo Y. Association between PTEN and clinical-pathological features of osteosarcoma. *Biosci Rep.* 2019;39(7).

39. Smida J, Xu H, Zhang Y, et al. Genome-wide analysis of somatic copy number alterations and chromosomal breakages in osteosarcoma. *Int J Cancer.* 2017;141(4):816-828.

40. Lafleur EA, Koshkina NV, Stewart J, et al. Increased Fas expression reduces the metastatic potential of human osteosarcoma cells. *Clin Cancer Res.* 2004;10(23):8114-8119.

41. Koshkina NV, Khanna C, Mendoza A, Guan H, DeLauter L, Kleinerman ES. Fas-negative osteosarcoma tumor cells are selected during metastasis to the lungs: the role of the Fas pathway in the metastatic process of osteosarcoma. *Mol Cancer Res.* 2007;5(10):991-999.

42. Worth LL, Lafleur EA, Jia SF, Kleinerman ES. Fas expression inversely correlates with metastatic potential in osteosarcoma cells. *Oncol Rep.* 2002;9(4):823-827.

43. Modiano JF, Bellgrau D, Cutter GR, et al. Inflammation, apoptosis, and necrosis induced by neoadjuvant fas ligand gene therapy improves survival of dogs with spontaneous bone cancer. *Mol Ther.* 2012;20(12):2234-2243.

44. Modiano JF, Bellgrau D. Fas ligand based immunotherapy: A potent and effective neoadjuvant with checkpoint inhibitor properties, or a systemically toxic promoter of tumor growth? *Discov Med.* 2016;21(114):109-116.

45. Filtz EA, Emery A, Lu H, Forster CL, Karasch C, Hallstrom TC. Rb1 and Pten Co-Deletion in Osteoblast Precursor Cells Causes Rapid Lipoma Formation in Mice. *PloS one.* 2015;10(8):e0136729.

46. Ng AJ, Mutsaers AJ, Baker EK, Walkley CR. Genetically engineered mouse models and human osteosarcoma. *Clin Sarcoma Res.* 2012;2(1):19.

47. Temiz NA, Moriarity BS, Wolf NK, et al. RNA sequencing of Sleeping Beauty transposon-induced tumors detects transposon-RNA fusions in forward genetic cancer screens. *Genome Res.* 2016;26(1):119-129.

48. Mavrakis KJ, McDonald ER, 3rd, Schlabach MR, et al. Disordered methionine metabolism in MTAP/CDKN2A-deleted cancers leads to dependence on PRMT5. *Science.* 2016;351(6278):1208-1213.

49. Kryukov GV, Wilson FH, Ruth JR, et al. MTAP deletion confers enhanced dependency on the PRMT5 arginine methyltransferase in cancer cells. *Science.* 2016;351(6278):1214-1218.

50. Tseng YY, Moriarity BS, Gong W, et al. PVT1 dependence in cancer with MYC copy-number increase. *Nature.* 2014;512(7512):82-86.

51. Zhou Y, Yang D, Yang Q, et al. Single-cell RNA landscape of intratumoral heterogeneity and immunosuppressive microenvironment in advanced osteosarcoma. *Nature communications.* 2020;11(1):6322.

52. Baccin C, Al-Sabah J, Velten L, et al. Combined single-cell and spatial transcriptomics reveal the molecular, cellular and spatial bone marrow niche organization. *Nat Cell Biol.* 2020;22(1):38-48.

53. Scott MC, Temiz NA, Sarver AE, et al. Comparative Transcriptome Analysis Quantifies Immune Cell Transcript Levels, Metastatic Progression, and Survival in

Osteosarcoma. *Cancer Res.* 2018;78(2):326-337.

54. Scott MC, Sarver AL, Gavin KJ, et al. Molecular subtypes of osteosarcoma identified by reducing tumor heterogeneity through an interspecies comparative approach. *Bone.* 2011;49(3):356-367.
55. Thayanithy V, Sarver AL, Kartha RV, et al. Perturbation of 14q32 miRNAs-cMYC gene network in osteosarcoma. *Bone.* 2012;50(1):171-181.
56. Lesluyes T, Delespaul L, Coindre JM, Chibon F. The CINSARC signature as a prognostic marker for clinical outcome in multiple neoplasms. *Sci Rep.* 2017;7(1):5480.
57. Thayanithy V, Park C, Sarver AL, et al. Combinatorial treatment of DNA and chromatin-modifying drugs cause cell death in human and canine osteosarcoma cell lines. *PloS one.* 2012;7(9):e43720.
58. Sarver AL, Thayanithy V, Scott MC, et al. MicroRNAs at the human 14q32 locus have prognostic significance in osteosarcoma. *Orphanet journal of rare diseases.* 2013;8:7.
59. Kelly AD, Haibe-Kains B, Janeway KA, et al. MicroRNA paraffin-based studies in osteosarcoma reveal reproducible independent prognostic profiles at 14q32. *Genome Med.* 2013;5(1):2.
60. Terashima A, Takayanagi H. The role of bone cells in immune regulation during the course of infection. *Semin Immunopathol.* 2019;41(5):619-626.
61. Sarver AL, Xie C, Riddle MJ, et al. Retinoblastoma tumor cell proliferation is negatively associated with an immune gene expression signature and increased immune cells. *Lab Invest.* 2021;101(6):701-718.
62. Lascelles BD, Dernell WS, Correa MT, et al. Improved survival associated with postoperative wound infection in dogs treated with limb-salvage surgery for osteosarcoma. *Annals of surgical oncology.* 2005;12(12):1073-1083.
63. Jeys LM, Grimer RJ, Carter SR, Tillman RM, Abudu A. Post operative infection and increased survival in osteosarcoma patients: are they associated? *Annals of surgical oncology.* 2007;14(10):2887-2895.
64. Wycislo KL, Fan TM. The immunotherapy of canine osteosarcoma: a historical and systematic review. *J Vet Intern Med.* 2015;29(3):759-769.
65. MacEwen EG, Kurzman ID, Rosenthal RC, et al. Therapy for osteosarcoma in dogs with intravenous injection of liposome-encapsulated muramyl tripeptide. *J Natl Cancer Inst.* 1989;81(12):935-938.
66. Mason NJ, Gnanandarajah JS, Engiles JB, et al. Immunotherapy with a HER2-Targeting Listeria Induces HER2-Specific Immunity and Demonstrates Potential Therapeutic Effects in a Phase I Trial in

Canine Osteosarcoma. *Clin Cancer Res.* 2016;22(17):4380-4390.

67. Meyers PA, Chou AJ. Muramyl tripeptide-phosphatidyl ethanolamine encapsulated in liposomes (L-MTP-PE) in the treatment of osteosarcoma. *Adv Exp Med Biol.* 2014;804:307-321.
68. Jimmy R, Stern C, Lisy K, White S. Effectiveness of mifamurtide in addition to standard chemotherapy for high-grade osteosarcoma: a systematic review. *JBI Database System Rev Implement Rep.* 2017;15(8):2113-2152.
69. Rebhun RB, York D, Cruz SM, et al. Inhaled recombinant human IL-15 in dogs with naturally occurring pulmonary metastases from osteosarcoma or melanoma: a phase 1 study of clinical activity and correlates of response. *J Immunother Cancer.* 2022;10(6).
70. Naik S, Galyon GD, Jenks NJ, et al. Comparative Oncology Evaluation of Intravenous Recombinant Oncolytic Vesicular Stomatitis Virus Therapy in Spontaneous Canine Cancer. *Mol Cancer Ther.* 2018;17(1):316-326.
71. Tawbi HA, Burgess M, Bolejack V, et al. Pembrolizumab in advanced soft-tissue sarcoma and bone sarcoma (SARC028): a multicentre, two-cohort, single-arm, open-label, phase 2 trial. *Lancet Oncol.* 2017;18(11):1493-1501.
72. D'Angelo SP, Richards AL, Conley AP, et al. Pilot study of bempegaldesleukin in combination with nivolumab in patients with metastatic sarcoma. *Nature communications.* 2022;13(1):3477.